

Determination of the Contributions of Light Duty and Heavy Duty Vehicle Emissions to Ambient Particles in California

Final Report (Contract #00-331)

Prepared for the California Air Resources Board and the California Environmental Protection Agency

May 20, 2005

Principal Investigator

Kimberly A. Prather

Primary Authors

Laura G. Shields

David A. Sodeman

Stephen M. Toner

Matthew T. Spencer

Thomas P. Rebotier

Secondary Authors

Deborah S. Gross

Sergio A. Guazzotti

Xueying Qin

David T. Suess

Department of Chemistry & Biochemistry
University of California San Diego
9500 Gilman Drive MC 0314
La Jolla, CA 92093-0314

Disclaimer

The statements and conclusions in this Report are those of the contractor and not necessarily those of the California Air Resources Board. The mention of commercial products, their source, or their use in connection with material reported herein is not to be construed as actual or implied endorsement of such products.

Acknowledgements

The authors of this report would like to acknowledge the people who made the studies possible. We thank the entire Prather group for their help over the past years in maintenance of the instrumentation, cooperation, participation in the setup and running of the studies, helpful discussions, and overall support. The authors express their gratitude to the Coordinating Research Council for their help and support in testing during CRC Project E55/E59, and the staff of the West Virginia University Transportable Heavy-Duty Emissions Testing Laboratory for their assistance with sample collection. For the operation of the light duty vehicle source study, we acknowledge the entire crew at the Hagen-Smit Laboratory in El Monte, CA. We also thank the staff at the Caldecott Tunnel in Berkeley, CA. We appreciate the assistance and side-by-side sampling of Michael Kleeman, Michael Robert, and Chris Jakober at several of the field studies. Finally, for all of his guidance and assistance in setting up the source testing and field studies, we thank Dr. William Vance.

This Final Report is submitted in fulfillment of Contract #00-331 (Determination of the Contributions of Light Duty and Heavy Duty Vehicle Emissions to Ambient Particles in California) by UCSD under the sponsorship of the California Air Resources Board. Work was completed as of January 31, 2005.

Table of Contents

<i>Section I: Introduction</i>	1
Introductory Remarks	2
1.1 Research Objectives	2
1.2 Instrumentation	4
1.3 Data Analysis Methods	5
1.4 Summary of Chapters	5
1.4.1 Introduction	5
1.4.2 Mobile Source Characterization Studies	6
1.4.3 Fuel and Oil Studies	7
1.4.4 Evaluation of Sources Signatures & Application to Apportionment Studies	7
1.4.5 Future Data Analysis Techniques	7
1.4.6 Conclusions	8
1.5 References	8
<i>Section II: Mobile Source Characterization Studies</i>	9
Determination of Single Particle Mass Spectral Signatures from Heavy Duty Vehicle Emissions in the 0.1 to 3 Micrometer Size Range	10
2.1 Introduction	10
2.2 Experimental Methods	11
2.2.1 Sampling Conditions	11
2.2.2 Instrumentation	13
2.2.3 Data Analysis Methods	16
2.3 Results and Discussion	16
2.3.1 Chemical Reproducibility	16
2.3.2 Effect of Dilution Conditions	17
2.3.3 Chemical Classes	20
2.3.4 Temporal and Cycle-to-Cycle Variation	29
2.3.5 Vehicle-to-Vehicle Variability	33
2.4 Implications	36
2.5 Acknowledgements	36
2.6 References	37
Single Particle Characterization of Ultrafine- and Fine-Mode Particles from Heavy Duty Diesel Vehicles using Aerosol Time-of-Flight Mass Spectrometry	43
3.1 Introduction	43
3.2 Experimental	44
3.3 Results and Discussion	46
3.3.1 Description of particle types observed with UF-ATOFMS	46
3.3.2 Analysis of Size Segregated Chemical Composition for each HDDV	53
3.3.3 Particle Composition as a Function of Driving Cycle & HDDV	57
3.3.4 Comparison of Ultrafine and Lower-Fine Mode to Fine/Coarse Mode Particles	57
3.3.5 Prospects for Apportionment	59
3.4 Summary	61
3.5 Acknowledgements	61
3.6 References	62

Determination of Single Particle Mass Spectral Signatures from Light Duty Vehicle Emissions	68
4.1 Introduction	68
4.2 Experimental	68
4.3 Results and Discussion	70
4.3.1 Scaling	70
4.3.2 Chemical Classes	72
4.3.3 Size	82
4.3.4 Vehicle and Cycle Variability	87
4.3.5 Cold Start	91
4.3.6 Exhaust Technology	93
4.4 Implications	95
4.5 Acknowledgements	95
4.6 References	96
<i>Section III: Fuel and Oil Studies</i>	102
Comparison of Oil and Fuel Aerosol Chemical Signatures with Heavy Duty and Light Duty Vehicle Emissions Using ATOFMS	103
5.1 Introduction	103
5.2 Experimental	103
5.2.1 Single Particle Analysis: ATOFMS	103
5.2.2 Fuel and Oil Aerosol Generation	103
5.2.3 ATOFMS Data Analysis	104
5.3 Results and Discussion	104
5.3.1 General Particle Classes	104
5.4 Conclusions	114
5.5 References	114
Analysis of Petroleum Based Lubricants with Different Detergent Additives and Used Engine Oils with Varying Soot Levels	118
6.1 Introduction	118
6.2 Experimental	118
6.2.1 Oil Aerosol Generation	118
6.2.2 Data Analysis	119
6.3 Results and Discussion	119
6.4 Conclusion	124
<i>Section IV: Evaluation of Source Signatures and Application to Apportionment Studies</i>	126
Comparison of Light Duty and Heavy Duty Vehicle Emissions from Dynamometer and Tunnel Studies Using ART-2a	127
7.1 Introduction	127
7.2 Experimental	128
7.3 Results and Discussion	130
7.3.1 Dynamometer Studies	130
7.3.2 Caldecott Tunnel Study	132
7.3.3 New Tunnel Classes	134
7.3.4 Size profiles	138
7.3.5 Temporal Trends	138
7.4 Implications	144

7.5 Acknowledgements	146
7.6 References	146
Using Mass Spectral Source Signatures to Apportion Exhaust Particles From Gasoline and Diesel Powered Vehicles in a Freeway Study	153
8.1 Overview of Freeway Study	153
8.2 Experimental Approach and Study Location.....	154
8.3 Results and Discussion	154
8.3.1 Quality assurance of ATOFMS data	154
8.3.2 Comparison with standard particle counts	157
8.3.3 Comparison of temporal trends from peripheral instruments	162
8.3.4 Comparison of particle phase and gas phase data	162
8.3.5 Upwind/Downwind Sampling.....	162
8.4 Data Analysis Approaches Used for Apportionment	175
8.4.1 ART-2a Analysis.....	175
8.4.2 Major particle types near roadway	179
8.5 Source apportionment progress	179
8.6 Conclusions and future work.....	185
8.7 Acknowledgements	185
<i>Section V: Future Data Analysis Techniques</i>	186
Identifying Particle Source in Ambient Air Using New Data Analysis Techniques.....	187
9.1 Introduction	187
9.2 Details of Future Data Analysis Methods Beyond ART-2a.....	190
9.2.1 Clustering as Narrowly as Possible.....	190
9.2.2 Regrouping and Labeling Microclusters.....	191
9.2.3 Using the Catalogue for Fast Recognition	193
9.3 Two Examples of Automatic Labeling Using Source Studies Method.....	193
9.3.1 Direct Apportionment by Nearest Neighbor.....	193
9.3.2 Regrouping Clusters by Analysis of Correlations	197
9.4 Other Modeling Approaches and Open Questions	200
9.5 Current Status and Next Steps.....	201
9.6 Conclusion	202
9.7 References	202
<i>Section VI: Conclusions</i>	204
Concluding Remarks.....	205
<i>Section VII: Appendices</i>	207
Publications and Presentations.....	208
A.1 List of Publications.....	208
A.2 List of Presentations	208
Reading Spectral Ternary Plots	211
B.1 Ternary Plots.....	211
Megaclusters for Fresno 20,000 Particles.....	214
C.1 Example 1: MEGA 1: Aged Organic Carbon.....	214
C.2 Example 2: MEGA 3: Biomass.....	215
C.3 Example 3: Clusters of “minor types” (not biomass or aged organic carbon).....	217

List of Figures

2.1 Driving cycles. Each of the six distinct stages is separated by approximately ten minutes...	14
2.2 Discontinuity between particle sizing instruments. The representative data taken from the Scanning Mobility Particle Sizer (SMPS) [○ – open circles] and the Aerodynamic Particle Sizer (APS) [■ – solid squares] show a difference in number concentration of more than an order of magnitude.....	15
2.3 An illustration of the centroid mass spectra for the most populated ART-2a cluster obtained from T3 driven through 2 complete CARB cycles. Note the excellent agreement between the 2 tests, with the black representing one test and the gray the subsequent test.....	19
2.4 Subtraction plot of digital mass spectra for less dilute sampling conditions (dilution factor of 48) minus more dilute sampling conditions (dilution factor of 124).....	21
2.5 Positive and negative ion weight vectors for the major particle classes observed in heavy duty diesel vehicle exhaust emissions: (a) Ca EC phosphate, (b) EC Ca phosphate sulfate, (c) Na Ca EC phosphate, (d) OC nitrate sulfate, (e) Fe Ca Al Na EC phosphate, (f) K Na Al Ca EC phosphate, (g) Na K nitrate sulfate, and (h) PAH sulfate nitrate.....	23
2.6 Relative fraction of each chemical class per 0.1 μm size bin.....	25
2.7 Relative fraction of each chemical class per 0.1 μm size bin for each vehicle.....	26
2.8 Average temporal variation in number concentration per mile driven and chemical composition of exhaust particles for all vehicles. (a) scaled to SMPS data in the 0.10 to 0.56 μm size range. (b) scaled to APS data in the 0.56 to 2.94 μm size range. Data are missing for the idle and extended idle cycles, since no miles were driven.....	30
2.9 Average temporal variation in number concentration per gram of carbon dioxide (CO ₂) emitted and chemical composition of exhaust particles for all vehicles. (a) scaled to SMPS data in the 0.10 to 0.56 μm size range. (b) scaled to APS data in the 0.56 to 2.94 μm size range.....	31
2.10 Size and cycle variation of number concentration and chemical composition of exhaust particles for each diesel truck. ATOFMS data are scaled to the SMPS in the 0.10 to 0.56 μm size range. Bars marked with an asterisk [*] indicate time periods in which there were not sufficient ATOFMS counts to allow proper scaling of the data.....	34
2.11 Size and cycle variation of number concentration and chemical composition of exhaust particles for each diesel truck. ATOFMS data are scaled to the APS in the 0.56 to 2.94 μm size range. Bars marked with an asterisk [*] indicate time periods in which there were not sufficient ATOFMS counts to allow proper scaling of the data.....	35
3.1 Sample collection system. (Figure derived from <i>Robert et al.</i> , 2005).....	48

3.2 (A – G), Positive and negative ion representative mass spectra / weight matrices for the particle classes from HDDV exhaust. A) <i>EC, Ca, OC, Phosphate</i> ; B) <i>OC, EC, Phosphate, Sulfate</i> ; C) <i>Ca, Na, EC, Phosphate, Sulfate</i> ; D) <i>Na, K, Ca, EC, PAH, Phosphate, Nitrate, Sulfate</i> ; E) <i>EC, Ca, Na, OC, Phosphate, Sulfate</i> ; F) <i>OC, Amines, Nitrates, Sulfates</i> ; G) <i>Na, K rich w/ Ca, Phosphate, Nitrates</i> . *Peaks labeled “CT” in negative ion spectra indicate signal “cross-talk” from the positive ion detector.....	49
3.3 Statistical breakdown of the particle classes observed from the HDDV exhaust.....	50
3.4 Average size distribution (from SMPS and APS) for all HDDVs during the 5-cycle tests. The solid colored lines on both plots are for the SMPS data and the dashed colored lines on the log-scale plot are for the APS measurements. The vertical dashed lines represent the sizing range of the UF-ATOFMS.....	54
3.5 (A - I), UF-ATOFMS size segregated chemical composition of particles observed for each HDDV for each driving test scaled to SMPS. Size bins are created from SMPS data, where certain bins were combined to provide 20-25nm size bins.....	56
3.6 (A – I), UF-ATOFMS particle classes scaled to SMPS for each HDDV on each test cycle. Note: The high-speed HHDDT65 cycle is denoted as H65, and the modified high-speed HDDT_S cycle is denoted as H_S.....	58
3.7 Comparison of top three HDDV particle classes with those observed of the same type in an ambient freeway study with the UF-ATOFMS. HDDV classes are labeled as HDDV# (+/-) and the classes from the freeway study are labeled likewise as FWY# (+/-). The “#” for HDDV and FWY refers to the cluster result as classified with ART-2a. The freeway study was classified with the same ART-2a parameters as the HDDV study. Similar classes are placed side-by-side.....	60
4.1 Speed-time trace for the three cycles tested; FTP, UC, and UCC50.....	71
4.2 Positive and negative ion average area matrices of the eleven chemical classes: a) EC-Ca-PO ₃ class. b) EC-Ca-SO ₄ . c) EC-Ca. d) OC- N class. e) OC- PAH class. f) EC-OC-Aromatic class. g) OC-V class. h) Ca-EC-PO ₃ class. i) Na-K class. j) Na-Ca class. k) Fe class.....	73
4.3 Positive and negative digital mass spectra of the eleven chemical classes: a) EC-Ca-PO ₃ class. b) EC-Ca-SO ₄ . c) EC-Ca. d) OC- N class. e) OC- PAH class. f) EC-OC-Aromatic class. g) OC-V class. h) Ca-EC-PO ₃ class. i) Na-K class. j) Na-Ca class. k) Fe class.....	75
4.4 Size resolved chemical composition for each car category in the a) 50 – 180 nm and b) 300 – 2550 nm size ranges. Note for the oxy-cat cycle, vehicle 23 (shown in Figure 4.6) was removed due to ATOFMS instrumental issues).....	83
4.5 Size resolved relative percentage of each chemical class for each car category in the a) 50 – 180 nm and b) 300 – 2550 nm size ranges.....	85

4.6 Scaled number concentrations (NEF values) of the thirteen classes for the TWC light duty trucks on three different cycles. Note the counts for bars with an (*) were multiplied by 100 and the bars with an (#) were divided by 10 in order to be visible on the same y-axis scale.....	88
4.7 NEFs of the thirteen classes for each vehicle. Bars with an (*) indicate multiplication by 100 and bars with an (#) indicate division by 10.....	89
4.8 Normalized fraction of thirteen classes for each vehicle.....	90
4.9 Two minute temporal profile of the thirteen classes for the ten LEV vehicles on the FTP cycle for all particles between 50 – 180 nm size range. A cooling period when the vehicle engine was off occurred from 20 – 32 minutes and then the cars were re-started at 32 minutes.....	92
4.10 NEFs of the thirteen classes for each of the car categories tested on the FTP cycle for particles in a) 50 – 180 nm and b) 300 – 2550 nm size range. Note the bars with an (+) indicates multiplication by 5 and the bars with an (#) indicates a division by 10. Note for the oxy-cat category, one vehicle (#23 shown in Figure 4.6 and 4.7) was removed due to ATOFMS instrumental issues.....	94
5.1 This histogram represents the contribution of each mass spectral class to the different oil and fuel samples that were analyzed using an ATOFMS. Each oil or fuel type is listed across the x-axis, and the normalized percentage of each mass spectral class is listed on the y-axis. Color corresponding mass spectral classes are listed on the right hand side of the figure.....	106
5.2 Positive and negative ion area matrices (AM) for all chemical classes seen in used and new oil, for both unleaded fuel and diesel fuel vehicles. The five different major classes shown are; a) Ca-Phosphate-OC , b) Ca-OC-Phosphate-NO ₂ -Na, c) Ca-PAH-OC-Phosphate, d) Ca-ECOC-Phosphate, and e) Ca-Na-ECOC-Phosphate.....	107
5.3 Positive and negative ion area matrices (AM) for the two classes seen in diesel fuel aerosols. a) PAH Containing, b) OC-Na-Sulfate-Phosphate. Unleaded fuel aerosol also contained the OC-Na-Sulfate-Phosphate particle class.....	110
5.4 Positive and negative ion area matrices (AM) for five chemical classes that are unique to unleaded fuel. The five different major classes shown are: a) PAH-Sulfate-NO ₂ -Cl, b) OC-K-Na-Sulfate-Phosphate, c) OC-Sulfate-Phosphate, d) OC-Sulfur containing, and e) OC-Sulfate-Other.....	111
5.5 Comparison of a) Ca-OC-Phosphate-NO ₂ -Na area matrix from used oil, b) the area matrix from the largest mass spectral class from the exhaust of heavy duty diesel trucks, and c) an area matrix from a class of particles which made up ~2% of “smoker” LDV mass spectra.....	113
6.1 Digital mass spectrum color stack for both positive and negative ions of a) fully formulated oil with a sulfonate detergent additive and b) sulfonate detergent additive package.....	120
6.2 Digital mass spectrum color stack for both positive and negative ions of a) fully formulated oil with a phenate detergent additive and b) phenate detergent additive package.....	121

6.3 Digital mass spectrum color stack for both positive and negative ions of a mineral base oil with no additives.....	122
6.4 EC/PAH ratio for m/z $^{48}\text{C}_4^-$, and m/z 205 ⁻ (triangles) and the ratio of the sum of EC peaks $^{24}\text{C}_2^-$, $^{36}\text{C}_3^-$, $^{48}\text{C}_4^-$ to the sum of PAH peaks 205 ⁻ and 219 ⁻ (squares) versus the percent of soot for each sample.....	123
7.1 Exclusive matching of HDV and LDV dynamometer particles. Fraction of HDV and LDV particles that matched to the HDV, LDV, or neither HDV nor LDV weight vectors for three size ranges; 50 – 100 nm, 100 – 1000 nm, and 1000 – 3000 nm.....	131
7.2 Comparison of three Caldecott Tunnel and dynamometer classes. a) Ca-EC-PO ₃ , b) EC-Ca-PO ₃ , and c) OC-N. Dot product (similarity) values are a) 0.88, b) 0.81, and c) 0.91. The thin black bars are the dynamometer classes, while the broad grey bars are the Caldecott Tunnel classes.....	133
7.3 Average area mass spectrum of Fe-Ba class.....	137
7.4 Relative size distributions of four chemical classes per size bin based on the ATOFMS raw counts. Each size bin displays the relative contribution of each chemical class for that size bin.....	139
7.5 Hourly unscaled ATOFMS counts of the three major chemical classes. a) Ca-EC-PO ₃ , b) EC-Ca-PO ₃ , and c) OC-N. HDV-LDV Bore indicates when sampling was conducted from the mixed bore. HDV-LDV Video indicates when sampling was under the influence of HDVs (i.e. at least 1.5% of the vehicles were HDVs) based on video counts. LDV only Bore indicates when sampling was conducted from the LDV only bore. LDV Video indicates when sampling was under a relatively low influence of HDVs based on video counts (i.e. HDV were less than 0.8% of the total vehicles).....	140
7.6 Hourly APS scaled ATOFMS number concentration of three chemical classes. a) Ca-EC-PO ₃ , b) EC-Ca-PO ₃ , and c) OC-N. HDV-LDV Bore indicates when sampling was conducted from the mixed bore. HDV-LDV Video indicates when sampling was under the influence of HDVs (i.e. at least 1.5% of the vehicles were HDVs). LDV only Bore indicates when sampling was conducted from the LDV only bore. LDV Video indicates when sampling was not under the influence of HDVs (i.e. HDV were less than 0.8% of the total vehicles).....	141
7.7 Ratios of HDV-LDV bore values divided by LDV only bore values for all EC particle types in the Caldecott Tunnel as a function of EC m/z fragments. Ratios greater than one indicate a higher detection of that m/z in the Caldecott Tunnel, whereas ratios less than one indicate lower detection of that m/z in the LDV dynamometer study.....	145
8.1 Aerial view of the UCSD campus showing the freeway upwind (yellow circle) and downwind (green circle) sampling sites.....	155
8.2 Temporal trends (30 minute resolution) showing those particles which scatter light versus those that scatter light and also produce a mass spectrum.....	158

8.3 Comparison of temporal trends for two ATOFMS instruments in the 100-1000 nm size range.....	159
8.4 Comparison of ATOFMS counts for sub-100 nm particles versus those measured by the scanning mobility particle sizing system.....	160
8.5 Comparison of temporal trends of aerodynamic particle sizer (APS) counts to the ATOFMS counts with 1 hour temporal resolution for the duration of the study.....	161
8.6 Temporal trends for the aethalometer (370 nm) versus gas phase NO _x concentrations.....	163
8.7 Temporal trends of NO _x , aethalometer, and particle number concentrations for sizes below 100 nm measured with the SMPS.....	164
8.8 Comparison of ATOFMS ultrafine particle counts with gas phase measurements of CO (top) and NO _x (bottom).....	165
8.9 Comparison of temporal trends of CO, NO _x , and UF-ATOFMS (50-100 nm) particle counts.....	166
8.10 Comparison of SMPS and APS concentrations at freeway and upwind sites.....	168
8.11 Comparison of ultrafine particle concentrations (upper) and 1000-2500 nm size ranges made using an SMPS and APS, respectively.....	169
8.12 Single particle spectra of meat cooking particles detected in ultrafine mode at upwind site and accumulation mode (100-1000 nm) at freeway site). Note unique signatures of odd spaced peaks at higher m/z ratios. These are indicative of fatty acids. See 8.13 for temporal trends.....	170
8.13 Temporal trends for meat cooking particles (oleic acid marker) for upwind (lab) and freeway locations.....	171
8.14 Size distributions for total hit particles as measured for the 3 ATOFMS instruments between July 24-31, 2004.....	173
8.15 Common V-containing particle type detected at both locations and temporal trends for 3 instruments.....	174
8.16 Particle population distribution in each of the 300 source clusters used for ambient matching.....	178
8.17 Weight matrices of two most common types of particles observed in the 50-300 nm size range during the freeway study. These types are very similar to the major types sampled from vehicles during previous HDDV and LDV dynamometer studies.....	180
8.18 Ultrafine EC particle counts detected by ATOFMS compared to aethalometer data.....	181

8.19 Source apportionment of LDV (cars) vs. HDDV (trucks) for 1 time period during the study for particles in the 100-1000 nm size range.....	182
8.20 Apportionment of ultrafine particles during 2 days on the weekend (top) and weekend (bottom). The arrows indicate how the proportion of LDV to HDDV shows the greatest differences in the late night-early morning hours.....	184
9.1 LDV particles projected in the plane of their spectra peak areas on peaks 12, 24 and 36. (See appendix A2 about ternary plots). The distribution is bimodal.....	189
9.2 Three representations of the same cluster. Fig. 10.2.a. (top left) shows the mean of the relative areas of peaks. Each peak is shown as a dark bar. Standard deviation is shown by a yellow bar extending the peak, and by a color change (blue to green) for the part of the bar stretching one standard deviation downwards of the mean. Fig 10.2.b (top right) shows the median of relative peak areas, indicating first quartile, median and third quartile with the blue/green/yellow color scheme. Fig. 10.2.c (bottom) shows for each peak the proportion of particles in the cluster that have areas larger than a given color-coded threshold. Large peak areas are in warm colors, so that a high reddish bar would indicate that most particles in the cluster have a large area for this particular peak.....	192
9.3 Above, Fresno particles labeled “Dust” by a nearest neighbor method. Below, sea salt and dust particles from CIFEX, selected by human criteria. Peak 27 is likely Aluminum, a crustal element frequently present in dust particles. Peak 46 can be either Na ₂ or an isotope of Ti. In salt, 46 tends to be Na ₂ , but in dust it is 6% of the Ti content, and peak 47 is then 7% of the same Ti content. Fresno particles labeled “dust” follow the same 46/47 ratio as CIFEX dust does...	194
9.4 Timeline for Fresno Nearest-Neighbor Apportionment: in 10.4A, we observe a decrease in particle count (measured particles) from Wed 1/24 to Mon 1/29. This coincides with a rise in the percentage of sea salt, dust, and biomass particles (10.4B). The daily timeline in 10.4C shows the biomass fraction peaking in the hours following sunset.....	195
9.5 Fresno Particle Apportionment, comparing the HDV, LDV and other particles at m/z 12, 24, and 36. Only LDV differs, but it still overlaps with HDV. The third plot is obtained from nebulized oil particles measured in the laboratory. Even this pure source in very controlled conditions presents the same variations as LDV do in ambient studies, which is further evidence the desorption process generates at least a substantial part of the spectral variation observed in ambient particles.....	196
9.6 The percent of particles, not from the lead microcluster, that match the type of this microcluster as a function of lead cluster size.....	199
B.1 Creating a ternary plot. From their 3-D coordinates (concentrations in [12], [24] and [36]), individual particles are projected into the triangle defined by (x+y+z =1). Here for example the green particles have strong peaks at m/z 12 whereas the red ones have only about 20% of [12]. The sides are labeled with a 0-100% scale and the peak that this scale applies to. Reference lines (dotted lines) allow a better reading of the particle composition.....	212

B.2 Reading relative composition from the ternary plot: the main component is the triangle corner that the point is closest to. In this case, peak 24. The composition is in proportion of the proximity to the pure peak corners. The exact composition can be read by projecting the point onto the axes by following lines opposite to the corner of which we are reading the percentage. In this case, the particle has [24] ~ 55% found by following the green line down to the green scale; [12] ~ 20% by following the red line, and [36] ~ 25% read by following the blue line.....213

List of Tables

1.1 Table showing non-attainment counties in California based on U.S. EPA report.....	3
2.1 Truck descriptions.....	12
2.2 ATOFMS chemical reproducibility.....	18
2.3 Degree of similarity (dot product values) among the area matrices of the eight major particle classes.....	27
3.1 Heavy Duty Diesel Vehicles (HDDVs) tested and driving cycles performed.....	45
3.2 Dilution ratios (DR) for each HDDV and cycle.....	47
4.1 List of make, model, year, and mileage for each vehicle, as well as the technology category, cycles tested and total particles analyzed by UF-ATOFMS (50 – 180 nm), and ATOFMS (300 – 2550 nm).....	69
4.2 List of possible PAHs for each m/z ratio.....	79
7.1 HDV-LDV and LDV only bores sampling times, along with available videotape of the traffic.....	129
7.2 Ratio of Caldecott values to the LDV Dynamometer values for individual m/z for average area mass spectrum and digital mass spectra for the organic carbon.....	135
7.3 List of the number of LDV per hour, HDV per hour, and percent of HDV for each videotape period.....	143
8.1 Instruments used for the upwind/downwind freeway study.....	156
8.2 Percentage of particles matched to dynamometer source seeds using a vigilance factor of 0.85 for all particles in the 100-300 nm (UF-ATOFMS) and 100-1000 nm (ATOFMS-1) size ranges.....	176

List of Abbreviations

AAMS: average area mass spectra
AM: area matrix
AMS: Aerodyne aerosol mass spectrometer
APS: aerodynamic particle sizer
ART-2a: adaptive resonance theory-based neural network algorithm
ATOFMS: aerosol time-of-flight mass spectrometry
CARB: California Air Resources Board
DA: discriminant analysis
EC: elemental carbon
EPA: Environmental Protection Agency
FTP: federal test procedure
GVW: gross vehicle weight
HDDV: heavy duty diesel vehicle
HDV: heavy duty vehicle
HHDDT: heavy heavy-duty diesel truck
ICA: independent component analysis
LDI: laser desorption/ionization
LDT: light duty truck
LDV: light duty vehicle
LEV: low emission vehicle
MOUDI: micro orifice uniform deposit impactor
NEF: number emission factor
Non-cat: non-catalyst
OC: organic carbon
Oxy-Cat: oxidation catalyst
PAH: polycyclic aromatic hydrocarbon
PAS: photoelectric aerosol sensor
PCA: principal component analysis
PM: particulate matter
PMF: positive matrix factorization
PMT: photomultiplier tube
SAHN: sequential, agglomerative, hierarchical, non-overlapping
SDT: stack dilution tunnel
SMPS: scanning mobility particle sizer
SOA: secondary organic aerosol
SPMS: single particle mass spectrometry
SVOC: semi-volatile organic compound
TDPBMS: thermal desorption particle beam mass spectrometer
TEOM: tapered element oscillating microbalance
THDVETL: transportable heavy duty vehicle emissions testing laboratory
TWC: three-way catalyst
UC: unified cycle

UCC50: unified cycle high speed correction 50
UCSD: University of California San Diego
UF-ATOFMS: ultrafine aerosol time-of-flight mass spectrometry
WDR: wide dynamic range
WM: weight matrix
ZDP: zinc dithiophosphate
ZDDP: zinc dialkyldithiophosphates

Abstract

A new approach for PM source apportionment has been developed and successfully tested, using meteorological, gas phase, and single particle source signatures to identify and apportion ambient particles in California. A central component of these studies involves using aerosol time-of-flight mass spectrometry (ATOFMS), a technique which analyzes the size and chemical composition of single particles in real-time, to determine the size-resolved mass spectral source signatures of the particulate exhaust emissions from heavy duty diesel vehicles (HDDV) and gasoline powered light duty vehicles (LDV) that can be used for ambient source apportionment. The source signatures were measured by directly sampling PM emissions from multiple vehicles operating on different driving cycles while on a chassis dynamometer. Differences between HDDV and LDV source seeds are discussed. The second and final phase of this project involved sampling ambient particles inside a tunnel and alongside a major freeway. In the freeway study, a high fraction (70-85%) of ambient particles were shown to match the dynamometer source seeds, showing the dynamometer seeds are indeed representative of “real-world” emissions. The difference signatures from LDV and HDDV allow for differentiation of ambient particles from multiple sources including vehicles, biomass, and meat cooking. The established ATOFMS signature libraries for HDDV and LDV exhaust particles will be used in future ATOFMS apportionment studies which will detail the fraction of vehicle emissions in particulate matter in ambient air throughout California.

Executive Summary

Background

Many studies have shown the effects ambient aerosols have on human health, as well as global and regional climate, and visibility. Thirteen California counties are on the EPA non-compliance list for PM_{2.5}. In order for policymakers to set appropriate regulations that will allow these regions in California to achieve compliance, we need a better understanding of the relative contributions of different PM sources to ambient air. In California, it is well documented that vehicle emissions from both light duty gasoline vehicles (LDV) and heavy duty diesel vehicles (HDDV) represent a significant source of ambient particles; however, there is quite a bit of debate regarding the relative fractions of ambient particles derived from these two vehicle sources. Some studies suggest LDV emissions represent the highest fraction of ambient particles, whereas historically it has been shown HDDV are the dominant ambient source. Much of this debate stems from large uncertainties which exist when performing source apportionment using ambient samples acquired on filters. Finding the appropriate tracers (i.e. metals, organics) that are robust under atmospheric conditions, and specific to only one source is challenging. The ultimate goal of this project is to take a new approach which involves using single particle mass spectral signatures to apportion ambient particles in studies conducted in the state of California.

Methods

In order to create source profiles which can be used for ambient apportionment studies, the chemical variability of each source must be examined thoroughly. The chemical composition and size of individual exhaust particles were analyzed using aerosol time-of-flight mass spectrometry (ATOFMS) during three separate dynamometer studies, two of which focused on the exhaust emissions of HDDV and one on the emissions of LDV. A total of thirteen HDDV and twenty-eight LDV were tested on chassis dynamometers using driving cycles designed to reflect real world driving conditions. The exhaust emissions passed through a dilution and residence chamber system to simulate atmospheric dilution conditions before being sampled by the ATOFMS. Different vehicle types and models and driving cycles were implemented to yield a broad range of representative source profiles.

Dynamometer studies permit control over the vehicles, driving conditions, and sampling conditions, but the relevance of the source signatures in ambient air must be evaluated. Single ambient particles were analyzed during two studies which were heavily influenced by vehicular emissions: a tunnel study, in which the HDDV were required to pass through only one bore of a two-bore system, and a freeway study situated alongside a major freeway in southern California.

Results

The combination of a chassis dynamometer and a dilution system yielded highly reproducible single particle mass spectral signatures. This suggests ATOFMS source profiles and chemical variations observed between vehicles, driving cycles, and other factors can be

attributed to actual chemical differences and not to instrumental variability or lack of statistically relevant samples. Several distinct chemical classes from each source were observed in the vehicle exhaust emissions during the dynamometer studies. The dominant particle types emitted by HDDV were soot (or elemental carbon) and particles formed from lubricant oil (Ca-, phosphate-containing). This was supported by matching the tailpipe emissions to particle spectra obtained directly from aerosolized vehicle fluids, oil, and fuel samples taken from these same vehicles. Whereas, HDV showed high concentrations of EC and oil, LDV emitted high amounts of organic carbon (OC) particles in the accumulation mode. Somewhat surprisingly, the ultrafine mode (<100 nm) produced by low emitting vehicles (LEV) LDV emissions were dominated by elemental carbon (EC). This suggests EC signatures alone cannot be used to distinguish HDV from LDV in ambient studies. However, single particle EC mass spectral signatures from diesel contained high amounts of Ca and phosphate signals in addition to the carbon peaks and thus this combination of species can be used to distinguish EC from HDV from LDV. Single particle analysis may be the only way to distinguish LDV EC emissions from HDV EC emissions in the ultrafine size range. High temporal resolution (2 minute) measurements made with the ATOFMS provided insight into the chemical composition of single exhaust particles as the driving conditions were changed on the dynamometer; the measurements revealed the preferential production of elemental carbon particle types during the beginning of the cold start of LDV and organic carbon enriched particles during the idling and low speed operation of HDDV. The particle types observed in the dynamometer studies were used to create source profiles for LDV and HDDV, which were applied and evaluated in a freeway apportionment study. The source signatures were detected in the tunnel study, and HDV emissions were clearly more abundant in the HDV+LDV tunnel compared to the LDV-only tunnel. Also, a new vehicle-related particle type (brake dust) was revealed indicated by the presence of Ba in the spectrum. The observation of the major source signatures observed during the dynamometer study in ambient air provides great promise for using these signatures in ambient apportionment studies. This was further validated in the freeway study. Significant fractions (close to 70% of accumulation mode and 80% of ultrafine mode) of ambient particles during the freeway study were well matched to the dynamometer signatures. Somewhat surprisingly, a major regional background of close to 30% was observed for accumulation mode particles in San Diego. Given the proximity of the freeway to the ocean making the freeway being the only major PM source, this high background was somewhat surprising. Preliminary analysis of the freeway study using ART-2a analysis of the single particle data showed a higher contribution from LDV compared to HDV (about 3:1). The freeway study demonstrated how the ATOFMS can also identify particle types from other major combustion sources in ambient air including biomass and meat cooking. This finding is significant because these particle types represent a significant fraction of anthropogenic particles in the accumulation mode, particularly in other regions of California such as central California. The freeway study demonstrated the strength of using a combination of gas and particle phase instruments coupled with meteorological data for source apportionment. Strong correlations were shown between the temporal variations of particle types measured with ATOFMS instruments and peripheral gas and particle phase instruments. Future plans will involve using time series data from meteorological, gas phase, and single particle signatures to perform complete source apportionment of the ambient data collected during the freeway study.

Section I

Introduction

Introductory Remarks

1.1 Research Objectives

As we gain more knowledge on the effects of ambient aerosols on human health and the influences that particulate matter (PM) has on climate conditions and visibility, our concern increases regarding which sources contribute the most to the anthropogenic production of aerosols. A recent report by the Environmental Protection Agency (EPA) states that 13 counties (Table 1.1) in California are designated areas of non-attainment for PM_{2.5}. California policymakers must understand the major sources of PM contributing in these areas before setting targeted regulations that may require technological advances. Vehicles, biomass burning, meat cooking, and dust (crustal) are some of the sources that contribute to the pollution in different regions of California. It is well documented that vehicle emissions from both light duty gasoline vehicles and heavy duty diesel vehicles represent a significant source of ambient particles especially in the Los Angeles air basin. Filter based PM sampling methods are the most common methods used for measuring composition information for source apportionment; with filter-based methods, it is very difficult to come up with robust and unique markers which allow one to unravel the relative contributions from different sources. In addition, filter based methods require long sampling times and can be quite costly methods for obtaining size-resolved composition information, and thus limited temporal and spatial information exists on PM sources in California. The ultimate goal of this project is to test aerosol time-of-flight mass spectrometry (ATOFMS) in a combination of lab (dynamometer) and field studies as a method that will provide a unique and complementary way for distinguishing between light duty and heavy duty vehicle emissions.

ATOFMS is one of a growing number of methods being developed that provide on-line measurements of particle size and composition. Instruments that characterize single particles one-by-one provide different yet complementary information to traditional bulk filter measurement techniques. In particular, the analysis of individual particles with high temporal resolution allows for the determination of chemical variability in particle types from a specific source. Because they avoid combining the different chemical signatures from multiple sources as filter methods do, the comparison of particles from various sources should show direct chemical differences at the single particle level. Therefore, the apportionment of ambient aerosols by using single particle source signature profiles established by the ATOFMS will add a new method which can be used for real-time source apportionment of PM in various regions of California.

In order to create the source profiles needed for apportionment studies, the chemical variability of each source must be examined thoroughly in studies with ATOFMS. Dynamometer studies permit complete control over the testing of vehicles, driving conditions, and sampling conditions. By sampling the emissions of both light duty gasoline and heavy duty diesel vehicles in dynamometer studies, unique source fingerprints can be established. It is

Table 1.1 U.S. EPA list of 13 California counties of non-attainment for PM_{2.5}.

State	Non-attainment Area Name	Counties
California	Los Angeles-South Coast Air Basin, CA	Los Angeles (P) Orange Riverside (P) San Bernardino(P)
	San Diego, CA	San Diego
	San Joaquin Valley, CA	Fresno Kern (P) Kings Madera Merced San Joaquin Stanislaus Tulare

important that these source characterization studies reflect the diversity in vehicle types and driving conditions so that the source profiles will be representative of real-world vehicular emissions. Because fuel and lubricating oil are two important components of the engine system that can contribute to the exhaust particles, it is also valuable to characterize the fuels and oils by themselves and establish a library of fingerprints. Once the source profiles are characterized, it is necessary to evaluate how representative the signatures are in apportionment studies. As a starting point, it is more straightforward to investigate ambient data sets known to be strongly influenced by vehicular emissions, such as tunnel and freeway studies, before beginning to analyze other ambient airsheds. Considering the initial studies use one specific neural network analysis method, it will also become important to evaluate other data analysis techniques and assess their relative performance in source apportionment investigations.

This report compiles all of the work completed thus far in the step-by-step progression taken to establish the capability of source apportionment of single ambient particles from light duty gasoline and heavy duty diesel vehicles using aerosol time-of-flight mass spectrometry.

1.2 Instrumentation

Aerosol time-of-flight mass spectrometry, ATOFMS, analyzes individual particle size and composition in near real-time. A detailed description of instrument operation and performance has been provided previously [*Gard et al.*, 1997], though a brief explanation is included here. The inlet region consists of a convergent nozzle, which is separated from vacuum by two skimmers. Upon introduction, the particles undergo supersonic expansion and are accelerated to velocities dependent on their aerodynamic size. The skimmers fulfill two primary functions: to permit differential pumping from atmospheric pressures to the pressures necessary to operate the mass spectrometer and to collimate the particle beam by removing those particles which do not follow a straight trajectory. The particle beam next enters the light-scattering region, which includes two continuous-wave diode lasers. These lasers are positioned orthogonal to the particle beam, so that when a particle passes through the laser beam, its scattered light is focused onto photomultiplier tubes (PMTs) by means of ellipsoidal mirrors. The PMTs send pulses to an electronic timing circuit that measures the time the particle takes to travel the known distance between the two laser beams. The velocity of the particle is calculated with the particle time of flight and the distance and is converted to a physical aerodynamic diameter via an external size calibration with particles of known size. With the determined particle velocity, the timing circuit counts down to when the tracked particle will reach the center of the ion source region of the mass spectrometer and sends a signal to the pulsed Nd:YAG laser (frequency quadrupled to 266 nm) to fire. Through direct laser desorption/ionization, the laser pulse produces ions, which are then mass analyzed in a dual-ion reflectron time-of-flight mass spectrometer. This ATOFMS instrumentation can analyze single particles with aerodynamic diameters of approximately 200 to 3000 nm.

Recently developed ultrafine aerosol time-of-flight mass spectrometry (UF-ATOFMS) focuses on particles in the fine (100-300 nm) and ultrafine (<100 nm) size ranges. It has been described in detail elsewhere [*Su et al.*, 2004]. The main difference between the standard ATOFMS instrument and the UF-ATOFMS instrument is the particle sampling inlet. In UF-ATOFMS, the original nozzle-skimmer interface is replaced with a critical orifice, an

aerodynamic lens system, and two skimmers. The aerodynamic lens efficiently focuses fine and ultrafine aerosols. The sizing and chemical analysis of particles is the same as that of the standard instrument.

1.3 Data Analysis Methods

A TOFMS generates large amounts of data; the instrumentation is capable of collecting size and chemical information on > 100 individual particles per minute, depending upon the atmospheric or sample concentrations. While simple laboratory experiments may run for only a few hours, ambient monitoring studies with ATOFMS may operate for weeks. For efficient analysis of such a volume of data, the data analysis technique must perform automatic sorting and classification of individual particles. The primary method employed within this report is an adaptive resonance theory-based neural network algorithm, ART-2a [Song *et al.*, 1999].

Though more detailed descriptions of the ART-2a algorithm have been provided elsewhere [Xie *et al.*, 1994; Hopke and Song, 1997], a brief description is included here. Using the spectral characteristics, ART-2a separates particles into distinct classes (clusters) of chemically similar particles within large ATOFMS data sets and generates new clusters whenever a data point (mass spectrum) falls outside the present proximity to all existing classes, thereby providing the advantage of determining contributions from previously detected particle classes while introducing information on new particle types. The ion peak positions and intensities in all positive and negative spectra (350 m/z units for each $\times 2 = 700$ total) for each particle are combined to form a weight vector in which the ion intensity at each m/z ratio is normalized with respect to the maximum peak intensity present in the vector. In the classification process, particles are selected randomly and their spectral information is compared to each particle class (weight vector) by calculating the dot product of the particle vector and weight vector. If the dot product value between the particle vector and any of the existing weight vectors is above the user-defined threshold (vigilance factor), the particle is added to the particle class with the highest dot product value. If the value is below, the particle defines a new class. As will be described herein, source classes (weight vectors) or seeds developed from dynamometer studies are then compared to ambient single particle data. In a procedure referred to herein as “matching”, the dot product of each ambient particle (particle vector) crossed with each ambient cluster weight vector is taken in direct analogy to the procedure used to initially analyze the data. The particle is placed in (or apportioned to) the ambient cluster that produces the highest dot product, assuming it is above a user-defined threshold (usually 0.85).

1.4 Summary of Chapters

1.4.1 Introduction

Chapter 1 provides an overview of the motivation and research directives behind the works presented in this report. It introduces the primary data analysis method (ART-2a) used in most of the chapters and provides a general description for how it is used in this project. It also presents a brief synopsis of each of the individual chapters.

1.4.2 Mobile Source Characterization Studies

Chapter 2 analyzes the chemical associations in unique single particle signatures in the exhaust emissions of heavy duty diesel vehicles. The emissions of seven in-use heavy duty diesel trucks, varying in manufacture year and make, passed through dilution and residence chambers to simulate the dilution conditions encountered by ambient particles before detection by ATOFMS. The vehicle operation was controlled with set driving cycles run on a chassis dynamometer that is part of an emissions testing laboratory. It verifies the sampling and chemical reproducibility of ATOFMS. This chapter describes eight main particle types that vary in chemical composition and aerodynamic size range, two of which govern the particle type fraction at 63 to 95% depending upon particle size. With the presence of oil additive species, such as calcium and phosphate, in the mass spectral signatures, the study determines that two dominating particle types show indicators associated with the lubricating oil. In this chapter, we also examine the chemical variation of exhaust particle as a function of driving conditions and vehicle. The single particle chemical signatures are used to make up the source profile for heavy duty diesel vehicles, which can then be applied in ambient source apportionment investigations.

Chapter 3 examines the chemical signatures of individual ultrafine and low-fine mode particles (50 – 300 nm) emitted by heavy duty diesel vehicles. Six in-use heavy duty diesel vehicles operated the heavy heavy-duty diesel truck five-cycle driving schedule under different simulated weight loads on a chassis dynamometer. An ultrafine ATOFMS sampled the exhaust particles in real-time after they passed through a dilution/residence system to simulate atmospheric dilution conditions. This chapter details seven distinct particle types observed in this size range, of which the top three types composed 91% of the total particles measured. It also investigates the effect of driving cycle, simulated weight load, and vehicle make/year on exhaust particulate size and composition. The signatures defined in this chapter extend the size range of the heavy duty diesel source profile used in apportioning ambient aerosols.

Chapter 4 characterizes the mass spectral signatures of single particle exhaust emissions from light duty vehicles. It examines the chemical signatures as a function of aerodynamic size from twenty-eight light duty gasoline vehicles that covered a range of catalytic converter and engine technologies. The vehicles followed driving cycles that mimic urban driving conditions, such as the Federal Testing Procedure, Unified Cycle, and Unified High Speed Correction Cycle, while operating on a chassis dynamometer. Two different ATOFMS instruments sampled the exhaust particles after dilution in a dilution and residence chamber system – a standard ATOFMS system with a measuring size range of 300 to 2550 nm and an ATOFMS system equipped with an aerodynamic lens with a size range of 50 to 300 nm. The chapter discusses the eleven distinct particle classes observed and their variability in the emissions within different vehicle categories and driving cycles. The high temporal resolution of the measurements reveals the preferential production of a particular particle type during the first two minutes of a cold start. With the observation that elemental carbon (EC) dominates the particle types in the ultrafine size range, it is apparent that the application of EC as a unique tracer for diesel vehicles is not a valid assumption. The single particle signatures established in this chapter are used to create the source profile for identifying particles originating from light duty gasoline vehicles in ambient apportionment studies.

1.4.3 Fuel and Oil Studies

Chapter 5 investigates the chemical composition of particles formed by aerosolizing various vehicle fluids: new gasoline auto oil, new diesel oil, used auto oil, used diesel oil, unleaded fuel, diesel fuel, and diesel fuel taken from the tank of heavy duty diesel vehicles. It compares the ATOFMS mass spectral signatures of these fluids with the signatures observed in vehicle exhaust. It determines a high degree of similarity between the mass spectra of oil aerosols and the mass spectra of heavy duty diesel exhaust emissions. This chapter provides insight into the origin of the chemical species on exhaust particles within the engine system.

Chapter 6 provides preliminary results on the analysis of lubricant oil packages using ATOFMS.

1.4.4 Evaluation of Sources Signatures & Application to Apportionment Studies

Chapter 7 applies the source signatures obtained for light duty and heavy duty vehicles obtained in the chassis dynamometer studies to ambient particles sampled in the first apportionment study. It discusses the similarity between the light duty and heavy duty vehicle particle types and evaluates the degree of uncertainty in matching those signatures using ART-2a. The chapter analyzes the employment of the signatures of multiple particle types in the two bore system of the Caldecott Tunnel that requires all heavy duty vehicles to travel in one bore (in theory). It also introduces a new particle type not seen in the dynamometer studies, which is ascribed to the wear of brake pads. With the detection of the dynamometer signatures in the Caldecott Tunnel, this study validates that single particle chemical classes observed in the controlled dynamometer studies with simulated dilution conditions are representative of vehicular particle types emitted in ambient conditions.

Chapter 8 describes the next step in ambient source apportionment using ATOFMS mass spectral signatures for light duty gasoline and heavy duty diesel vehicles for source apportionment in a study which was heavily influenced by vehicle sources. Both a standard-inlet ATOFMS and an ultrafine ATOFMS, among several other instruments, sampled ambient air alongside a major freeway in southern California over the period of one month. The chapter describes results obtained by using the dynamometer signatures in apportioning ambient particles.

1.4.5 Future Data Analysis Techniques

Chapter 9 outlines the steps needed in order to reach the ultimate goal of performing source apportionment of ambient particles in real-time using ATOFMS. It considers the limitations of the clustering algorithm currently in use, ART-2a, and introduces several new data analysis techniques for single particle source apportionment. The chapter provides preliminary results on using these new techniques to apportion aged ambient particles collected in central California. It discusses the current status and future steps that will be required to achieve real-time apportionment.

1.4.6 Conclusions

Chapter 10 summarizes the major findings presented in this report and provides future directions.

1.5 References

- Gard, E., J.E. Mayer, B.D. Morrical, T. Dienes, D.P. Fergenson, and K.A. Prather, Real-time analysis of individual atmospheric aerosol particles - design and performance of a portable ATOFMS, *Analytical Chemistry*, 69 (20), 4083-4091, 1997.
- Hopke, P.K., and X.H. Song, Classification of single particles by neural networks based on the computer-controlled scanning electron microscopy data, *Analytica Chimica Acta*, 348 (1-3), 375-388, 1997.
- Song, X.H., P.K. Hopke, D.P. Fergenson, and K.A. Prather, Classification of single particles analyzed by ATOFMS using an artificial neural network, ART-2A, *Analytical Chemistry*, 71 (4), 860-865, 1999.
- Su, Y., Sipin, M.F., Furutani, H., and K.A. Prather, Development and characterization of an aerosol time-of-flight mass spectrometer with increased detection efficiency, *Analytical Chemistry*, 76, 712-719, 2004.
- Xie, Y., P.K. Hopke, and D. Wienke, Airborne particle classification with a combination of chemical composition and shape index utilizing an adaptive resonance artificial neural network, *Environmental Science & Technology*, 28 (11), 1921-1928, 1994.

Section II

Mobile Source Characterization

Studies

Determination of Single Particle Mass Spectral Signatures from Heavy Duty Vehicle Emissions in the 0.1 to 3 Micrometer Size Range

2.1 Introduction

Detailed characterization of emissions from anthropogenic sources that contribute to atmospheric particulate matter is essential for apportionment studies. These studies are important to policy makers and others, who decide which technological advances and regulations are needed in order to meet compliance. Particulate matter below 2.5 micrometers (PM_{2.5}) is of great concern to the community due to its effects on public health and the environment. For example, epidemiological studies have shown an association between increased exposure to particles in this size range and mortality [Pope, 2000; Schwartz *et al.*, 1996]. From an environmental perspective, aerosols play a significant role in reducing visibility and influencing the climate.

One substantial source of fine particles is the exhaust emissions from diesel engines [Kirchstetter *et al.*, 1999; Schauer *et al.*, 1996]. Though they represent only a small fraction of the mobile fleet (2% in California), the use of diesel engines is increasing worldwide, given their higher fuel efficiency and lower maintenance costs [Dunlap, 1998]. However, diesel engine particulate matter mass emissions are 1 to 2 orders of magnitude higher than spark ignition vehicles per vehicle [Kittelson, 1998]. In some areas of the world, such as London, approximately two-thirds of the mass of all particles with aerodynamic diameters smaller than 10 μm have been attributed to diesel engines [Colville *et al.*, 2001].

A number of previous studies have focused primarily on the size and number concentrations of particles emitted by diesel vehicles; however the chemical composition of the exhaust needs to be considered as well. Exhaust emitted from heavy duty diesel vehicles (HDDV) constitutes a complex mixture of gaseous compounds and particulate matter (PM) with a significant number of adsorbed and condensed phase species [Kittelson, 1998; Yanowitz *et al.*, 2000]. Diesel PM is composed of elemental carbon (soot), inorganic salts, trace metals, and semivolatile organic species, including polycyclic aromatic hydrocarbons (PAHs) [Burtcher *et al.*, 1998; Lyyranen *et al.*, 1999; Sakurai *et al.*, 2003a]. Many different PAH species, including carcinogenic and mutagenic compounds, have been identified in diesel exhaust [Durant *et al.*, 1996; Marr *et al.*, 1999; Mi *et al.*, 2000]. In particular, a toxicological study on pyrene in diesel exhaust particles found that it has specific influences on various parts of the immune system, in addition to those involved with atopic diseases [Bommel *et al.*, 2003]. The evidence of negative health effects from diesel PM is convincing enough for the California Air Resources Board (CARB) to include the substance on their list of toxic air contaminants (www.arb.ca.gov). Atmospheric reactions with diesel PM have been the focus of some recent investigations, which have begun to expose the impact it can have on the surrounding environment [Geiger *et al.*, 2002; Lee *et al.*, 2004]. For example, smog chamber studies have shown that diesel exhaust

causes a significant increase in ozone formation [Geiger *et al.*, 2002]. Because certain chemical compounds have more serious effects than others, knowing the detailed chemical makeup of particles in a specific size range from a source is essential for understanding their participation in atmospherically relevant reactions and their toxicological effects.

Given the potential threats of diesel PM to public health and the environment, it is crucial that source apportionment studies accurately quantify the contribution of diesel emissions to ambient particles. There has been some variability in the choice of chemical species that can serve as markers or tracers for particles originating from diesel engine emissions, as it is difficult to find robust tracers unique to a specific source [Fraser *et al.*, 2003]. For instance, elemental carbon (EC) has been used as a tracer for diesel PM in past studies without considering the contributions from other sources to EC in the atmosphere, such as coal-fired and fuel oil-fired power plants and gasoline powered vehicles [Schauer, 2003]. Complete characterization of all potential sources and careful consideration of plausible tracers are necessary for source apportionment models that utilize molecular markers.

Particles emitted by diesel vehicles conventionally are collected on filters and analyzed off-line after accumulating sufficient mass. One of the disadvantages of this method is the low temporal resolution. Ideally, instruments need to acquire chemical data on a near real time basis, in order to accurately interpret trends of emissions in terms of engine speed or other operating conditions [Moosmuller *et al.*, 2001]. For example, only instruments with high temporal resolution can capture the impact of hard accelerations on HDDV emissions. Single particle mass spectrometry (SPMS) techniques, such as aerosol time-of-flight mass spectrometry (ATOFMS), are a collection of on-line analytical instruments that measure the size and chemical composition of individual particles [Suess and Prather, 1999]. This combination of size and chemical information of single particles coupled with high temporal resolution provides unique information on source emissions, which can be applied in apportioning ambient particles.

The goal of this study is to determine the unique associations of chemical species in single particles observed in the exhaust of heavy duty diesel vehicles run on a chassis dynamometer. The results presented are part of a series of studies that apportion ambient aerosols to gasoline or diesel vehicles on a single particle basis by accomplishing the following tasks: the elucidation of multiple single particle signatures of exhaust emissions from light duty (gasoline) vehicles [Sodeman *et al.*, 2005a] and heavy duty (diesel) vehicles (this work, ultrafine size range [Toner *et al.* 2005]) and the evaluation of these chassis dynamometer particle signatures in real world tunnel [Sodeman *et al.*, 2005b] and roadside (conducted in the summer of 2004) studies.

2.2 Experimental Methods

2.2.1 Sampling Conditions

Exhaust emissions from seven heavy duty diesel trucks were analyzed between August 26 and November 3, 2001 at the Ralph's Distribution center in Riverside, CA. The fleet of trucks from which PM samples were measured varied by vehicle year, manufacturer, gross vehicle weight (GVW), and miles driven, as described in Table 2.1. The chosen vehicles were tested under the same sampling conditions, which include driving cycle and dilution conditions. The sampling procedure required driving each truck on a heavy duty dynamometer operated by

Table 2.1 Truck Descriptions

CRC #	Year	Type	Make	Engine	Model	GVW (lbs)	Miles
3	1985	HDD Tractor	International	Cummins	NTCC-300	32000	501,586
6	1995	HDD Tanker	Freightliner	Cummins	-	45000	689,536
7	1990	HDD Tractor	Peterbilt	Detroit Diesel	Series 60	50000	399,224
8	1996	HDD Tractor	Kenworth	Cummins	M11-300	32000	507,855
9	1998	HDD Tractor	Peterbilt	Caterpillar	C12	48000	607,968
10	1998	HDD Tractor	Sterling	Detroit Diesel	Series 60	52000	21,631
11	2000	HDD Tractor	Freightliner	Cummins	ISM	35000	17,048

West Virginia University. This transportable heavy duty vehicle emissions testing laboratory allowed reproducible aerosol emissions from HDDV exhaust emissions to be studied. The dynamometer system has been described elsewhere [Clark *et al.*, 1995]. For this study, a number of different driving cycles were employed to determine the effect of driving conditions on the exhaust aerosol chemical composition. The main driving cycle, developed by the CARB, was composed of six regimes: idle, creep, transient, cruise, extended idle, and extended creep, which are illustrated in Figure 2.1. The truck was maintained at idle during the first stage (idle). The creep phase consisted of small accelerations and decelerations with a top speed of less than 10 mph, while the transient stage involved fast and short periods of accelerations and decelerations with a top speed of nearly 50 mph. The truck operated between 50 and 60 mph for the majority of the cruise section, though the end of the cycle resembled a lower speed transient phase. The extended idle stage was a double length idle mode, whereas the extended creep phase comprised four creep phases back-to-back. All data presented in this work were collected under laden driving conditions, using a load of 56,000 lbs. The diesel exhaust flows through a dilution tunnel, which is part of the emissions testing laboratory, and then a portion of the dilute emissions is transferred to a residence chamber [McDonald *et al.*, 2000]. The residence chamber established an equilibrium between the gas and particle phase of the semivolatile organic components [Hildemann *et al.*, 1989]. Dilution ratios close to those reported for roadway situations [Dolan and Kittelson, 1979] were employed to simulate realistic conditions which determine the ultimate particle size and composition. All vehicles used fuels with low sulfur content (California, Federal, and Emissions Control Diesel fuels). The setup is similar to the one illustrated in Figure 3.1, only a standard ATOFMS instrument and copper tubing were used.

2.2.2 Instrumentation

Single particle size and chemical composition were measured using a transportable aerosol time-of-flight mass spectrometer. Details on the function of the transportable instrument are described elsewhere [Gard *et al.*, 1997]. ATOFMS data reported herein correspond to particles with aerodynamic diameters between 0.1 and 3 μm . It is important to note that the ATOFMS acquires both positive and negative ion mass spectra for each particle, providing information on all cations and anions simultaneously. Detection of both polarities provides for more detailed chemical information, allowing for enhanced possibility of differentiating signatures from specific sources [Lighty *et al.*, 2000]. All data presented herein include only the individual particles for which the ATOFMS collected mass spectra for both polarities.

To account for the ATOFMS transmission efficiency which decreases with decreasing particle size, ATOFMS chemical composition data are scaled to particle size distribution data measured concurrently with the ATOFMS data [Allen *et al.*, 2000]. The Scanning Mobility Particle Sizer (SMPS, TSI Model 3081 Electrostatic Classifier and TSI Model 3010 Condensation Particle Counter) and the Aerodynamic Particle Sizer (APS, TSI Model 3320) are considered reliable in their ability to collect number concentrations as a function of aerosol size in near real-time [Shen *et al.*, 2002]. ATOFMS data in the 0.10 to 0.56 μm size range are scaled to the SMPS data, while data in the 0.56 to 2.94 μm size range are scaled to the APS data. Figure 2.2 shows particle size distributions of a representative 80 second time interval for the SMPS and APS instruments. Note the two orders of magnitude discontinuity between number

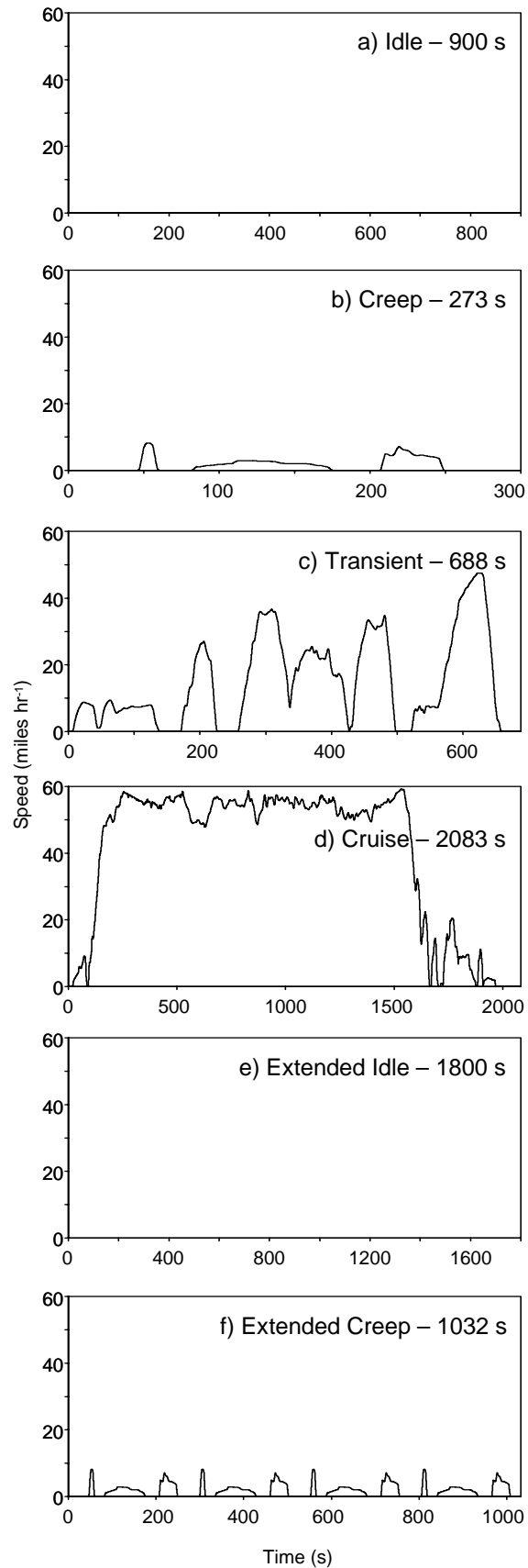


Figure 2.1 Driving cycles. Each of the six distinct stages is separated by approximately ten minutes.

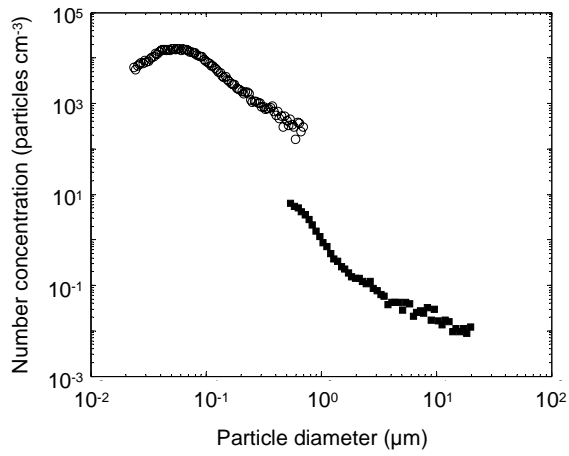


Figure 2.2 Discontinuity between particle sizing instruments. The representative data taken from the Scanning Mobility Particle Sizer (SMPS) [\circ – open circles] and the Aerodynamic Particle Sizer (APS) [\blacksquare – solid squares] show a difference in number concentration of more than an order of magnitude.

concentrations measured by the two sizing instruments; this observation has been noted in another study [Morawska *et al.*, 1998]. A combination of factors may have contributed to this discontinuity, including differences in the measuring techniques of the sizing instruments. For example, the SMPS scanned over each size bin every 80 second time period, while the APS averaged each size bin simultaneously during every 20 second time period. In addition, the SMPS and APS measure different diameters (mobility diameter vs. aerodynamic diameter, respectively). Studies have shown how the fractal-like shape of diesel exhaust particles leads to inaccurate measurement of these diameters by these techniques [Van Gulijk *et al.*, 2004]. However, using the most extreme dynamic shape factor and density values determined by Park *et al.*, it was calculated that the conversion between mobility (SMPS) and aerodynamic (ATOFMS) diameters does not affect the scaled chemical class percentages significantly (< 1%) in the SMPS size range, only the absolute number concentrations [Park *et al.*, 2004]. Since shape factor and density values for diesel exhaust particles have not been determined over the entire SMPS size range used in this work (0.10 to 0.56 μm), the ATOFMS data were scaled directly to SMPS data. There may be other limitations of the sizing instruments, such as the counting efficiency of the APS [Armendariz and Leith, 2002]. Corrections were not implemented, because their inclusion can only account for a small portion of the discontinuity. The high concentrations and rapid changes in vehicular operation suggest that most of the difference can be attributed to the scanning technique of the SMPS, which is too slow relative to the rapid changes in the driving cycle, because this discontinuity is not observed to the same extent in ambient measurements. Therefore, the plots in this work with SMPS and APS scaled data will be addressed separately.

2.2.3 Data Analysis Methods

Automated sorting and classification of particles with similar spectral characteristics were achieved using an adaptive resonance theory-based neural network algorithm, ART-2a [Song *et al.*, 1999]. General descriptions of the ART-2a algorithm have been presented in previous publications [Hopke and Song, 1997; Xie *et al.*, 1994].

2.3 Results and Discussion

2.3.1 Chemical Reproducibility

Using ART-2a analysis, numerous particle types are produced from each vehicle during dynamometer testing. Typically, 10-20 clusters can be used to describe at least 80% of the total particles sampled. For different trucks, the distribution of numbers of particles in each type varies. Certain questions rise. Are these different types truly distinct types or just variations in the sampling and/or ATOFMS analysis conditions? How reproducible are these different types and the numbers of particles occurring in each type from cycle-to-cycle and vehicle-to-vehicle? Much work has been done previously to sample combustion sources in a manner that reproducibly simulates ambient dilution conditions [Kittelson, 1998; Lighty *et al.*, 2000]. To date, the focus of these combustion studies has been on the size distribution measurements, and the chemical reproducibility of these sampling conditions has not been fully characterized. Likewise, the reproducibility of the SMPS instruments has not been examined using a highly complex sample, such as particle emissions from HDDV. To investigate the single particle

chemical reproducibility of ATOFMS for characterizing HDDV emissions, an initial analysis of the emissions from three trucks (T1, T2, and T3) chosen at random was performed.

Table 2.2 quantifies the chemical reproducibility of the single particle measurements by reporting the linear regression, r^2 values, from the analyses for each truck and between two different trucks. First, average area mass spectra (AAMS) are produced for all sampled particles from each test, and the r^2 values between the reproduced test AAMS for all detected 700 m/z values vary between 0.979 and 0.994 with less similarity observed between vehicles (0.805). The average area matrix shows how much the average intensities of all particles sampled from each vehicle vary. Next, ART-2a was applied to this data set. For this initial analysis, the vigilance factor, iterations, and learning rate are set at 0.5, 20, and 0.1, respectively. No further manual combination of clusters was performed. Here, the r^2 values compare the percentage of particles within each of the mass spectral ART-2a clusters. Between successive tests, the r^2 values vary from 0.940 to 0.970, showing a strong correlation for each of the three trucks. Interestingly, the r^2 value shows a poor correlation, 0.158, when comparing identical runs of different trucks, T1 and T3. Figure 2.3 shows two centroid mass spectra, or AAMS, for consecutive identical tests, one in black and the other in gray, representing all particles in the most populated cluster, Cluster 1, from the ART-2a analysis for T3. Cluster 1 represents 15 and 14% of the total sampled particle spectra from the reproduced tests. This figure illustrates the SPMS chemical reproducibility, $r^2 = 0.998$ between these two centroid mass spectra, for all detected 700 m/z values present within this cluster collected during subsequent tests. These analyses illustrate that there are chemical compositional differences between trucks and the high level of reproducibility between subsequent tests.

This initial analysis is the first to demonstrate that the sampling conditions used to study a complex combustion aerosol source yield highly reproducible chemical compositions at the single particle level. Even with all of the possible complications due to the laser desorption/ionization process and the relatively low sampling efficiency associated with ATOFMS, the chemical reproducibility of the technique is illustrated by ART-2a and AAMS analyses from the reproduced truck emissions. These observations allow for the conclusion that a statistically significant number of particles are being sampled during the transient truck driving cycles by ATOFMS. Determination of a single particle source profile from HDDV is the basis for this study, and it is well known that the more reproducible the analysis, the more reliable the source profile. This analysis is the first to confirm the single particle chemical reproducibility of the dynamometer and other sampling conditions, which consist of the dilution and residence chambers as well as the ATOFMS. Therefore, ATOFMS source profiles and chemical variations observed between trucks, driving cycles, and other factors, which will be presented in detail herein, can now be attributed to actual chemical differences and not to innate variations from instrumental variability or lack of a statistically relevant sample.

2.3.2 Effect of Dilution Conditions

The carefully designed dilution tunnel and residence chamber system allows for adequate mixing between the exhaust emissions and the dilution air, so that when the emissions are measured at ambient temperature, the exhaust compounds in both the gas and particle phases should have undergone the same condensation and adsorption reactions that they would have experienced in the atmosphere [Hildemann *et al.*, 1989]. Studies have shown how the dilution

Table 2.2 ATOFMS chemical reproducibility

Analysis method	T1 r^2	T2 r^2	T3 r^2	T1 & T3 r^2
All particles AAMS ^a	0.994	0.979	0.991	0.805
ART-2a Clusters ^b	0.954	0.970	0.940	0.158
Cluster 1—AAMS ^a	0.999	0.998	0.998	0.938

^aValues for r^2 are calculated between average ion intensities for each cation and anion m/z value between 0 and 350.

^bValues for r^2 are calculated between the percentage of particles within each of the 107 ART-2a clusters.

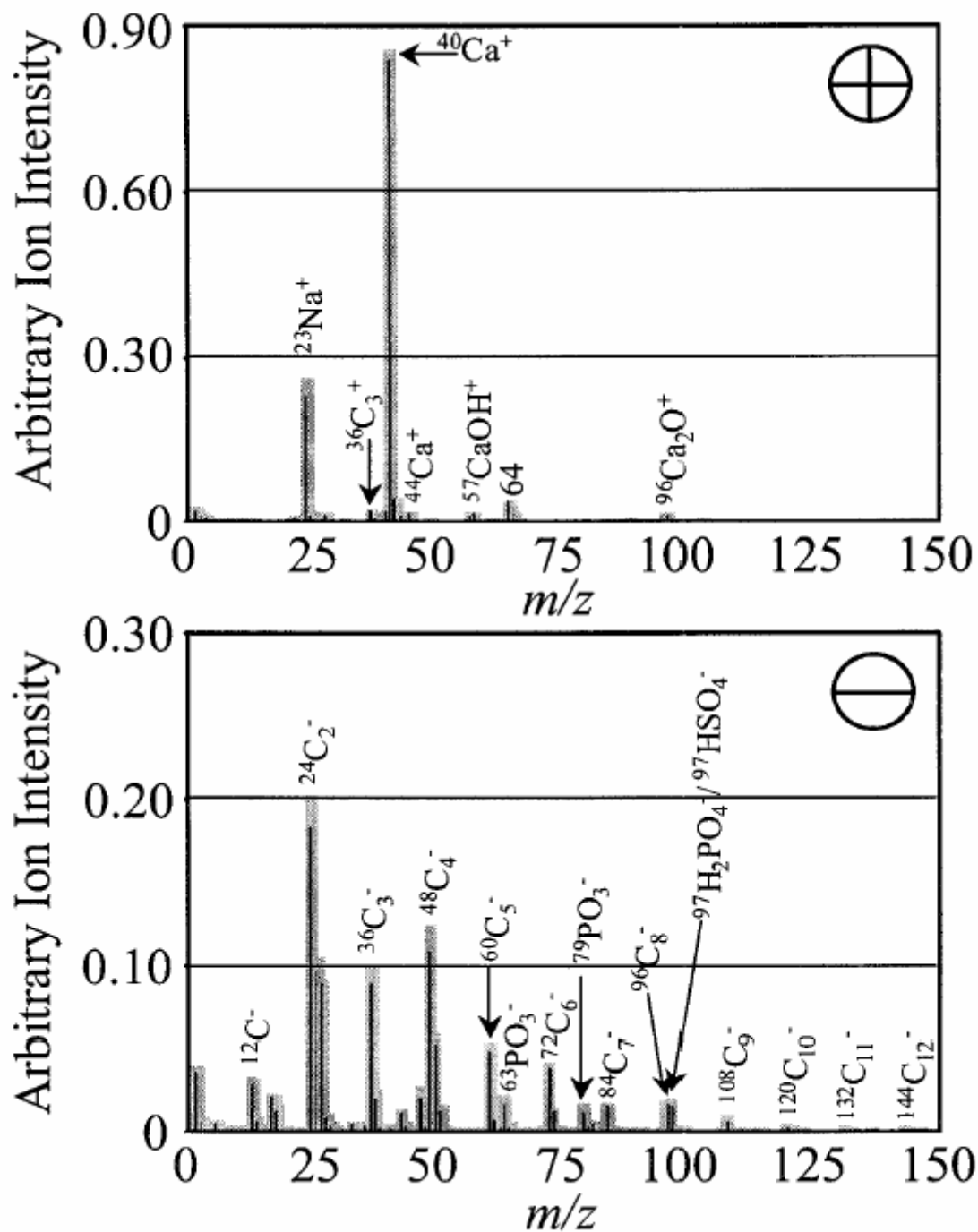


Figure 2.3 An illustration of the centroid mass spectra for the most populated ART-2a cluster obtained from T3 driven through 2 complete CARB cycles. Note the excellent agreement between the 2 tests, with the black representing one test and the gray the subsequent test.

conditions and its parameters, such as the dilution ratio, mixing time, temperature, and relative humidity, can change the number concentration and size distribution of the exhaust particles [Graskow *et al.*, 2000; Kawai *et al.*, 2004; Mathis *et al.*, 2004]. The influence of dilution conditions on the chemical composition of single particles can be examined by ATOFMS, as shown in the following experiment.

For example, polycyclic aromatic hydrocarbons (PAHs) need time to establish equilibrium between the gas and the particle phases; therefore, the dilution conditions and residence time can affect the relative fraction of PAH in the particulate phase. Figure 2.3 shows an example of how two dilution factors (DF 48 and 124) change the chemical associations in particles emitted during idling conditions from the same truck (CRC 3) in two consecutive tests run 3.5 hours apart. These particles were collected directly from the dilution tunnel without passing through the residence chamber. For all particles collected under each dilution condition, a digital mass spectrum, determined by the fraction of particles in that group that have a peak above a set threshold value, was created. For example, if a particular m/z peak in a digital mass spectrum has a height of 0.90, this means that 90% of the particles represented in that spectrum have a peak at that m/z above the threshold. The two spectra for each dilution condition are subtracted from one another to show the major differences between them, as shown in Figure 2.4. The peaks with positive intensities are more representative of chemical species in particles collected under less dilute conditions (lower dilution factor) and those with negative intensities under more dilute conditions (higher dilution factor). The figure shows positive peaks in the 160-300 mass-to-charge range to highlight the peaks from the chemical species of interest. The presence of PAH peaks with positive intensities indicates that more PAHs in the particle phase are favored in the less diluted conditions. When the exhaust is diluted more, PAHs in the gas phase also are diluted more, leading to the transfer of PAH species on the particles to the gas phase to reestablish equilibrium between the two phases. Possible contributions to m/z 178 are anthracene and phenanthrene with its dimethyl derivative at m/z 206 and trimethyl derivative at 220. The peaks at m/z 216, 230, and 244 possibly may be accounted for by benzo[b]fluorene and its methyl derivatives.

The increased presence of PAHs in the particle phase under less dilute conditions agrees with the size distribution shift seen between two different dilution factors. In the work of Graskow *et al.*, a comparison of size distributions between two different dilution factor conditions showed that the mean diameter of the particles is higher under less dilute conditions [Graskow *et al.*, 2000]. In other words, the growth of particles occurs under less dilute conditions which favor the condensation and adsorption of semi-volatile organics (e.g. PAHs) onto the non-volatile EC cores. Based on this knowledge, it is essential that the exhaust in dynamometer studies is properly diluted so that the data accurately simulate environmental diesel engine exhaust. Therefore, all remaining data herein have been measured under optimized dilution conditions with the dilution tunnel and residence chamber to mimic the influence of the atmosphere on the size and chemical composition of particles emitted from the exhaust pipe.

2.3.3 Chemical Classes

Linking chemical species to the specific engine source of particles in diesel exhaust is important for understanding the observed variations in diesel PM emitted from different vehicles

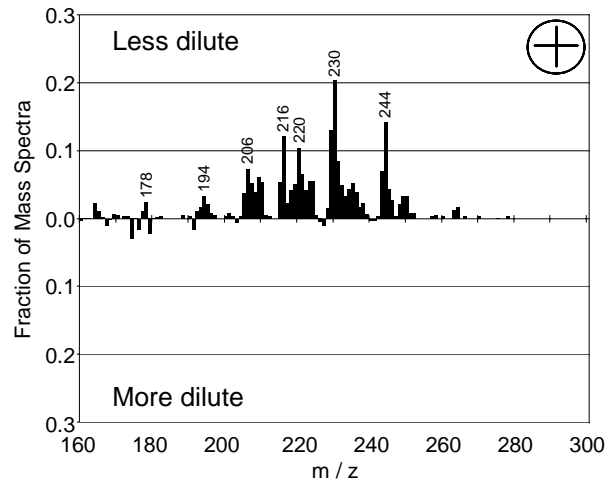


Figure 2.4 Subtraction plot of digital mass spectra for less dilute sampling conditions (dilution factor of 48) minus more dilute sampling conditions (dilution factor of 124).

during different driving cycle regimes. Fuel and lubricant oil were identified as the two main sources of chemical compounds within the internal combustion system in the exhaust particles in several forms: as unburned compounds, partially oxidized products, products of pyrolysis, and combinations of these [Rogge *et al.*, 1993]. Previous reports show that elemental carbon (soot) accounts for a large fraction (41% of the mass) of the particulate matter emitted by diesel engines [Burtscher *et al.*, 1998; Kittelson, 1998]. Although there is excess air to combust all of the fuel injected into the engine cylinder, the method of fuel injection creates local regions within the fuel spray which are either overlean or undermixed, leaving unburned and partially oxidized fuel compounds in the cylinder [Heywood, 1988]. These gas-phase species, particularly acetylene and PAHs, condense and react to form nuclei soot particles with diameters between 2-3 nm [Heywood, 1988]. Coagulation, agglomeration, condensation, and adsorption cause the growth of these soot-core particles [Kittelson, 1998]. Because the purpose of many lubricant additives is to prevent engine wear by mechanical (abrasion) and chemical (corrosion) processes due to the buildup of soot particles in the oil, the exhaust particles may also provide evidence of interactions between soot particles and the oil [Rudnick, 2003].

The main ART-2a parameters (vigilance factor, number of iterations, and learning rate), were set to 0.85, 20, and 0.05 for this detailed analysis. Similar particle types were further combined manually based upon chemical and size information. For example, two clusters were combined if they displayed the same size distributions and mass spectral information but showed slight differences in the intensities of the same m/z ratios. The eight main particle types that resulted after manually combining clusters are described below.

The positive and negative area vectors (average mass spectral signatures) for each of the eight major particle chemical classes are shown in Figure 2.5. Each particle class is labeled according to the most significant chemical features in both area vectors and described in detail below. Depending upon formation mechanisms, particle classes may have different size distributions; therefore, the relative fraction that each particle class represents of all particles of a particular size is shown in 0.1 μm size bin increments in Figure 2.6. Corresponding plots for all particles measured from the individual vehicles are shown in Figure 2.7. Table 2.3 provides the degree of similarity (dot product values) among the area matrices of the eight particle classes.

Class 1 (Ca EC phosphate sulfate): This chemical class is distinguished by the dominant calcium peak at m/z 40 [Ca]⁺ and additional calcium peaks at 57 [CaOH]⁺, 96 [Ca_2O]⁺, and 103 [CaPO_3]⁺ in the positive area vector [Figure 2.5 (a)]. During a roadside study, a high contribution of calcium to fine particles was observed, and its origin was associated with anthropogenic sources, rather than crustal material [Harrison *et al.*, 2003]. The existence of calcium on diesel exhaust particles results from common detergent additives to vehicular lubricants, such as calcium carbonate and calcium sulfonate; these basic additives neutralize acidic combustion byproducts and suspend the resulting salts, thus preventing the accumulation of deposits [Rudnick, 2003]. The negative area vector is composed mostly of elemental carbon (EC) peaks at [C_n]⁻ ($n = 1 - 12$) (ascribed to the anticipated soot core) and also indicates the presence of phosphate with peaks at 63 [PO_2]⁻, 79 [PO_3]⁻, and 97 [$\text{H}_2\text{O}\cdot\text{PO}_3$]⁻. Another engine oil additive, zinc dithiophosphate (ZDP), which functions as an antiwear agent, is one likely source for phosphate in diesel aerosols [Gautam *et al.*, 1999]. ATOFMS is less sensitive to zinc ions, which explains why there is a lack of peaks that can be associated to zinc isotopes when their presence is expected from ZDP. Additional negative peaks indicate that nitrate (46 [NO_2]⁻, 62 [NO_3]⁻) and sulfate (64 [SO_2]⁻, 80 [SO_3]⁻, 97 [HSO_4]⁻) adsorbed and condensed on the individual

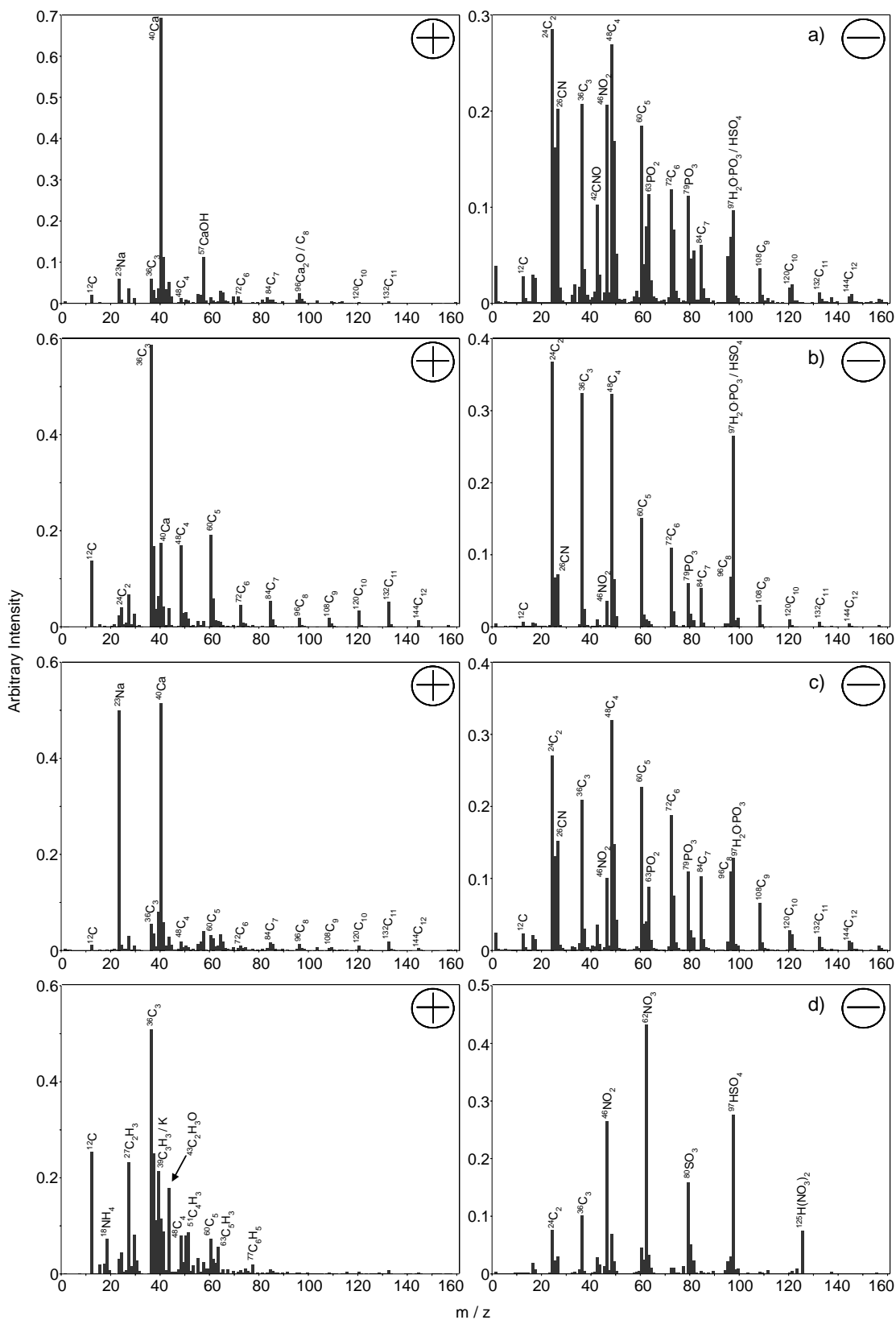


Figure 2.5 Positive and negative ion area vectors for the major particle classes observed in heavy duty diesel vehicle exhaust emissions: (a) Ca EC phosphate, (b) EC Ca phosphate sulfate, (c) Na Ca EC phosphate, and (d) OC nitrate sulfate.

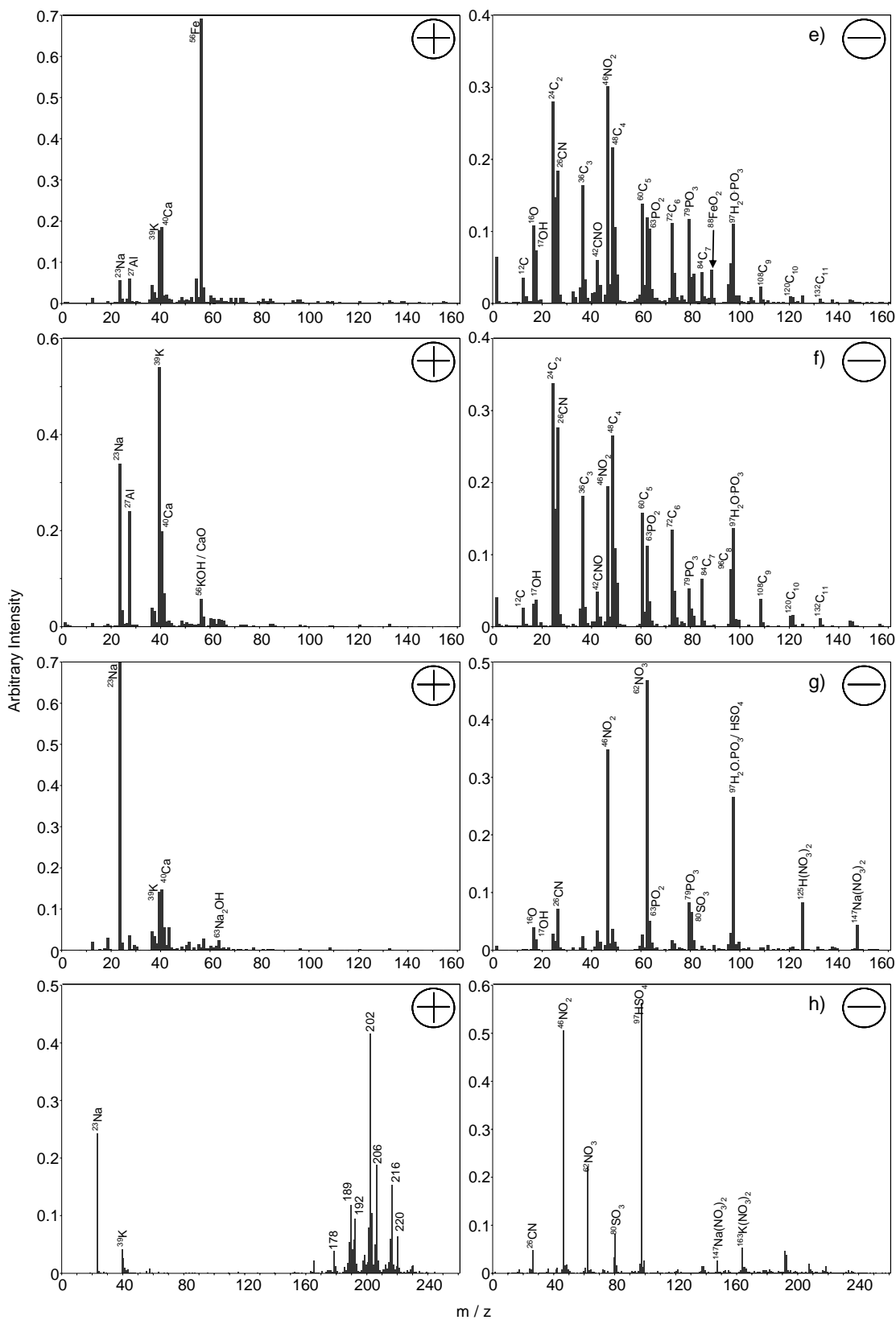


Figure 2.5 continued Positive and negative ion area vectors for the major particle classes observed in heavy duty diesel exhaust emissions: (e) Fe Ca Al Na EC phosphate, (f) K Na Al Ca EC phosphate, (g) Na K nitrate sulfate, and (h) PAH sulfate nitrate.

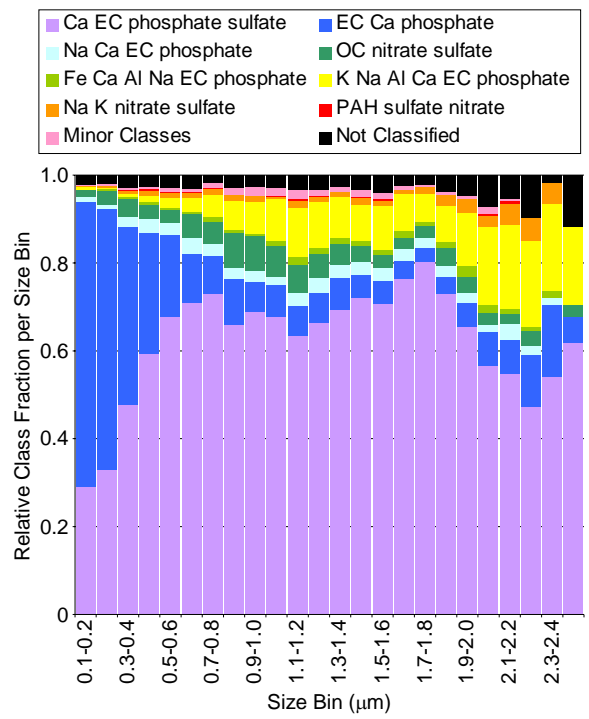


Figure 2.6 Relative fraction of each chemical class per 0.1 μm size bin.

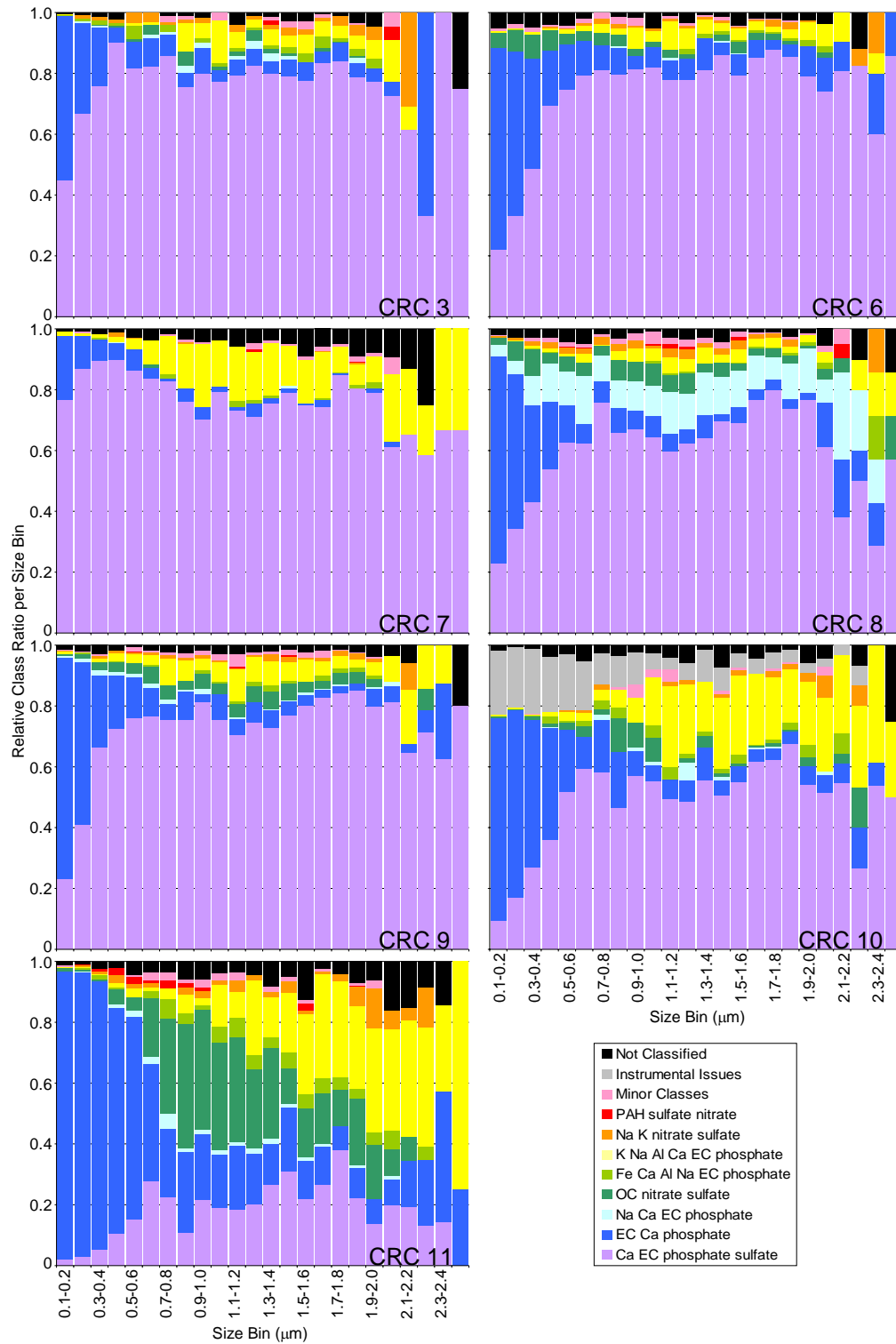


Figure 2.7 Relative fraction of each chemical class per 0.1 μm size bin for each vehicle.

Table 2.3 Degree of similarity (dot product values) among the area matrices of the eight major particle classes.

	Ca EC phosphate sulfate	EC Ca phosphate	Na Ca EC phosphate	OC nitrate sulfate	Fe Ca Al Na EC phosphate	K Na Al Ca EC phosphate	Na K nitrate sulfate	PAH sulfate nitrate
Ca EC phosphate sulfate	1.000							
EC Ca phosphate	0.5841	1.000						
Na Ca EC phosphate	0.8599	0.5908	1.000					
OC nitrate sulfate	0.4105	0.6803	0.3587	1.000				
Fe Ca Al Na EC phosphate	0.6044	0.4474	0.5584	0.3931	1.000			
K Na Al Ca EC phosphate	0.6647	0.5475	0.7762	0.4976	0.6465	1.000		
Na K nitrate sulfate	0.3878	0.2436	0.6152	0.5534	0.3733	0.5940	1.000	
PAH sulfate nitrate	0.2523	0.2084	0.3070	0.4247	0.3017	0.3489	0.6444	1.000

particles, as well. The presence of sulfur can be attributed to the additives such as calcium sulfonate or the intrinsic low sulfur levels in the fuel. Given the close resemblance of this chemical class to the major particle type in nebulized used diesel oil analyzed by ATOFMS, it is highly probable that these individual particles each have an EC nucleus surrounded by a coating of unburned lubricant oil compounds [Spencer and Prather].

Class 2 (EC Ca phosphate): These particles are differentiated by the elemental carbon peaks in both the positive and the negative spectra [Figure 2.5 (b)], including higher mass carbon clusters. Furthermore, other peaks display the presence of calcium and phosphate. Note that the size distribution of this particle class dramatically differentiates from the Ca EC class (Figure 2.6); EC Ca particles comprise a significant fraction (~60%) of the observed particles with diameters less than 0.3 μm , whereas the Ca EC particles cover both the fine and coarse size ranges (0.10 to 2.5 μm). Given the mass spectral and size information, the probability that the EC Ca class represents single particles with a larger EC core and/or less oil coating is high. The temporal resolution of the two particle types may give insight into any differences in the mechanisms of formation between these classes. Because these two particle types constitute the majority of diesel exhaust particles and have similar oil-derived chemical compositions, these results support the findings of Sakurai et al. that unburned oil contributes to at least 95% of the mass of the total diesel particles in the accumulation-mode particle size range [Sakurai et al., 2003b].

Class 3 (Na Ca EC phosphate): The positive area vector [Figure 2.5 (c)] for Class 3 is composed of metal peaks, particularly sodium (23 $[\text{Na}]^+$) and calcium coupled with elemental carbon cluster peaks. Corresponding carbon cluster peaks also appear in the negative area vector, in addition to phosphate and nitrate. With the exception of the intense sodium peak, this class closely resembles the previous two classes, implying similar formation mechanisms. The size profile of this particle type resembles that of the Ca EC class, which is more evidence of a similar formation mechanism. The two classes also have a high degree of similarity in their spectral characteristics [Table 2.3]. The increase in the sodium peak may be from increased impurity levels in the fuel and additive packages.

Class 4 (OC nitrate sulfate): This class is an organic carbon (OC) particle type, indicated by the hydrocarbon envelopes in the positive area vector [Figure 2.5 (d)], such as 27 $[\text{C}_2\text{H}_3]^+$ / $[\text{NCH}]^+$ and 43 $[\text{C}_2\text{H}_3\text{O}]^+$ / $[\text{CHNO}]^+$. Nitrate and sulfate are present in the negative ion area vector. This chemical class lacks the calcium and phosphate ions, which dominate the Ca EC and EC Ca particle type spectra, suggesting a different formation mechanism. Its gas-phase precursors (unburned fuel hydrocarbons, NO, SO₂) may escape through the exhaust system before cooling and condensing onto EC nuclei. The OC coating may be thick enough to preclude the ATOFMS from detecting the EC signatures of the soot core. The formation of these particles can be attributed mostly to the fuel, especially considering the sulfur content of diesel fuel. This chemical class is consistent with the hypothesis proposed by Canagaratna and coworkers using an aerosol mass spectrometer (AMS) in chase studies that sulfate and organic species are internally mixed in single diesel exhaust aerosols [Canagaratna et al., 2004].

Class 5 (Fe Ca Al Na EC phosphate): This particle type has a metal dominated positive area vector [Figure 2.5 (e)] with peaks indicative of iron (56 $[\text{Fe}]^+$), calcium, aluminum (27 $[\text{Al}]^+$), and sodium. In contrast, the carbonaceous negative area vector exhibits elemental carbon clusters ions, as well as phosphate and nitrate. Likely sources of the iron are the fuel, wearing exhaust pipes, and abrasion of the engine block itself [Ulrich and Wichser, 2003].

Class 6 (K Na Al Ca EC phosphate): These particles compose another metal/carbonaceous chemical class. The metals include potassium (39 [K]⁺), sodium, aluminum, and calcium. The positive peak [Figure 2.5 (f)] at m/z 56 could signify the presence of iron; however, the absence of iron isotopes at 54 and 57 and the abundance of potassium at m/z 39 indicate that KOH⁺/CaO⁺ is a better assignment for this peak. The negative area vector closely resembles that of the Class 5 with its negative peaks of elemental carbon, nitrate, and phosphate.

Class 7 (Na K nitrate sulfate): This class is dominated by metal ions in the positive spectrum (sodium, potassium) with a very different negative area vector [Figure 2.5 (g)] when compared to the other metal dominated particle classes. The negative ions in the Na K class are dominated by nitrate and sulfate. This particle class closely resembles an inorganic salt type observed near a high speed highway with a heavy influence by HDDV in Germany [Vogt *et al.*, 2003].

Class 8 (PAH sulfate nitrate): This particle type is distinguished by the dominant presence of PAH peaks in the positive ion area vector [Figure 2.5 (h)]. It is important to note that PAH also occurred in some of the other particle types, but they were not the dominant peaks as with this chemical class. The peak at m/z 202 could be pyrene or fluoranthene, while m/z 216 is the methyl derivative. Sulfate and nitrate dominate the negative spectrum. The presence of the characteristic 26 [CN]⁻ and 46 [NO₂]⁻ peaks in the negative area vector can be indicators of N-organic species and nitro-PAH compounds, respectively [Bezabeh *et al.*, 1997]. Without the negative ion spectra for these particles, it would be difficult to differentiate between nitro-PAHs and unsubstituted PAHs using only the positive ion spectral information. A radiotracer study determined that approximately one-third of the PAH species in diesel engine emissions originate from the fuel through incomplete combustion [Rhead and Hardy, 2003]. Other sources of PAHs include the lubricant oil or reacted products of pyrolysis [Marr *et al.*, 1999].

The above eight particle types account for 97% of the particles. Individual particles that were not classified into one of these eight classes were placed into one of two other categories: “not classified” and “minor” classes. The “not classified” category contains those individual particles which were not matched by ART-2A (~2.5%). The “minor classes” category (<1%) is a collection of classified particle types that constituted small fractions of all measured aerosols. Of particular interest in this group is the vanadium particle type. These particles are distinguished by positive ion peaks of vanadium at m/z 51 [V]⁺ and vanadium oxide at m/z 67 [VO]⁺. Aerosols with these markers have been observed during ambient monitoring and associated with fuel oil combustion [Lake *et al.*, 2004]. However, since this chemical class represents such a small percentage (<1%) of the total collected particles, it is labeled as a minor class.

2.3.4 Temporal and Cycle-to-Cycle Variation

On-line sampling by ATOFMS allows for the collection of size-resolved information on particles with high temporal resolution, which is important for observing rapid changes during dynamometer tests. Figures 2.8 and 2.9 show the temporal response of the number concentration scaled to miles driven and grams of CO₂ emitted during the six stages of the CARB cycle separated by engine soaks of approximately ten minutes. Each plot represents the average CARB cycle for all seven trucks tested, and each bar represents the average chemical composition of 80 second time bins. The time resolution is limited by the scanning period of the

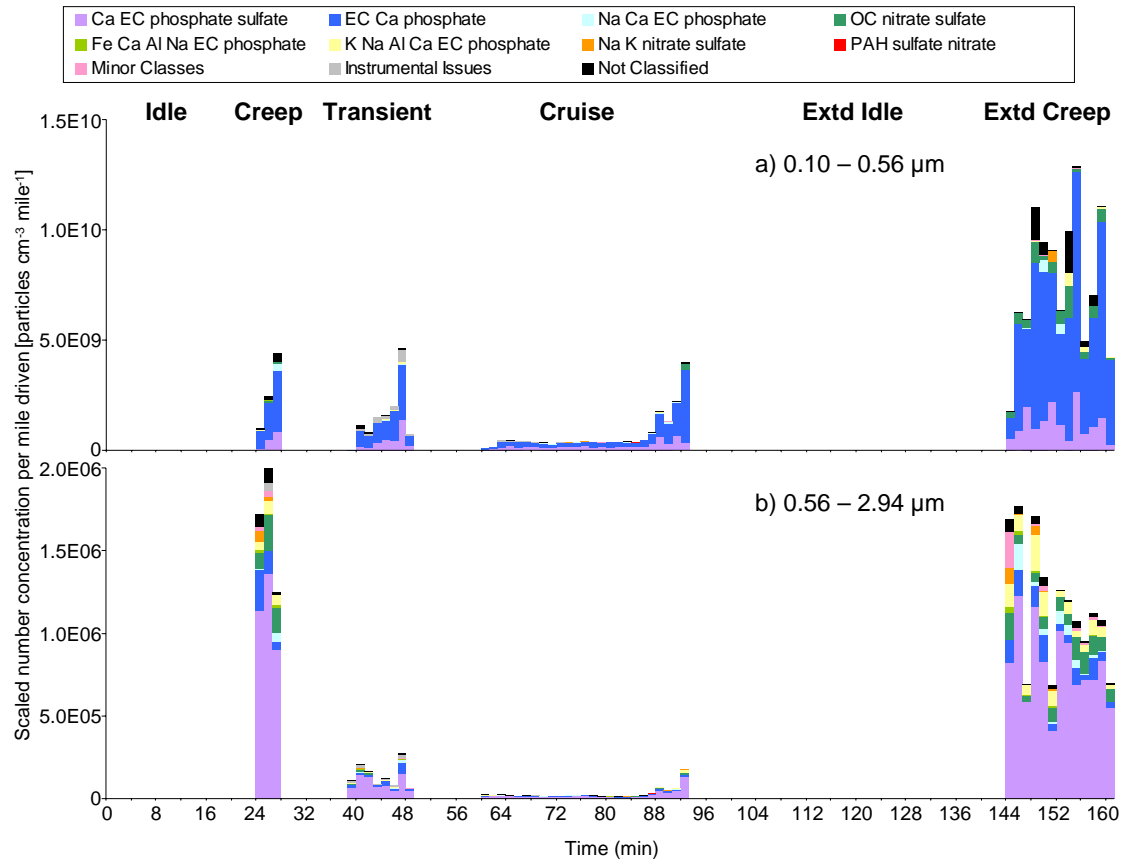


Figure 2.8 Average temporal variation in number concentration per mile driven and chemical composition of exhaust particles for all vehicles. (a) scaled to SMPS data in the 0.10 to 0.56 μm size range. (b) scaled to APS data in the 0.56 to 2.94 μm size range. Data are missing for the idle and extended idle cycles, since no miles were driven.

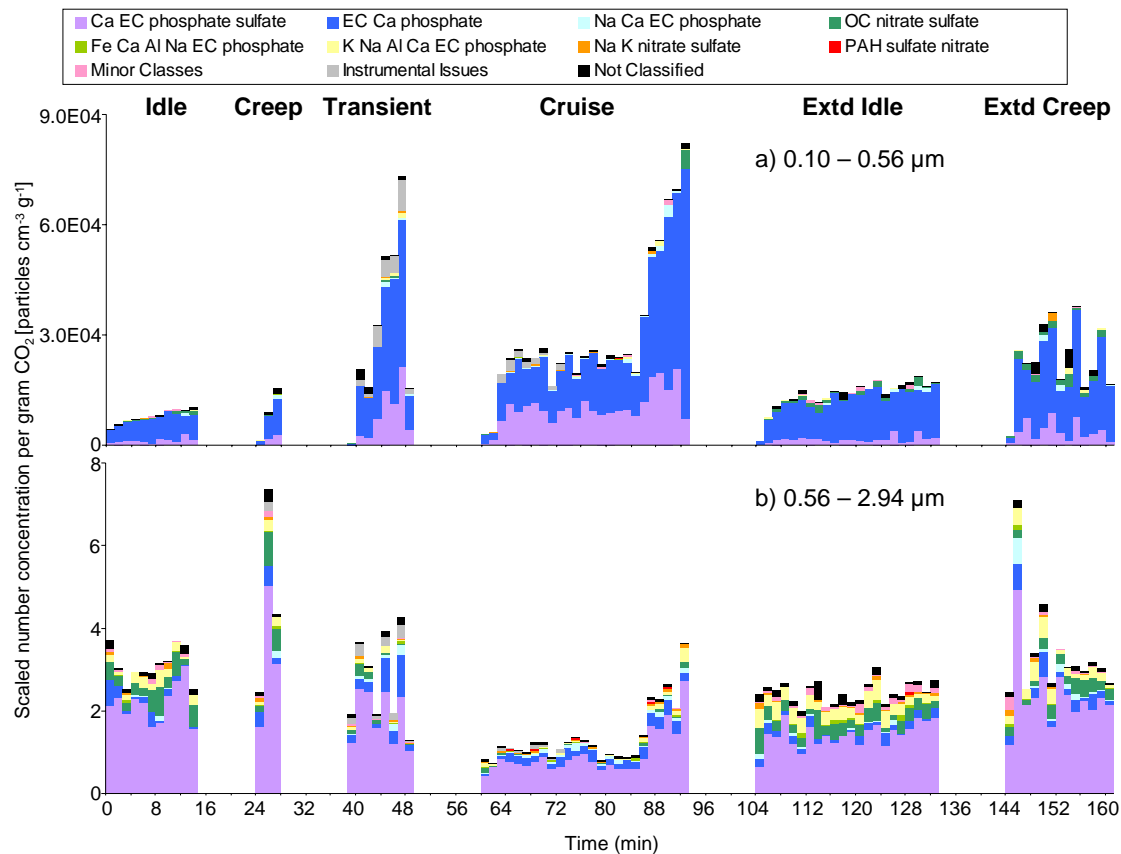


Figure 2.9 Average temporal variation in number concentration per gram of carbon dioxide (CO₂) emitted and chemical composition of exhaust particles for all vehicles. (a) scaled to SMPS data in the 0.10 to 0.56 μm size range. (b) scaled to APS data in the 0.56 to 2.94 μm size range.

SMPS. If the final 80 second bin of any cycle represents less than 75% of the full time period, it is not shown in these plots. The data in Figure 2.8 (a) and (b) are scaled to the SMPS and APS data and have units of scaled number concentration per number of miles driven. There are no data shown for the idle and extended idle phases in these plots, because no mileage was traveled. Units of per mile driven is most common in the literature, as it can be directly applied in any emission inventory calculations by activity (travel) based models, such as CARB's Emission Factor (EMFAC) [Dreher and Harley, 1998].

During the testing of the CRC 10 truck (1998 Sterling Detroit Diesel), a data acquisition board on the ATOFMS malfunctioned, affecting the positive ion spectra during the transient and cruise cycles. Without the positive ion signal, it is difficult to classify the individual particles and, therefore, the particles influenced by this instrumental issue are placed in a separate class ("Instrumental Issues"). Although the chemical information is lost, the temporal and size information are still important for comparison purposes, warranting their inclusion in the plots.

The creep and extended creep cycles produced the highest number concentrations of emitted particles per mile driven by nearly an order of magnitude. It is possible that a portion of the high number concentration may be an artifact of the normalization method due to the very short distances covered during the creep phases. The cruise phase yielded the lowest number concentrations of emitted particles per mile, which agrees with the findings of Shah *et al.* [Shah *et al.*, 2004]. Without normalization by distance traveled, the stages producing the highest number concentrations were the transient and cruise cycles for the 0.10 to 0.56 micrometer size range and the creep cycle for the 0.56 to 2.94 micrometer size range.

To explore the effects of scaling on overall concentrations further, Figures 2.9 (a) and (b) display the same data as shown in Figure 2.8, only the scaled number concentrations are normalized by the grams of CO₂ emitted. The amount of CO₂ emitted closely tracks the amount of fuel consumed by means of the carbon balance [Yanowitz *et al.*, 2000]; therefore, these units are proportional to number concentration per gram of fuel burned and are a good substitute when the actual fuel consumption is not measured. Unlike the distance based figures, the fuel based figures allow comparison of the idle and extended idle conditions; the emissions during these cycles remain uniform, particularly for particles in the 0.10 to 0.56 micrometer size range. Such homogeneity is anticipated, given the consistent demand upon the engine during the idling.

The advantages of expressing results in terms of fuel (CO₂) based emissions versus emissions per mile driven include the decreased influence of driving conditions (e.g. level roads versus uphill grades) over the estimated emissions; vehicles operating on harder driving conditions burn more fuel but travel the same distance. Another benefit is the availability of data on volumes of fuel purchased in order to calculate the contribution of diesel particles to region-wide inventories [Dreher and Harley, 1998]. The fuel basis factors minimize the affect of vehicle load and speed [Yanowitz *et al.*, 1999]. In addition, diesel particles emitted during idling periods are not considered in distance-based measurements. For these reasons, the remaining data are normalized to grams of CO₂ emitted.

One interesting temporal feature is the transition from high speed cruise to low speed accelerations and decelerations during the cruise cycle, as shown in Figures 2.8 and 2.9. The high speed portion displays constant number concentration and chemical composition. During the final section of the cruise phase, the emitted number concentration increases considerably, resembling the emissions of the transient cycle, as expected due to the conversion to rapid accelerations and decelerations.

The temporal plots demonstrate how dominant the Ca EC and EC Ca particles are in all cycles. However, the ratio of number concentrations of particles in the EC Ca to Ca EC classes changes for each cycle: the higher the speed, the lower the ratio in the 0.10 to 0.56 micrometer size range. For example, the mean (± 1 standard deviation) ratio is 5.8 (± 3.3) for the idle cycle and 1.4 (± 0.31) for the high speed cruise section of the cruise cycle. Therefore, more lubricant oil is consumed during higher speed operating conditions. Another chemical class is preferentially produced at specific conditions. The OC chemical class is formed more during the idle and creep cycles. This observation is consistent with the findings of other researchers [Fraser *et al.*, 2002; Robert *et al.*, 2004]. The engine operating conditions during these low speed phases generate lower cylinder temperatures, which allow for more condensation. It is interesting to note that even when the OC particle class is preferentially produced, the EC classes still dominate over all size ranges, unlike in the accumulation mode particle emissions of light duty vehicles [Sodeman *et al.*, 2005a].

The fuel based plots in Figure 2.9 show small variations in number concentrations from cycle to cycle. The diesel trucks emitted the highest concentration of particles in the smaller size range during the transient stage and the highest concentration of particles in the 0.56 to 2.94 micrometer size range during the creep and extended creep phases. On the basis of this difference, it is worthwhile to compare cycles using smaller size bins.

2.3.5 Vehicle-to-Vehicle Variability

The chemical composition of diesel particles as a function of cycle and size is illustrated in Figure 2.10 (a – g) for each vehicle. In these plots, the ATOFMS data are scaled in four size bins [0.10 – 0.20; 0.20 – 0.29; 0.29 – 0.41; and 0.41 – 0.56 μm] to the size distribution data collected by the SMPS. The absence of chemical composition information for some cycles in these plots indicates time periods in which there were not enough ATOFMS counts in that particular size bin to accurately scale the data.

For every size bin for each vehicle, the number concentration per gram of CO_2 emitted is highest for the acceleration cycles (creep and transient) and lowest for the more steady-state cycles (cruise and idle). Highest particulate emissions during transient cycles have been observed in other studies as well [Lehmann *et al.*, 2003]. This pattern is justified by the efficiency of the diesel engines during each cycle; the engine is designed to operate more efficiently during the cruise cycle while it maintains a fairly constant high speed and has few accelerations. During optimal operation, the combustion processes are more complete, producing fewer diesel particles and more combustion products such as carbon dioxide. On the other hand, when the vehicle is required to accelerate and decelerate quickly, the amount of injected fuel may be too little or too much, causing more incomplete combustion. Here, the truck functions less efficiently and yields more particles.

Figure 2.11 (a – g) displays the chemical, cycle, and size data scaled to the APS data for each vehicle. The scaled data are divided into six size bins [0.56 – 0.75; 0.75 – 1.00; 1.00 – 1.33; 1.33 – 1.78; 1.78 – 2.05; and 2.05 – 2.94 μm]. In these larger size ranges, the creep cycle in each size bin generally exhibits the highest number concentration per gram of CO_2 emitted, because the transition of the highest PM emitting cycle from the transient to the creep cycle for each vehicle generally occurred around 0.3 μm for each vehicle. Fast accelerations produce more small particles.

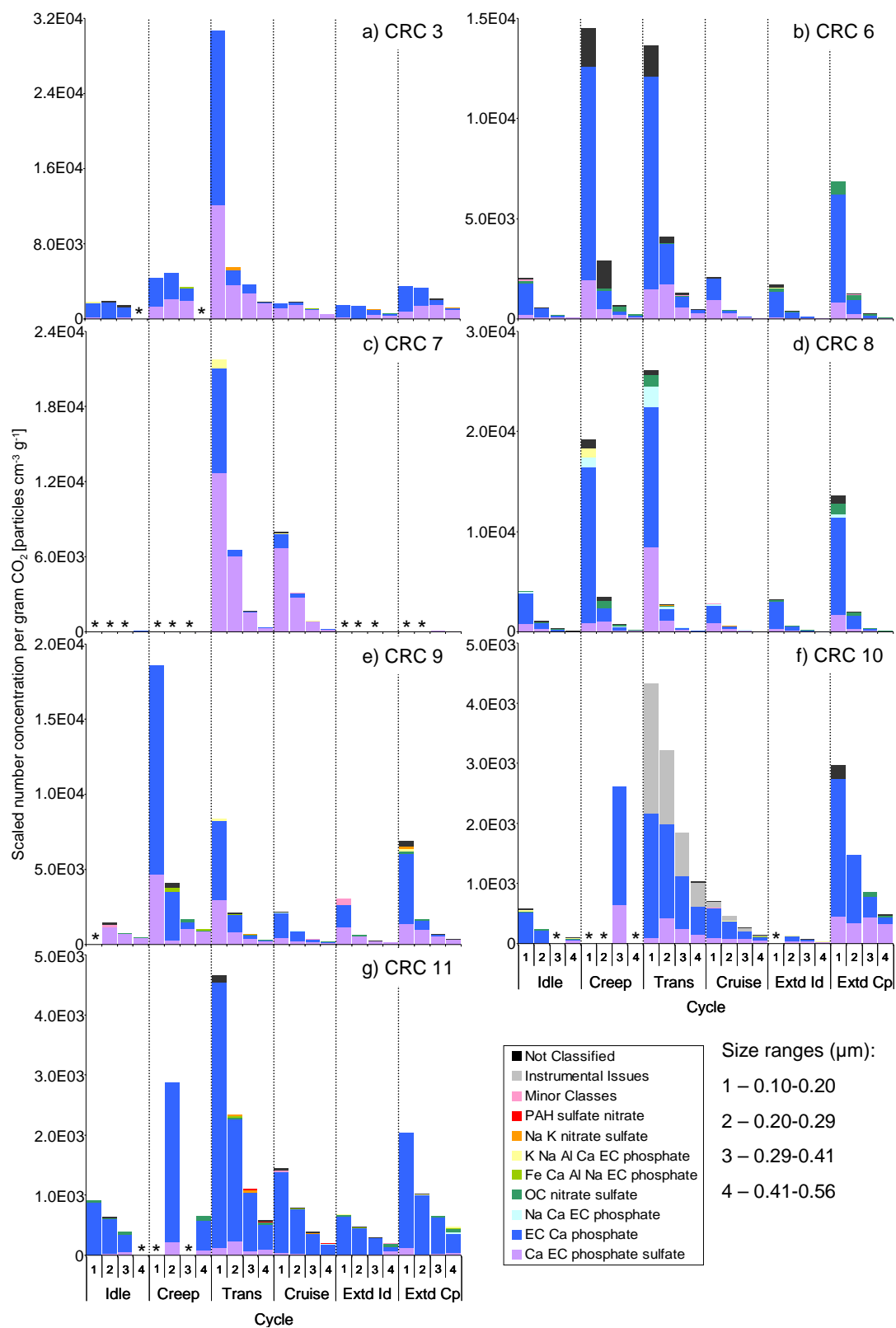


Figure 2.10 Size and cycle variation of number concentration and chemical composition of exhaust particles for each diesel truck. ATOFMS data are scaled to the SMPS in the 0.10 to 0.56 μm size range. Bars marked with an asterisk [*] indicate time periods in which there were not sufficient ATOFMS counts to allow proper scaling of the data.

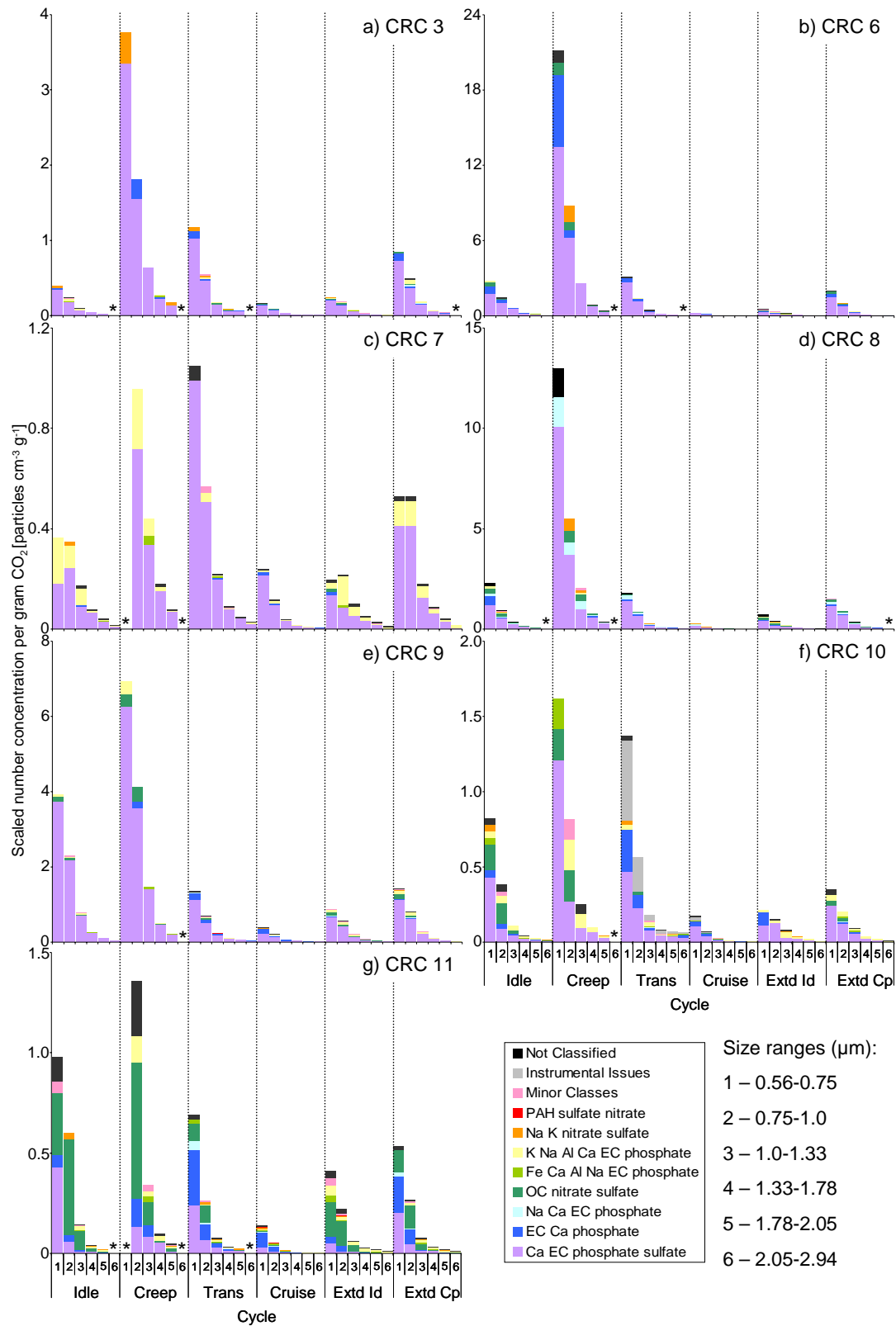


Figure 2.11 Size and cycle variation of number concentration and chemical composition of exhaust particles for each diesel truck. ATOFMS data are scaled to the APS in the 0.56 to 2.94 µm size range. Bars marked with an asterisk [*] indicate time periods in which there were not sufficient ATOFMS counts to allow proper scaling of the data.

While the smaller size bins are primarily composed of EC Ca and Ca EC particles for all vehicles, there is considerably more variation in chemical composition in the larger size bins. In particular, the Na Ca EC class in the CRC 8 truck (1996 Kenworth Cummins), the K Na Al Ca particle type in the CRC 7 truck (1990 Peterbilt Detroit Diesel), and the OC class in the CRC 11 truck (2000 Freightliner Cummins) contribute to large fractions of the chemical compositions. As mentioned above, the Na Ca EC particle type closely resembles the main oil-derived particle classes with the exception of the intense sodium peak. Analysis of fuel and oil samples from the CRC 8 truck by ATOFMS revealed a strong presence of sodium in the oil, which most likely can be attributed to a component in the additive package, when compared to the other used oil samples [Spencer and Prather]. In this same study by Spencer and Prather, no anomalous increased presence of potassium was detected in the fuel and oil samples of the CRC 7 truck, implying that another variable within this specific engine system caused the higher production of the K Na Al Ca particle type.

Although it can be difficult to specify any trends of chemical composition with vehicle age or mileage using a dataset of only seven trucks, it is worthy to note that the vehicles with the lowest mileage (CRC 11 and CRC 10, even with its instrumental issues) have the highest diversity in chemical composition. In other words, although Ca EC and EC Ca type particles still account for the majority (63-95%) of the total emitted particles, aerosols of other particle types compose a larger fraction in low mileage trucks. It is interesting to note that these trucks also produced less exhaust particles overall. Because these two low mileage trucks also are two of the newer vehicles in this dataset, more measurements would be necessary to determine if this chemical variation is due to technological advances or if all low mileage vehicles display this same characteristic. However, the increased domination of the main oil-derived particle class (Ca EC) for the high mileage vehicles could indicate that worn engine parts permit more oil inside the combustion chamber [Pedersen *et al.*, 1980].

2.4 Implications

In this study, the sampling and chemical reproducibility of ATOFMS was verified. Eight distinct particle types were found to describe the majority of single particles emitted by heavy duty diesel vehicles, and these chemical classes were highly reproducible from one vehicle to another. Now that the HDV exhaust has been characterized, the evaluation of how well the signatures apply in apportionment studies must be examined in an ambient data set known to be heavily influenced by vehicular emissions, such as a tunnel study [Sodeman *et al.*, 2005b], before applying the signatures to other ambient studies.

2.5 Acknowledgements

The authors express their gratitude to the Coordinating Research Council for their help and support in testing during CRC Project E55/E59, and the staff of the West Virginia University Transportable Heavy-Duty Emissions Testing Laboratory for their assistance with sample collection. The authors would like to acknowledge West Virginia University personnel, Benji Staggs, Tim Hall, Andy Williams, and Chris Rowe. In addition, thanks are extended to Pat

Arnott and Dave Campbell from Desert Research Institute for their assistance in the use of their residence chamber. Finally, the authors would like to thank William Vance from California Air Resources Board for assistance throughout this project and providing invaluable advice along the way. Funding for this project was supplied by the California Air Resources Board (00-331).

2.6 References

- Allen, J.O., D.P. Fergenson, E.E. Gard, L.S. Hughes, B.D. Morrical, M.J. Kleeman, D.S. Gross, M.E. Galli, K.A. Prather, and G.R. Cass, Particle detection efficiencies of aerosol time of flight mass spectrometers under ambient sampling conditions, *Environmental Science & Technology*, 34 (1), 211-217, 2000.
- Armendariz, A.J., and D. Leith, Concentration measurement and counting efficiency for the aerodynamic particle sizer 3320, *Journal of Aerosol Science*, 33 (1), 133-148, 2002.
- Bezabeh, D.Z., T.M. Allen, E.M. McCauley, P.B. Kelly, and A.D. Jones, Negative ion laser desorption ionization time-of-flight mass spectrometry of nitrated polycyclic aromatic hydrocarbons, *Journal of the American Society for Mass Spectrometry*, 8 (6), 630-636, 1997.
- Bommel, H., M. Haake, P. Luft, J. Horejs-Hoeck, H. Hein, J. Bartels, C. Schauer, U. Poschl, M. Kracht, and A. Duschl, The diesel exhaust component pyrene induces expression of IL-8 but not of eotaxin, *International Immunopharmacology*, 3 (10-11), 1371-1379, 2003.
- Burtscher, H., S. Kunzel, and C. Hüglin, Characterization of particles in combustion engine exhaust, *Journal of Aerosol Science*, 29 (4), 389-396, 1998.
- Canagaratna, M.R., J.T. Jayne, D.A. Ghertner, S. Herndon, Q. Shi, J.L. Jimenez, P.J. Silva, P. Williams, T. Lanni, F. Drewnick, K.L. Demerjian, C.E. Kolb, and D.R. Worsnop, Chase studies of particulate emissions from in-use New York City vehicles, *Aerosol Science & Technology*, 38 (6), 555-573, 2004.
- Clark, N.N., M. Gautam, R.M. Bata, W.-G. Wang, J.L. Loth, G.M. Palmer, and D.W. Lyons, Technical Report: Design and operation of a new transportable laboratory for emissions testing of heavy duty trucks and buses, *Int. J. of Vehicle Design*, 2 (3/4), 308-322, 1995.
- Colvile, R.N., E.J. Hutchinson, J.S. Mindell, and R.F. Warren, The transport sector as a source of air pollution [Review], *Atmospheric Environment*, 35 (9), 1537-1565, 2001.
- Dolan, D.F., and D.B. Kittelson, Roadway measurements of diesel exhaust aerosols, *Society of Automotive Engineers Technical Paper Series*, 790492, 9 pp., 1979.
- Dreher, D.B., and R.A. Harley, A fuel-based inventory for heavy-duty diesel truck emissions, *Journal of the Air & Waste Management Association*, 48 (4), 352-358, 1998.

- Dunlap, J., New truck inspection programs in California aim to reduce emissions, *Diesel Progress North American Edition*, 64 (6), 94-96, 1998.
- Durant, J.L., W.F. Busby, A.L. Lafleur, B.W. Penman, and C.L. Crespi, Human cell mutagenicity of oxygenated, nitrated and unsubstituted polycyclic aromatic hydrocarbons associated with urban aerosols, *Mutation Research: Genetic Toxicology*, 371 (3-4), 123-157, 1996.
- Fraser, M.P., B. Buzcu, Z.W. Yue, G.R. McGaughey, N.R. Desai, D.T. Allen, R.L. Seila, W.A. Lonneman, and R.A. Harley, Separation of fine particulate matter emitted from gasoline and diesel vehicles using chemical mass balancing techniques, *Environmental Science & Technology*, 37 (17), 3904-3909, 2003.
- Fraser, M.P., K. Lakshmanan, S.G. Fritz, and B. Ubanwa, Variation in composition of fine particulate emissions from heavy-duty diesel vehicles - art. no. 8346, *Journal of Geophysical Research-Atmospheres*, 107 (D21), 8346, 2002.
- Gard, E., J.E. Mayer, B.D. Morrical, T. Dienes, D.P. Fergenson, and K.A. Prather, Real-time analysis of individual atmospheric aerosol particles - design and performance of a portable ATOFMS, *Analytical Chemistry*, 69 (20), 4083-4091, 1997.
- Gautam, M., K. Chitoor, M. Durbha, and J.C. Summers, Effect of diesel soot contaminated oil on engine wear - investigation of novel oil formulations, *Tribology International*, 32 (12), 687-699, 1999.
- Geiger, H., J. Kleffmann, and P. Wiesen, Smog chamber studies on the influence of diesel exhaust on photosmog formation, *Atmospheric Environment*, 36 (11), 1737-1747, 2002.
- Graskow, B.R., M.R. Ahmadi, J.E. Morris, and D.B. Kittelson, Influence of fuel additives and dilution conditions on the formation and emission of exhaust particulate matter from a direct injection spark ignition engine, *Society of Automotive Engineers, [Special Publication] SP, SP-1551* (Diesel and Gasoline Performance and Additives), 261-271, 2000.
- Harrison, R.M., R. Tilling, M.S.C. Romero, S. Harrad, and K. Jarvis, A study of trace metals and polycyclic aromatic hydrocarbons in the roadside environment, *Atmospheric Environment*, 37 (17), 2391-2402, 2003.
- Heywood, J.B., *Internal combustion engine fundamentals*, xxix, 930 p., McGraw-Hill, New York, 1988.
- Hildemann, L.M., G.R. Cass, and G.R. Markowski, A dilution stack sampler for collection of organic aerosol emissions: design, characterization and field tests, *Aerosol Science and Technology*, 10 (1), 193-204, 1989.

- Hopke, P.K., and X.H. Song, Classification of single particles by neural networks based on the computer-controlled scanning electron microscopy data, *Analytica Chimica Acta*, 348 (1-3), 375-388, 1997.
- Kawai, T., Y. Goto, and M. Odaka, Influence of dilution process on engine exhaust nanoparticles, *Society of Automotive Engineers, [Special Publication] SP, SP-1862* (Emissions Measurement & Testing), 113-119, 2004.
- Kirchstetter, T.W., R.A. Harley, N.M. Kreisberg, M.R. Stolzenburg, and S.V. Hering, On-road measurement of fine particle and nitrogen oxide emissions from light- and heavy-duty motor vehicles, *Atmospheric Environment*, 33 (18), 2955-2968, 1999.
- Kittelson, D.B., Engines and nanoparticles - a review, *Journal of Aerosol Science*, 29 (5-6), 575-588, 1998.
- Lake, D.A., M.P. Tolocka, M.V. Johnston, and A.S. Wexler, The character of single particle sulfate in Baltimore, *Atmospheric Environment*, 38 (31 Special Issue SI), 5311-5320, 2004.
- Lee, S.D., M.S. Jang, and R.M. Kamens, SOA formation from the photooxidation of alpha-pinene in the presence of freshly emitted diesel soot exhaust, *Atmospheric Environment*, 38 (16), 2597-2605, 2004.
- Lehmann, U., M. Mohr, T. Schweizer, and J. Rutter, Number size distribution of particulate emissions of heavy-duty engines in real world test cycles, *Atmospheric Environment*, 37 (37), 5247-5259, 2003.
- Lighty, J.S., J.M. Veranth, and A.F. Sarofim, Combustion aerosols: Factors governing their size and composition and implications to human health [Review], *Journal of the Air & Waste Management Association*, 50 (9), 1565-1618, 2000.
- Lyyranen, J., J. Jokiniemi, E.I. Kauppinen, and J. Joutsensaari, Aerosol characterisation in medium-speed diesel engines operating with heavy fuel oils, *Journal of Aerosol Science*, 30 (6), 771-784, 1999.
- Marr, L.C., T.W. Kirchstetter, R.A. Harley, A.H. Miguel, S.V. Hering, and S.K. Hammond, Characterization of polycyclic aromatic hydrocarbons in motor vehicle fuels and exhaust emissions, *Environmental Science & Technology*, 33 (18), 3091-3099, 1999.
- Mathis, U., M. Mohr, and R. Zenobi, Effect of organic compounds on nanoparticle formation in diluted diesel exhaust, *Atmospheric Chemistry & Physics*, 4, 609-620, 2004.
- McDonald, J.D., B. Zielinska, E.M. Fujita, J.C. Sagebiel, J.C. Chow, and J.G. Watson, Fine particle and gaseous emission rates from residential wood combustion, *Environmental Science & Technology*, 34 (11), 2080-2091, 2000.

- Mi, H.H., W.J. Lee, C.B. Chen, H.H. Yang, and S.J. Wu, Effect of fuel aromatic content on PAH emission from a heavy-duty diesel engine, *Chemosphere*, 41 (11), 1783-1790, 2000.
- Moosmuller, H., W.P. Arnott, C.F. Rogers, J.L. Bowen, J.A. Gillies, W.R. Pierson, J.F. Collins, T.D. Durbin, and J.M. Norbeck, Time resolved characterization of diesel particulate emissions. 1. Instruments for particle mass measurements, *Environmental Science & Technology*, 35 (4), 781-787, 2001.
- Morawska, L., N.D. Bofinger, L. Kocis, and A. Nwankwoala, Submicrometer and supermicrometer particles from diesel vehicle emissions, *Environmental Science & Technology*, 32 (14), 2033-2042, 1998.
- Park, K., D.B. Kittelson, and P.H. McMurry, Structural properties of diesel exhaust particles measured by transmission electron microscopy (TEM): Relationships to particle mass and mobility, *Aerosol Science & Technology*, 38 (9), 881-889, 2004.
- Pedersen, P.S., J. Ingwersen, T. Nielsen, and E. Larsen, Effects of fuel, lubricant, and engine operating parameters on the emission of polycyclic aromatic hydrocarbons, *Environmental Science and Technology*, 14 (1), 71-9, 1980.
- Pope, C.A., Review: Epidemiological basis for particulate air pollution health standards, *Aerosol Science & Technology*, 32 (1), 4-14, 2000.
- Rhead, M.M., and S.A. Hardy, The sources of polycyclic aromatic compounds in diesel engine emissions, *Fuel*, 82 (4), 385-393, 2003.
- Robert, M.A., C.A. Jakober, S. VanBergen, and M.J. Kleeman, Size and composition distribution of particular matter emitted from light duty gasoline and heavy duty diesel vehicles, *submitted for publication, Environmental Science & Technology*, 2004.
- Rogge, W.F., L.M. Hildemann, M.A. Mazurek, G.R. Cass, and B.R.T. Simoneit, Sources of fine organic aerosol 2: Nuncatalyst and catalyst-equipped automobiles and heavy-duty diesel trucks, *Environmental Science & Technology*, 27 (4), 636-651, 1993.
- Rudnick, L.R., *Lubricant additives : chemistry and applications*, xiii, 735 pp., Marcel Dekker, New York, 2003.
- Sakurai, H., K. Park, P.H. McMurry, D.D. Zarling, D.B. Kittelson, and P.J. Ziemann, Size-dependent mixing characteristics of volatile and nonvolatile components in diesel exhaust aerosols, *Environmental Science & Technology*, 37 (24), 5487-5495, 2003a.
- Sakurai, H., H.J. Tobias, K. Park, D. Zarling, S. Docherty, D.B. Kittelson, P.H. McMurry, and P.J. Ziemann, On-line measurements of diesel nanoparticle composition and volatility, *Atmospheric Environment*, 37 (9-10), 1199-1210, 2003b.

- Schauer, J.J., Evaluation of elemental carbon as a marker for diesel particulate matter, *Journal of Exposure Analysis and Environmental Epidemiology*, 13 (6), 443-453, 2003.
- Schauer, J.J., W.F. Rogge, L.M. Hildemann, M.A. Mazurek, and G.R. Cass, Source apportionment of airborne particulate matter using organic compounds as tracers, *Atmospheric Environment*, 30 (22), 3837-3855, 1996.
- Schwartz, J., D.W. Dockery, and L.M. Neas, Is daily mortality associated specifically with fine particles, *Journal of the Air & Waste Management Association*, 46 (10), 927-939, 1996.
- Shah, S.D., D.R. Cocker, J.W. Miller, and J.M. Norbeck, Emission rates of particulate matter and elemental and organic carbon from in-use diesel engines, *Environmental Science & Technology*, 38 (9), 2544-2550, 2004.
- Shen, S., P.A. Jaques, Y.F. Zhu, M.D. Geller, and C. Sioutas, Evaluation of the SMPS-APS system as a continuous monitor for measuring PM_{2.5}, PM₁₀ and coarse (PM_{2.5-10}) concentrations, *Atmospheric Environment*, 36 (24), 3939-3950, 2002.
- Sodeman, D.A., S.M. Toner, and K.A. Prather, Determination of single particle mass spectral signatures from light duty vehicle emissions, *accepted for publication, Environmental Science & Technology*, 2005a.
- Sodeman, D.A., S.M. Toner, L.G. Shields, D.T. Suess, D.S. Gross, and K.A. Prather, Comparison of light duty and heavy duty vehicle emissions from dynamometer and tunnel studies using ART-2a, *manuscript in preparation, Aerosol Science & Technology*, 2005b.
- Song, X.H., P.K. Hopke, D.P. Fergenson, and K.A. Prather, Classification of single particles analyzed by ATOFMS using an artificial neural network, ART-2A, *Analytical Chemistry*, 71 (4), 860-865, 1999.
- Spencer, M.T., and K.A. Prather, Comparison of oil and fuel signatures with gasoline and diesel emissions, *in preparation*.
- Suess, D.T., and K.A. Prather, Mass spectrometry of aerosols [Review], *Chemical Reviews*, 99 (10), 3007-3035, 1999.
- Toner, S.M., D.A. Sodeman, and K.A. Prather, Single particle characterization of ultrafine- and fine-mode particles from heavy duty diesel vehicles using aerosol time-of-flight mass spectrometry, *in preparation*.
- Ulrich, A., and A. Wichser, Analysis of additive metals in fuel and emission aerosols of diesel vehicles with and without particle traps, *Analytical & Bioanalytical Chemistry*, 377 (1), 71-81, 2003.

- Van Gulijk, C., J.C.M. Marijnissen, M. Makkee, J.A. Moulijn, and A. Schmidt-Ott, Measuring diesel soot with a scanning mobility particle sizer and an electrical low-pressure impactor: performance assessment with a model for fractal-like agglomerates, *Journal of Aerosol Science*, 35 (5), 633-655, 2004.
- Vogt, R., U. Kirchner, V. Scheer, K.P. Hinz, A. Trimborn, and B. Spengler, Identification of diesel exhaust particles at an Autobahn, urban and rural location using single-particle mass spectrometry, *Journal of Aerosol Science*, 34 (3), 319-337, 2003.
- Xie, Y., P.K. Hopke, and D. Wienke, Airborne particle classification with a combination of chemical composition and shape index utilizing an adaptive resonance artificial neural network, *Environmental Science & Technology*, 28 (11), 1921-1928, 1994.
- Yanowitz, J., M.S. Graboski, L.B.A. Ryan, T.L. Alleman, and R.L. McCormick, Chassis dynamometer study of emissions from 21 in-use heavy duty diesel vehicles, *Environmental Science & Technology*, 33 (2), 209-216, 1999.
- Yanowitz, J., R.L. McCormick, and M.S. Graboski, In-use emissions from heavy-duty diesel vehicles, *Environmental Science & Technology*, 34 (5), 729-740, 2000.

Single Particle Characterization of Ultrafine- and Fine-Mode Particles from Heavy Duty Diesel Vehicles using Aerosol Time-of-Flight Mass Spectrometry

3.1 Introduction

Of the anthropogenic sources of particles, diesel powered vehicles have been of increasing environmental concern. While they tend to have lower fuel consumption and CO₂ emissions, they have greater (by one to two orders of magnitude) particulate matter emissions than do gasoline powered vehicles [Kittelson, 1998]. Many studies have been conducted on the particulate matter released in diesel emissions. These studies have included insight as to possible health effects [Dybdahl *et al.*, 2004; Pourazar *et al.*, 2004; Reed *et al.*, 2004; Zhao *et al.*, 2004], as well as size and number concentrations of particles emitted by diesel vehicles [Khalek *et al.*, 2003; Kwon *et al.*, 2003; Lehmann *et al.*, 2003; Lyyranen *et al.*, 1999a; Moosmuller *et al.*, 2001; Reilly *et al.*, 1998; Sakurai *et al.*, 2003a; Schauer *et al.*, 1999; Shi *et al.*, 2000; Virtanen *et al.*, 2004; Yanowitz *et al.*, 1999]. Many of these studies have shown that the emissions from diesel engines produce high number concentrations of ultrafine particles, especially during idle and low RPM engine operation. While some studies have included diesel particulate matter chemical composition, they generally use filter techniques such as Micro Orifice Uniform Deposit Impactors (MOUDI) to collect particles of different size ranges and can not provide single particle chemical information or high temporal resolution of chemical species. Analysis of the particles collected on filters can be useful for determining organic species and mass of different species, but they can not provide details on individual particle types. Detailed information of individual particle types emitted by diesel engines is crucial for understanding their origin as well as what kind of environmental and health impacts they may have. With such a large fraction of the particles emitted from diesels occurring in the low fine and ultrafine size range, it is important to be able to characterize these particles on the single particle level.

Single particle mass spectrometry techniques, such as aerosol time-of-flight mass spectrometry (ATOFMS), are very useful in characterizing particles in the fine (100 – 1000nm) and coarse (>1000nm) size ranges. Recently, the ATOFMS instrument has been fitted with an aerodynamic lens for improved transmission of smaller fine and ultrafine particles [Su *et al.*, 2004]. This instrument has been used for this study to provide single particle characterization of ultrafine and fine diesel emissions and is referred to as an ultrafine aerosol time-of-flight mass spectrometer (UF-ATOFMS). Other particle mass spectrometers, such as the thermal desorption particle beam mass spectrometer (TDPBMS) [Sakurai *et al.*, 2003b; Tobias *et al.*, 2001; Tobias *et al.*, 2000] and the Aerodyne aerosol mass spectrometer (AMS) [Canagaratna *et al.*, 2004; Jayne *et al.*, 2000], have been used to characterize particles emitted from diesels engines. However, these techniques are not sensitive to non-volatile components in particles, such as elemental carbon, that make up a large fraction of diesel emissions.

The goal of this study is to chemically characterize the ultrafine and low-fine mode (50 – 300 nm) diesel exhaust particles to determine single particle mass spectral signatures that are unique to heavy duty diesel vehicles (HDDVs). These signatures can then be used with those obtained from previous ATOFMS studies for HDDV exhaust (100 – 3000 nm) and gasoline vehicle (LDV) exhaust (50 – 3000 nm) for the purpose of ambient source apportionment of HDDV and LDV exhaust, which will be tested on data obtained during a freeway-side ATOFMS study.

3.2 Experimental

Six HDDVs were analyzed between June and July in 2003 at the Ralph's Distribution center in Riverside, CA. A description of each truck is provided in Table 3.1, including the vehicle/engine year, manufacturer, engine power, miles driven, and driving cycles performed. The HDDVs were tested under the same sampling conditions, including the driving schedule and real-world dilution conditions, so the major aerosol chemical disparities observed between trucks are attributed to the differences between trucks and not sampling and/or instrumental variability [Suess and Prather, 2002].

The sampling conditions consisted of driving each truck on a heavy duty dynamometer operated by West Virginia University personnel. This transportable heavy duty vehicle emissions testing laboratory (THDVETL) is used to obtain reproducible aerosol emissions from HDDV and is described elsewhere [Bata *et al.*, 1991; Clark *et al.*, 1995]. For this study, the heavy heavy-duty diesel truck (HHDDT) five-cycle driving schedule under different simulated weight loads was used to determine the effect of driving conditions on the exhaust aerosol's chemical composition. The HHDDT five-cycle schedule was developed by the California Air Resources Board (CARB) and consists of an idle, creep, transient, cruise, and a high-speed cycle. The idle stage consists of the truck idling for 30 minutes with no acceleration periods. The creep stage consists of small accelerations and decelerations, maintaining speeds less than 10 mph, which simulates heavy traffic conditions. The transient stage consists of fast and short periods of accelerations and decelerations with speeds up to 50 mph and is a simulation of city-street and some highway driving conditions. The cruise cycle mimics driving conditions encountered on highways and maintains speeds between 50 - 60 mph for the majority of the cycle. The final cycle of the 5-cycle test, named HDDT_S / HHDDT65, is a simulation of higher speed driving and acceleration, with speeds up to 65 mph. The high-speed cycle was altered during the study from a 31 minute test (HHDDT65) to a 13 minute test (HDDT_S) for efforts of stress relief on the dynamometer.

Three different (on axle) simulated weight loads were used to determine the effect of engine load on exhaust emissions. These loads were 56,000 lbs, 66,000 lbs, and 75,000 lbs, representing increasingly laden driving conditions. The different loads were not tested on all HDDVs; however, all vehicles except one were tested at the 56,000 lbs load. Only one truck was able to be tested at 75,000 lbs and one other at 66,000 lbs due to stress issues on the dynamometer. The truck tested at 66,000 lbs was also tested at 56,000 lbs, and the differences in loads, as it pertains to particle composition, will be discussed.

Upon exiting the exhaust pipe of the HDDV, the diesel exhaust is passed through a constant volume sampling system, which is part of the THDVETL [Bata *et al.*, 1991; Clark *et*

Table 3.1 Heavy Duty Diesel Vehicles (HDDVs) tested and driving cycles performed.

E55CRC (truck)	Vehicle Model Year	Vehicle Manufacturer	Engine Model Year	Engine Manufacturer	Engine Model	Engine Power (hp)	Mileage	Tests Performed
E55CRC-27	2000	Freightliner	1999	Detroit	Diesel Series 60	500	420,927	C*
E55CRC-28	1999	Freightliner	1998	Detroit	Diesel Series 60	500	539,835	IC, A*
E55CRC-30	1999	Freightliner	1998	Detroit	Diesel Series 60	500	138,553	IC, A
E55CRC-31	1998	Kenworth	1997	Cummins	N14-460E+	460	587,265	A, B
E55CRC-32	1992	Volvo	1991	Caterpillar	3406B	280	595,258	A
E55CRC-33	1985	Freightliner	1984	Caterpillar	3,406	310	988,823	A

Five cycle test at A) 56,000 lbs / B) 66,000 lbs / C) 75,000 lbs

30 min idle

10 min soak

17 min creep

10 min soak

11 min transit

10 min soak

34 min cruise with speeds at 55 mph

10 min soak

13 min "high speed" HDDT_S cycle at 65 mph *(31 min "high speed" HHDDT65 at 65 mph)

stop cycle

56,000 lbs idle-creep cycle (IC)

Idle truck for 30 min

run at "creep" speeds for 17 min

10 min soak with engine off

repeat 5x

al., 1995], and is used for primary dilution. Secondary dilution was achieved by sampling off of the primary dilution tunnel with a Stack Dilution Tunnel (SDT) at a constant flow [McDonald *et al.*, 2000]. The secondary dilution with the SDT was used to simulate realistic atmospheric dilution conditions, allowing for equilibrium of the semi-volatile organic fraction between the gas and particle phase [Hildemann *et al.*, 1989]. Dilution ratios for each HDDV and cycle performed are summarized in Table 3.2.

For this study, an ultrafine aerosol time-of-flight mass spectrometer (UF-ATOFMS) was used to size and chemically characterize HDDV exhaust particles between 50 and 300 nm. The UF-ATOFMS instrument along with an aerodynamic particle sizer (APS) (TSI Model 3321 – Minnesota) and a scanning mobility particle sizer (SMPS) (TSI Model 3936L10 – Minnesota) sampled off of the SDT residence chamber continuously for each truck testing period. Stainless steel sampling lines were used to sample from the residence chamber to the instrumentation and were coupled to the instruments with black conductive tubing (TSI). A diagram of the sampling system is provided in Figure 3.1 [Robert *et al.*, 2004].

Data obtained from this study were imported into Matlab 6.1.0.450 (Release 12.1) and analyzed with the ART-2a neural network data analysis algorithm [Hopke and Song, 1997; Song *et al.*, 1999; Xie *et al.*, 1994] with a vigilance factor of 0.85, learning rate of 0.05 and 20 iterations. This method of analysis has been shown to be reliable for ATOFMS data and is used for this study for consistency as well as to compare to previous and future studies using the same technique. For this paper, the focus is on the emissions sampled with the UF-ATOFMS instrument and the SMPS. Single particle HDDV emissions (100 – 3000nm) have been sampled and reported with a standard-inlet ATOFMS instrument previously [Shields *et al.*, 2005] and will be used as a basis of comparison in this paper.

3.3 Results and Discussion

3.3.1 Description of particle types observed with UF-ATOFMS

Formation of diesel exhaust particles in the fine and ultrafine size mode has been studied and described elsewhere [Burtscher *et al.*, 1998; Kittelson, 1998; Tobias *et al.*, 2001]. These previous accounts of HDDV exhaust have mainly focused on size profiles of the exhaust particles, or chemical composition through bulk analysis on filters. This study, however, reports the first single particle chemical composition analysis of ultrafine and fine mode particles from HDDV exhaust. As previously stated, the data were imported into Matlab and analyzed with the ART-2a neural network data analysis technique, where particles are grouped into clusters (classes) based on their similarity of mass spectra. Performing this data analysis technique resulted in seven main particle classes for this HDDV data set with 100 % of the sampled particles being classified. Representative spectra / weight-matrices for the seven classes are shown in Figure 3.2 (A-G), and Figure 3.3 shows the statistical breakdown of these classes (in the same order of spectra shown).

The top particle class (Figure 3.2A and labeled as *EC*, *Ca*, *OC*, *Phosphate* in Figure 3.3) makes up 78% of the particles sampled by UF-ATOFMS in the ultrafine and fine particle modes. The positive ion mass spectra for this class consist of elemental carbon (EC) ($^{12}\text{C}_1^+$, $^{24}\text{C}_2^+$, $^{36}\text{C}_3^+$, $^{48}\text{C}_4^+$, $^{60}\text{C}_5^+$), calcium ($^{40}\text{Ca}^+$, $^{56}\text{CaO}^+$), and organic carbon (OC) seen as peaks at m/z 27⁺ and 29⁺.

Table 3.2 Dilution ratios (DR) for each HDDV and cycle.

HDDV	Cycle	Cycle time (sec)	Dilution Ratio Information		Cycle DR
			WVU Primary Dilution	UCD Secondary Dilution	
E55CRC-27 5-cycle 75,000lbs	Idle	1800	130.0	10.0	1300.0
	Creep	1032	77.0	10.0	770.0
	Trans	688	17.0	10.0	170.0
	Cruise	2083	12.0	9.7	116.4
	HHDDT65	739	7.0	9.0	63.0
E55CRC-28 Idle/Creep	Idle/Creep	2831	117.9	5.2	618.2
	Idle/Creep	2831	117.4	5.2	615.5
	Idle/Creep	2831	119.7	5.2	627.4
	Idle/Creep	2831	117.1	5.2	614.1
	Idle/Creep	2831	121.4	5.2	636.6
E55CRC-28 5-cycle 56,000lbs	Idle	1799	139.9	30.1	4211.0
	Creep	1031	101.0	35.2	3555.2
	Trans	687	24.4	26.6	649.0
	Cruise	2082	13.0	26.6	345.8
	HHDDT65	1899	12.0	27.8	333.6
E55CRC-30 Idle/Creep	Idle/Creep	2831	110.2	5.2	573.0
	Idle/Creep	2831	110.5	5.2	573.3
	Idle/Creep	2831	111.2	5.2	577.0
	Idle/Creep	2831	113.4	5.2	588.4
	Idle/Creep	2831	115.1	5.2	597.0
E55CRC-30 5-cycle 56,000lbs	Idle	1799	121.9	10.0	1221.1
	Creep	1031	73.3	10.0	734.1
	Trans	687	19.7	9.7	189.8
	Cruise	2082	13.4	9.3	125.2
	HDDT S	759	9.1	9.0	82.6
E55CRC-31 5-cycle 56,000lbs	Idle	1799	133.3	10.0	1334.9
	Creep	1031	78.7	10.0	788.0
	Trans	687	20.7	10.0	207.7
	Cruise	2082	13.4	9.7	129.2
	HDDT S	759	9.8	9.3	91.4
E55CRC-31 5-cycle 66,000lbs	Idle	1799	129.4	10.0	1296.0
	Creep	1031	80.2	10.0	803.6
	Trans	687	20.5	10.0	205.7
	Cruise	2082	15.0	9.7	144.6
	HDDT S	759	10.1	9.3	93.8
E55CRC-32 5-cycle 56,000lbs	Idle	1799	120.2	9.7	1160.6
	Creep	1031	84.4	10.0	845.8
	Trans	687	26.0	9.7	251.1
	Cruise	2082	14.8	9.0	133.6
	HDDT S	759	12.2	8.8	106.8
E55CRC-33 5-cycle 56,000lbs	Idle	1799	122.7	10.0	1229.3
	Creep	1031	84.2	10.0	843.2
	Trans	687	24.7	9.5	234.1
	Cruise	2082	15.1	8.8	132.6
	HDDT S	759	10.1	8.5	85.8

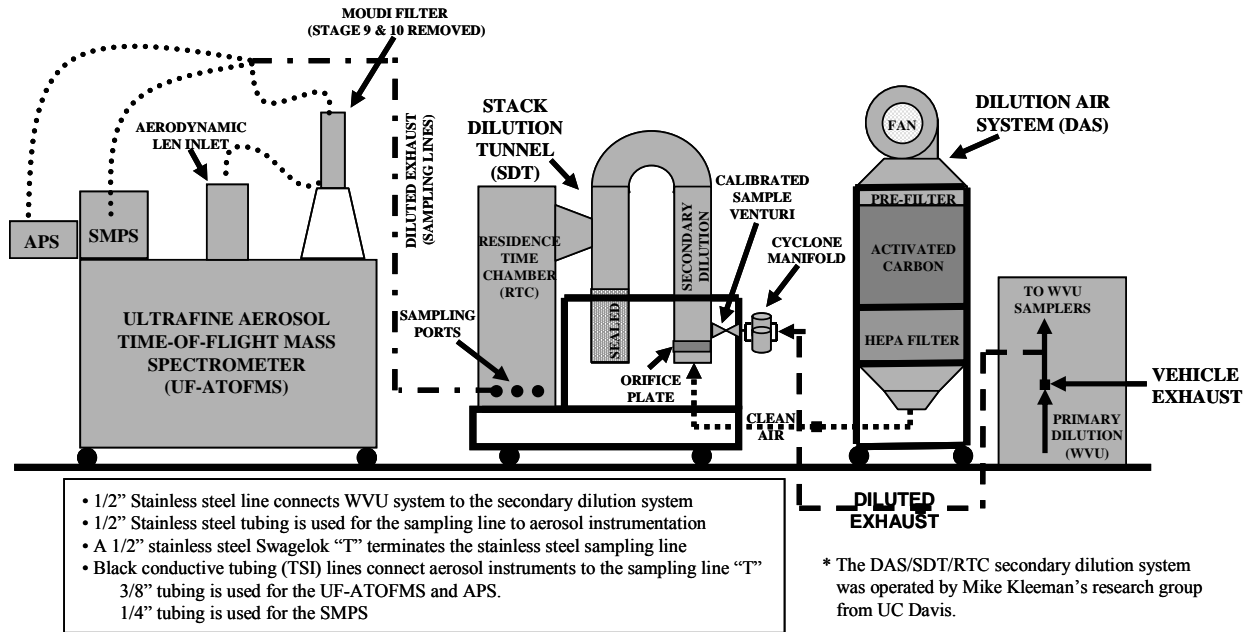


Figure 3.1 Sample collection system. (Figure derived from *Robert et al.*, 2004)

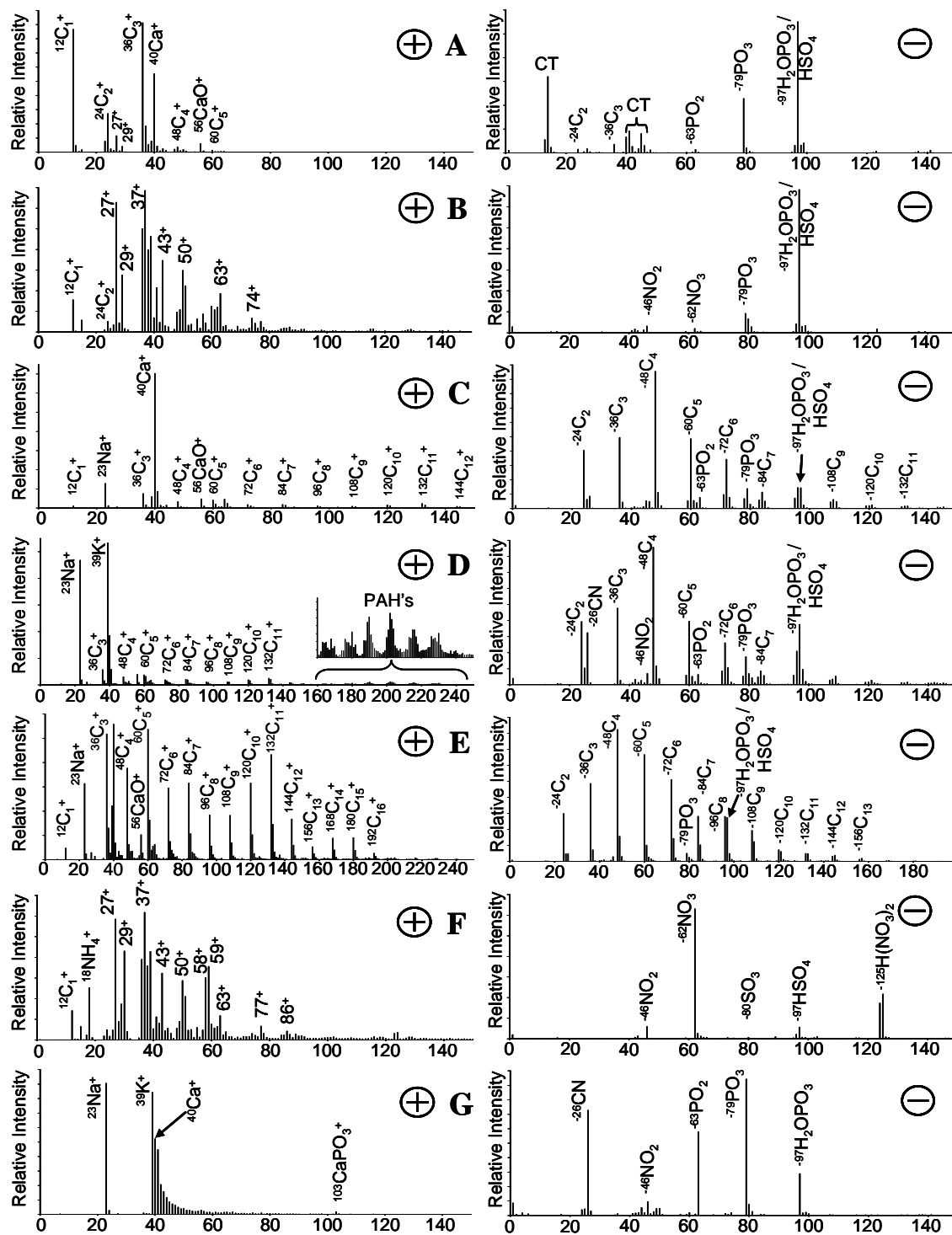


Figure 3.2 (A – G), Positive and negative ion representative mass spectra / weight matrices for the particle classes from HDDV exhaust. A) *EC, Ca, OC, Phosphate*; B) *OC, EC, Phosphate, Sulfate*; C) *Ca, Na, EC, Phosphate, Sulfate*; D) *Na, K, Ca, EC, PAH, Phosphate, Nitrate, Sulfate*; E) *EC, Ca, Na, OC, Phosphate, Sulfate*; F) *OC, Amines, Nitrates, Sulfates*; G) *Na, K rich w/ Ca, Phosphate, Nitrates*. *Peaks labeled “CT” in negative ion spectra indicate signal “cross-talk” from the positive ion detector.

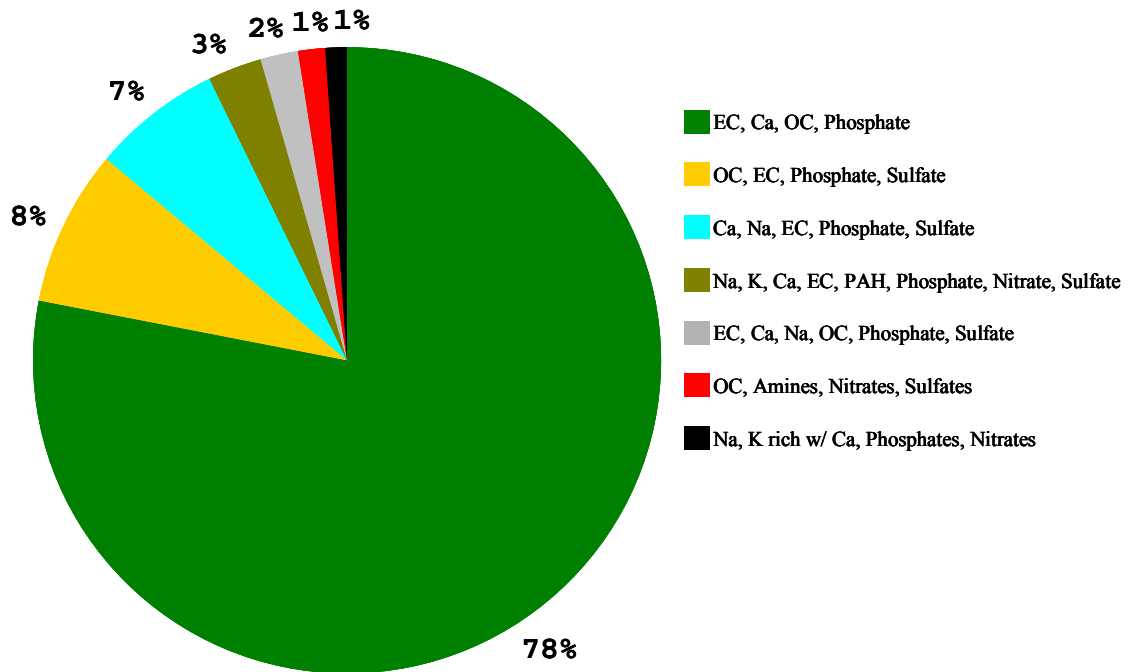


Figure 3.3 Statistical breakdown of the particle classes observed from the HDDV exhaust.

The negative ion spectra contain peaks due to phosphate ($^{-97}\text{H}_2\text{OPO}_3$, $^{-79}\text{PO}_3$, $^{-63}\text{PO}_2$) and some EC ($^{-24}\text{C}_2$, $^{-36}\text{C}_3$). The peak at m/z -97 can also be attributed to $^{-97}\text{HSO}_4$. Based on the spectrum, it would appear that the EC in this class are primarily short chain EC (C_n^+ where $n < 6$). This could be the case, however, it has been shown that as particle size goes down (especially in the ultrafine and low fine size range), the extent of fragmentation through laser desorption/ionization (LDI) techniques goes up [Schoolcraft *et al.*, 2001; Schoolcraft *et al.*, 2000]. While the EC in this class could actually be short-chained, the effect of LDI on small particles would also provide a good explanation as to why this class appears to be composed of short chained EC. Another note to make about the EC peaks in this class is that the peak for $^{36}\text{C}_3^+$ is larger than that of $^{12}\text{C}_1^+$. This finding is significant and will be addressed later in the discussion when referring to the prospects for ambient apportionment. The presence of calcium and phosphate in this class is consistent with additives typically found in diesel engine lubrication oil [Gautam *et al.*, 1999; Harrison *et al.*, 2003; Rudnick, 2003]. Calcium is added to vehicle lubricants commonly in the form of calcium carbonate and calcium sulfonate to act as a detergent to neutralize acidic combustion byproducts and to prevent accumulation of deposits in the engine [Rudnick, 2003]. Phosphate is typically added to engine lubricants in the form of organic zinc phosphates and functions as an anti-wear agent [Gautam *et al.*, 1999]. The nebulization of the oil and fuel samples retrieved from each truck sampled during the HDDV study and analysis with an ATOFMS show the presence of these additives in similar amounts to those detected in the HDDV exhaust spectra [Spencer *et al.*, 2005]. The lack of zinc detected in this type (and others) is likely due to the insensitivity of ATOFMS towards that particular metal. For other particle types, the m/z peaks of Zn (m/z 64, 66, 68) can be masked by peaks from organic carbon. These findings strongly suggest that this main class of particles seen in HDDV exhaust is from engine lubricating oil or coagulation of lubricating oil aerosols with EC from incomplete combustion. These results agree with the findings by other researchers that lubricating oil is found in the majority of diesel exhaust particles [Canagaratna *et al.*, 2004; Jung *et al.*, 2003; Lyyranen *et al.*, 1999b; Okada *et al.*, 2003; Sakurai *et al.*, 2003b; Tobias *et al.*, 2001; Vilhunen *et al.*, 1999].

The second most abundant particle type is shown in Figure 3.3B (labeled as *OC, EC, Phosphate, Sulfate* in Figure 3.3) and makes up 8% of the particles characterized with the ATOFMS. The positive ion mass spectra of this class are dominated by peaks due to the fragmentation of organic carbon, which are labeled by mass-to-charge (as there are many possibilities to their organic compositions), and to a lesser extent, the presence of EC. While LDI causes extensive fragmentation of organics present on particles and makes it difficult to identify the parent species, it is possible to distinguish certain types of organics. In the case of this positive ion spectrum, the presence of m/z 63^+ and 74^+ can be attributed to aromatic containing organics which have been previously characterized using an ATOFMS [Silva and Prather, 2000]. The presence of low mass organic fragments m/z 27^+ , 29^+ , 37^+ , 43^+ and 50^+ are typically associated with long-chain aliphatic organics, but can also result from the fragmentation of many other types of organic species. These fragments can also occur from reactions of radicals and/or ions in the ion plume created by the LDI process. The negative ion mass spectra are similar to those seen in the top class, containing $^{-97}\text{H}_2\text{OPO}_3$ / $^{-97}\text{HSO}_4$, and $^{-79}\text{PO}_3$, however, this class also contains ions due to NO_x species ($^{-46}\text{NO}_2$, $^{-62}\text{NO}_3$). The presence of NO_x species in the particles can indicate incomplete combustion of air in the engine or possible high exhaust temperatures. They could also derive from oxidation of the nitrogen-containing organics from the diesel fuel [Arens *et al.*, 2001; Hughey *et al.*, 2001]. The presence of phosphates in the

negative ion mass spectra makes this class appear to be from engine oil lubricant. However, in the positive ion spectra, there is no presence of calcium. This might suggest that this particle type originated from lubricating oil as an indicator of the job being performed by the ZDP additive, scavenging engine deposits before being emitted into the exhaust. Another possibility is that there was a sufficient amount of an organic coating to effectively suppress the presence of calcium and EC (given the high surface area of EC—this is highly likely) in the particle. The incomplete combustion of fuel would provide semi-volatile organic species that could condense onto these particles, thus contributing to the OC content of the particle.

The third most abundant particle type observed makes up 7% of the HDDV exhaust particles classified with the ATOFMS and is represented in Figure 3.2C (labeled as *Ca, Na, EC, Phosphate, Sulfate* in Figure 3.3). This particular class contains a strong ion signal due to calcium ($^{40}\text{Ca}^+$) in the positive ion mass spectra, as well as lesser peaks due to sodium ($^{23}\text{Na}^+$), long-chained EC (C_n^+ where $n \geq 6$) and potassium ($^{39}\text{K}^+$). The negative ion mass spectra are also dominated by long-chained EC and contain peaks due to $^{-97}\text{H}_2\text{OPO}_3$ / $^{-97}\text{HSO}_4$, $^{-79}\text{PO}_3$, and $^{-63}\text{PO}_2$ as well. This class appears to have originated from lubricating oil as it is very similar to the top class, except for that this class contains sodium and higher m/z EC fragments. The presence of sodium can be from a variety of sources, including impurities in the lubricating oil and/or from the diesel fuel. The ATOFMS lab-analyzed diesel fuel samples show the presence of sodium more frequently than in the oil samples. The presence of sodium on these oil-type particles may be from the oil itself or from the release of sodium during the diesel fuel combustion where the freed sodium could adhere to other particles. The higher m/z EC fragments seen in these spectra could also be from a variety of reasons. The most reasonable explanations could be that the EC in this particle type is from more developed, longer chained soot/EC, or it could also result from the LDI process. It is known that soot can form long-chain EC/soot agglomerates, and this process occurs in the ultrafine and fine size modes [Arens *et al.*, 2001; Kittelson, 1998; Shi *et al.*, 2000; Van Gulijk *et al.*, 2004; Walker, 2004]. The issue of the LDI process on these particles always remains though. It has been shown that there are differences with ATOFMS spectra for the same particle type based solely on the LDI laser [Wenzel and Prather, 2004]. These effects include ionizing the particle in cold or hot spots of the laser beam where the power density is different enough to cause softer or harder ionization (respectively).

The fourth most abundant classified particle type makes up 3% of the total particles and is represented in Figure 3.2D (labeled as *Na, K, Ca, EC, PAH, Phosphate, Nitrate, Sulfate* in Figure 3.3). This class consists of positive ion mass spectra with strong potassium ($^{39}\text{K}^+$) and sodium ($^{23}\text{Na}^+$) signals, as well as smaller peaks attributed to EC (C_{1-11}^+) and peaks due to polycyclic aromatic hydrocarbons (PAH's) in the higher mass range (m/z 163, 168, 176, 180, 190, 202, 216, 226 and 230). Since the ATOFMS is very sensitive to both potassium and sodium, their peak intensities are greater than those of the EC and PAH's which makes it difficult to see them in the representative weight matrix (which is sensitive to relative areas). The negative ion mass spectra for this class consist of EC, phosphates, sulfate, $^{-46}\text{NO}_2$ and ^{-26}CN . This particle type may be due to the incomplete combustion of lubricating oil (as the negative ion spectra suggests) however, it appears to be more from a mixture of diesel oil and fuel combustion. Spectra showing sodium and potassium with such strong intensities resemble those detected in the lab-analyzed diesel fuel samples [Spencer *et al.*, 2005]. The presence of PAH's has been seen in both fuel and oil samples and could be from either source, or could have formed during combustion and condensed onto the particles.

The fifth most abundant class, making up 2% of the total HDDV exhaust particles, is represented in Figure 3.2E (labeled *EC, Ca, Na, OC, Phosphate, Sulfate* in Figure 3.3). This class has positive ion mass spectra containing calcium, long-chained EC (C_{1-16}^+), sodium, and some minor peaks attributed to OC. The negative ion mass spectra are composed of long-chained EC (C_{1-13}), $^{-97}H_2OPO_3$ / $^{-97}HSO_4$, and $^{-79}PO_3$. While this class has a very similar composition to that of the third class, the major difference is that this class has much more intense EC ion intensities, and the presence of some OC. Despite the differences, this class does appear to be from the same source as the third class.

The sixth class, represented in Figure 3.2F (labeled *OC, Amines, Nitrates, Sulfates* in Figure 3.3), makes up 1% and appears to be from incomplete combustion of the diesel fuel. The positive ions for this class are composed primarily of peaks due to OC, as well as peaks due to amines (or possibly nitrogen containing organics) at m/z 58^+ , 59^+ , and 86^+ [Angelino *et al.*, 2001], and peaks due to aromatic organics (m/z 63^+ and 77^+). While the negative ion spectra contain peaks for $^{-46}NO_2$, $^{-62}NO_3$, $^{-125}H(NO_3)_2$, $^{-80}SO_3$, and $^{-97}HSO_4$ (generically labeled as nitrates and sulfates, respectively). The peaks in the negative ions due to the nitrate species is an indication of incomplete combustion, and the presence of the sulfate species (with no presence of phosphate species) indicates that this is more likely from the combustion of fuel than from the lubricating oil. This source assignment is corroborated by the laboratory ATOFMS analysis of diesel fuel [Spencer *et al.*, 2005].

The final class, making up the remaining 1% of the total particles, is represented in Figure 3.2G (labeled *Na, K rich w/Ca, Phosphates, Nitrates* in Figure 3.3). This class is very unique, compared to the other classes, in that it is only composed of inorganic species. The positive ion mass spectra contain sodium, potassium, calcium and calcium phosphate ($^{103}CaPO_3^+$). While the negative ion mass spectra contain phosphates ($^{-97}H_2OPO_3$, $^{-79}PO_3$, $^{-63}PO_2$), ^{-26}CN , and $^{-46}NO_2$. The species present in this class would indicate that it is the result of the salts in the additives from the lubricating oil and fuel combining after combustion.

3.3.2 Analysis of Size Segregated Chemical Composition for each HDDV

Prior studies on HDDV exhaust have included in-depth accounts of particle size distributions based on engine load and speed [Khalek *et al.*, 2003; Kwon *et al.*, 2003; Lehmann *et al.*, 2003; Lyyranen *et al.*, 1999a; Moosmuller *et al.*, 2001; Reilly *et al.*, 1998; Sakurai *et al.*, 2003a; Schauer *et al.*, 1999; Shi *et al.*, 2000; Virtanen *et al.*, 2004]. For this study, not only was size information obtained with the UF-ATOFMS instrument, but with a scanning mobility particle sizer (SMPS) and an aerodynamic particle sizer (APS) as well. The SMPS was used to obtain “true” sizing information and for the purpose of scaling the UF-ATOFMS data. The average size distribution (from SMPS and APS) for all HDDVs during their five-cycle tests is shown in Figure 3.4. While this is an average for all HDDVs tested, the profile for each stage of the 5-cycle test is relatively consistent for each HDDV. What this figure shows, which correlates with the aforementioned studies, is that particle number concentrations peak in the ultrafine size mode under lower engine loads (lower rpm). Also, as engine loads increase (increasing rpm), the particle number concentrations go down in the ultrafine mode and shift more to the accumulation mode range. The vertical dashed lines on the plot indicate the particle sizing range of the UF-ATOFMS. Since the lower particle size limit of the UF-ATOFMS is at 50nm, the hierarchy of particle number concentration based on cycle will be different for the UF-ATOFMS. Studies by

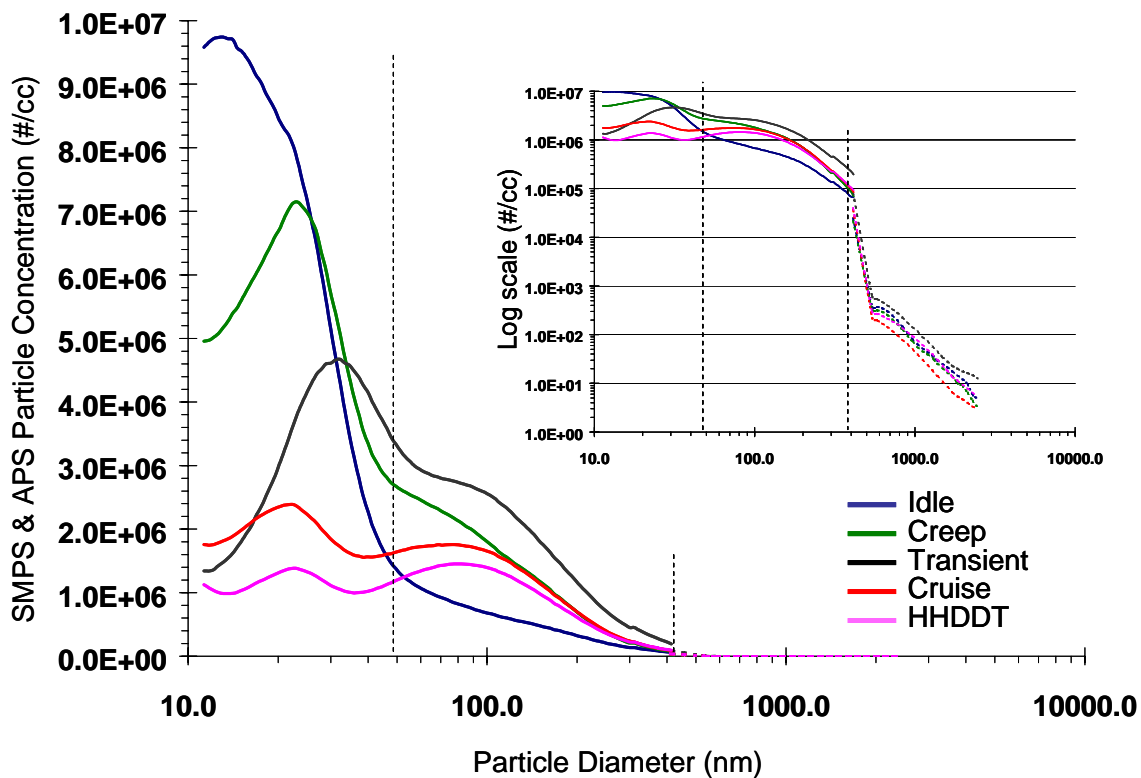


Figure 3.4 Average size distribution (from SMPS and APS) for all HDDVs during the 5-cycle tests. The solid colored lines on both plots are for the SMPS data and the dashed colored lines on the log-scale plot are for the APS measurements. The vertical dashed lines represent the sizing range of the UF-ATOFMS.

Tobias *et al*, and Sakurai *et al*, have included chemical composition analysis of particles by size for HDDV engines, but not on the single particle level, nor with the ability to detect refractory materials such as EC, metals, and metal oxides. One of the unique abilities of an ATOFMS is that both organic and inorganic species can be detected and their associations analyzed for single particles in real time. This allows us to provide size segregated chemical composition information about the particle classes observed for each HDDV, and this is shown in Figure 3.5(A-I).

Figure 3.5 shows the UF-ATOFMS particle classes scaled to the SMPS number concentrations for combined size bins for each HDDV on each test. Combining certain SMPS size bins allows us to ensure that there are enough UF-ATOFMS particle counts in each particular bin to provide reliable particle statistics. Data missing from a certain size bin indicates that there were not enough UF-ATOFMS particle counts for that particular bin to make scaling for that size bin statistically acceptable. The rule set for scaling was that for each size bin there had to be at least eight particles. Also, the data in each plot have been multiplied by a factor (indicated on each plot) to keep them all on the same scale.

As Figure 3.5 shows, the main particle type for generally all size bins and for each HDDV is that of the top particle class (*EC, Ca, OC, Phosphate*). This is particularly true for the smaller size bins, but as particle size goes up, the composition changes for some HDDVs. E55CRC-30 (Figure 3.5D,E) is an anomaly to this scenario, where the idle/creep cycle (3.5D) is dominated by the second particle class (*OC, EC, Phosphate, Sulfate*) for all size bins and still contains a significant amount of this class for the size bins in the 5-cycle test (3.5E). Since the HDDVs E55CRC-27, 28, and 30 (Figure 3.5A-D) have enough counts to show scaled data out to 294nm, they can show a trend of particle composition as size increases. The larger size bins show that some of the more minor classes (especially the organic carbon containing classes) start to become more prevalent as particle size increases. This is an indication of semi-volatile organic vapors condensing onto HDDV exhaust particle EC cores to create larger particles with more of an organic coating. For each HDDV, from 50-178nm, the overall particle class breakdown per size bin seems to be relatively constant. That is, to say, that there is not much variation per size bin composition for a given HDDV (excluding E55CRC-27 and 30).

Another feature to note about Figure 3.5 concerns the number concentration per size bin for each HDDV. The scale is set by E55CRC-30 (Figure 3.5D) during the idle/creep cycle, where the particle concentrations peaked in the 50-75nm size bin. The number concentration falls quite dramatically with this particular HDDV as particle size goes up, but this is expected of an idle/creep cycle. The idle/creep cycle for E55CRC-28 (Figure 3.5B) does not show this type of trend though, which is particularly interesting since they are of the same make/model and year (and E55CRC-28 has higher engine mileage). Another interesting note is about the E55CRC-31 which ran the 5-cycle test at 56,000 lbs and 66,000 lbs (Figure 3.5F,G). The particulate emissions for the 66,000 lbs test were a little over 1.5 times more per size bin than for the 56,000 lbs test. However, it is noticeable that for each size bin, the relative particle compositions remain fairly constant between the two loads. Another trend that can be noted from all the HDDVs (excluding E55CRC-30) is that particle number concentrations over all size bins (50-294nm) tend to increase with older HDDV models.

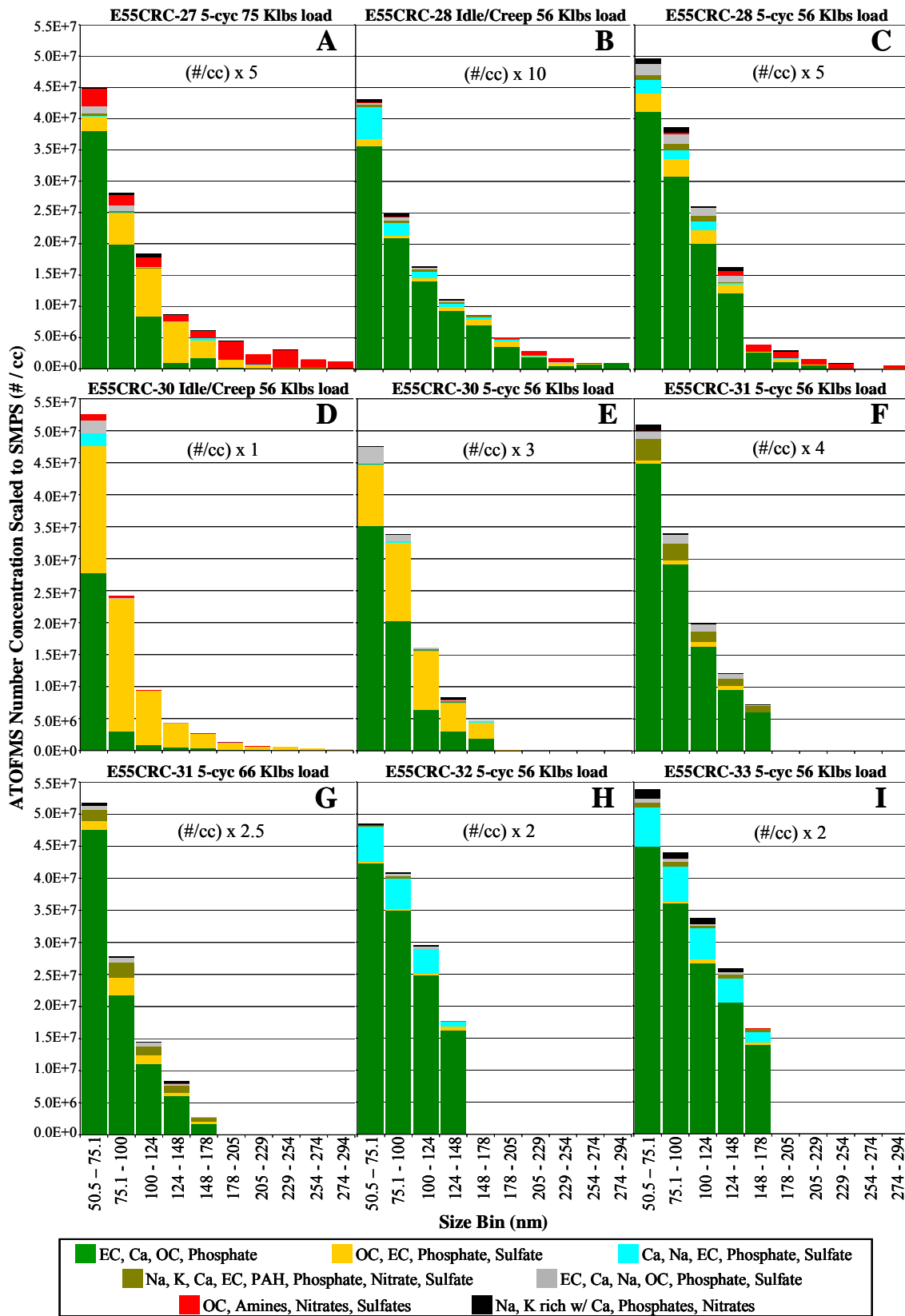


Figure 3.5 (A - I), UF-ATOFMS size segregated chemical composition of particles observed for each HDDV for each driving test scaled to SMPS. Size bins are created from SMPS data, where certain bins were combined to provide 20-25nm size bins.

3.3.3 Particle Composition as a Function of Driving Cycle & HDDV

It is expected that different HDDVs will contain particles with a range of compositions in their exhaust. Differences in fuel, oil, engine technology and engine wear would account for some of the major factors in these particle composition variations. Figure 3.6(A-I) shows the UF-ATOFMS particle classes scaled to the SMPS number concentrations for each HDDV on each test cycle. Since the UF-ATOFMS is unable to detect particles below 50nm, the number concentration trends per cycle for these plots in Figure 3.6 will follow the trend for each cycle within the dashed lines as previously discussed in Figure 3.4. Also, the data from each plot in Figure 3.6 have been multiplied by a factor (indicated on each plot) to keep them all on the same scale.

As shown in Figures 3.3 and 3.5, the major class for each cycle on most trucks is that of the top particle class (*EC, Ca, OC, Phosphate*). E55CRC-27 and 30 show the most variation where there is a major influence from organic containing particles. One of the most important functions of these plots is that they can show what kind of driving conditions produce certain types of particles. This is more clearly noticed with the minor classes, as they may only be in just one cycle for a particular HDDV. These plots (as well as in the previous figure) show that not all HDDVs produce the same particle types. This is even true for E55CRC-28 and -30 (Figure 3.6B-E), which are of the same make/model and year, but emit different particle types and different amounts of the same particle types for the same driving cycles.

Since there were only six HDDVs tested in this study, it is rather difficult to make a generalization for all HDDVs and driving cycles based on these results. One trend that remains consistent for all tests and vehicles is the presence of the top particle class (*EC, Ca, OC, Phosphate*). While this may not always be the dominant class for each cycle and size bin, it is consistently present for each HDDV tested and may therefore be useful for ambient apportionment purposes, which will be discussed later.

3.3.4 Comparison of Ultrafine and Lower-Fine Mode to Fine/Coarse Mode Particles

As described at the beginning of this chapter, a previous study on HDDV particulate emissions was conducted with a standard inlet ATOFMS on the same dynamometer system in Riverside, CA in 2001 [*Shields et al., 2005*]. While the ATOFMS instrument used for the earlier study was tuned to characterize particles down to 100nm, it had a much lower transmission efficiency for smaller particles than the UF-ATOFMS [*Su et al., 2004*]. This overlap allows for comparison of particle types seen in the same size range for two different ATOFMS instruments; however, it is important to note that the UF-ATOFMS will have better compositional statistics at smaller sizes based on its greater transmission efficiency.

As with the particle classes in the 2003 study, the top particle classes from the 2001 study were dominated by particles attributed to the combustion (or incomplete combustion) of diesel lubricating oil. With the standard inlet ATOFMS, as the particle size gets smaller, the particle classes match well with those obtained with UF-ATOFMS. The top particle class seen with both instruments in the 100 to 300nm size range is the *EC, Ca, OC, Phosphate* type. Comparing the weight matrices of the top ART-2a cluster for this class between the two studies in an m/z correlation plot yields an r^2 value of 0.95. The other main class seen with the standard inlet ATOFMS matches the third most abundant class (*Ca, Na, EC, Phosphate, Sulfate*) seen with the

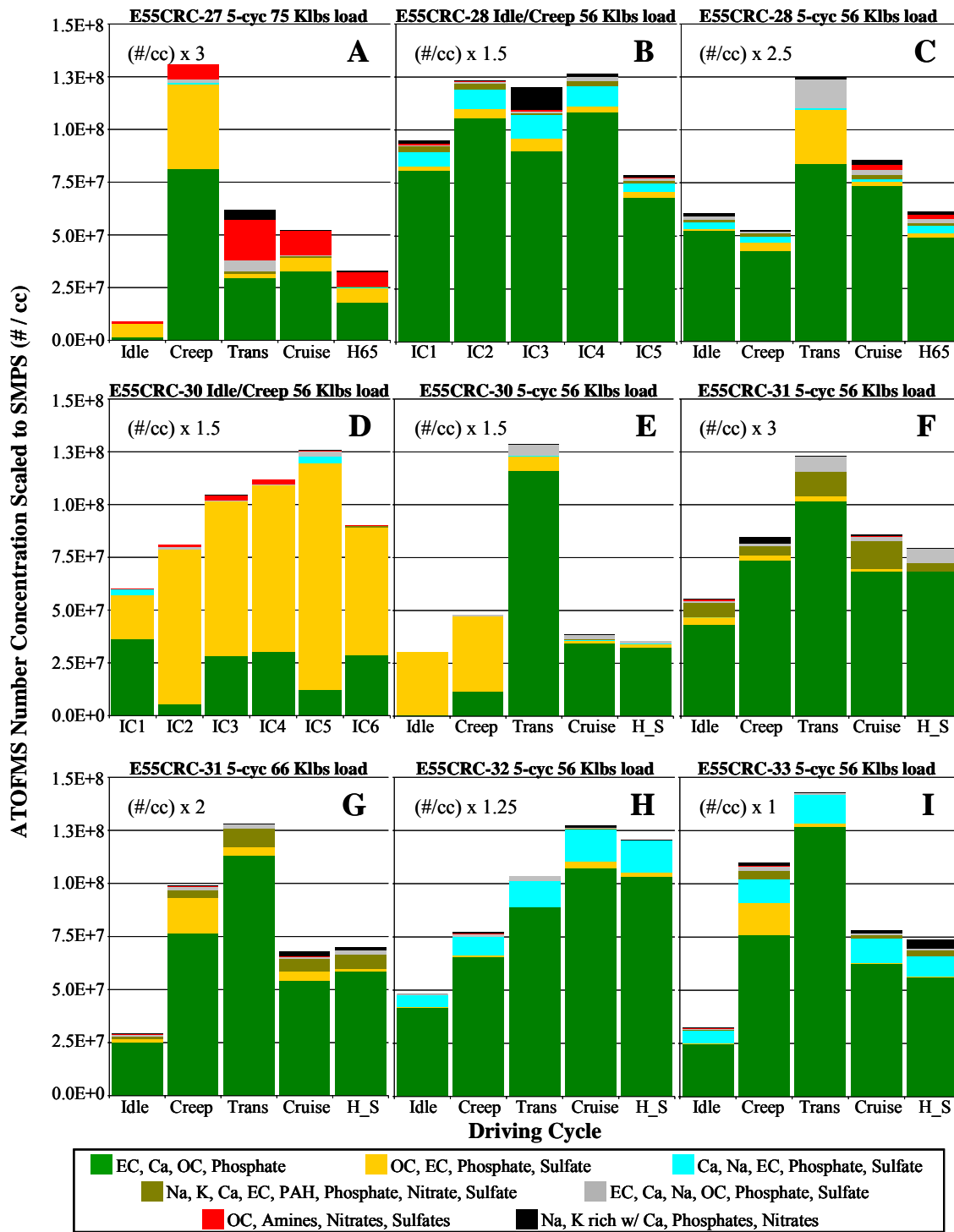


Figure 3.6 (A – I), UF-ATOFMS particle classes scaled to SMPS for each HDDDV on each test cycle. Note: The high-speed HHDDT65 cycle is denoted as H65, and the modified high-speed HHDDT_S cycle is denoted as H_S.

UF-ATOFMS and also shows a correlation with an r^2 of 0.95. Classes containing fewer particles, such as the sixth (*OC, Amines, Nitrates, Sulfates*) and the seventh classes (*Na, K rich w/Ca, Phosphates, Nitrates*) are also seen in this overlapping 100 – 300nm size range with r^2 correlations of 0.88 and 0.87. The other particle types classified with the UF-ATOFMS (the 2nd, 4th, and 5th classes listed in this chapter) were also detected in the previous study with the standard inlet instrument; however, the particle counts for these types were not sufficient to be included as their own classes and were grouped into the “minor classes” category. Because of the overall higher transmission of particles in this size range in the UF-ATOFMS, there is a better statistical representation of the classes containing fewer particles that allows them to be classified into their own distinct chemical category with the UF-ATOFMS.

The above comparison focuses on the comparison of particle signatures only for particles of the same size. When comparing the composition of all particle sizes, both instruments see most of the same particle types. Such classes include the top class (*EC, Ca, OC, Phosphate*), the third class (*Ca, Na, EC, Phosphate, Sulfate*), the sixth class (*OC, Amines, Nitrates, Sulfates*) and the seventh class (*Na, K rich w/Ca, Phosphates, Nitrates*) with r^2 correlations of 0.89, 0.81, 0.78 and 0.76 respectively. These correlations were higher than expected given that the two instruments detect the majority of their particles in different size ranges. Typically, as the particle grows larger, so does the complexity of its mass spectrum. That is to say that for particles classified as the same type between the two studies, the larger particles detected with the standard inlet ATOFMS would result in somewhat more complex spectra than would be seen with the UF-ATOFMS for the same classified particle type in the smaller sizes. While these particles are classified as the same type, there are (in general for this comparison) higher mass peaks attributed to EC for the particles detected with the standard inlet ATOFMS than with the UF-ATOFMS, which is reflected in their lower r^2 correlations. The fact that the chemistry and particle types doesn't change significantly as particle size increases, only the intensities get larger, suggests that particle growth via agglomeration is the main growth mechanism for these particles types. In the atmosphere, since agglomeration occurs between particles from different sources with different compositions, one would expect larger particles to have distinctly different compositions than smaller particles. In fact, this is indeed what is observed in ambient ATOFMS studies.

Other classes detected with the standard inlet instrument resemble those detected with the ultrafine instrument, however, they also contain different inorganic species (such as iron or aluminum) and/or the relative peak intensities for EC versus OC ions are different. These changes occur through particle agglomeration and accumulation of coatings as particle size increases. Also, mechanical wear (which typically produces super-micron particles) of engine surfaces accounts for the metals detected in particles with only the standard inlet ATOFMS, since they are above the detectable size range for the UF-ATOFMS.

3.3.5 Prospects for Apportionment

There is some concern as to whether ATOFMS mass spectral signatures obtained from laboratory and dynamometer experiments on different sources are relevant to ambient measurements and can be used for source apportionment purposes. Certain sources, such as sea salt, dust, biomass burning, coal combustion, meat cooking, and fireworks have proven to be readily distinguishable in ATOFMS ambient measurements by using source signatures to

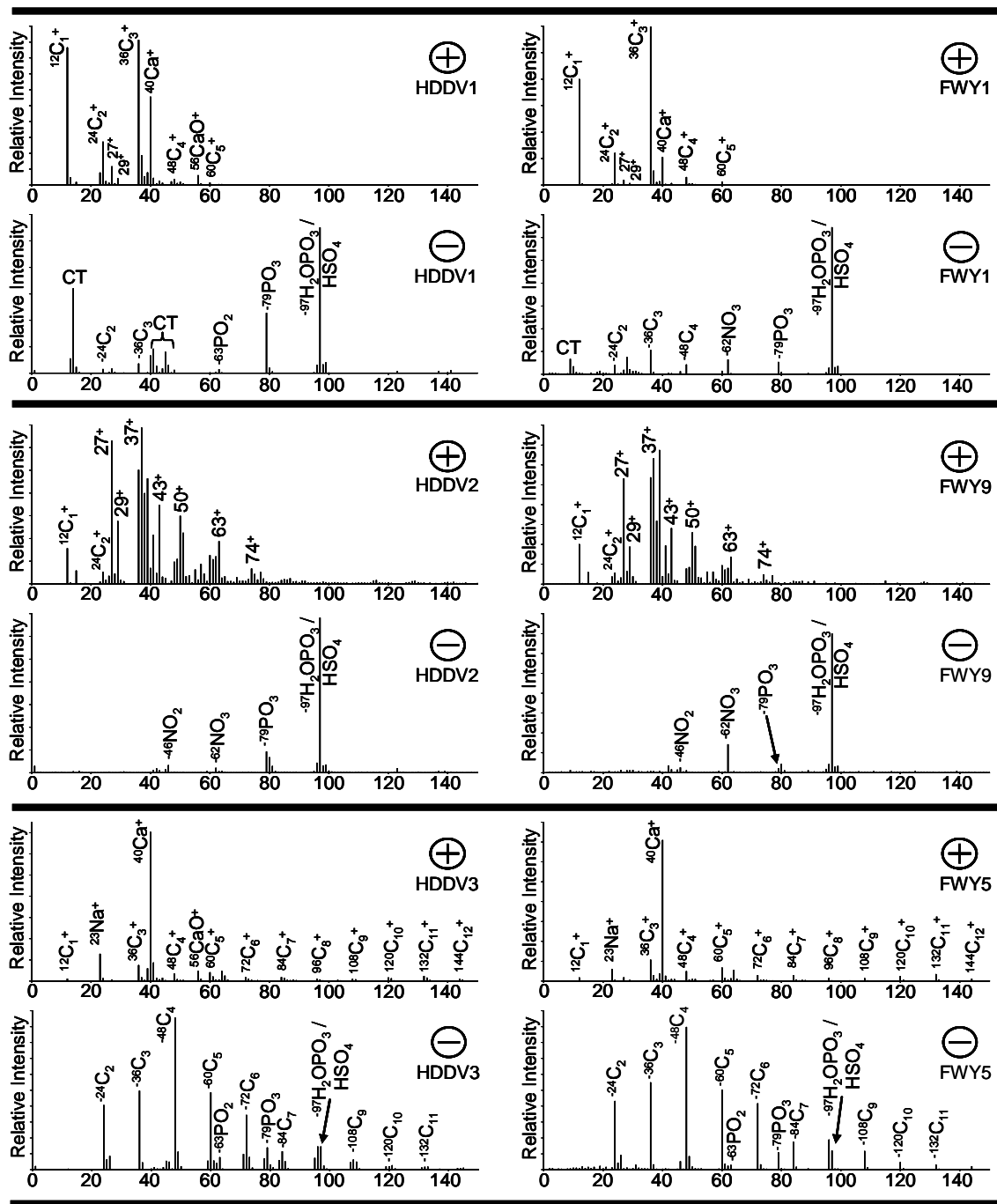


Figure 3.7 Comparison of top three HDDV particle classes with those observed of the same type in an ambient freeway study with the UF-ATOFMS. HDDV classes are labeled as HDDV# (+/-) and the classes from the freeway study are labeled likewise as FWY# (+/-). The “#” for HDDV and FWY refers to the cluster result as classified with ART-2a. The freeway study was classified with the same ART-2a parameters as the HDDV study. Similar classes are placed side-by-side.

apportion them [Gard *et al.*, 1998; Guazzotti *et al.*, 2003; Liu *et al.*, 1997; Liu *et al.*, 2003; Silva *et al.*, 2000; Silva *et al.*, 1999; Suess, 2002]. A far bigger challenge involves distinguishing exhaust particles from gasoline powered vehicles and diesel powered vehicles in an ambient environment. Comparing the source signatures for gasoline powered light duty vehicles (LDV) versus those obtained for HDDV with ATOFMS have already shown that the particles from these sources are distinguishable from one another [Sodeman *et al.*, 2005]. Some of the features that distinguish HDV from LDV are that HDV particles have a more intense peak for calcium, they contain a stronger presence of phosphates, and the peak of $^{36}\text{C}_3^+$ is greater than that of $^{12}\text{C}_1^+$ for EC particles. One of the key purposes of this study was to not only characterize particle types seen from HDDV exhaust, but to obtain source signatures for HDDVs that can be used for apportionment purposes in ambient studies. There is an issue that particles sampled from the tail-pipe of HDDVs (through dilution and residence systems) still do not properly mimic the dilution and aging that occurs on these particles in real on-road driving [Graskow *et al.*, 2000; Kawai *et al.*, 2004].

Figure 3.7 displays the top three ART-2a clusters/classes from this study compared to three clusters observed with the UF-ATOFMS sampling alongside a freeway. When peaks for each m/z of the weight matrices (representative spectra) of the compared classes are plotted against each other, the comparisons show very close correlation with R^2 values of 0.89, 0.95, and 0.97 for HDV1-FWY1, HDV2-FWY9, and HDV3-FWY5 respectively. As shown here, the dynamometer classes are detected in ambient air with almost identical signatures at the single particle level, thus showing promise that dynamometer signatures can be used for ambient source apportionment. This study was completed at the end of this project (August 2004) allowing only a brief inspection of the data. A more detailed analysis of the ambient freeway study will be forthcoming as part of a future CARB project.

3.4 Summary

Ultrafine and low-fine mode diesel exhaust particles (50 - 300nm) were examined on the single particle level to determine their chemical composition for the purpose of finding unique chemical signatures that can be used for ambient apportionment studies. Six in-use heavy duty diesel vehicles (HDDVs) were operated on a chassis dynamometer using the heavy heavy-duty diesel truck (HHDDT) five-cycle driving schedule under different simulated weight loads. The exhaust emissions passed through a dilution/residence system to simulate atmospheric dilution conditions, after which an ultrafine aerosol time-of-flight mass spectrometer (UF-ATOFMS) was used to sample and characterize the HDDV exhaust particles in real-time. The top three particle classes observed with the UF-ATOFMS comprise 91% of the total particles sampled and are believed to originate primarily from engine lubricating oil.

3.5 Acknowledgements

The authors express their gratitude to the Coordinating Research Council for their help and support in testing during CRC Project E55/E59, and the staff (including Nigel Clark, Tom Long, Curt Leasor, Chris Rowe, and Adam Leach) of the West Virginia University Transportable

Heavy-Duty Emissions Testing Laboratory for their assistance with sample collection. We also sincerely thank Michael Kleeman, Michael Robert, and Chris Jakober for operating the secondary dilution and residence chamber. We would like to acknowledge William Vance at CARB for his assistance in organizing this study and many discussions. Funding for this project was supplied by the California Air Resources Board (CARB).

3.6 References

- Angelino, S., D.T. Suess, and K.A. Prather, Formation of aerosol particles from reactions of secondary and tertiary alkylamines: Characterization by aerosol time-of-flight mass spectrometry, *Environmental Science and Technology*, 35 (15), 3130-3138, 2001.
- Arens, F., L. Gutzwiller, U. Baltensperger, H.W. Gaeggeler, and M. Ammann, Heterogeneous reaction of NO₂ on diesel soot particles, *Environmental Science and Technology*, 35 (11), 2191-2199, 2001.
- Bata, R., N. Clark, M. Gautam, A. Howell, T. Long, J. Loth, D. Lyons, G. Palmer, J. Smith, and W. Wang, A transportable heavy duty engine testing laboratory, *SAE Trans.*, 100, 433-440, 1991.
- Burtscher, H., S. Kunzel, and C. Hüglin, Characterization of particles in combustion engine exhaust, *Journal of Aerosol Science*, 29 (4), 389-396, 1998.
- Canagaratna, M.R., J.T. Jayne, D.A. Ghertner, S. Herndon, Q. Shi, J.L. Jimenez, P.J. Silva, P. Williams, T. Lanni, F. Drewnick, K.L. Demerjian, C.E. Kolb, and D.R. Worsnop, Chase studies of particulate emissions from in-use New York City vehicles, *Aerosol Science & Technology*, 38 (6), 555-573, 2004.
- Clark, N.N., M. Gautam, R.M. Bata, W.-G. Wang, J.L. Loth, G.M. Palmer, and D.W. Lyons, Technical Report: Design and operation of a new transportable laboratory for emissions testing of heavy duty trucks and buses, *Int. J. of Vehicle Design*, 2 (3/4), 308-322, 1995.
- Dybdahl, M., L. Risom, J. Bornholdt, H. Autrup, S. Loft, and H. Wallin, Inflammatory and genotoxic effects of diesel particles in vitro and in vivo, *Mutation Research*, 562 (1-2), 119-131, 2004.
- EPA, NAAQS - PM_{2.5} NAAQS Implementation - PM Standards, http://www.epa.gov/ttn/naaqs/pm/pm25_stand.html.
- Gard, E.E., M.J. Kleeman, D.S. Gross, L.S. Hughes, J.O. Allen, B.D. Morrical, D.P. Fergenson, T. Dienes, M.E. Galli, R.J. Johnson, G.R. Cass, and K.A. Prather, Direct observation of heterogeneous chemistry in the atmosphere, *Science (Washington, D. C.)*, 279 (5354), 1184-1187, 1998.

- Gautam, M., K. Chitoor, M. Durbha, and J.C. Summers, Effect of diesel soot contaminated oil on engine wear - investigation of novel oil formulations, *Tribology International*, 32 (12), 687-699, 1999.
- Graskow, B.R., M.R. Ahmadi, J.E. Morris, and D.B. Kittelson, Influence of fuel additives and dilution conditions on the formation and emission of exhaust particulate matter from a direct injection spark ignition engine, *Society of Automotive Engineers, [Special Publication] SP, SP-1551* (Diesel and Gasoline Performance and Additives), 261-271, 2000.
- Guazzotti, S.A., D.T. Suess, K.R. Coffee, P.K. Quinn, T.S. Bates, A. Wisthaler, A. Hansel, W.P. Ball, R.R. Dickerson, C. Neususs, P.J. Crutzen, and K.A. Prather, Characterization of carbonaceous aerosols outflow from India and Arabia: biomass/biofuel burning and fossil fuel combustion, *Journal of Geophysical Research, [Atmospheres]*, 108 (D15), ACL13/1-ACL13/14, 2003.
- Harrison, R.M., R. Tilling, M.S.C. Romero, S. Harrad, and K. Jarvis, A study of trace metals and polycyclic aromatic hydrocarbons in the roadside environment, *Atmospheric Environment*, 37 (17), 2391-2402, 2003.
- Hildemann, L.M., G.R. Cass, and G.R. Markowski, A dilution stack sampler for collection of organic aerosol emissions: Design, characterization and field tests, *Aerosol Science and Technology*, 10 (1), 193-204, 1989.
- Hopke, P.K., and X.H. Song, Classification of single particles by neural networks based on the computer-controlled scanning electron microscopy data, *Analytica Chimica Acta*, 348 (1-3), 375-388, 1997.
- Hughey, C.A., C.L. Hendrickson, R.P. Rodgers, and A.G. Marshall, Elemental composition analysis of processed and unprocessed diesel fuel by electrospray ionization Fourier transform ion cyclotron resonance mass spectrometry, *Energy & Fuels*, 15 (5), 1186-1193, 2001.
- Jayne, J.T., D.C. Leard, X. Zhang, P. Davidovits, K.A. Smith, C.E. Kolb, and D.R. Worsnop, Development of an aerosol mass spectrometer for size and composition analysis of submicron particles, *Aerosol Science and Technology*, 33 (1-2), 49-70, 2000.
- Jung, H., D.B. Kittelson, and M.R. Zachariah, The influence of engine lubricating oil on diesel nanoparticle emissions and kinetics of oxidation, *Society of Automotive Engineers, [Special Publication] SP, SP-1802* (Diesel Particulate Systems, Engines and Components, and Engine Performance Additives), 217-226, 2003.
- Kawai, T., Y. Goto, and M. Odaka, Influence of dilution process on engine exhaust nanoparticles, *Society of Automotive Engineers, [Special Publication] SP, SP-1862* (Emissions Measurement & Testing), 113-119, 2004.

- Khalek, I.A., M. Spears, and W. Charmley, Particle size distribution from a heavy-duty diesel engine: Steady-state and transient emission measurement using two dilution systems and two fuels, *Society of Automotive Engineers, [Special Publication] SP, SP-1755* (Diesel Emission Measurement and Modeling), 1-11, 2003.
- Kittelson, D.B., Engines and nanoparticles - a review, *Journal of Aerosol Science*, 29 (5-6), 575-588, 1998.
- Kwon, S.-B., K.W. Lee, K. Saito, O. Shinozaki, and T. Seto, Size-dependent volatility of diesel nanoparticles: Chassis dynamometer experiments, *Environmental Science and Technology*, 37 (9), 1794-1802, 2003.
- Lehmann, U., M. Mohr, T. Schweizer, and J. Rutter, Number size distribution of particulate emissions of heavy-duty engines in real world test cycles, *Atmospheric Environment*, 37 (37), 5247-5259, 2003.
- Liu, D.-Y., D. Rutherford, M. Kinsey, and K.A. Prather, Real-time monitoring of pyrotechnically derived aerosol particles in the troposphere, *Analytical Chemistry*, 69 (10), 1808-1814, 1997.
- Liu, D.-Y., R.J. Wenzel, and K.A. Prather, Aerosol time-of-flight mass spectrometry during the Atlanta Supersite Experiment: 1. Measurements, *Journal of Geophysical Research, [Atmospheres]*, 108 (D7), SOS 14/1-SOS 14/16, 2003.
- Lyyranen, J., J. Jokiniemi, E.I. Kauppinen, and J. Joutsensaari, Aerosol characterisation in medium-speed diesel engines operating with heavy fuel oils, *Journal of Aerosol Science*, 30 (6), 771-784, 1999a.
- Lyyranen, J., J. Jokiniemi, E.I. Kauppinen, and J. Joutsensaari, Aerosol characterization in medium-speed diesel engines operating with heavy fuel oils, *Journal of Aerosol Science*, 30 (6), 771-784, 1999b.
- McDonald, J.D., B. Zielinska, E.M. Fujita, J.C. Sagebiel, J.C. Chow, and J.G. Watson, Fine particle and gaseous emission rates from residential wood combustion, *Environmental Science & Technology*, 34 (11), 2080-2091, 2000.
- Moosmuller, H., W.P. Arnott, C.F. Rogers, J.L. Bowen, J.A. Gillies, W.R. Pierson, J.F. Collins, T.D. Durbin, and J.M. Norbeck, Time resolved characterization of diesel particulate emissions. 1. Instruments for particle mass measurements, *Environmental Science & Technology*, 35 (4), 781-787, 2001.
- Okada, S., C.-B. Kweon, J.C. Stetter, D.E. Foster, M.M. Shafer, C.G. Christensen, J.J. Schauer, A.M. Schmidt, A.M. Silverberg, and D.S. Gross, Measurement of trace metal composition in diesel engine particulate and its potential for determining oil consumption: ICPMS (inductively coupled plasma mass spectrometer) and ATOFMS

- (Aerosol time of Flight mass spectrometer) measurements, *Society of Automotive Engineers, [Special Publication] SP, SP-1737 (CI Engine Combustion Processes & Performance with Alternative Fuels)*, 59-72, 2003.
- Pourazar, J., A.J. Frew, A. Blomberg, R. Helleday, F.J. Kelly, S. Wilson, and T. Sandstrom, Diesel exhaust exposure enhances the expression of IL-13 in the bronchial epithelium of healthy subjects, *Respiratory Medicine*, 98 (9), 821-5., 2004.
- Reed, M.D., A.P. Gigliotti, J.D. McDonald, J.C. Seagrave, S.K. Seilkop, and J.L. Mauderly, Health effects of subchronic exposure to environmental levels of diesel exhaust, *Inhalation Toxicology*, 16 (4), 177-193, 2004.
- Reilly, P.T.A., R.A. Gieray, W.B. Whitten, and J.M. Ramsey, Real-time characterization of the organic composition and size of individual diesel engine smoke particles, *Environmental Science and Technology*, 32 (18), 2672-2679, 1998.
- Robert, M.A., C.A. Jakober, S. VanBergen, and M.J. Kleeman, Size and composition distribution of particulate matter emitted from light duty gasoline and heavy duty diesel vehicles, *Environmental Science & Technology*, Submitted, 2004.
- Rudnick, L.R., *Lubricant additives : chemistry and applications*, xiii, 735 pp., Marcel Dekker, New York, 2003.
- Sakurai, H., K. Park, P.H. McMurry, D.D. Zarling, D.B. Kittelson, and P.J. Ziemann, Size-dependent mixing characteristics of volatile and nonvolatile components in diesel exhaust aerosols, *Environmental Science and Technology*, 37 (24), 5487-5495, 2003a.
- Sakurai, H., H.J. Tobias, K. Park, D. Zarling, K.S. Docherty, D.B. Kittelson, P.H. McMurry, and P.J. Ziemann, On-line measurements of diesel nanoparticle composition and volatility, *Atmospheric Environment*, 37 (9-10), 1199-1210, 2003b.
- Schauer, J.J., M.J. Kleeman, G.R. Cass, and B.R.T. Simoneit, Measurement of emissions from air pollution sources. 2. C-1 through C-30 organic compounds from medium duty diesel trucks, *Environmental Science & Technology*, 33 (10), 1578-1587, 1999.
- Schoolcraft, T.A., G.S. Constable, B. Jackson, L.V. Zhigilei, and B.J. Garrison, Molecular dynamics simulations of laser disintegration of amorphous aerosol particles with spatially nonuniform absorption, *Nuclear Instruments & Methods in Physics Research, Section B: Beam Interactions with Materials and Atoms*, 180, 245-250, 2001.
- Schoolcraft, T.A., G.S. Constable, L.V. Zhigilei, and B.J. Garrison, Molecular dynamics simulation of the laser disintegration of aerosol particles, *Analytical chemistry*, 72 (21), 5143-50., 2000.

- Shi, J.P., D. Mark, and R.M. Harrison, Characterization of particles from a current technology heavy-duty diesel engine, *Environmental Science & Technology*, 34 (5), 748-755, 2000.
- Shields, L.G., D.T. Suess, S.A. Guazzotti, and K.A. Prather, Determination of single particle mass spectral signatures from heavy duty vehicle emissions in the 0.1 to 3 micrometer size range, *Environmental Science & Technology, manuscript in preparation*, 2005.
- Silva, P.J., R.A. Carlin, and K.A. Prather, Single particle analysis of suspended soil dust from Southern California, *Atmospheric Environment*, 34 (11), 1811-1820, 2000.
- Silva, P.J., D.-Y. Liu, C.A. Noble, and K.A. Prather, Size and chemical characterization of individual particles resulting from biomass burning of local southern California species, *Environmental Science and Technology*, 33 (18), 3068-3076, 1999.
- Silva, P.J., and K.A. Prather, Interpretation of mass spectra from organic compounds in aerosol time-of-flight mass spectrometry, *Analytical Chemistry*, 72 (15), 3553-3562, 2000.
- Sodeman, D.A., S.M. Toner, L.G. Shields, D.T. Suess, D.S. Gross, and K.A. Prather, Comparison of light duty and heavy duty vehicle emissions from dynamometer and tunnel studies using ART-2a, *Environmental Science & Technology, in preparation for submission*, 2005.
- Song, X.H., P.K. Hopke, D.P. Fergenson, and K.A. Prather, Classification of single particles analyzed by ATOFMS using an artificial neural network, ART-2A, *Analytical Chemistry*, 71(4), 860-865, 1999.
- Spencer, M.T., L.G. Shields, S.M. Toner, D.A. Sodeman, T. Suess David, and K.A. Prather, Atomization of gasoline and diesel fuel and oil, *manuscript in preparation*, 2005.
- Su, Y., M.F. Sipin, H. Furutani, and K.A. Prather, Development and characterization of an aerosol time-of-flight mass spectrometer with increased detection efficiency, *Analytical Chemistry*, 76 (3), 712-719, 2004.
- Suess, D.T., Single particle mass spectrometry combustion source characterization and atmospheric apportionment of vehicular, coal and biofuel exhaust emissions, 2002.
- Suess, D.T., and K.A. Prather, Reproducibility of single particle chemical composition during a heavy duty diesel truck dynamometer study, *Aerosol Science and Technology*, 36 (12), 1139-1141, 2002.
- Tobias, H.J., D.E. Beving, P.J. Ziemann, H. Sakurai, M. Zuk, P.H. McMurry, D. Zarling, R. Waytulonis, and D.B. Kittelson, Chemical analysis of diesel engine nanoparticles using a nano-DMA/thermal desorption particle beam mass spectrometer, *Environmental Science and Technology*, 35 (11), 2233-2243, 2001.

- Tobias, H.J., P.M. Kooiman, K.S. Docherty, and P.J. Ziemann, Real-time chemical analysis of organic aerosols using a thermal desorption particle beam mass spectrometer, *Aerosol Science and Technology*, 33 (1-2), 170-190, 2000.
- Van Gulijk, C., J.C.M. Marijnissen, M. Makkee, J.A. Moulijn, and A. Schmidt-Ott, Measuring diesel soot with a scanning mobility particle sizer and an electrical low-pressure impactor: performance assessment with a model for fractal-like agglomerates, *Journal of Aerosol Science*, 35 (5), 633-655, 2004.
- Vilhunen, J.K., A. Von Bohlen, M. Schmeling, L. Rantanen, S. Mikkonen, R. Klockenkamper, and D. Klockow, Trace element determination in diesel particulates by total-reflection x-ray fluorescence analysis, *Mikrochimica Acta*, 131 (3-4), 219-223, 1999.
- Virtanen, A.K.K., J.M. Ristimaeki, K.M. Vaaraslahti, and J. Keskinen, Effect of engine load on diesel soot particles, *Environmental Science and Technology*, 38 (9), 2551-2556, 2004.
- Walker, A.P., Controlling particulate emissions from diesel vehicles, *Topics in Catalysis*, 28 (1-4), 165-170, 2004.
- Wenzel, R.J., and K.A. Prather, Improvements in ion signal reproducibility obtained using a homogeneous laser beam for on-line laser desorption/ionization of single particles, *Rapid Communications in Mass Spectrometry*, 18 (13), 1525-1533, 2004.
- Xie, Y., P.K. Hopke, and D. Wienke, Airborne particle classification with a combination of chemical composition and shape index utilizing an adaptive resonance artificial neural network, *Environmental Science & Technology*, 28 (11), 1921-1928, 1994.
- Yanowitz, J., M.S. Graboski, L.B.A. Ryan, T.L. Alleman, and R.L. McCormick, Chassis dynamometer study of emissions from 21 in-use heavy duty diesel vehicles, *Environmental Science & Technology*, 33 (2), 209-216, 1999.
- Zhao, H.W., M.W. Barger, J.K.H. Ma, V. Castranova, and J.Y.C. Ma, Effects of exposure to diesel exhaust particles (DEP) on pulmonary metabolic activation of mutagenic agents, *Mutation Research*, 564 (2), 103-113, 2004.

Determination of Single Particle Mass Spectral Signatures from Light Duty Vehicle Emissions

4.1 Introduction

This study investigates the aerodynamic size and chemical composition of particles emitted from low emission vehicles (LEV), three-way catalyst (TWC), oxidation catalyst (Oxy-Cat), and non-catalyst equipped vehicles (Non-Cat), as well as vehicles emitting visible amounts of blue smoke (Smoker) which signifies oil emissions. Particles are analyzed semi-continuously within two size ranges (aerodynamic diameters 50 – 300 nm and 300 – 2550 nm) by two different ATOFMS systems. Vehicle-to-vehicle variability in size and chemical composition for cars with the same technologies driven on the same cycles as well as different cycles was examined. The particle types based on distinct chemical signatures for light duty gasoline vehicle emissions are presented. The temporal evolution is shown for the chemical classes over time with two-minute temporal resolution during the Federal Test Procedure (FTP) cycle. This represents the first time this level of chemical composition detail with this size and temporal resolution has been shown for particles produced by vehicular emissions.

4.2 Experimental

Twenty-eight light duty vehicles were tested on a chassis dynamometer at the California Air Resources Board Haagen-Smit Laboratory in El Monte, California. The make, model, year, and mileage as well as catalytic converter category of each of the twenty-eight vehicles tested are listed in Table 4.1. These vehicles span a wide range of different exhaust technologies and production years. Two of the vehicles exhibited the burning of oil and thus were classified as smokers. The remaining vehicles had the following catalytic converter types: no catalyst (two vehicles), oxidation catalyst (three vehicles), three-way catalyst (eleven vehicles), and low emission vehicles (LEV, three-way catalyst with emissions control) (ten vehicles). Also included in Table 4.1 are the cycle(s) that each vehicle was driven through. Each of these vehicles was tested under one or more of the following cycles: Federal Test Procedure (FTP), Unified Cycle (UC), and Unified Cycle High Speed Correction 50 (UCC50). A brief description of the cycles is given below. The emissions from the tailpipe traveled through a constant volume sampler, into a dilution and residence chamber set-up [Hildemann *et al.*, 1989] before being sampled with the following instrumentation: a scanning mobility particle sizer (SMPS TSI model 3081 electrostatic classifier and TSI model 3010 condensation particle counter), an aerodynamic particle sizer (APS TSI model 3321), an aerosol time-of-flight mass spectrometer (ATOFMS), and an ultrafine aerosol time-of-flight mass spectrometer (UF-ATOFMS). The ATOFMS and the UF-ATOFMS have been described in detail elsewhere [Gard *et al.*, 1997; Su *et al.*, 2004]. Both the ATOFMS and the UF-ATOFMS measure the aerodynamic size and the positive and negative

Table 4.1 List of make, model, year, and mileage for each vehicle, as well as the technology category, cycles tested and total particles analyzed by UF-ATOFMS (50 – 180 nm), and ATOFMS (300 – 2550 nm).

#	Make	Model	Year	Mileage	Category	Cycles	UF-ATOFMS	ATOFMS
1	Toyota	Camry	1999	43160	LEV	1C	225	56
2	Nissan	Sentra	1999	52630	LEV	1C	425	120
3	Honda	Civic	1996	77703	LEV	1C	729	105
4	Chevrolet	Monte Carlo	2002	20230	LEV	1C	262	195
5	Honda	Accord	1998	97811	LEV	1C	381	248
6	Ford	Explorer	1998	82513	LEV	1C	319	90
7	Nissan	Pathfinder	2002	8169	LEV	1C	484	338
8	Chevrolet	Silverado	2003	1264	LEV	1C	721	275
9	Jeep	Grand Cherokee	2000	31751	LEV	1C	746	93
10	Toyota	Tacoma	2000	51554	LEV	1C	345	247
11	Plymouth	Horizon	1988	32097	TWC	1C:2C	165:154	158:253
12	Toyota	Camry	1991	95532	TWC	1C:2C	108:143	115:122
13	Acura	Integra	1994	104441	TWC	1C:2C	91:100	53:55
14	Ford	Mustang	1998	10697	TWC	1C:2C	80:74	43:22
15	Ford	Taurus	1991	136983	TWC	1C:2C	212:195	280:281
16	Cadillac	Sedan DeVille	1999	35320	TWC	1C:2C	250:131	258:208
17	Dodge	Caravan	1989	207104	TWC	3H:4H:5H	55:203:83	469:936:188
18	Nissan	Frontier Pickup	1996	55940	TWC	3H:4H:5H	70:154:88	278:987:37
19	Toyota	SR5 Pickup	1989	59231	TWC	3H:4H:5H	159:226:78	259:96:20
20	Suzuki	Samari	1987	57124	TWC	3H:4H:5H	123:181:95	382:1784:52
21	Chevrolet	Suburban	1995	91618	TWC	3H:4H:5H	106:83:53	666:66:78
22	Mercedes	280E	1977	118119	Oxy	1C	118	119
23	Honda	Accord	1980	88642	Oxy	1C	***	397
24	Toyota	Corolla	1979	8661	Oxy	1C	112	131
25	Chevrolet	Bel Air	1953	96176	Non	1C	154	85
26	Ford	Mustang	1966	55280	Non	1C	83	208
27	Chevrolet	S10 Blazer	1993	162750	Smoker	1C	***	69
28	Mercury	Cougar	1968	63622	Smoker	1C	***	1297

LEV = Low Emission Vehicle	1 = FTP	C = Cold Start
TWC = Three Way Catalytic Converter	2 = UC	H = Hot Start
Oxy = Oxidation Catalytic Converter	3 = UC bag 1&2	
Non = No Catalytic Converter	4 = UCC50	***: Instrumental issue.
Smoker = exhibits smoke in exhaust	5 = FTP bag 1&2	See text for explanation

ion mass spectra of single particles. The ATOFMS has a size range of 300 – 3000 nm. The UF-ATOFMS has a size range of 50 – 300 nm, and much higher transmission efficiency (at least three orders of magnitude) of particles in this size range compared to the ATOFMS. The last two columns in Table 4.1 show the total number of particles that were chemically analyzed by the UF-ATOFMS and the ATOFMS.

The FTP cycle is a transient cycle that lasts for a total of 1879 seconds with an average speed of 21.2 mph, and a top speed of 56.7 mph (Figure 4.1). After 1374 seconds, the engine was turned off, the sampling was stopped and the engine was allowed to soak for 10 minutes before resuming the last 505 seconds, at an identical speed-time trace as the first 505 seconds. The UC cycle is also a transient cycle, but with higher speeds and a total duration of 1735 seconds. It has an average speed of 22.8 mph with a top speed of 67.2 mph. After 1435 seconds the engine was turned off and allowed to soak for 10 minutes before resuming the last 300 seconds, at an identical speed-time trace as the first 300 seconds. The UCC50 cycle is a high-speed cruise cycle with a duration of 2191 seconds, and an average speed of 42.9 mph and a top speed of 71.6 mph.

For the five TWC light duty trucks (LDTs), the FTP and UC cycles were only run through the initial 1374 and 1435 seconds, respectively. These shorter FTP and UC cycles are referred to as FTPb12 and UCb12. The FTPb12 and UCb12 cycles had average speeds of 19.5 mph and 24.6 mph, respectively. With the exception of the TWC LDTs, all vehicles were run 'cold,' while the TWC LDTs were run 'hot'. Hot means that the vehicle was prepped by driving the vehicle at 50 mph for 10 minutes before being run through the testing cycle. Cold means that the vehicle was prepped and then kept in a temperature-controlled room for at least 12 hours prior to testing and then pushed onto the dynamometer immediately prior to testing.

4.3 Results and Discussion

4.3.1 Scaling

The same procedures used to scale ATOFMS counts to an optical particle counter as described in Allen *et al.* and Wenzel *et al.* were applied in this study, except an SMPS and APS were used as the reference instruments in place of an optical particle counter [Allen *et al.*, 2000; Wenzel *et al.*, 2003]. Raw ATOFMS counts were scaled to either the SMPS or the APS depending on the size range of interest. The SMPS was used to scale particles from the UF-ATOFMS instrument in the size range of 50 – 180 nm. No corrections were made to the SMPS mobility diameters prior to scaling the ATOFMS aerodynamic diameters since proper correction requires known densities of the particles which are currently unknown [Van Gulijk *et al.*, 2004]. It has been shown that due to their fractal geometries, the mobility diameters of diesel soot particles are larger than their aerodynamic diameters, and thus the contribution of the EC types which dominate the smaller sizes may be over-estimated since they are being scaled by a larger number [Van Gulijk *et al.*, 2004].

The APS was used to scale particles from the ATOFMS instrument in the 300 – 2550 nm size range. Briefly, the ratio of the raw ATOFMS number concentration for a given size range to the reference number concentration of the same size range gives the particle detection efficiency for that size range. The inverse of this ratio gives the scaling factor needed to convert the raw

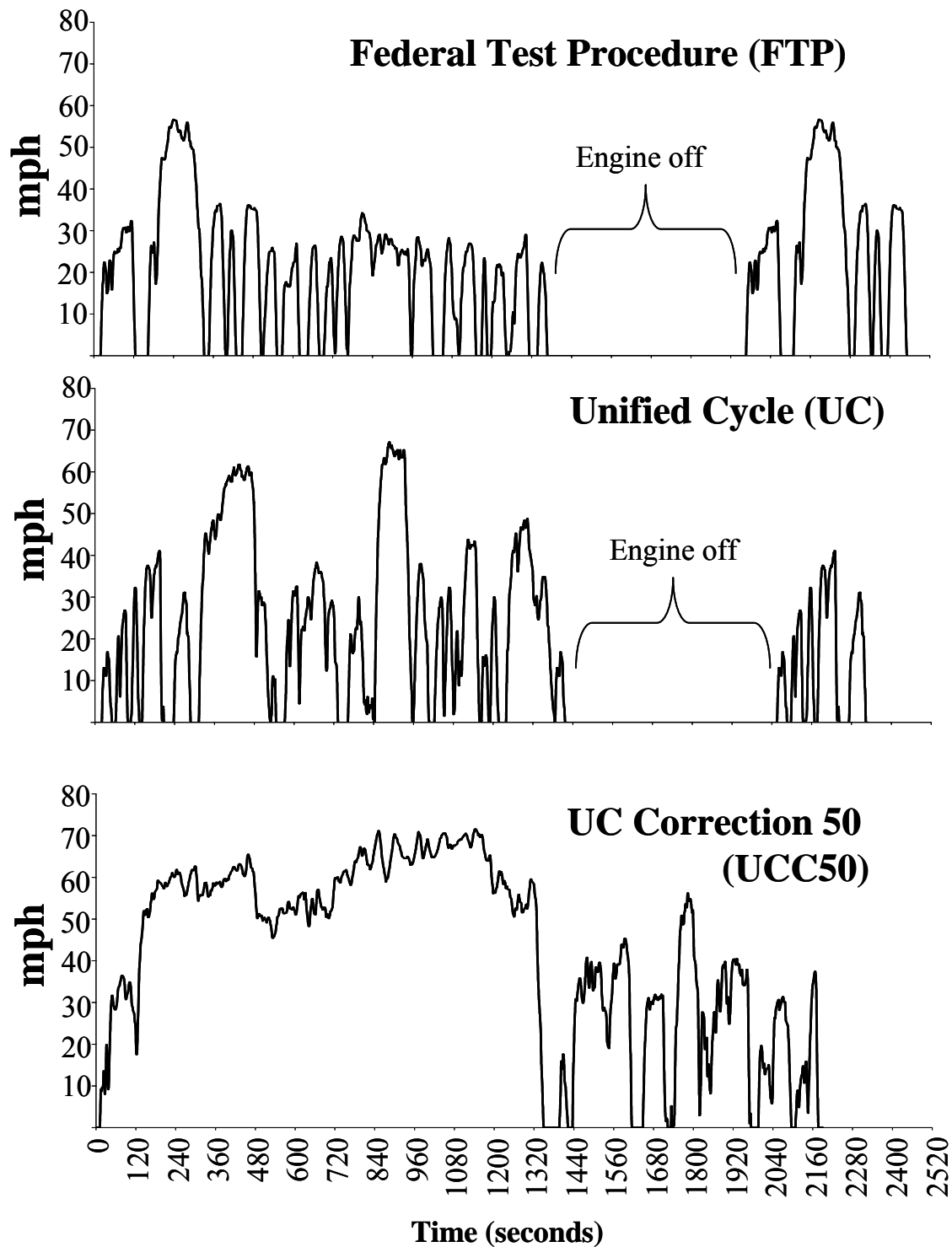


Figure 4.1 Speed-time trace for the three cycles tested; FTP, UC, and UCC50.

ATOFMS number concentration to an actual number concentration. The scaling factors were calculated for five bins in the 50 – 180 nm size range and twelve bins in the 300 – 2550 nm size range. An average scaling factor was calculated for each size bin for each vehicle each time it was tested on a different cycle. All of the data presented in this paper have been scaled to take into account the transmission and detection efficiencies, as well as dilution conditions used during the sampling. The data are reported as number emission factors (NEFs or number of particles emitted from the vehicle per mile driven on the cycle) for particles in both size ranges (50 – 180 nm or 300 – 2550 nm).

In some instances, statistically there were not enough UF-ATOFMS counts to accurately scale the chemical information. To preserve the total number concentration and size profiles, the number concentration of the non-scaled size bins were added as the “§” class and treated the same as the other classes. The chemically resolved UF-ATOFMS data were not scaled for the two smoker vehicles. The particle concentrations produced by these two vehicles were so high that the UF-ATOFMS experienced coincidence errors which made the size data unreliable [Dahneke, 1976]. However, since the UF-ATOFMS utilizes a micro-orifice uniform deposit impactor (MOUDI, with the last stage removed) as an upper size cut, the particles analyzed were predominately less than 300 nm. Thus, the chemical types of particles for the smoker vehicles will be discussed, but not their absolute or relative number concentrations. No new particle types were detected by the UF-ATOFMS from the smoker vehicles.

4.3.2 Chemical Classes

In this section, the compositions of the basic particle types observed are described. A total of 31,725 particles were analyzed from all vehicles and tests, as we chose to analyze only those particles which produced both a positive and negative ion mass spectrum. This choice was made because the ultimate goal of these vehicle studies is to determine single particle signatures for ambient source apportionment and both polarities are necessary to perform accurate source apportionment [Spencer and Prather, 2005]. The basic general types were determined for all particles collected with both instruments. The particle spectra were classified into general classes using a neural network (ART-2a) which groups particle mass spectra into clusters based on similarities in their ion patterns. A vigilance factor of 0.85, a learning rate of 0.05, and 20 iterations were used [Phares *et al.*, 2001; Song *et al.*, 1999]. Digital mass spectra [Liu *et al.*, 2003] for each resulting cluster were plotted and used to determine which clusters could be manually combined into one of eleven simplified classes by examining the spectral characteristics of each ART-2a cluster. A twelfth class (unknown) is all particles that did not fit into any of eleven classes. This class (originally 12% of the dataset) was rerun through ART-2a at a lower vigilance factor and manually combined, when appropriate, with the other classes. After this analysis, the unknown class contained 1% of the total particles. Positive and negative ion average area matrices for the eleven classes are presented in Figure 4.2. Positive and negative ion digital mass spectra for the same eleven classes are presented in Figure 4.3. Both are used as part of the analysis as they provide complementary information. The area matrices provide an indication of the relative intensity of each of the ion peaks in the single particle mass spectra for a given class. Digital mass spectra display the fraction of particles in each class that contains a peak above a threshold value (area greater than 50 arbitrary units). For example, about 85% of all

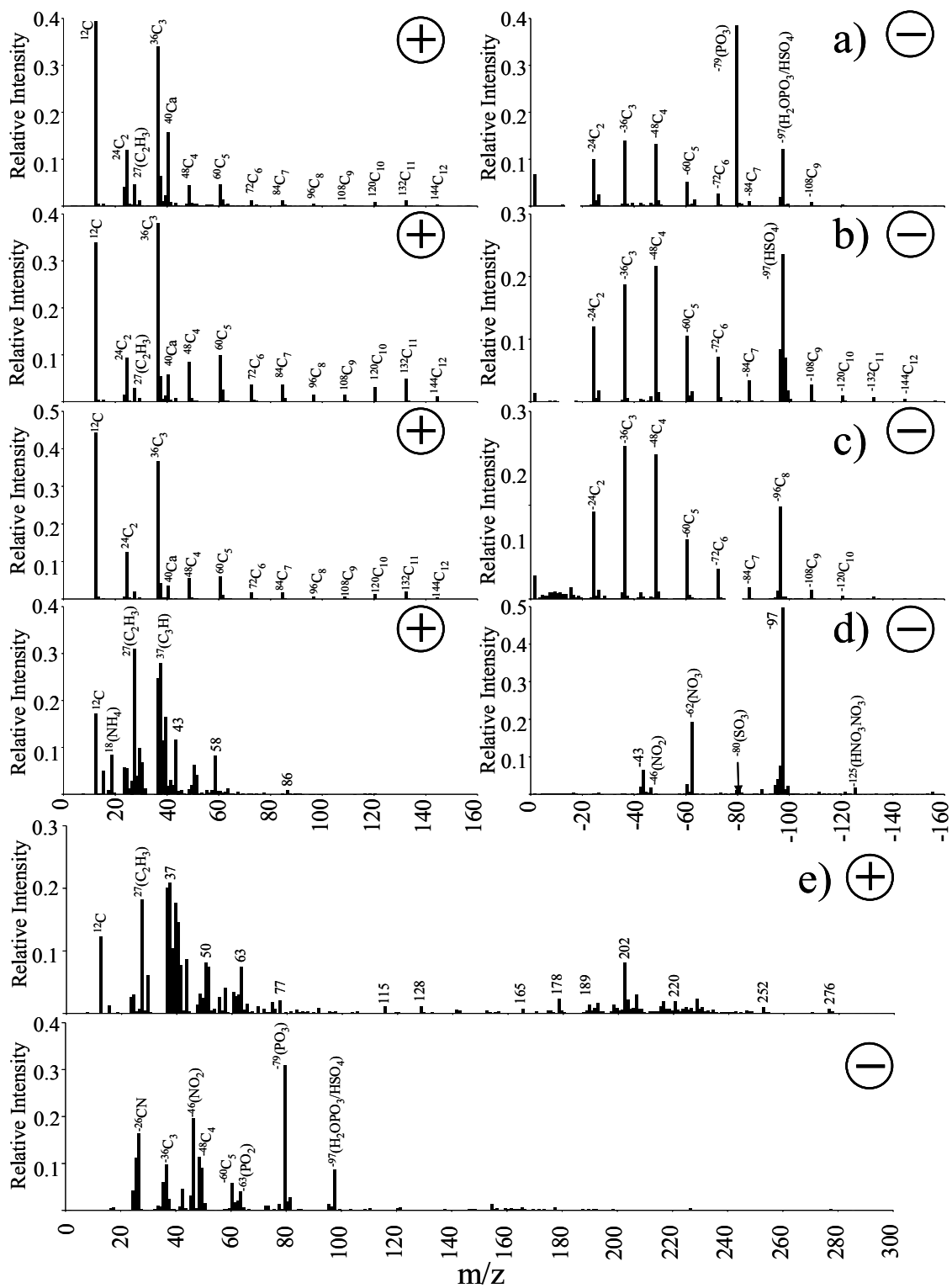


Figure 4.2 Positive and negative ion average area matrices of the eleven chemical classes: a) EC-Ca-PO₃ class. b) EC-Ca-SO₄. c) EC-Ca. d) OC- N class. e) OC- PAH class.

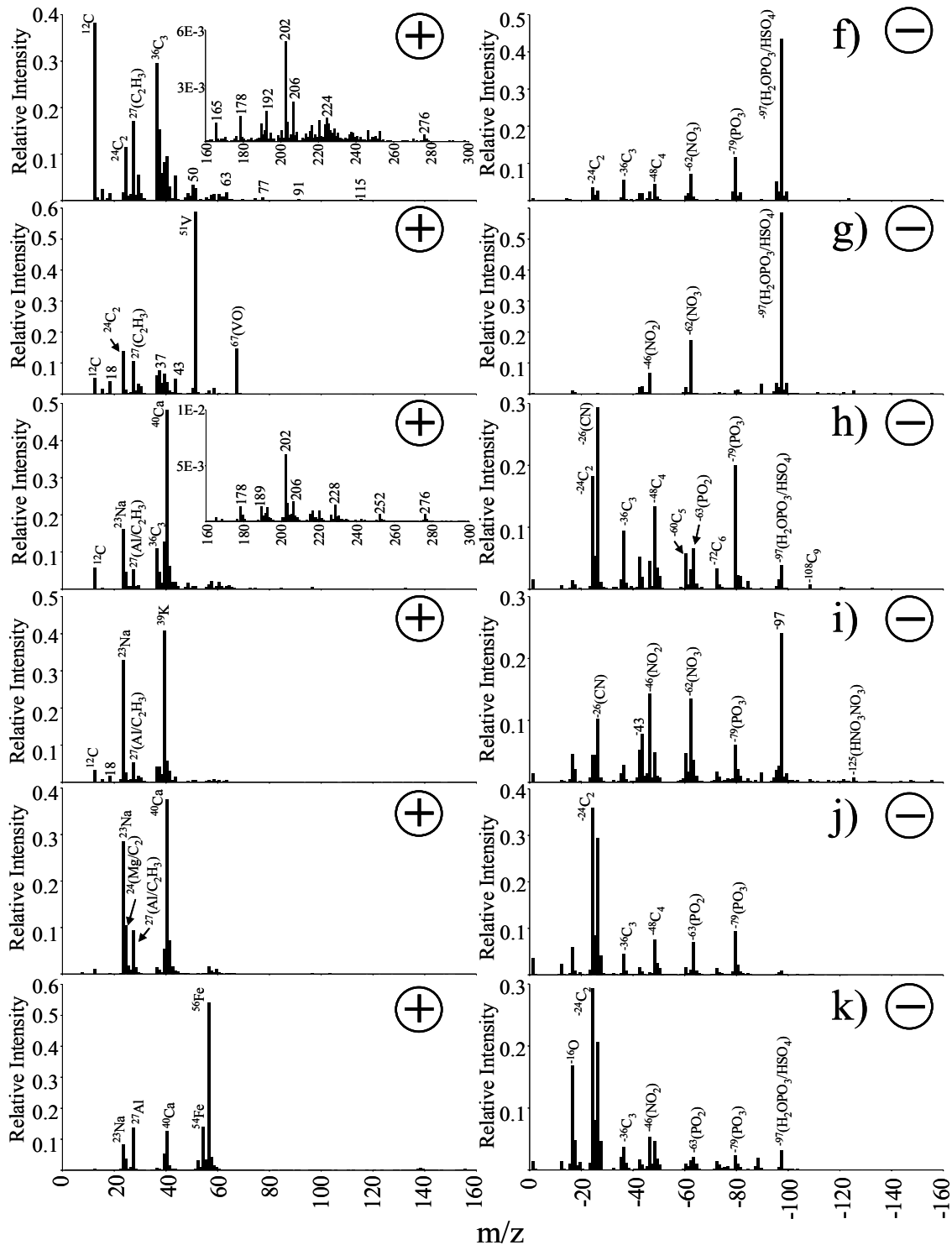


Figure 4.2 continued: Positive and negative ion average area matrices of the eleven chemical classes: f) EC-OC-Aromatic class. g) OC-V class. h) Ca-EC-PO3 class. i) Na-K class. j) Na-Ca class. k) Fe class.

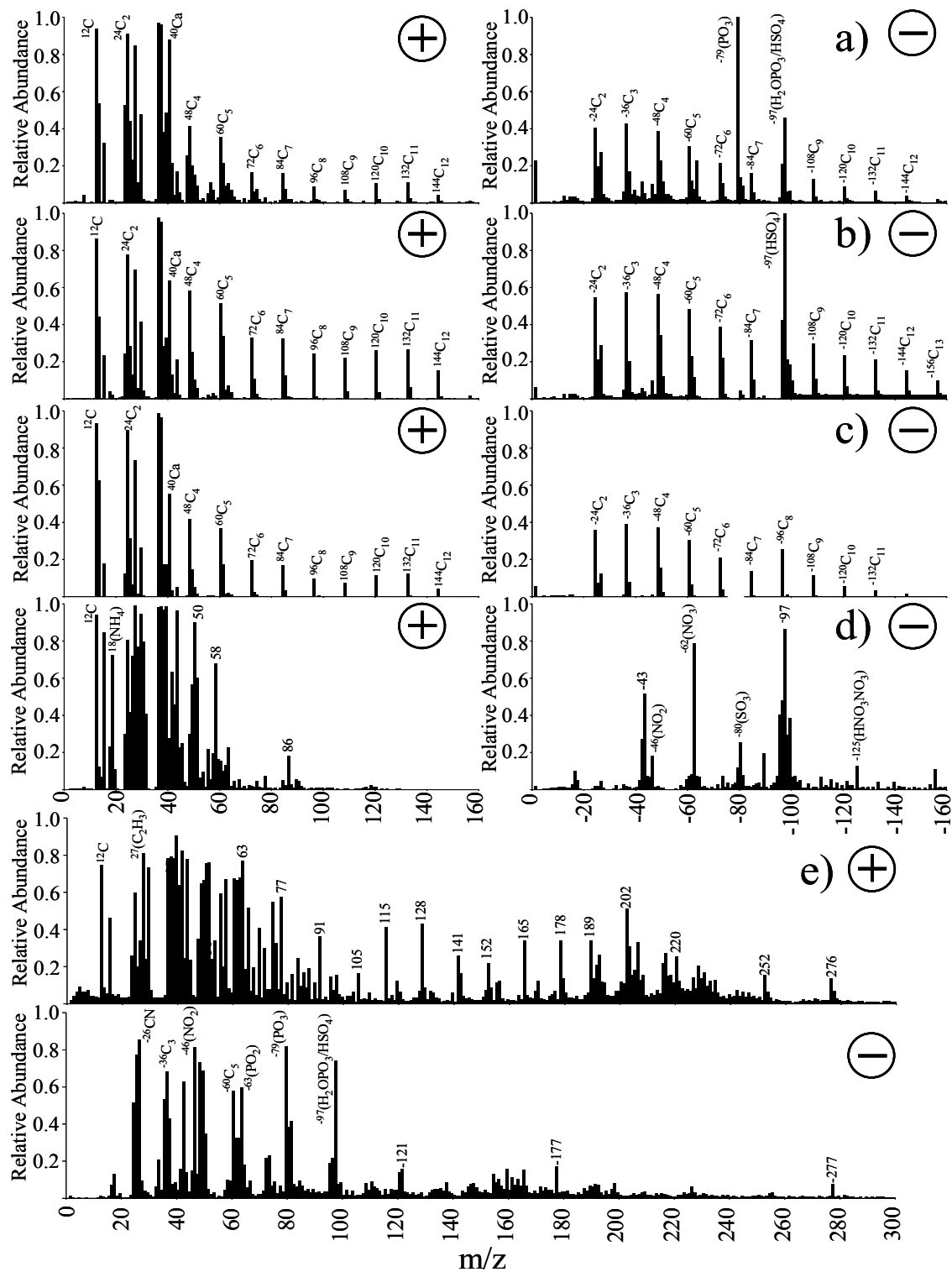


Figure 4.3 Positive and negative digital mass spectra of the eleven chemical classes: a) EC-Ca-PO₃ class. b) EC-Ca-SO₄. c) EC-Ca. d) OC-N class. e) OC-PAH class.

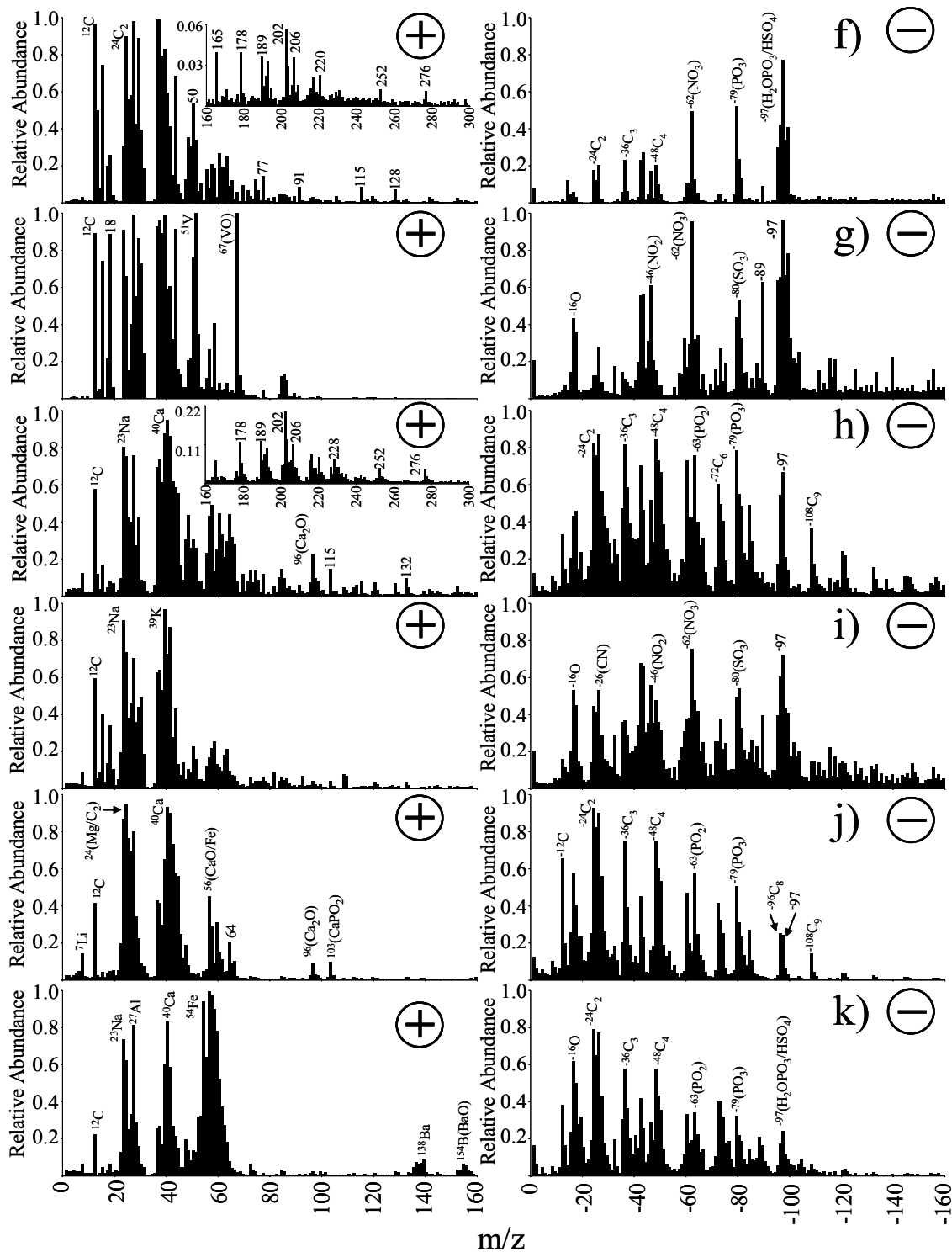


Figure 4.3 continued: Positive and negative digital mass spectra of the eleven chemical classes: f) EC-OC-Aromatic class. g) OC-V class. h) Ca-EC-PO3 class. i) Na-K class. j) Na-Ca class. k) Fe class.

particles in Carbon Class 1 have a peak at m/z 27 with an area greater than 50 arbitrary units, Figure 4.3a.

For the class descriptions below, the percentage of a chemical species (i.e. nitrate, sulfate, etc.) for a given class is derived from the digital mass spectra. The percentages of phosphate and sulfate are often given as a range since both species can occur at the same m/z ratio (-97). The peak at m/z -97 is considered sulfate unless there is also a major peak at $^{-79}(\text{PO}_3)$ in the same spectrum. For these particles, the values at $^{-79}(\text{PO}_3)$ and $^{-80}(\text{SO}_3)$ are the lower range for phosphate and sulfate, respectively, while $^{-97}(\text{H}_2\text{OPO}_3/\text{HSO}_4)$ is the upper value for both phosphate and sulfate. For each chemical class, a brief descriptive name is given for each class based on several prevalent m/z peaks in the positive and negative ion mass spectra. These names are used to refer to the classes in the figures and discussions in later sections; however, the reader is directed to the following paragraphs for a comprehensive description of the chemical classes. Though these LDV chemical classes are similarly labeled to those in Chapters 2 and 3, they are actually distinct from heavy duty diesel vehicle (HDDV) particle types. If all LDV and HDDV particles were combined in a single ART-2a classification, particles from the two sources would not necessarily be classified together.

4.3.2.1 Carbon Class 1 (EC-Ca-PO₃)

Peaks that correspond to elemental carbon (EC: m/z C_n, where n = 1–12), calcium (^{40}Ca), and phosphate ($^{-79}\text{PO}_3$) dominate this class. Other peaks indicate the presence of sulfate and organics. See Figures 4.2a and 4.3a for ion peak assignments. Nearly 100% of the time, calcium and phosphate are present in the same particle. This high co-occurrence implies that they are from the same source. The calcium is added to the oil as a detergent in the form of calcium sulfonate, phenate, salicylate, or carbonate and is used to neutralize acids and keep insoluble contaminants in suspension. The phosphate is added to the oil in the form of zinc dialkyldithiophosphate as an antioxidant and antiwear additive [Willermet, 1998; Yamaguchi *et al.*, 2002]. Thus, whenever calcium and phosphate appear in the same particle, it is highly likely that at least a portion of the particle originated from oil, via either complete or partial combustion. EC (peaks at repeating C_n ion clusters) forms from the incomplete combustion of fuel and possibly oil. The organic carbon (OC) fragments (m/z 27 and 29) are most likely from semivolatile species vaporized from the gasoline fuel or combustion by-products (see Carbon Class 6 in Figure 4.2f and 4.3f). When EC particles are absorbed into the oil, the dispersants bind with the EC particles, keeping them from agglomerating together. The particles in this class most likely possess an EC core with OC on the surface which is consistent with the findings by Sakurai *et al.* in previous vehicle studies [Sakurai *et al.*, 2003]. Previous roadside studies have proposed that the sub-micrometer calcium is being emitted from vehicles (gasoline and diesel) and the work herein supports those findings [Harrison *et al.*, 2003; Singh *et al.*, 2002; Vogt *et al.*, 2003].

4.3.2.2 Carbon Class 2 (EC-Ca-SO₄)

This class is very similar to Carbon Class 1 (EC-Ca-PO₃) class, except particles in this class contain no mass spectral peaks from phosphate and show more intense peaks due to sulfate (~100%), Figures 4.2b and 4.3b. The sulfate could be from the oil additive in the form of

calcium sulfonate or from the small fraction of sulfur in the gasoline fuel. Given the lack of phosphate associated with this particle class, this class probably originated from the complete or partial combustion of gasoline fuel, as OC fragments (m/z 27 and 29) are also present in this class.

4.3.2.3 Carbon Class 3 (EC-Ca)

This class is very similar to the first two Carbon Classes (EC-Ca-PO₃ and the EC-Ca-SO₄), except particle mass spectra in this class contain only elemental carbon peaks in the negative ion spectra with no contributions from phosphate or sulfate, Figures 4.2c and 4.3c. The calcium ion intensity in this class is the least intense of Carbon Classes 1 – 3. This could indicate on a relative basis, there is less calcium associated with this particle type than the EC-Ca-PO₃ and EC-Ca-SO₄ classes. It is important to note that given the higher sensitivity of ATOFMS to metals compared to carbonaceous species [Gross *et al.*, 2000], the amount of calcium in all three of these particle types is a small fraction of the total particle. This class most likely originates from the complete or partial combustion of gasoline fuel or oil. The term ‘the three EC-Ca classes’ will be used to collectively refer to Carbon Classes 1 – 3 in later sections, while the term ‘EC-Ca’ refers to Carbon Class 3. There is a possibility that particles in Carbon Classes 1 – 3 are all the same particle types, and the particles were just desorbed/ionized by different laser powers in the inhomogeneous beam producing different ion patterns [Wenzel and Prather, 2004]. However, the particles in these classes showed distinct size, temporal, and vehicle characteristics indicating they were indeed of different origin and thus were kept in separate classes.

4.3.2.4 Carbon Class 4 (OC-N)

This carbon class contains OC, sulfate (90%), and nitrate (82%) in addition to semivolatile species including ammonium (85%) nitrate and possibly amines, Figures 4.2d and 4.3d. Ammonia (which can react with nitric acid to form ammonium nitrate) can be formed in the three way catalytic converter as a by-product of the process which reduces NO_x to N₂ under rich fuel – air mixtures conditions [Fraser and Cass, 1998]. This class is seen in all of the vehicles equipped with three way catalytic converters. Markers used to identify amines occur at ⁵⁸(C₃H₅N) and ⁸⁶(C₅H₁₂N) [Angelino *et al.*, 2001]. For this study, the m/z 86 peak is not as prevalent, thus, it is likely that other species contribute to the m/z 58 peak. Other signatures (m/z 27, 29, 43, and 50) in the mass spectra indicate the presence of unburned and/or partially burned gasoline fuel.

4.3.2.5 Carbon Class 5 (OC-PAH)

Particle spectra in this carbon class show the presence of PAHs, along with phosphate, OC, and EC, Figures 4.2e and 4.3e, and were observed in most of the vehicles. PAHs were detected at m/z 128, 152, 178, 192, 202, 206, 216, 220, 228, 252, and 276. Due to the high laser fluence used in this study, extensive fragmentation occurred for organic compounds, however, PAHs have been shown to also yield parent ions under these laser power conditions [Silva and Prather, 2000]. In this previous study by Silva and Prather, the higher m/z peaks in Figure 4.2e and 4.3e were attributed to PAHs. Fragments of the PAHs and/or monoaromatics (especially for

Table 4.2 List of possible PAHs for each m/z ratio

m/z	PAH
128	naphthalene
152	acenaphthylene
178	anthracene
178	phenanthrene
192	methyl anthracene
192	methyl phenanthrene
202	pyrene
202	fluoranthene
206	dimethyl anthracene
206	dimethyl phenanthrene
216	methyl pyrene
216	methyl fluoranthene
220	trimethyl anthracene
220	trimethyl phenanthrene
228	chrysene
228	benzo[a]anthracene
252	benzo[a]pyrene
252	benzo[b]fluoranthene
276	benzo[ghi]perylene
276	indeno[123cd]pyrene

the lower masses) are seen at m/z 63, 77, 91, 115, 165, and 189. Table 4.2 shows some possible PAHs that could account for each of these ion peaks. Each PAH listed in Table 4.2 has been identified in previous dynamometer studies [Cadle *et al.*, 2001; Cadle *et al.*, 1999; Sagebiel *et al.*, 1997; Schauer *et al.*, 2002] and except for the methyl-substituted PAHs, identified in liquid gasoline samples [Marr *et al.*, 1999]. The methyl-substituted PAHs listed in Table 4.2 were detected in used gasoline oil [Wang *et al.*, 2000]. The PAHs detected in this study have also been identified in tunnel and/or roadside studies [Harrison *et al.*, 2003; Miguel *et al.*, 1998; Pereira *et al.*, 2002; Venkataraman *et al.*, 1994; Wingfors *et al.*, 2001]. The OC-PAH class is from the combustion of gasoline and oil and mostly likely also coated with incomplete combustion by-products from the gasoline fuel.

Harrison *et al.* found a strong correlation between calcium and methyl-PAHs along a road in Birmingham, UK suggesting exhaust emissions as the source of the non-crystal calcium [Harrison *et al.*, 2003]. This study supports that link as both calcium and methyl-PAHs were detected in this study. Interestingly, in this study, only 60% of the PAH-containing particles contain calcium (Figure 4.3e). However, calcium is the most commonly observed metal in light duty vehicular emissions and it could be that calcium is at the core of the PAH-containing particles and the laser desorption ionization process did not penetrate into the core far enough to allow detection of the calcium. The beam quality of the desorption/ionization laser (Nd:YAG at 266nm) used in this study is spatially inhomogeneous. When particles are analyzed in the ‘cold’ spot of the laser, less of the particle is sampled and the surface species are preferentially detected [Wenzel and Prather, 2004].

4.3.2.6 Carbon Class 6 (EC-OC-Aromatic)

This class of particles has peaks indicative of EC (^{12}C , $^{24}\text{C}_2$, $^{36}\text{C}_3$, $^{-24}\text{C}_2$, $^{-36}\text{C}_3$, and $^{-48}\text{C}_4$) and organic fragments ($^{27}(\text{C}_2\text{H}_3)$, $^{37}(\text{C}_3\text{H})$, 43, and 50). The particle spectra for this type also contained sulfate (20 – 78%) and phosphate (50 – 75%), Figures 4.2f and 4.3f. The peaks at m/z 50, 51, 63, 77, and 91 are most likely fragments of substituted monoaromatic compounds [McLafferty and Tureček, 1993; Silva and Prather, 2000]. The peaks at m/z 15, 27, 29, 41, and 43 are most likely alkyl fragments from the substituted monoaromatic compounds. This class also contains a small percentage (6%) of PAHs. These PAHs are the same PAHs observed in the OC-PAH class. The mass spectra of particles in this class are nearly identical to the mass spectra produced by nebulizing gasoline [Spencer and Prather, 2005]. Thus, this class is most likely unburned gasoline fuel or combustion by-products condensed onto an insoluble core, like EC, as EC fragments are also observed in the spectra. This finding is not surprising given that gasoline vapor has been shown to form aerosols and represents a dominant contributor to secondary organic aerosol formation in the atmosphere [Odum *et al.*, 1997].

4.3.2.7 Carbon Class 7 (OC-V)

This class of carbon particle spectra contains strong signals from vanadium and vanadium oxide, in addition to OC, sulfate (50 – 95%), nitrate (95%), ammonium (90%), and phosphate (45 – 95%), Figures 4.2g and 4.3g. Vanadium is naturally present in petroleum [Barceloux, 1999; Nriagu and Pacyna, 1988]. Since it is not added as an additive, it is not expected to be a dominant class and should have low concentrations in the exhaust. This class represented only

1% of the total particle counts but it is highlighted because of health effects concerns [Sabbioni *et al.*, 1996]. It was detected in nearly all of the vehicles tested, and thus, a possible candidate for a vehicular marker for source apportionment studies when used in conjunction with other ion markers in the same spectra. This particle type has been identified in past ATOFMS studies, although usually in small abundance.

4.3.2.8 Inorganic Class 1 (Ca-EC-PO₃)

This class is a mixture of organic and elemental carbon with phosphate, sulfate, and nitrate mixed with several different metals, Figures 4.2h and 4.3h. The metals include calcium, sodium, magnesium, aluminum, and potassium. A small percentage (20%) of the particles in this class also contained PAH species. These PAHs are the same as those observed in the OC-PAH class. This class differs from the three EC-Ca classes (Carbon Class 1 – 3) in that for this class, the calcium peak is more intense than the rest of the carbonaceous peaks in the mass spectrum. In the three EC-Ca classes, the calcium peak is less intense than the elemental carbon peaks. Also, the Ca-EC-PO₃ class and the three EC-Ca classes have different size distributions. The three EC-Ca classes peak in the ultrafine mode (particles with aerodynamic diameters (D_a) less than 100 nm) while the Ca-EC-PO₃ class peaks in the fine mode (D_a between 100 and 1000 nm) and some particles are even detected in the coarse mode (D_a greater than 1000 nm).

4.3.2.9 Inorganic Class 2 (Na-K)

Particles in this class contain sodium, potassium, magnesium, and aluminum along with EC (60%), OC (60%), phosphate (50 – 70%), sulfate (55 – 70%) and nitrate (75%), Figures 4.2i and 4.3i. This class is seen in the nebulization of gasoline fuel [Spencer and Prather, 2005] and is likely the result of incomplete combustion of gasoline fuel.

4.3.2.10 Inorganic Class 3 (Na-Ca)

This class contains primarily metals (sodium, calcium, potassium, magnesium, and aluminum) with EC (70%), OC (30%), phosphate (25 – 50%), and sulfate (25 – 30%), Figures 4.2j and 4.3j. One significant source of this class is oil additives. Antiwear additives in the oil polymerize, forming films of 20 – 100 nm thick consisting of iron or the overbase metal (calcium or magnesium), phosphorus, sulfur, and oxygen as well as some organic material [Willermet, 1998]. These films can be mechanically broken up and emitted through the exhaust system as particles. This class could also originate from the combustion of the gasoline fuel. Sodium, magnesium, aluminum, potassium, and calcium have been detected in automobile exhaust particles during dynamometer studies [Cadle *et al.*, 2001; Cadle *et al.*, 1997; Kleeman *et al.*, 2000]. In general, all particles in the inorganic classes detected during this study show strong resemblances to atmospheric dust and soil particles. In fact, particles with similar signatures to this class have been detected near an Autobahn using single particle mass spectrometry and named “mineral and carbonaceous” and attributed to soil dust [Vogt *et al.*, 2003]. This shows the importance of performing dynamometer source testing in order to establish signature libraries for specific sources.

4.3.2.11 Inorganic Class 4 (Fe)

This class contains strong ion signals from iron, along with sodium, calcium, aluminum, elemental carbon (60%), phosphate (25 – 30%), and sulfate (20 – 30%), Figures 4.2k and 4.3k. The majority of this class was seen in the older vehicles (the oxidation catalyst and non-catalyst vehicles) and only in the larger sized particles (D_a greater than 500 nm). This class could have originated from the polymerization of the antiwear additives in oil [Willermet, 1998]. These particles could have also originated from engine and exhaust pipe wear. Iron has also been detected in previous light duty dynamometer studies [Cadle *et al.*, 2001; Cadle *et al.*, 1997; Kleeman *et al.*, 2000].

4.3.3 Size

Figure 4.4 shows the average scaled ATOFMS number emission factor (NEF) of the thirteen classes in two different size ranges (50 – 180 nm and 300 – 2550 nm) for the different car categories (relative percentages in Figure 4.5). The size range between 180 and 300 nm is not shown due to low particle counts. This break occurs due to the lack of overlap between the sizes detected by the two ATOFMS instruments. The UF-ATOFMS samples from a MOUDI, replacing the last stage which has a 50% size cut at 100 nm to remove the majority of particles larger than 250 nm [Su *et al.*, 2004] while the standard ATOFMS had very low transmission efficiency for particles smaller than 300 nm during this study [Allen *et al.*, 2000]. Therefore, the UF-ATOFMS instrument was used to analyze particles in the 50 – 180 nm size range, while the standard ATOFMS instrument analyzed particles in the 300 – 2550 nm size range.

In the 50 – 100 nm size range, of the chemically resolved fraction, slightly less than 60% of the particles belong to the three EC-Ca classes. Several dynamometer studies on LDV have indicated that LDV emit primarily OC particles and very little EC [Cadle *et al.*, 1997; Kleeman *et al.*, 2000; Schauer *et al.*, 1996]. However, other LDV dynamometer studies show variations between 2 and 38% in the EC to total carbon ratio [Cadle *et al.*, 1999; Sagebiel *et al.*, 1997; Watson *et al.*, 1994]. It should be noted that all previous dynamometer studies base their percentages on mass, whereas in this study the percentages are number fractions. This is an important difference as EC could have an effective density substantially lower than 1 g cm^{-3} , while OC is assumed to be 1.2-g cm^{-3} [McMurry *et al.*, 2002; Rogge *et al.*, 1993; Turpin and Lim, 2001]. To convert number concentrations to mass concentrations, the aerodynamic diameters must be converted to physical diameters, and to do this the effective density and shape factors need to be known. It should also be noted that the three EC-Ca classes are not pure EC particles. These classes do have some OC associated with them (i.e. 70 – 85% of the particles in these classes have a detectable organic carbon peak, $^{27}(\text{C}_2\text{H}_3^+)$), although it is currently not known how much OC is present on these elemental carbon particles. Also, the EC/OC split is sensitive to the temperature program [Chow *et al.*, 2001; Schauer *et al.*, 2003] and could indicate a bias for one form of carbon over the other. All of these issues (the EC/OC split, mass versus number, and the density of EC versus OC) could explain the differences seen in this paper and the previous dynamometer studies.

In the 100 – 180 nm size range, the EC-OC-Aromatic and the OC-N classes are more abundant than in the smaller size bins. The three EC-Ca classes are less abundant than in the smaller size bins. This is expected because the EC-OC-Aromatic and the OC-N classes most

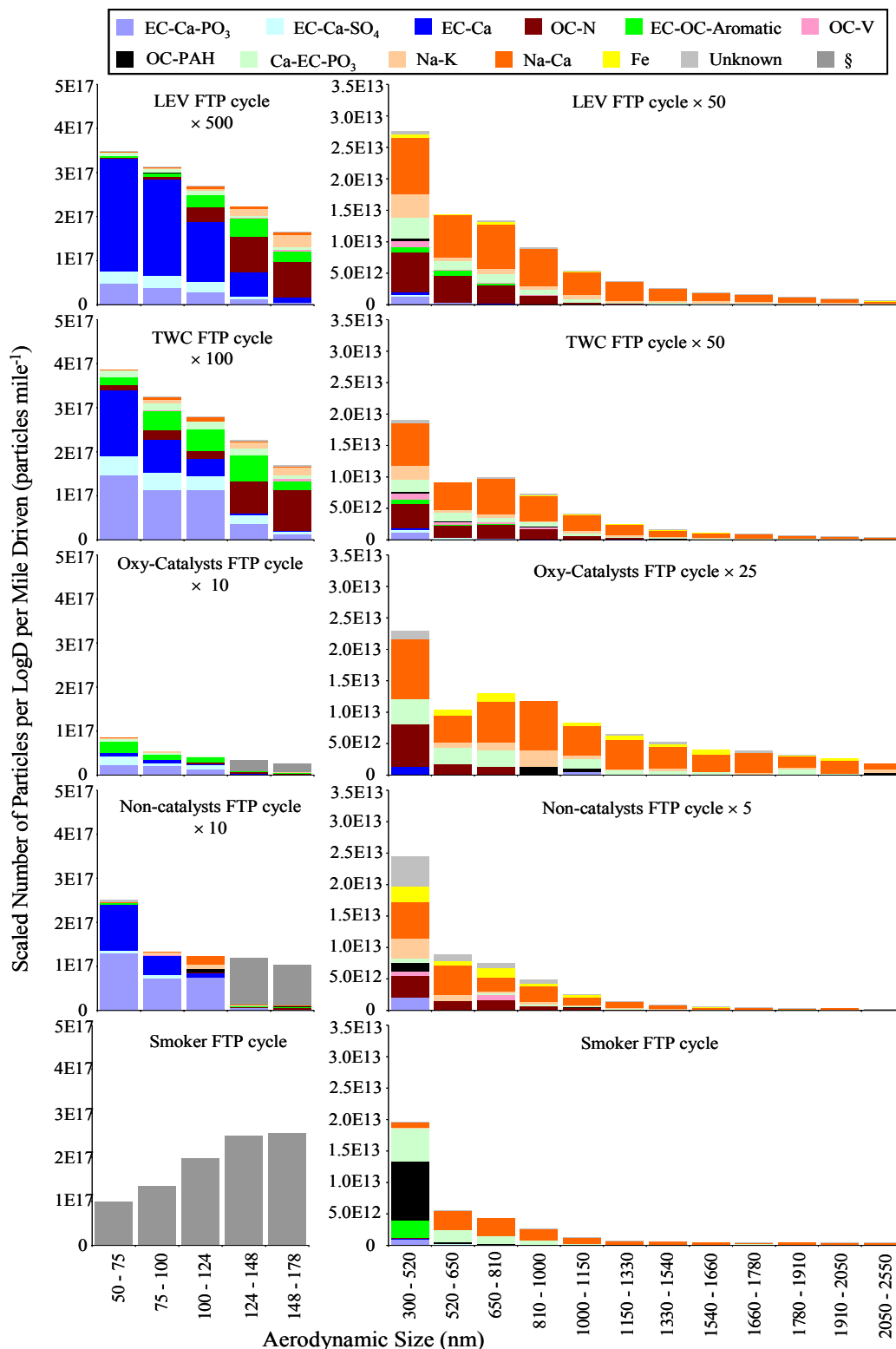


Figure 4.4 Size resolved chemical composition for each car category in the a) 50 – 180 nm and b) 300 – 2550 nm size ranges. Note for the oxy-cat cycle, vehicle 23 (shown in Figure 4.7) was removed due to ATOFMS instrumental issues).

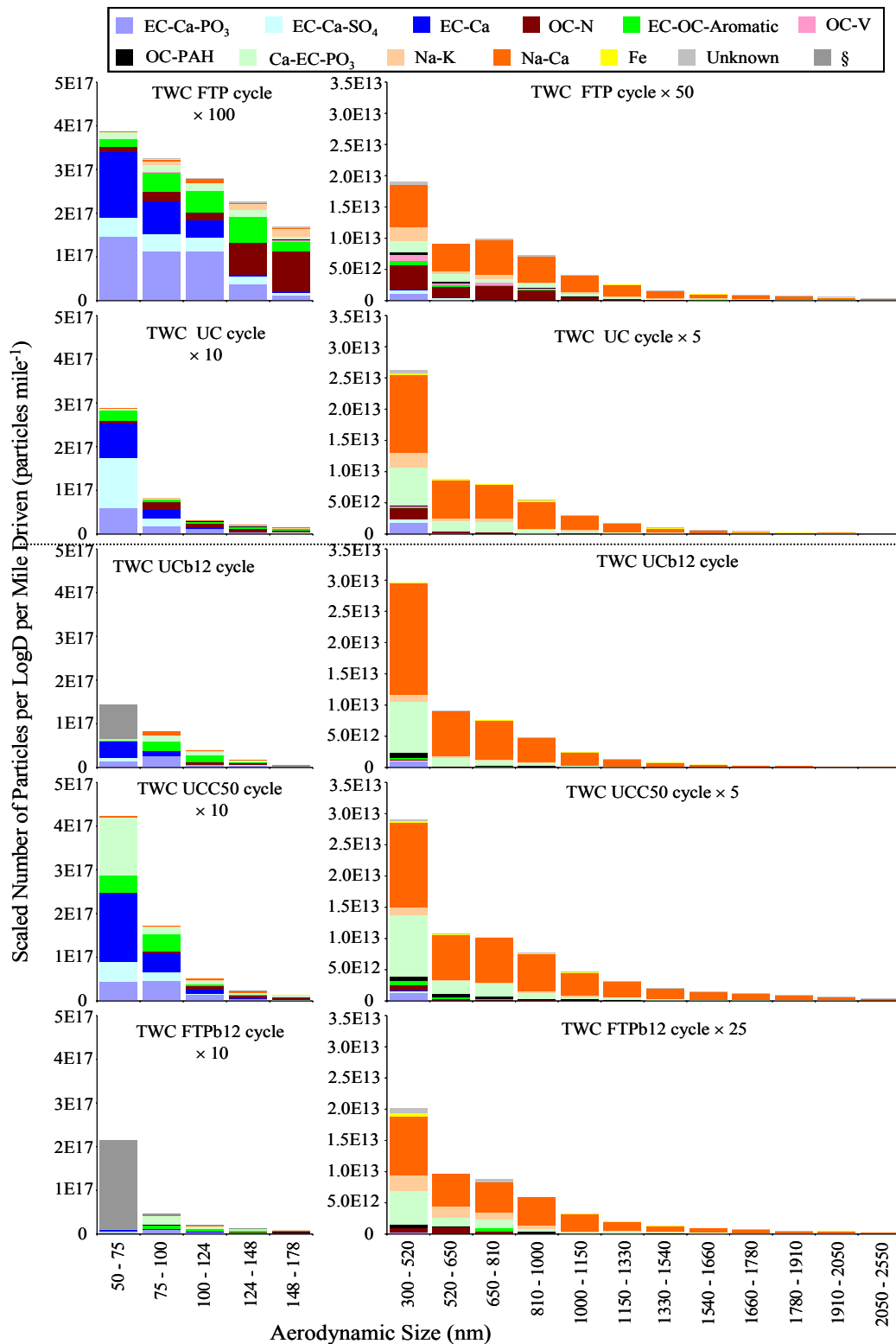


Figure 4.4 continued Size resolved chemical composition for each car category in the a) 50 – 180 nm and b) 300 – 2550 nm size ranges.

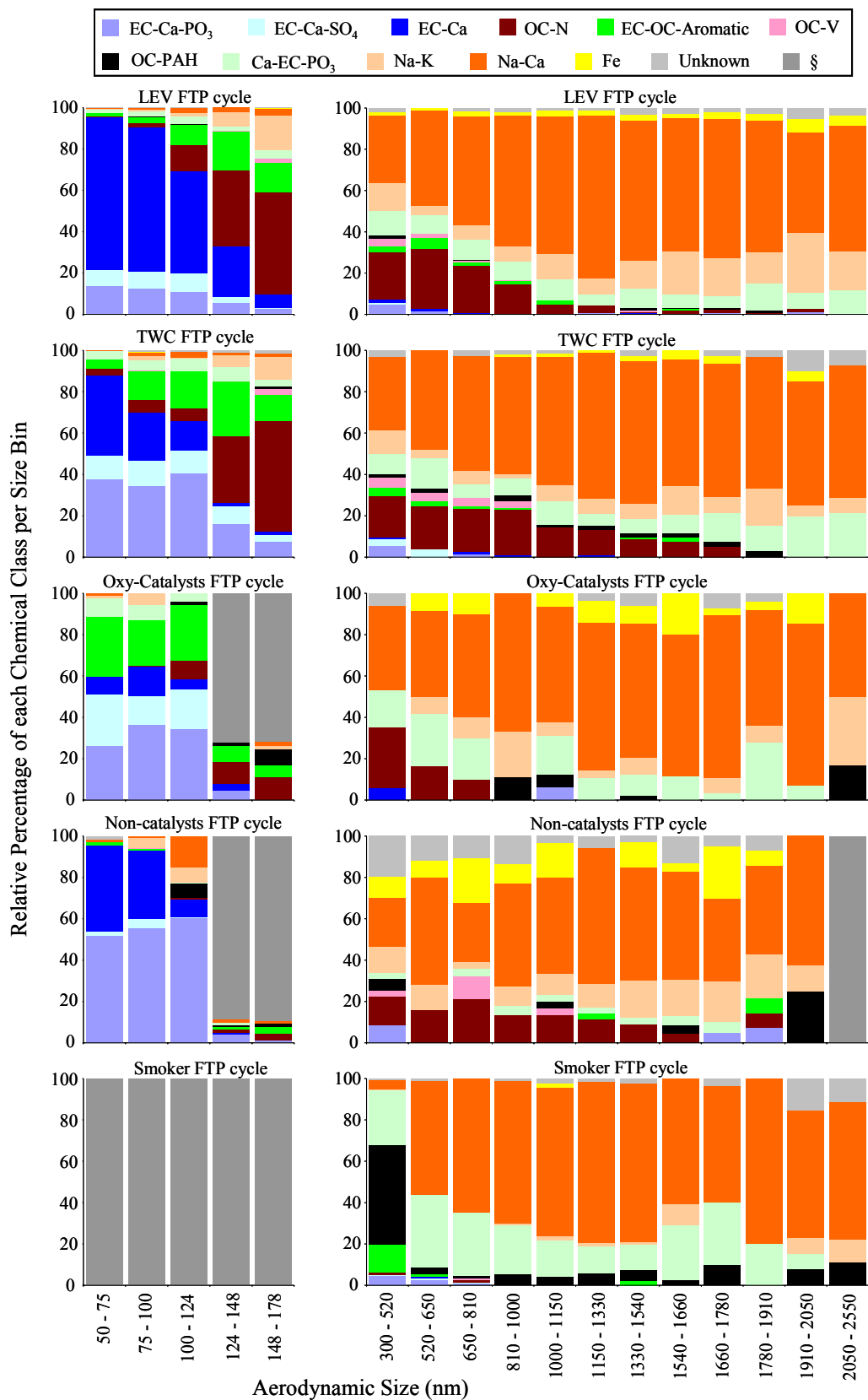


Figure 4.5 Size resolved relative percentage of each chemical class for each car category in the a) 50 – 180 nm and b) 300 – 2550 nm size range.

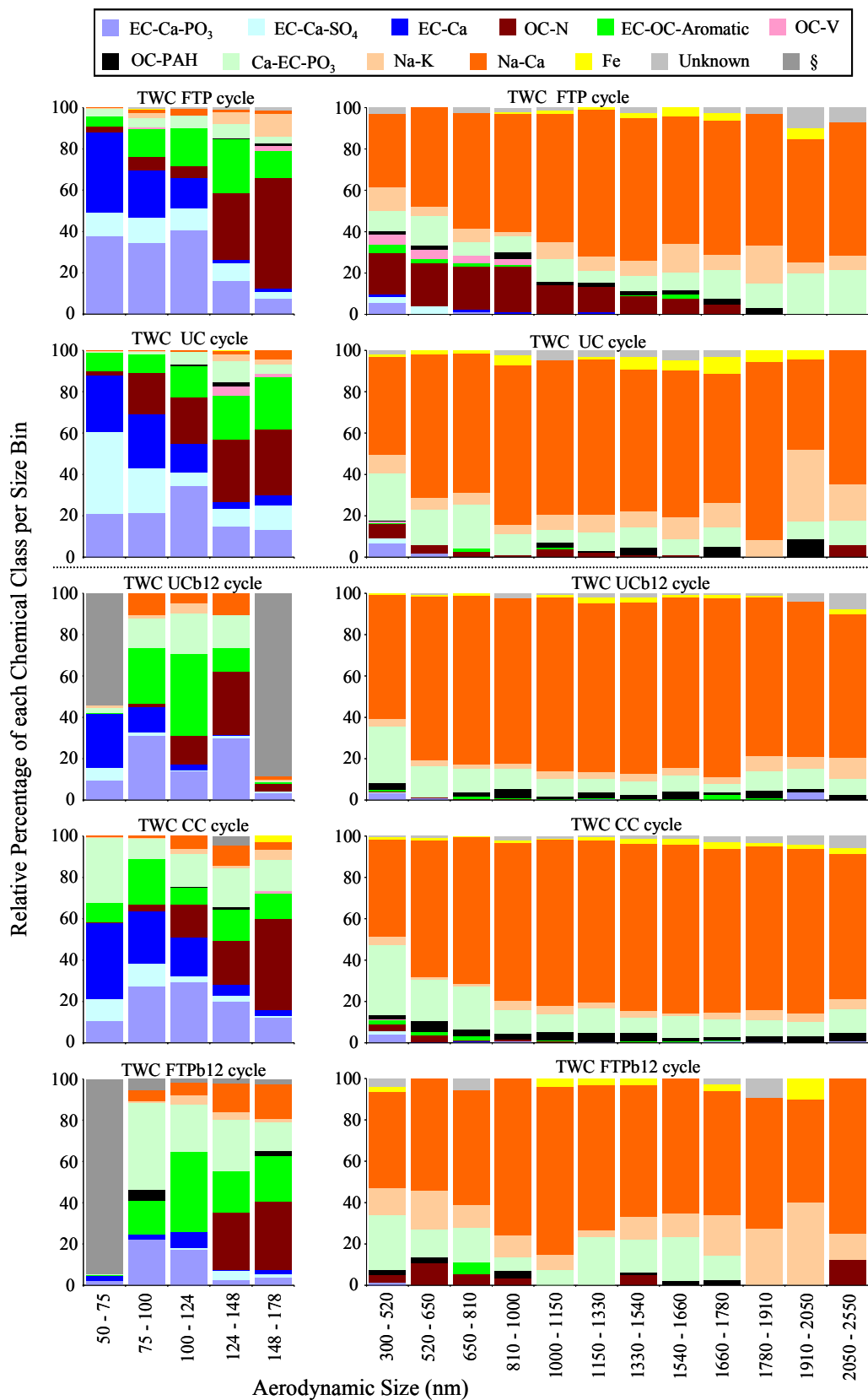


Figure 4.5 continued Size resolved relative percentage of each chemical class for each car category in the a) 50 – 180 nm and b) 300 – 2550 nm size ranges.

likely result from particles in the three EC-Ca classes becoming more coated with semivolatile organic carbon species. The results for this size range agree with other dynamometer studies which show mostly organic carbon above 100 nm [Cadle *et al.*, 1997; Cadle *et al.*, 1999; Kleeman *et al.*, 2000; Sagebiel *et al.*, 1997; Schauer *et al.*, 2002].

Above 500 nm, the fraction of inorganic classes increases relative to the organic classes with increasing aerodynamic diameters. However, it should be pointed out that the inorganic particles also contain carbonaceous compounds. The mass spectrometer utilized in this experiment for the larger sizes had a much higher sensitivity towards metals than carbonaceous species [Gross *et al.*, 2000], and thus a significant fraction of the particles could originate from carbonaceous species even though the bulk of the mass spectral ion intensities are from metals and their oxides. It is important to note that after this study was completed, it was determined that the detector had worn down so a higher voltage was needed to increase the contributions from the lower intensity carbon species. With the Na-Ca class being formed in the engine via mechanical breakdown of the antiwear film, it is expected that the Na-Ca particles would be in the larger size fractions. Another possible formation process for the Na-Ca class is liberation when the oil additives are combusted; however, this should result in the formation of particles with aerodynamic diameters less than 500 nm. This class is the dominant class above 500 nm. In the 1000 to 2550 nm size range bin, the Na-Ca class is even more dominant and the Carbon classes are only present in small amounts (<10%). This is not surprising given the large amount of surface area of inorganic particles available to which the carbon species can partition. It is possible these particles are ash-like in nature and thus highly porous [Hsieh and Tsai, 2003]. In summary, the less than 100 nm sized particles were mostly elemental carbon with calcium, phosphate, sulfate, and organic carbon, while particles larger than 500 nm were mostly composed of the inorganic particles mixed with organic species, mostly from the oil lubricants. The particles with sizes between 100 and 180 nm contain a mixture of particles from the three EC-Ca classes and several OC classes.

4.3.4 Vehicle and Cycle Variability

Figure 4.6 displays the scaled ATOFMS NEFs for particles in the size range of 50 – 180 nm for each of the five TWC LDTs on three cycles. The “§” class is large for the Dodge Caravan due to low UF-ATOFMS counts in the smallest size bins. This has a significant effect overall because the smaller the size bin, the larger the contribution of that size bin to the total concentration. The reader is referred back to the Scaling Section for a more complete explanation of the “§” class. The larger size ranges (300 – 2550 nm) are not shown since there were not enough particles detected by the ATOFMS in each size bin for each vehicle on the different cycles to accurately scale the data. There is a significant amount of variation in the total NEFs and chemical composition within the TWC LDT category. In fact, there were large variations between vehicles in all of the car categories. See Figure 4.7 for plots for the other car categories analogous to Figure 4.6. Figure 4.8 is the same plot as Figure 4.7, except each vehicle is normalized to itself. Figure 4.7 displays the total NEF, whereas Figure 4.8 displays the relative NEFs of each chemical class for each vehicle. For most of the LDT vehicles and cycles, the three EC-Ca classes were the dominant particle types. For the Suzuki Samari and Chevrolet Suburban, a higher fraction of particles in the EC-OC-Aromatic and OC-PAH classes was made to the total NEFs.

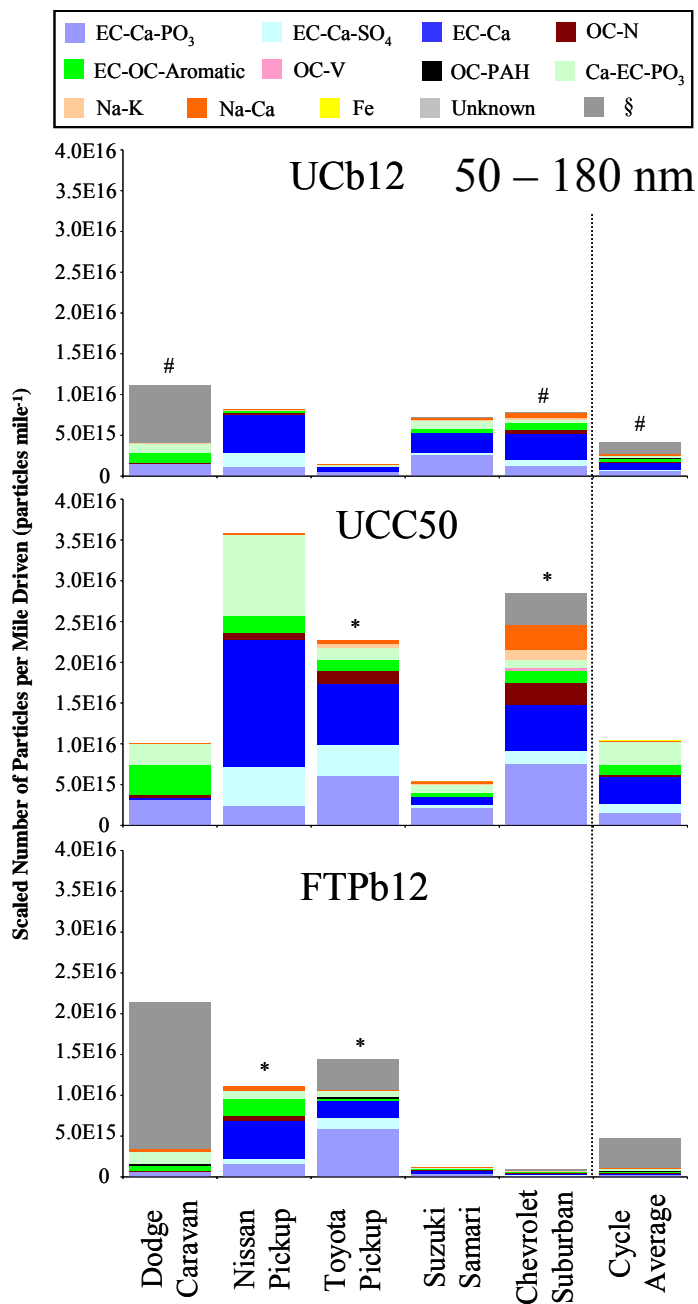


Figure 4.6 Scaled number concentrations (NEF values) of the thirteen classes for the TWC light duty trucks on three different cycles. Note the counts for bars with an (*) were multiplied by 100 and the bars with an (#) were divided by 10 in order to be visible on the same y-axis scale.

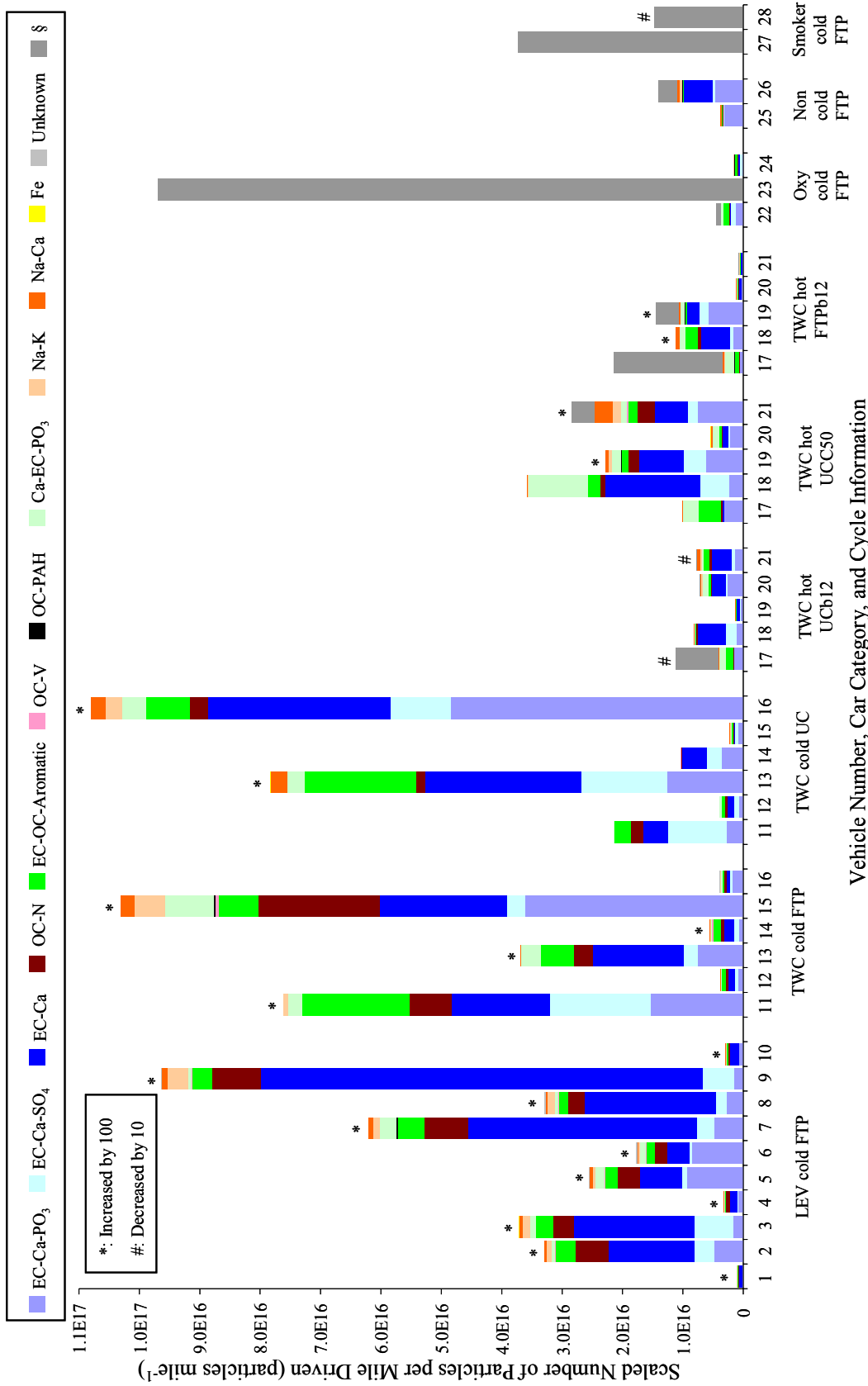


Figure 4.7 NEFs of the thirteen classes for each vehicle. Bars with an (*) indicate multiplication by 100 and bars with an (#) indicate division by 10.

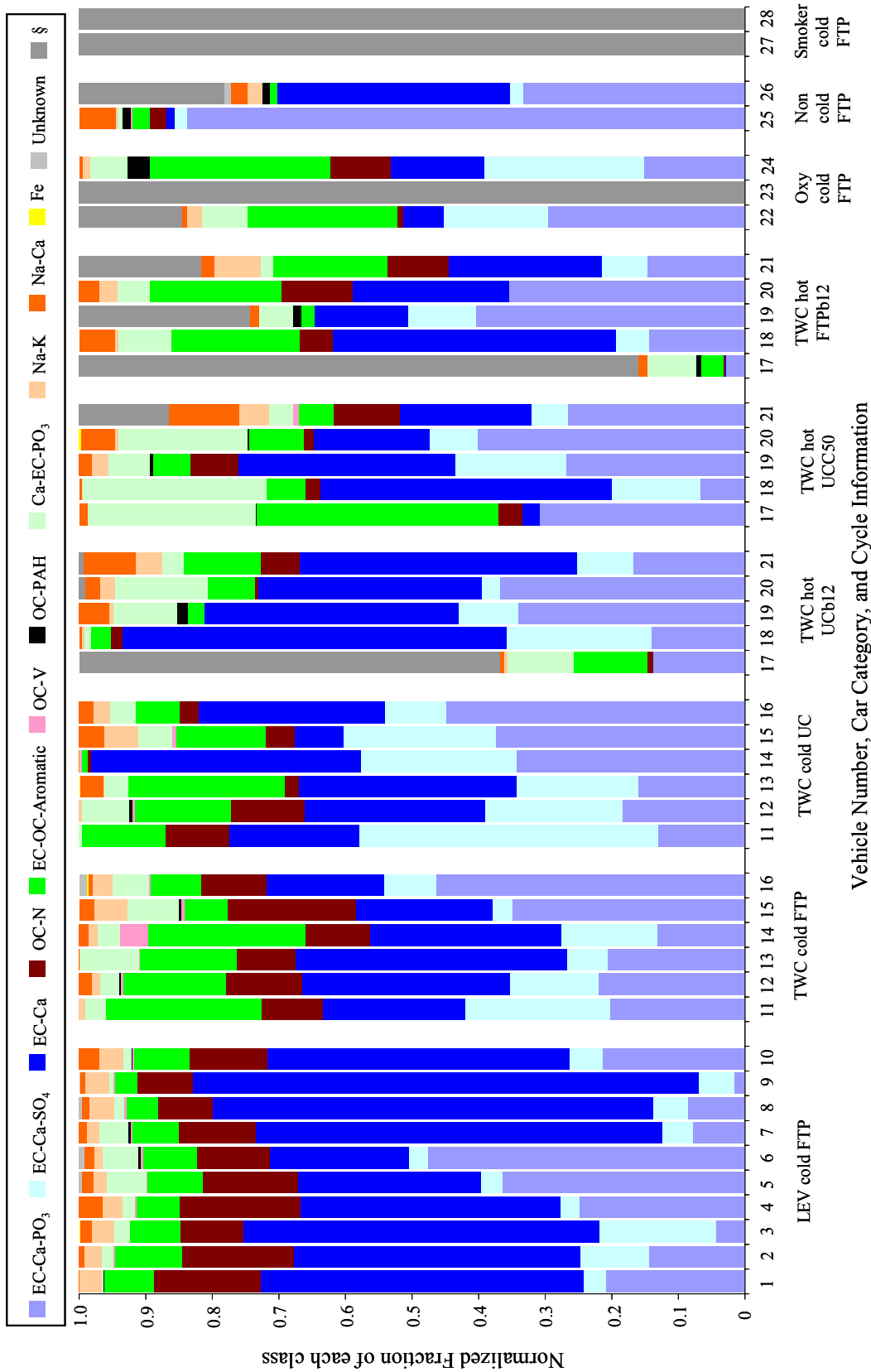


Figure 4.8 Normalized fraction of thirteen classes for each vehicle.

Four of the five vehicles produced higher NEFs on the UCb12 cycles (shorter UC cycle) than the UCC50 cycle and the shorter FTP (FTPb12) cycle. As described in the experimental section, both the UC and the FTP cycles are transient cycles, with the UC cycle having significantly faster accelerations/decelerations and higher speeds. The UCC50 cycle is mostly a high-speed cruise cycle. See Figure 4.1 for the time-speed trace for all of the cycles. Overall, the five light duty trucks produced more particles under faster accelerations and at higher speeds. The effect was also seen on the six TWC passenger cars, which were tested on the FTP and UC cycles as shown in Figure 4.7. It is important to note that in general for unscaled ATOFMS counts, a higher relative fraction of OC to EC particle types were observed on the FTP cycle than the UC cycles. However, since the EC particle types are in general the most abundant type in the sub-100 nm size bin, their relative amounts end up being larger after scaling since they are multiplied by a larger number. This finding suggests more EC particles are produced overall during faster accelerations and higher speeds conditions.

Reported NEFs values range from 3×10^{11} to 10^{15} particles mile⁻¹, with the majority of the reported values in the 10^{13} – 10^{15} range [Gramotnev *et al.*, 2003; Jamriska and Morawska, 2001; Ketzler *et al.*, 2003; Kristensson *et al.*, 2004; Ristovski *et al.*, 1998]. Only the LEVs in this study have NEFs below 10^{15} particles mile⁻¹ (an average of 3×10^{14} particles mile⁻¹, with a range from 1×10^{13} to 1×10^{15} particles mile⁻¹). The non-LEVs in this study have NEFs that range from 5.6×10^{13} to 1.5×10^{17} particles mile⁻¹. The higher values for this study compared to previous studies could be due to the small number of vehicles sampled and/or the different driving cycles used in each study. However, the observation that the oxidation catalysts, non-catalysts, and smoker vehicles have higher NEFs is consistent with them having older engine and catalytic converter technologies.

4.3.5 Cold Start

It has been documented that cold starts produce the majority of the emissions [Farrauto and Heck, 1999; Heck and Farrauto, 2001; Kaspar *et al.*, 2003]. But little research has been reported regarding the chemical composition of the particle types emitted during the early stages of the FTP cycle due to difficulties associated with obtaining enough material for chemical analysis in such a short time period. Since ATOFMS measures particles in real-time, it is feasible that it could shed some light on the chemical composition of cold starts. In order to obtain enough particles with short time resolution, the counts for all ten LEV vehicles which were tested on the FTP cycle with a cold start were compiled. Figure 4.9 displays the temporal evolution with two minute resolution of the scaled ATOFMS NEFs of the thirteen classes in the size range of 50 – 180 nm. The NEF decreases as the engine temperature increases (a factor of five from two to six minutes after the cycle starts and a factor of 50 after ten minutes). The EC-Ca-PO₃ and the EC-Ca classes are the two dominant classes produced during the cold start. The absolute (and relative) NEFs of the EC-Ca-PO₃ class decreases as the engine warms up (a factor of nine after two minutes and greater than 75 times after six minutes). In the raw ATOFMS data, the OC-dominant classes became more abundant than the EC types after 10 minutes in the FTP cycle. Upon scaling, as discussed before, this composition change is not as apparent. The first 505 seconds of the FTP cycle are repeated after a ten-minute 'soak' (the hot engine is turned off) and the NEF for the hot start (first two minutes) does not reach the same levels as the cold start (a factor of 24 lower). In the hot start, the dominant classes are again the EC-Ca-PO₃

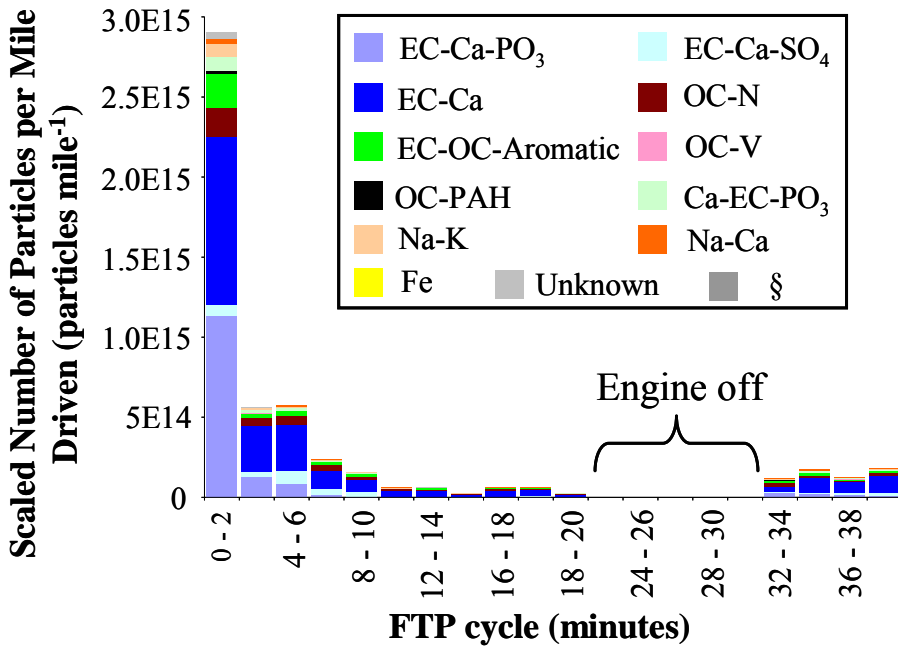


Figure 4.9 Two minute temporal profile of the thirteen classes for the ten LEV vehicles on the FTP cycle for all particles between 50 – 180 nm size range. A cooling period when the vehicle engine was off occurred from 20 – 32 minutes and then the cars were re-started at 32 minutes.

and the EC-Ca classes. The NEF of the EC-Ca-PO₃ class dropped 70% by the end of the FTP cycle as compared to its hot start value. With the exception of the Na-K class (which only contributes less than 10% of the total NEF), no other chemical class had such a decrease in their NEF value. The majority of the chemical classes had an increase in their NEFs at the end of the FTP cycle as compared to their hot start values. In summary, compared to the other chemical classes, the EC-Ca-PO₃ class is preferentially produced during starts (cold and hot); however, the most obvious change was in the total absolute number concentration as previously reported.

4.3.6 Exhaust Technology

Figure 4.10 shows the NEFs for each of the car categories tested on the FTP cycle for the 50 – 180 nm (Figure 4.10a) and 300 – 2500 nm (Figure 4.10b) size ranges. Each bar represents the average NEFs for all vehicles in each category. This figure shows that regardless of the engine technology, the same major particle types are present for all vehicles, and the absolute number concentrations vary. The general composition differences are most apparent when comparing the different size fractions with EC particle types occurring more in the small sizes and OC particle types more in the larger sizes. With the exception of the smoker category (9×10^{16} particles per mile), the general trend is older engine technologies (non-cat, oxy-cat) produced the most particles and newer technologies (LEV, TWC: 3×10^{14} particles mile⁻¹ and 2×10^{15} particles mile⁻¹, respectively) the least. This finding is consistent with the work by Bishop and Stedman which reports that 10% of the vehicle fleet (high emitters) emits over 50% of the emissions [Bishop and Stedman, 1996]. The vehicles equipped with three way catalytic converters (LEV and TWC) produced, on a relative basis, more particles in the OC-N class than the rest of the vehicle categories. As discussed in the chemical classes section, this particle type contained ammonium, which is a by-product of the reduction of NO_x to N₂ under rich fuel – air mixture conditions in three way catalytic converters [Fraser and Cass, 1998].

Seagrave *et al.* (2002) found that PM and semivolatile organic compounds (SVOCs) from high PM emitting vehicles have higher toxicity per unit mass than normal emitting vehicles [Seagrave *et al.*, 2002]. This is most likely at least partly due to the higher fraction of aromatic and PAHs produced from high PM emitting (smoker) vehicles, as reported in this work and others [Cadle *et al.*, 2001; Cadle *et al.*, 1999; Sagebiel *et al.*, 1997]. In this study, for the 300 – 2550 nm size range, the EC-OC-Aromatic and the OC-PAH classes accounted for 48% (by number) of the total particle concentration, which is a factor of ~18 times higher than the average of the rest of the car categories. Note that both of these classes show phosphate associations as well (60 - 80%), suggesting lubrication oil was associated with most of the smoker particles. Similar particle types were observed in the smaller particle size range. Note that due to the inability to scale the smoker category for the smaller sizes due to the extremely high number of particles produced, the calculated percentage is based on the raw particle counts. In the smaller size range (50 – 300 nm), 26% of the particles detected by UF-ATOFMS belonged to the EC-OC-Aromatic and OC-PAH classes, which is ~6 times higher than the average of the rest of the car categories. The largest fraction (approximately 50%) of the smallest particles emitted from the smoker were in the EC-Ca-PO₃ and Ca-EC-PO₃ classes which are indicators of lubricating oil. This finding is consistent with the cars in this class being labeled as “blue” smokers which are known to release oil. The only other vehicle category to produce as high of a fraction of particles in the EC-Ca-PO₃ and Ca-EC-PO₃ classes was the non-catalyst category which showed

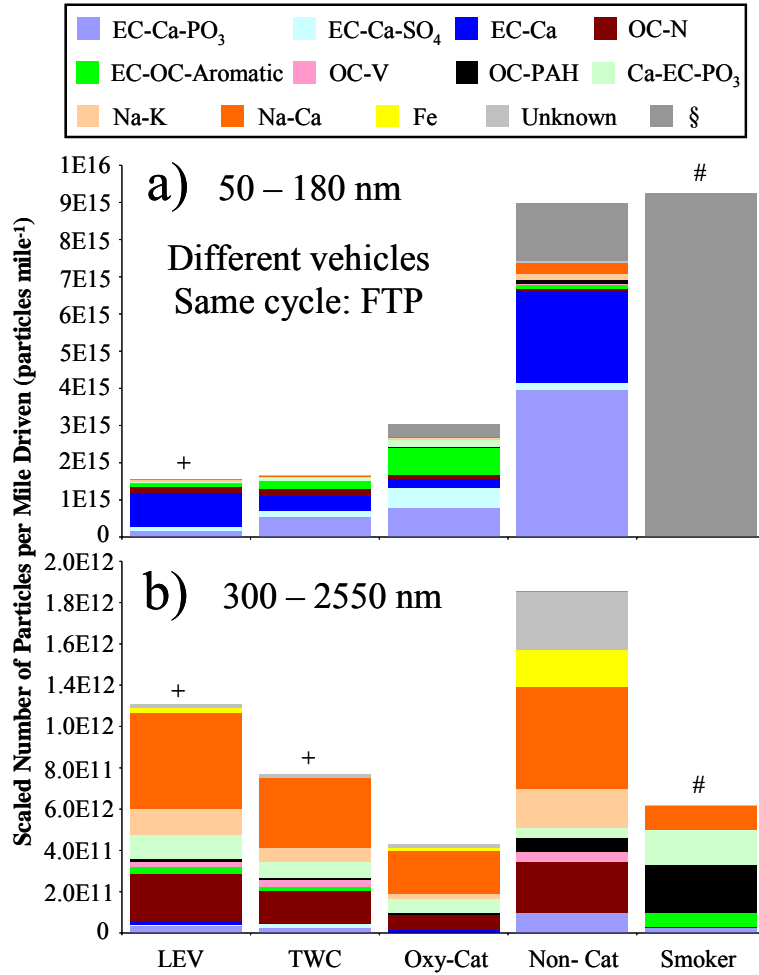


Figure 4.10 NEFs of the thirteen classes for each of the car categories tested on the FTP cycle for particles in a) 50 – 180 nm and b) 300 – 2550 nm size range. Note the bars with an (+) indicates multiplication by 5 and the bars with an (#) indicates a division by 10. Note for the oxy-cat category, one vehicle (#23 shown in Figure 4.7 and 4.8) was removed due to ATOFMS instrumental issues).

a 95% contribution (but far fewer particles overall). In the 300 – 2550 nm size range, these classes accounted for 30% of the total NEF, which is on average, two to three times higher than the other vehicle categories driven on the same FTP cycle.

The OC-PAH class was the only chemical class in which $^{46}\text{(NO}_2\text{)}$ was present in more particles than $^{62}\text{(NO}_3\text{)}$. Nitrate-containing particles, when analyzed with ATOFMS, yield peaks at $^{62}\text{(NO}_3\text{)}$ and $^{46}\text{(NO}_2\text{)}$ and usually, the $^{46}\text{(NO}_2\text{)}$ peak shows a lower abundance than $^{62}\text{(NO}_3\text{)}$. Since the OC-PAH showed the reverse trend with $^{46}\text{(NO}_2\text{)}$ greater than $^{62}\text{(NO}_3\text{)}$, this may be an indication of other species, such as nitro-PAHs, contributing to $^{46}\text{(NO}_2\text{)}$. In previous laser desorption/ionization studies of nitro-PAH, these species have been shown to rapidly fragment and produce a strong peak at $^{46}\text{(NO}_2\text{)}$ [Bezabeh *et al.*, 1997]. Nitro-PAHs are highly carcinogenic and mutagenic [Durant *et al.*, 1996; Yaffe *et al.*, 2001] and have been previously detected in vehicle exhaust [Dimashki *et al.*, 2000; Hayakawa *et al.*, 2000]. Therefore, reducing the number of high PM emitters on the road would not only have a dramatic effect in lowering the amount of PM and SVOCs released into the environment from vehicle traffic, but would also substantially lower the amount of mutagenic and carcinogenic compounds released as well.

4.4 Implications

This chapter characterizes the particulate matter emissions from light duty vehicles on a chassis dynamometer. A total of twenty-eight vehicles were tested on one or more of three cycles; the FTP (a transient cycle), the UC (a transient cycle with higher speeds than the FTP cycle), and/or the UCC50 (a high speed cruise cycle). The twenty-eight vehicles were broken down based on their exhaust technology; low emission vehicles (LEVs), three way catalytic converters (TWCs), oxidation catalytic converters (Oxy), no catalytic converters (Non), and vehicles that exhibit the burning of oil (Smokers). In the ultrafine size range (50 – 100 nm), three elemental carbon classes dominated the scaled number concentration. In the fine mode, an organic carbon with ammonium and some amines was the dominate particle type. The larger sized particles (greater than 500 nm) showed markers for inorganic species coupled with organic and elemental carbon. The smoker vehicles not only emitted the highest number concentration, but their emissions had the largest fraction of polycyclic aromatic hydrocarbons (PAHs) and substituted aromatic particles. A two minute temporal resolution was utilized to gain insight into the chemical composition of the emitted particles from all of the LEVs tested on the FTP cycle. An elemental carbon with calcium, phosphates, and organic carbon class was preferentially emitted during cold and hot starts. This was the first time that this level of chemical composition detail with this particle size and temporal resolution has been shown for vehicular emissions.

4.5 Acknowledgements

The authors would like to sincerely thank Shane Michael and the rest of the crew at the Hagen-Smit Laboratory in El Monte for driving the vehicles and hard work and dedication to this project. In addition, we acknowledge Hector Maldonado of CARB, who provided useful information on vehicle classes and the final test matrix. We also sincerely thank Michael

Kleeman, Michael Roberts, and Chris Jakober for operating the dilution and residence chamber. Funding for this project was supplied by the California Air Resources Board.

4.6 References

- Allen, J.O., D.P. Fergenson, E.E. Gard, L.S. Hughes, B.D. Morrical, M.J. Kleeman, D.S. Gross, M.E. Galli, K.A. Prather, and G.R. Cass, Particle detection efficiencies of aerosol time of flight mass spectrometers under ambient sampling conditions, *Environmental Science & Technology*, 34 (1), 211-217, 2000.
- Angelino, S., D.T. Suess, and K.A. Prather, Formation of aerosol particles from reactions of secondary and tertiary alkylamines: Characterization by aerosol time-of-flight mass spectrometry, *Environmental Science & Technology*, 35 (15), 3130-3138, 2001.
- Barceloux, D.G., Vanadium, *Journal of Toxicology - Clinical Toxicology*, 37 (2), 265-278, 1999.
- Bezabeh, D.Z., T.M. Allen, E.M. McCauley, P.B. Kelly, and A.D. Jones, Negative ion laser desorption ionization time-of-flight mass spectrometry of nitrated polycyclic aromatic hydrocarbons, *Journal of the American Society for Mass Spectrometry*, 8 (6), 630-636, 1997.
- Bishop, G.A., and D.H. Stedman, Measuring the emissions of passing cars, *Accounts of Chemical Research*, 29 (10), 489-495, 1996.
- Cadle, S.H., P. Mulawa, P. Groblicki, C. Laroo, R.A. Ragazzi, K. Nelson, G. Gallagher, and B. Zielinska, In-use light-duty gasoline vehicle particulate matter emissions on three driving cycles, *Environmental Science & Technology*, 35 (1), 26-32, 2001.
- Cadle, S.H., P.A. Mulawa, J. Ball, C. Donase, A. Weibel, J.C. Sagebiel, K.T. Knapp, and R. Snow, Particulate emission rates from in use high emitting vehicles recruited in Orange County, California, *Environmental Science & Technology*, 31 (12), 3405-3412, 1997.
- Cadle, S.H., P.A. Mulawa, E.C. Hunsanger, K. Nelson, R.A. Ragazzi, R. Barrett, G.L. Gallagher, D.R. Lawson, K.T. Knapp, and R. Snow, Composition of light-duty motor vehicle exhaust particulate matter in the Denver, Colorado area, *Environmental Science & Technology*, 33 (14), 2328-2339, 1999.
- Chow, J.C., J.G. Watson, D. Crow, D.H. Lowenthal, and T. Merrifield, Comparison of IMPROVE and NIOSH carbon measurements, *Aerosol Science & Technology*, 34 (1), 23-34, 2001.
- Dahneke, B., Aerosol Beams, in *Recent Developments in Aerosol Science*, edited by D. Shaw, Wiley, New York, 1976.

- Dimashki, M., S. Harrad, and R.M. Harrison, Measurements of nitro-PAH in the atmospheres of two cities, *Atmospheric Environment*, 34 (15), 2459-2469, 2000.
- Durant, J.L., W.F. Busby, A.L. Lafleur, B.W. Penman, and C.L. Crespi, Human cell mutagenicity of oxygenated, nitrated and unsubstituted polycyclic aromatic hydrocarbons associated with urban aerosols, *Mutation Research: Genetic Toxicology*, 371 (3-4), 123-157, 1996.
- Farrauto, R.J., and R.M. Heck, Catalytic converters: State of the art and perspectives, *Catalysis Today*, 51 (3-4), 351-360, 1999.
- Fraser, M.P., and G.R. Cass, Detection of excess ammonia emissions from in-use vehicles and the implications for fine particle control, *Environmental Science & Technology*, 32 (8), 1053-1057, 1998.
- Gard, E., J.E. Mayer, B.D. Morrical, T. Dienes, D.P. Fergenson, and K.A. Prather, Real-time analysis of individual atmospheric aerosol particles: Design and performance of a portable ATOFMS, *Analytical Chemistry*, 69 (20), 4083-4091, 1997.
- Gramotnev, G., R. Brown, Z. Ristovski, J. Hitchins, and L. Morawska, Determination of average emission factors for vehicles on a busy road, *Atmospheric Environment*, 37 (4), 465-474, 2003.
- Gross, D.S., M.E. Galli, P.J. Silva, and K.A. Prather, Relative sensitivity factors for alkali metal and ammonium cations in single particle aerosol time-of-flight mass spectra, *Analytical Chemistry*, 72 (2), 416-422, 2000.
- Harrison, R.M., R. Tilling, M.S.C. Romero, S. Harrad, and K. Jarvis, A study of trace metals and polycyclic aromatic hydrocarbons in the roadside environment, *Atmospheric Environment*, 37 (17), 2391-2402, 2003.
- Hayakawa, K., T. Murahashi, K. Akutsu, T. Kanda, N. Tang, H. Kakimoto, A. Toriba, and R. Kizu, Comparison of polycyclic aromatic hydrocarbons and nitropolycyclic aromatic hydrocarbons in airborne and automobile exhaust particulates, *Polycyclic Aromatic Compounds*, 20 (1-4), 179-190, 2000.
- Heck, R.M., and R.J. Farrauto, Automobile exhaust catalysts, *Applied Catalysis A-General*, 221 (1-2), 443-457, 2001.
- Hildemann, L.M., G.R. Cass, and G.R. Markowski, A dilution stack sampler for collection of organic aerosol emissions: Design, characterization and field-tests, *Aerosol Science and Technology*, 10 (1), 193-204, 1989.
- Hsieh, Y.M., and M.S. Tsai, Physical and chemical analyses of unburned carbon from oil-fired fly ash, *Carbon*, 41 (12), 2317-2324, 2003.

- Jamriska, M., and L. Morawska, A model for determination of motor vehicle emission factors from on-road measurements with a focus on submicrometer particles, *Science of the Total Environment*, 264 (3), 241-255, 2001.
- Kaspar, J., P. Fornasiero, and N. Hickey, Automotive catalytic converters: Current status and some perspectives, *Catalysis Today*, 77 (4), 419-449, 2003.
- Ketzel, M., P. Wahlin, R. Berkowicz, and F. Palmgren, Particle and trace gas emission factors under urban driving conditions in Copenhagen based on street and roof-level observations, *Atmospheric Environment*, 37 (20), 2735-2749, 2003.
- Kleeman, M.J., J.J. Schauer, and G.R. Cass, Size and composition distribution of fine particulate matter emitted from motor vehicles, *Environmental Science & Technology*, 34 (7), 1132-1142, 2000.
- Kristensson, A., C. Johansson, R. Westerholm, E. Swietlicki, L. Gidhagen, U. Wideqvist, and V. Vesely, Real-world traffic emission factors of gases and particles measured in a road tunnel in Stockholm, Sweden, *Atmospheric Environment*, 38 (5), 657-673, 2004.
- Liu, D.Y., R.J. Wenzel, and K.A. Prather, Aerosol time-of-flight mass spectrometry during the Atlanta Supersite Experiment: 1. Measurements, *Journal of Geophysical Research-Atmospheres*, 108 (D7), 8426, 2003.
- Marr, L.C., T.W. Kirchstetter, R.A. Harley, A.H. Miguel, S.V. Hering, and S.K. Hammond, Characterization of polycyclic aromatic hydrocarbons in motor vehicle fuels and exhaust emissions, *Environmental Science & Technology*, 33 (18), 3091-3099, 1999.
- McLafferty, F.W., and F. Tureček, *Interpretation of mass spectra*, 371 pp., University Science Books, Mill Valley, Calif., 1993.
- McMurry, P.H., X. Wang, K. Park, and K. Ehara, The relationship between mass and mobility for atmospheric particles: A new technique for measuring particle density, *Aerosol Science & Technology*, 36 (2), 227-238, 2002.
- Miguel, A.H., T.W. Kirchstetter, R.A. Harley, and S.V. Hering, On-road emissions of particulate polycyclic aromatic hydrocarbons and black carbon from gasoline and diesel vehicles, *Environmental Science & Technology*, 32 (4), 450-455, 1998.
- Nriagu, J.O., and J.M. Pacyna, Quantitative assessment of worldwide contamination of air, water, and soils by trace-metals, *Nature*, 333 (6169), 134-139, 1988.
- Odum, J.R., T.P.W. Jungkamp, R.J. Griffin, R.C. Flagan, and J.H. Seinfeld, The atmospheric aerosol-forming potential of whole gasoline vapor, *Science*, 276 (5309), 96-99, 1997.

- Pereira, P.A.D., J.B. de Andrade, and A.H. Miguel, Measurements of semivolatile and particulate polycyclic aromatic hydrocarbons in a bus station and an urban tunnel in Salvador, Brazil, *Journal of Environmental Monitoring*, 4 (4), 558-561, 2002.
- Phares, D.J., K.P. Rhoads, A.S. Wexler, D.B. Kane, and M.V. Johnston, Application of the ART-2a algorithm to laser ablation aerosol mass spectrometry of particle standards, *Analytical Chemistry*, 73 (10), 2338-2344, 2001.
- Ristovski, Z.D., L. Morawska, N.D. Bofinger, and J. Hitchins, Submicrometer and supermicrometer particulate emission from spark ignition vehicles, *Environmental Science & Technology*, 32 (24), 3845-3852, 1998.
- Rogge, W.F., M.A. Mazurek, L.M. Hildemann, G.R. Cass, and B.R.T. Simoneit, Quantification of urban organic aerosols at a molecular level: Identification, abundance and seasonal variation, *Atmospheric Environment*, 27 (8), 1309-1330, 1993.
- Sabbioni, E., J. Kueera, R. Pietra, and O. Vesterberg, A critical review on normal concentrations of vanadium in human blood, serum, and urine, *Science of the Total Environment*, 188 (1), 49-58, 1996.
- Sagebiel, J.C., B. Zielinska, P.A. Walsh, J.C. Chow, S.H. Cadle, P.A. Mulawa, K.T. Knapp, and R.B. Zweidinger, PM₁₀ exhaust samples collected during IM-240 dynamometer tests of in-service vehicles in Nevada, *Environmental Science & Technology*, 31 (1), 75-83, 1997.
- Sakurai, H., H.J. Tobias, K. Park, D. Zarling, S. Docherty, D.B. Kittelson, P.H. McMurry, and P.J. Ziemann, On-line measurements of diesel nanoparticle composition and volatility, *Atmospheric Environment*, 37 (9-10), 1199-1210, 2003.
- Schauer, J.J., M.J. Kleeman, G.R. Cass, and B.R.T. Simoneit, Measurement of emissions from air pollution sources 5: C-1-C-32 organic compounds from gasoline-powered motor vehicles, *Environmental Science & Technology*, 36 (6), 1169-1180, 2002.
- Schauer, J.J., B.T. Mader, J.T. Deminter, G. Heidemann, M.S. Bae, J.H. Seinfeld, R.C. Flagan, R.A. Cary, D. Smith, B.J. Huebert, T. Bertram, S. Howell, J.T. Kline, P. Quinn, T. Bates, B. Turpin, H.J. Lim, J.Z. Yu, H. Yang, and M.D. Keywood, ACE-Asia intercomparison of a thermal-optical method for the determination of particle-phase organic and elemental carbon, *Environmental Science & Technology*, 37, 993-1001, 2003.
- Schauer, J.J., W.F. Rogge, L.M. Hildemann, M.A. Mazurek, and G.R. Cass, Source apportionment of airborne particulate matter using organic compounds as tracers, *Atmospheric Environment*, 30 (22), 3837-3855, 1996.
- Seagrave, J., J.D. McDonald, A.P. Gigliotti, K.J. Nikula, S.K. Seilkop, M. Gurevich, and J.L. Mauderly, Mutagenicity and in vivo toxicity of combined particulate and semivolatile

- organic fractions of gasoline and diesel engine emissions, *Toxicological Sciences*, 70 (2), 212-226, 2002.
- Silva, P.J., and K.A. Prather, Interpretation of mass spectra from organic compounds in aerosol time-of-flight mass spectrometry, *Analytical Chemistry*, 72 (15), 3553-3562, 2000.
- Singh, M., P.A. Jaques, and C. Sioutas, Size distribution and diurnal characteristics of particle-bound metals in source and receptor sites of the Los Angeles Basin, *Atmospheric Environment*, 36 (10), 1675-1689, 2002.
- Song, X.H., P.K. Hopke, D.P. Fergenson, and K.A. Prather, Classification of single particles analyzed by ATOFMS using an artificial neural network, ART-2A, *Analytical Chemistry*, 71 (4), 860-865, 1999.
- Spencer, M.T., and K.A. Prather, Atomization of gasoline and diesel fuel and oil, *in preparation*, 2005.
- Su, Y.X., M.F. Sipin, H. Furutani, and K.A. Prather, Development and characterization of an aerosol time-of-flight mass spectrometer with increased detection efficiency, *Analytical Chemistry*, 76 (3), 712-719, 2004.
- Turpin, B.J., and H.J. Lim, Species contributions to PM_{2.5} mass concentrations: Revisiting common assumptions for estimating organic mass, *Aerosol Science & Technology*, 35 (1), 602-610, 2001.
- Van Gulijk, C., J.C.M. Marijnissen, M. Makkee, J.A. Moulijn, and A. Schmidt-Ott, Measuring diesel soot with a scanning mobility particle sizer and an electrical low-pressure impactor: performance assessment with a model for fractal-like agglomerates, *Journal of Aerosol Science*, 35 (5), 633-655, 2004.
- Venkataraman, C., J.M. Lyons, and S.K. Friedlander, Size distributions of polycyclic aromatic hydrocarbons and elemental carbon 1: Sampling, measurement methods, and source characterization, *Environmental Science & Technology*, 28 (4), 555-562, 1994.
- Vogt, R., U. Kirchner, V. Scheer, K.P. Hinz, A. Trimborn, and B. Spengler, Identification of diesel exhaust particles at an Autobahn, urban and rural location using single-particle mass spectrometry, *Journal of Aerosol Science*, 34 (3), 319-337, 2003.
- Wang, J., C.R. Jia, C.K. Wong, and P.K. Wong, Characterization of polycyclic aromatic hydrocarbons created in lubricating oils, *Water, Air, & Soil Pollution*, 120 (3-4), 381-396, 2000.
- Watson, J.G., J.C. Chow, D.H. Lowenthal, L.C. Pritchett, C.A. Frazier, G.R. Neuroth, and R. Robbins, Differences in the carbon composition of source profiles for diesel-powered and gasoline-powered vehicles, *Atmospheric Environment*, 28 (15), 2493-2505, 1994.

- Wenzel, R.J., D.Y. Liu, E. Edgerton, and K.A. Prather, Aerosol time-of-flight mass spectrometry during the Atlanta Supersite Experiment: 2. Scaling procedures, *Journal of Geophysical Research-Atmospheres*, 108 (D7), 8427, 2003.
- Wenzel, R.J., and K.A. Prather, Improvements in ion signal reproducibility obtained using a homogeneous laser beam for on-line laser desorption/ionization of single particles, *Rapid Communications in Mass Spectrometry*, 18, 1525-1533, 2004.
- Willermet, P.A., Some engine oil additives and their effects on antiwear film formation, *Tribology Letters*, 5 (1), 41-47, 1998.
- Wingfors, H., A. Sjodin, P. Haglund, and E. Brorstrom-Lunden, Characterization and determination of profiles of polycyclic aromatic hydrocarbons in a traffic tunnel in Gothenburg, Sweden, *Atmospheric Environment*, 35 (36), 6361-6369, 2001.
- Yaffe, D., Y. Cohen, J. Arey, and A.J. Grosovsky, Multimedia analysis of PAHs and nitro-PAH daughter products in the Los Angeles basin, *Risk Analysis*, 21 (2), 275-294, 2001.
- Yamaguchi, E.S., S.H. Roby, M.M. Francisco, S.G. Ruelas, and D. Godfrey, Antiwear film formation by ZnDTP, detergent, and dispersant components of passenger car motor oils, *Tribology Transactions*, 45 (3), 425-429, 2002.

Section III

Fuel and Oil Studies

Comparison of Oil and Fuel Aerosol Chemical Signatures with Heavy Duty and Light Duty Vehicle Emissions Using ATOFMS

5.1 Introduction

LDV and HDDV emissions are comprised of a significant amount of particles containing combinations of EC, OC, trace metals, and salts [Burtcher *et al.*, 1998; Kittelson, 1998; Kleeman *et al.*, 2000; Schauer *et al.*, 2002; Silva and Prather, 1997; Suess and Prather, 2002]. Differentiating between LDV and HDDV aerosols is crucial in evaluating the environmental and health impacts of each. Oil and fuel formulations can influence the amount of EC, OC, metals and salts that are emitted from vehicles [Alander *et al.*, 2004; Isotalo *et al.*, 2002; Wang *et al.*, 2000]], and these formulations can vary by brand and type [Marr *et al.*, 1999]. Therefore, identical vehicles operating on similar fuel and oil, but from different vendors, could potentially emit chemically different aerosols. Determining whether the majority of particulate phase chemicals from LDV and HDDV emissions are present from incomplete fuel combustion, unburned oil, or engine block elements will be useful in identifying chemical markers for evaluating LDV and HDDV particulate emissions. This could lead to better petroleum formulations or engine design for abiding to more stringent pollution regulations.

An ATOFMS was used to analyze sixteen different aerosolized vehicular related fluids: new auto oil, new diesel oil, used auto oil, three used diesel oils, four unleaded fuels from different public gas stations, four diesel fuels from different public gas stations and three diesel fuels taken from the fuel tank of different diesel trucks. The aim of this work is to look for ion markers which can be used to relate mass spectral signatures from oil and fuel aerosols to LDV and HDDV emission particles and to shed light on which vehicular related fluids are significant contributors to vehicular particulate emissions. Further, comparison between the oil and fuels themselves is made, and the mass spectral fingerprints of each are discussed.

5.2 Experimental

5.2.1 Single Particle Analysis: ATOFMS

Single particle chemical analysis was performed using a transportable dual ion aerosol time-of-flight mass spectrometer (ATOFMS). A detailed instrumental description has been previously reported [Gard *et al.*, 1997]. Briefly, an ATOFMS measures in real-time the aerodynamic size and chemical composition of individual particles between 0.2 and 3.0 microns.

5.2.2 Fuel and Oil Aerosol Generation

Unleaded and diesel fuel samples numbered 1-4 were purchased from public gas stations in the San Diego, California area from: 1) Arco, 2) Shell, 3) Chevron, and 4) Unocal 76. New oil samples were purchased from a Unocal 76 gas station. New auto oil was a 10W-30 blend, and new diesel oil was a 15W-40 blend. Auto fuel was 87 octane (regular) unleaded and both diesel and unleaded fuel samples (1-4) were stored in a plastic petroleum storage container for 1 week prior to sampling. HDDV fuel and oil numbered (1-3) were obtained from: 1) 1995 Freightliner, 2) 1990 Peterbilt, and 3) 1996 Kenworth. Used light duty vehicle oil was obtained from a 2000, V6, Toyota truck. All used oil samples had a dark black visual appearance and were stored in glass containers.

Aerosols of the fuels and oils were generated using a Collison nebulizer [May, 1973], followed by two dilution chambers. Laboratory generated, charcoal filtered, dry, particle free air was used for aerosol production and subsequent dilution. A two liter dilution chamber was utilized first, followed by a 1 L chamber. Each dilution chamber was made of Pyrex glass. The dilution chambers each gave about a 10-fold dilution for an overall dilution of the initial particle stream of 100-fold. Aerosol size distributions were measured using the ATOFMS, an Aerodynamic Particle Sizer (APS, TSI Inc. model 3321), and a Scanning Mobility Particle Sizer (SMPS, TSI Inc. models 3080 and 3010).

5.2.3 ATOFMS Data Analysis

Data were imported into Matlab Version 6.1.0.450 release 12.1 (The Math Works, Inc.) containing YAADA version 1.2 [<http://www.yaada.org/>]. Comparisons between HDDV and oil/fuel samples were performed using components of the YAADA toolkit.

Particle types were grouped using a neural network, adaptive resonance theory (ART-2a) [Hopke and Song, 1997; Song et al., 2001; Song et al., 1999]. ART-2a groups similar particles together based on similarities between ion peak intensities. The parameters used for ART-2a in this experiment were: learning rate = 0.05, vigilance factor = 0.85, iterations = 20. This grouping of similar particles generates a weight matrix (WM). The WM represents a weighted average of a group of mass spectra that were found to be similar using ART-2a. The WM of different particle types can then be analyzed by hand and further refined into distinct chemical classes. From this grouping of similar particles an area matrix (AM) can then be generated. This AM is the non-weighted average intensity for each m/z for all particles within a group. In general, the AM strongly resembles the individual mass spectra of a particle within a group.

5.3 Results and Discussion

5.3.1 General Particle Classes

Throughout the following discussion the presence and relative intensities of certain ion peaks are used to distinguish the presence of either EC or OC. EC is characterized by carbon cluster peaks at positive and negative m/z (12, 24, 36... C_n) that are generally higher in intensity than other surrounding OC peaks at m/z 15⁺, 27⁺, 29⁺, 43⁺, 25⁻, and 26⁻ that might be present. OC peaks at these m/z could be assigned to many different organic ions known to form during organic fragmentation processes [McLafferty, 1980]. Some of these include, ¹⁵(CH₃)⁺, ²⁷(C₂H₃)⁺,

$^{27}(\text{CNH})^+$, $^{29}(\text{C}_2\text{H}_5)^+$, $^{29}(\text{COH})^+$, $^{43}(\text{CHNO})^+$, $^{43}(\text{C}_2\text{H}_3\text{O})^+$, $^{43}(\text{C}_3\text{H}_7)^+$, $^{91}(\text{C}_7\text{H}_7)^+$, $^{25}(\text{C}_2\text{H})^-$, $^{26}(\text{CN})^-$. Pure organic compounds can also form ions during laser ablation at positive and negative m/z of (12, 24, 36... C_n) [Silva and Prather, 2000]; however, these occur at lower intensity relative to the organic markers at m/z 15^+ , 27^+ , 29^+ , 43^+ , 25^- , and 26^- and, therefore are not attributed to EC.

Generated oil and diesel fuel particles ranged in size between 500nm – 5000nm. Oil aerosol had a mode at roughly 2.3 micron and the diesel fuel aerosol had a mode at 1.0 micron as measured by the APS. Unleaded fuel aerosols had a size range from 20 nm to 1500 nm as measured by the APS and SMPS. Unleaded fuel aerosols contained a mode at 670 nm on the APS, and 100 nm on the SMPS. These size distributions are likely a consequence of how the aerosols were generated, and a different method could yield different size distributions. The ATOFMS used in this experiment is able to analyze particles with an aerodynamic diameter within 200-3000 nm in size.

Figure 5.1 shows a histogram of the different particle types that were observed in each oil or fuel sample. From this figure you can see similarities and differences in the type of chemical classes that make up each series of samples. Assuming that each sample is well mixed and uniform in its contents, then each sample might be expected to generate only one unique mass spectrum based on its composition. However, because of inhomogeneities in the laser beam energy profile, different amounts of energy can be imparted on similar particles leading to differences in fragmentation and thus formation of different ions.

New oil samples are dominated by a Ca-Phosphate-OC chemical class, whereas the used HDDV oil samples are dominated by a Ca-OC-Phosphate- NO_2 -Na, and Ca-ECOC-Phosphate particle type. Used car oil also contains the Ca-OC-Phosphate- NO_2 -Na type, however it differs from used HDDV oil by the presence of a Ca-PAH-OC-Phosphate particle type. HDDV used oil #3 is unique from the other used oils in that it contains a particle class labeled Ca-ECOC-Na-Phosphate. Diesel fuel aerosols were dominated by two chemical classes, a PAH containing class and an OC-Na-Sulfate-Phosphate class. This OC-Na-Sulfate-Phosphate class is also seen in all the unleaded fuel samples however not as many of them were generated. Each of the four unleaded fuel samples also contained a PAH-Sulfate- NO_2 -Cl, and an OC-K-Na-Sulfate-Phosphate particle class. This OC-K-Na-Sulfate-Phosphate particle class is the dominant particle class in each unleaded fuel sample. Unleaded fuel samples #1 and #3 are differentiated from the other two unleaded fuel samples by the presence of an OC-Sulfate-Phosphate chemical class. Unleaded fuel sample #2 contains an OC-Sulfur-Containing class which is unique to unleaded #2 and unleaded sample #4 contains an OC-Sulfur-Other class which is unique to unleaded #4.

The new diesel and auto oil both contained a particle type classified as Ca-Phosphate-OC. Figure 5.2 (a-f) contains the AM for the different particle classes detected in the new and used oils. Figure 5.2a is the AM of a particle type containing Ca-phosphate-OC that was observed almost exclusively from the new auto and new diesel oils. Oil from Truck #1 did produce a very small fraction (<1%) of this particle type; however, the positive ion mass spectra of particles in this cluster are dominated by a very strong $^{40}\text{Ca}^+$ peak. Peaks are also seen for $^{57}\text{CaOH}^+$, $^{96}\text{Ca}_2\text{O}^+$, and m/z 27^+ . Mass to charge 27^+ is likely $^{27}\text{HCN}^+$ and attributed to the presence of nitrogen containing organics. Further evidence for the presence of these nitrogen containing organics is the presence of a intense $^{26}(\text{CN})^-$. The corresponding negative ion spectrum of Figure 5.2a shows the presence of phosphate ($^{63}\text{PO}_2^-$, $^{79}\text{PO}_3^-$, and $^{95}\text{PO}_4^-$), carbon clusters out to $^{60}\text{C}_5^-$, $^{26}(\text{CN})^-$, $^{42}\text{CNO}^-$, and $^{111}(\text{CH}_3\text{SO}_4)^-$. Ca is expected to be present in oil because it is added to engine lubricants as part of a detergent complex [Lyyranen *et al.*, 1999].

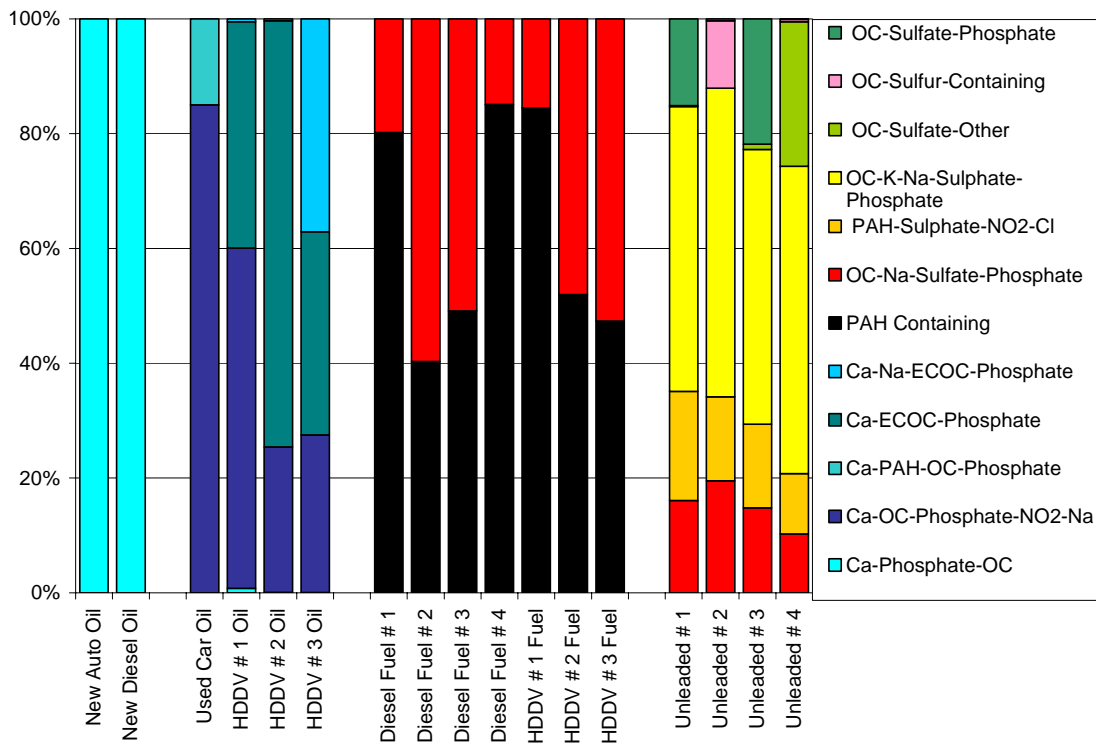


Figure 5.1 This histogram represents the contribution of each mass spectral class to the different oil and fuel samples that were analyzed using an ATOFMS. Each oil or fuel type is listed across the x-axis, and the normalized percentage of each mass spectral class is listed on the y-axis. Color corresponding mass spectral classes are listed on the right hand side of the figure.

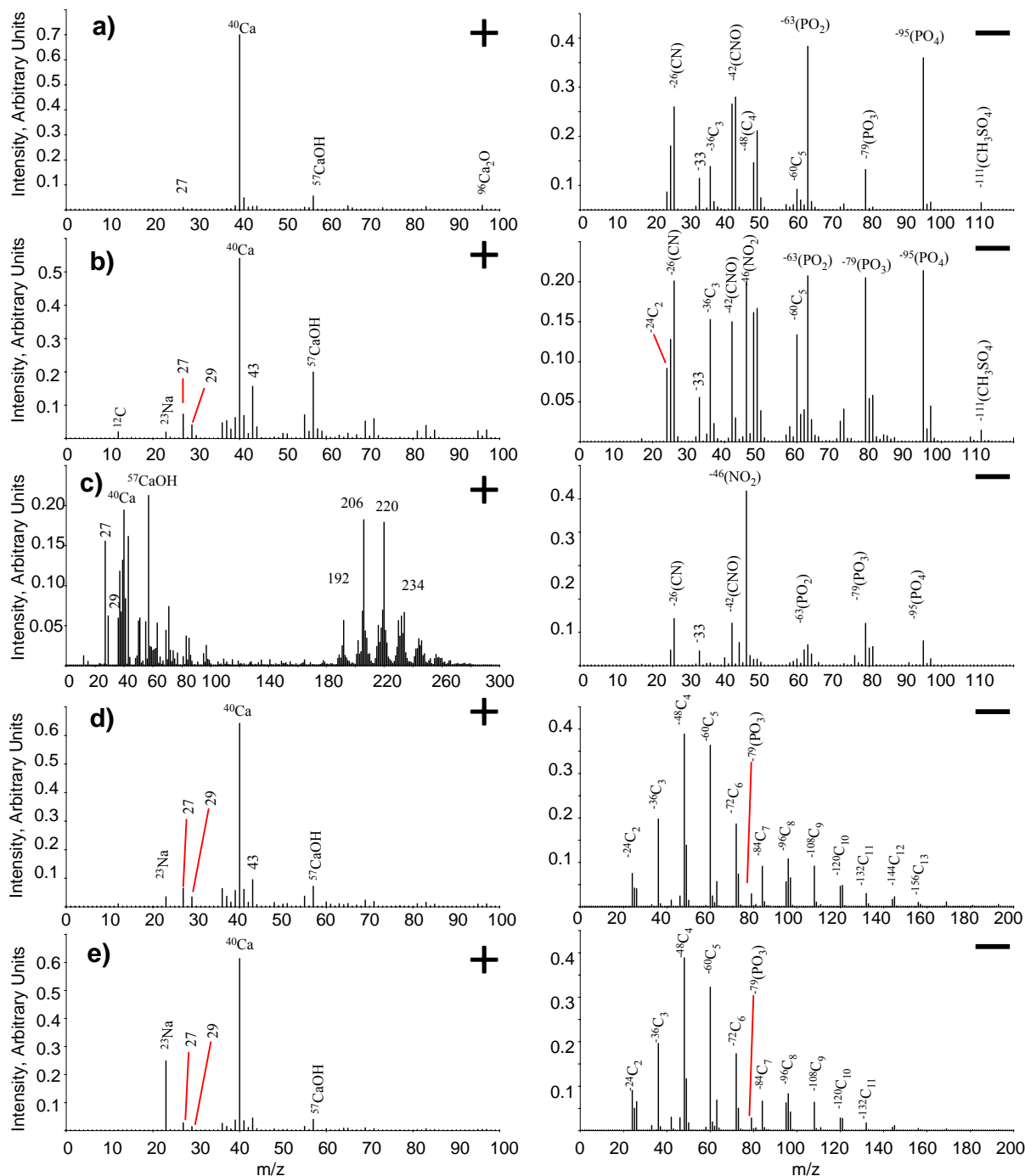


Figure 5.2 Positive and negative ion area matrices (AM) for all chemical classes seen in used and new oil, for both unleaded fuel and diesel fuel vehicles. The five different major classes shown are; a) Ca-Phosphate-OC , b) Ca-OC-Phosphate-NO₂-Na, c) Ca-PAH-OC-Phosphate, d) Ca-ECOC-Phosphate, and e) Ca-Na-ECOC-Phosphate

These detergents help neutralize and stabilize highly polar compounds that are formed during the combustion process. Without these detergents, polar compounds tend to separate out of the non-polar environment of the lubricant and cause surface deposits and clogging within an engine [Rudnick, 2003]. Zinc dialkyldithiophosphates (ZDDP) are added to commercial lubricants and serve as anti-wear and extreme-pressure agents [Gautam *et al.*, 1999]. ZDDP and the thermo-oxidative break down products orthophosphate and pyrophosphate have been measured in lubricant films, so the presence of phosphates and phosphites is expected [Canning *et al.*, 1999; Willermet *et al.*, 1992]. The presence of zinc is also expected, however due to the nature of the organic matrix, zinc ions were not formed during laser ablation.

Figure 5.2b shows the AM for a Ca-OC-Phosphate-NO₂-Na particle type. It is easily distinguished from Figure 5.2a by the increased amount of OC markers at 27⁺, 29⁺, 43⁺, the presence of ²³Na⁺, and the presence of an intense peak at ⁴⁶(NO₂)⁻. NO_x formation can occur during the combustion process from reactions between oxygen and nitrogen found in the fuel-air mixture [Heywood, 1988]. Some of these nitrogen species can then be absorbed into the oil and be stabilized as inorganic salts [Rudnick, 2003]. It has also been shown that nitro-PAH's fragment into CN⁻ and NO₂⁻ when ionized using a 266nm laser as was done in this experiment [Bezabeh *et al.*, 1997]. Peaks at ²⁶(CN)⁻ and ⁴⁶(NO₂)⁻ could therefore be from nitro-PAH's. Nitro-PAH's have been measured in both used oil and diesel particulates [Bezabeh *et al.*, 1997; Zielinska *et al.*, 2004]. An increase in OC content within used oil would be expected, because a function of the oil is to stabilize polar organics that are formed during the combustion process [Rudnick, 2003]. This Ca-OC-Phosphate-NO₂-Na particle type is seen only within the used auto and truck oil samples.

Used diesel oil and used auto oil samples can be differentiated from each other by the presence of PAH's in the used auto oil. Figure 5.2c shows the AM for a Ca-PAH-OC-Phosphate particle class found only in the used auto oil. It is characterized by a peak for ⁴⁰Ca⁺, OC peaks at 27⁺, 29⁺, and intense ion signals attributed to PAH's at 192⁺, 206⁺, 220⁺, 234⁺. Each of these PAH is separated by a mass of 14 which suggests they could be phenanthrene or anthracene with increasing numbers of methyl or ethyl substituents. These types of PAH's have been measured in oil, fuel, and tailpipe emissions [Zielinska *et al.*, 2004]. It has been shown that lube oil in gasoline engines contains a larger amount of PAH's as compared to diesel oil [Zielinska *et al.*, 2004]. Furthermore, it has been shown that diesel oil PAH did not match diesel emission PAH and it is suggested that diesel PAH emissions are not a component of unburned diesel oil [Zielinska *et al.*, 2004].

All three used truck oils contain a unique particle class containing Ca-ECOC-Phosphate, which is shown in Figure 5.2d. This class also differentiates used diesel oil from the used auto oil. The positive ion AM in Figure 5.2d shows dominant peaks such as ⁴⁰Ca⁺, ⁵⁷CaOH⁺, ⁹⁶Ca₂O⁺, and OC peaks 27⁺, 29⁺, 43⁺. A carbon envelope out to ¹⁵⁶C₁₃⁻ and the presence of ⁶³PO₂⁻, ⁷⁹PO₃⁻, and ⁹⁵PO₄⁻ can be seen in the negative ion AM. It has been well documented that diesel powered engines generate more EC than spark ignition engines [Burtscher *et al.*, 1998; Zielinska *et al.*, 2004]. One function of lubricating oil is to help disperse agglomerated EC particles that form in the oil. Because diesel engines generate more EC, one would expect to find more EC agglomerates in a sample of used diesel oil verses used auto oil. A comparison of this particle class with HDDV particles yielded only a small fraction of particles with an identical mass spectral fingerprint. A possible explanation for this is that the EC particles from diesel trucks are fresh un-agglomerated EC and much smaller in size. Shields *et al.* (2005), and Toner *et al.*

(2005) state that a dominant particle class from diesel trucks from 100-500 nm is indeed an EC-Ca particle type. This differs from the Ca-ECOC-Phosphate type here by the intensity of the carbon clusters in the positive ion mass spectra vs the Ca peak intensity. This would suggest that EC particles between 100nm and 500nm from diesel trucks are a mixture of freshly generated EC with a small fraction of unburned oil.

Figure 5.2e is the AM for the Ca-Na-ECOC-Phosphate class, which is unique to HDDV oil #3. It is easily distinguished from the increased peak intensity from $^{23}\text{Na}^+$. This $^{23}\text{Na}^+$ is possibly from impurities in the oil or from impurities in the fuel which then were absorbed into the oil. All other characteristics of this AM are very similar to the Ca-ECOC-Phosphate class. Work by *Shields et al.* (2005) show that the particulate emissions from this truck in particular contained a particle class with an intense Na^+ peak. This is evidence that fresh truck particulates contain a significant fraction of unburned oil.

Diesel fuel and regular unleaded fuel aerosols are easily distinguished from each other based on the presence of unique PAH ions. Figure 5.3a shows the AM that makes up from 40-80% of the diesel fuel particulate mass spectra. This class is labeled PAH-Containing and is comprised of any clusters that contained intense ion signals at m/z 181⁺, 195⁺, 206⁺, 220⁺, 234⁺ and at m/z 193⁻, 207⁻, 222⁻, and 236⁻ in the negative ions. PAH compounds have been shown to comprise a large fraction of diesel fuel [*Rhead and Hardy*, 2003]. The formation of a negative ion PAH is a very distinct feature of the diesel fuel AM shown here. A possible explanation for this is that these negative ion PAH's contain an electronegative functionality such as oxygen. Oxy-PAH's have been measured in diesel fuel [*Zielinska et al.*, 2004]. Anthraquinone for example has a mass of 208, and a methyl-anthraquinone would have a mass of 222, peaks at both of these m/z are seen in Figure 5.3a. It must be noted, however, that assignment of these negative ions to these oxy-PAHs is highly speculative. Peaks for OC are also observed at m/z , 27⁺, 29⁺, 43⁺ and $^{26}\text{CN}^-$.

Both diesel fuel and unleaded fuel contain a OC-Na-Sulphate-Phosphate particle class. Figure 5.3b is the AM for this class, and is characterized by the presence of OC peaks at 27⁺, 29⁺, 43⁺, 91⁺ and 25⁻, sulfate peak at $^{97}(\text{HSO}_4)^-$, phosphate peak at $^{79}(\text{PO}_3)^-$. Higher molecular weight ions at 165⁻, 179⁻, and 193⁻ are also present. These ions are attributed to a nitrogen containing aromatic with alkyl substitutions. A parent ion with an odd mass, such as m/z 165, 179, 193, will likely contain an odd number of nitrogens [*McLafferty*, 1980]. Further, fragment ions at m/z 119⁺, 105⁺, 91⁺ are attributed to fragmentation from phenylalkyl type compounds [*McLafferty*, 1980]. Definitive assignment of these peaks is quite difficult, however, due to the enormous number of organics that could be derived from in the gasoline and diesel fuel.

Figure 5.4 (a-e) contain the AM for the five different particle classes that are unique to the unleaded fuel samples. Figure 5.4a is the AM of a PAH-Sulfate-NO₂-Cl particle class, which is present in each unleaded fuel sample. This AM is characterized by intense peaks attributed to PAH ions at m/z , 191⁺, 205⁺, 218⁺, 230⁺, and 242⁺. The ions at m/z 218⁺, 230⁺, and 242⁺ are separated by 12 amu, which suggests that m/z 230⁺ and 242⁺ are likely the addition of one or two unsaturated ^{12}C . OC peaks are also seen at m/z 43⁺, 57⁺, and 25⁻ along with peaks from $^{35}\text{Cl}^-$, $^{97}(\text{HSO}_4)^-$, and $^{46}(\text{NO}_2)^-$. The negative ion AM also contains intense peaks at m/z 109⁻, 123⁻, and 137⁻, which are probably due to alkyl fragmentation.

The largest fraction of mass spectra from unleaded fuel was an OC-K-Na-Sulfate-Phosphate particle type. An AM for this particle class is shown in Figure 5.4b. The presence of potassium in the unleaded fuel distinguishes it from the diesel fuel. Potassium is not generally

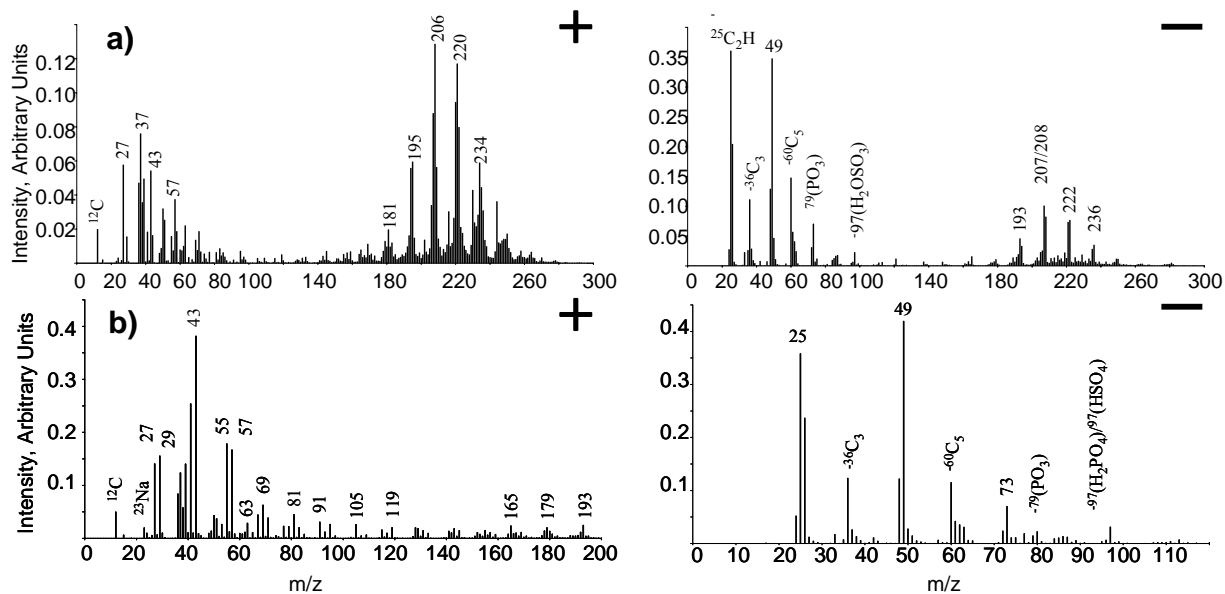


Figure 5.3 Positive and negative ion area matrices (AM) for the two classes seen in diesel fuel aerosols. a) PAH Containing, b) OC-Na-Sulfate-Phosphate. Unleaded fuel aerosol also contained the OC-Na-Sulfate-Phosphate particle class.

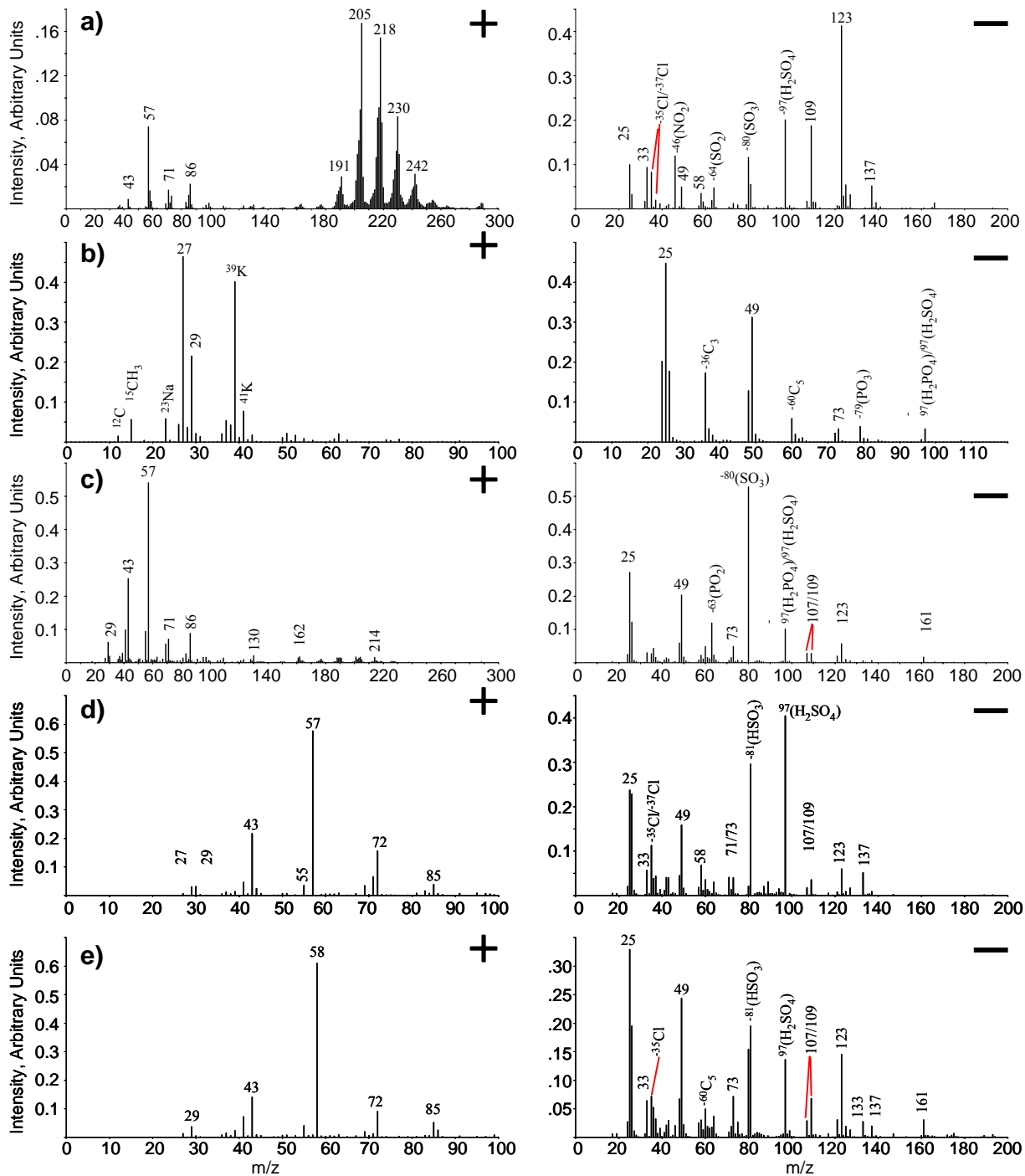


Figure 5.4 Positive and negative ion area matrices (AM) for five chemical classes that are unique to unleaded fuel. The five different major classes shown are; a) PAH-Sulfate-NO₂-Cl, b) OC-K-Na-Sulfate-Phosphate, c) OC-Sulfate-Phosphate, d) OC-Sulfur containing, and e) OC-Sulfate-Other

added as part of a fuel additive; however it is clearly present in all the unleaded fuel samples. The presence of potassium is thought to come from Na/K/Sulfur contamination of ethanol, which is an unleaded fuel additive (Personal Communication, Conoco-Phillips Corp.). Peaks are also observed for OC at $^{15}\text{CH}_3^+$, 27^+ , 29^+ , and 25^- . Sulfate and phosphate ions are seen at $^{97}(\text{HSO}_4)^-$, and $^{79}(\text{PO}_3)^-$. C_n peaks are also detected in the negative ion spectra out to m/z 72 $^-$. A mass spectral class containing Na and K has been observed in LDV emissions using ATOFMS [Sodeman *et al.*, 2005]. Na and K metals found in LDV emissions could very likely be from the combustion of the fuel.

Unleaded fuel sample #1 and #3 contain an OC-Sulfate-Phosphate particle class which is unique to these samples. The AM for this OC-Sulfate-Phosphate particle class is shown in Figure 5.4c. OC peaks at m/z 29 $^+$, 43 $^+$, 57 $^+$, and 25 $^-$ are seen along with peaks at 130 $^+$, 162 $^+$, and 214 $^+$. An intense $^{80}(\text{SO}_3)^-$ sulfate ion along with a less intense $^{97}(\text{HSO}_4)^-$ are also observed. Other peaks in the negative ion AM are a phosphate peak at $^{63}(\text{PO}_2)^-$, and peaks at 49 $^-$, 73 $^-$, 107 $^-$, 109 $^-$, 123 $^-$, and 161 $^-$. Figure 5.4d is the AM for a particle class unique to unleaded fuel sample #2. This AM contains OC peaks at 27 $^+$, 29 $^+$, 43 $^+$, 57 $^+$, and 25 $^-$ and other peaks at 72 $^+$, and 85 $^+$. Sulfate peaks are present at $^{81}(\text{HSO}_3)^-$, $^{97}(\text{HSO}_4)^-$, and a chlorine peak at $^{35}\text{Cl}^-$. As seen in Figure 5.4c peaks at 49 $^-$, 73 $^-$, 107 $^-$, 109 $^-$, and 123 $^-$ are also present and likely formed from alkyl fragmentation. The AM shown in Figure 5.4e is unique to unleaded fuel sample #4. It is labeled as OC-Sulfate-Other. It is similar to the AM in Figure 5.5d; however, it contains an intense peak at m/z 58 $^+$. The negative ion AM for this class contains peaks for sulfate at $^{81}(\text{HSO}_3)^-$, $^{97}(\text{HSO}_4)^-$, and a chlorine peak at $^{35}\text{Cl}^-$. Alkyl fragment ions at m/z 49 $^-$, 73 $^-$, 107 $^-$, 109 $^-$, 123 $^-$, and 161 $^-$ are also present.

Comparisons of the Ca-OC-Phosphate- NO_2 -Na particle class with the particle classes from HDDV trucks run on a dynamometer have a high degree of similarity. Figure 5.5 (a-b) show the positive and negative ion AM for the Ca-OC-Phosphate- NO_2 -Na mass spectral class, attributed to used oil, compared to the AM for the most abundant particle class detected in a HDDV dynamometer study using ATOFMS [Shields *et al.*, 2005]. This finding is consistent with a previous report that states up to 95% of the volatile component of nanoparticles and accumulation-mode particles emitted from diesel trucks are from unburned oil [Sakurai *et al.*, 2003]. In a study by Wang, *et al.* (2003), they report that the emission of Ca and other metals from a diesel engine could be fully explained by the consumption rate of metals in the fuel [Wang *et al.*, 2003]. This led these authors to conclude that crustal elements (Al, Ca, Fe, Mg, and Si) present in diesel exhaust particles came primarily from the fuel. Data reported here would suggest the vast majority of Ca in diesel exhaust is from unburned oil, not from diesel fuel. A comparison of the Ca-OC-Phosphate- NO_2 -Na particulate class with LDV exhaust particle classes did not yield many similarities between the two, suggesting that LDV emissions normally are not composed of a large fraction of unburned oil. However, a “smoker” LDV that emits heavy amounts of smoke from its tailpipe did contain a small fraction (~2%) of this Ca-OC-Phosphate- NO_2 -Na particle class shown in Figure 5.5c [Sodeman *et al.*, 2005].

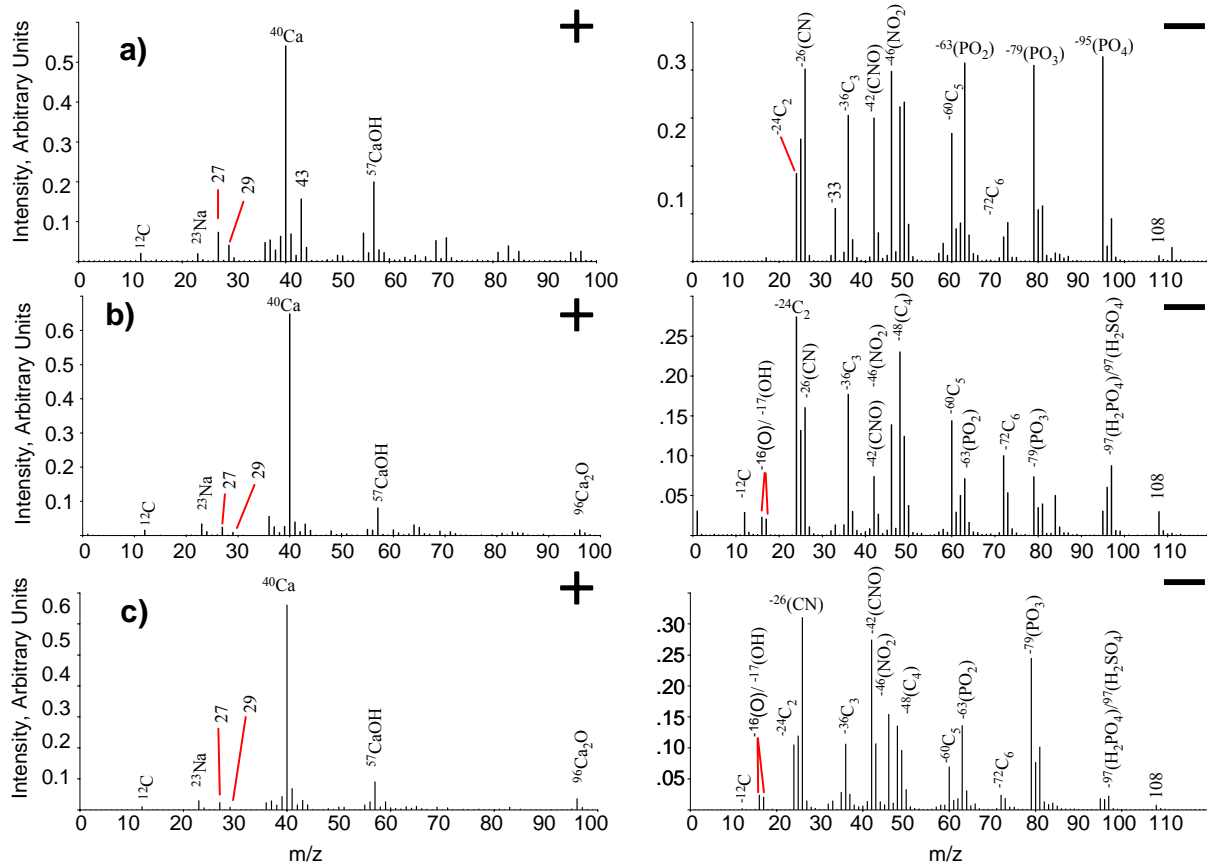


Figure 5.5 Comparison of a) Ca-OC-Phosphate-NO₂-Na area matrix from used oil, b) the area matrix from the largest mass spectral class from the exhaust of heavy duty diesel trucks, and c) an area matrix from a class of particles which made up ~2% of “smoker” LDV mass spectra.

5.4 Conclusions

A large fraction of freshly emitted diesel particulate matter in the size range of 0.5 to 2.5 microns has the same mass spectral fingerprint as used diesel oil aerosols in the same size range. Used oil that contained larger amounts of Na also corresponded to particulate emissions containing Na⁺ and other elements found in oil. This suggests that a large fraction of particles emitted from HDDV in this size range contain unburned lubricating oil. Diesel particulate matter between 0.1 to 0.5 microns does not contain a majority of mass spectral fingerprints that are closely matched to used diesel oil, however ions such as ⁴⁰Ca⁺ along with intense EC peaks suggest that these particles contain some unburned lubrication oil along with freshly generated EC. A good surrogate for HDDV aerosols in the laboratory might be used diesel oil aerosols. In this respect, one could possibly use diesel oil aerosols in health affect studies and atmospheric chemistry as a HDDV aerosol component. This would allow researchers to generate HDDV particulate matter isolated from the rest of the exhaust gas.

Although diesel fuel contained more PAH containing compounds compared to unleaded fuel, used diesel oil contained fewer PAH containing spectra as compared to used auto oil. A possible explanation for this is that the majority of PAH compounds in the diesel fuel are readily converted to soot during the combustion process and this soot is taken up by the oil. PAH compounds are believed to be the precursors to soot [Dobbins *et al.*, 1998].

Unleaded fuel and diesel fuel aerosols did not contain many similarities to particles emitted from LDV and HDDV vehicles, suggesting particulates from both LDV and HDDV do not contain a large fraction of unburned fuel aerosol. Presumably, this dissimilarity is because the fuels sampled in this experiment have not undergone combustion. Elements such as potassium, sodium, and chlorine, which have been measured in LDV and HDDV particles, were present in the fuel samples. This suggests that these elements could likely be coming from the fuel. A comparison of LDV particle mass spectra with used oil mass spectra did not yield many similarities, except in the case of a “smoker”. This would indicate that most LDV are not emitting a large fraction of unburned oil because they lacked the used oil mass spectral fingerprint. LDV particulates could be a mix of combusted fuel components, and unburned oil whose mass spectral fingerprint is different. Further studies with the aim of determining how LDV and HDDV particles change chemically as they age within the atmosphere are currently under progress.

5.5 References

- Alander, T.J.A., A.P. Leskinen, T.M. Raunemaa, and L. Rantanen, Characterization of diesel particles: Effects of fuel reformulation, exhaust aftertreatment, and engine operation on particle carbon composition and volatility, *Environmental Science & Technology*, 38 (9), 2707-2714, 2004.
- Bata, R., N. Clark, M. Gautam, A. Howell, T. Long, J. Loth, D. Lyons, G. Palmer, J. Smith, and W. Wang, A transportable heavy duty engine testing laboratory, *SAE Trans.*, 100, 433-440, 1991.

- Bezabeh, D.Z., T.M. Allen, E.M. McCauley, P.B. Kelly, and A.D. Jones, Negative ion laser desorption ionization time-of-flight mass spectrometry of nitrated polycyclic aromatic hydrocarbons, *Journal of the American Society for Mass Spectrometry*, 8 (6), 630-636, 1997.
- Burtscher, H., S. Kunzel, and C. Huglin, Characterization of particles in combustion engine exhaust, *Journal of Aerosol Science*, 29 (4), 389-396, 1998.
- Canning, G.W., M.L.S. Fuller, G.M. Bancroft, M. Kasrai, J.N. Cutler, G. De Stasio, and B. Gilbert, Spectromicroscopy of tribological films from engine oil additives. Part I. Films from ZDDP's, *Tribology Letters*, 6 (3-4), 159-169, 1999.
- Dobbins, R.A., R.A. Fletcher, and H.C. Chang, The evolution of soot precursor particles in a diffusion flame, *Combustion and Flame*, 115 (3), 285-298, 1998.
- Gard, E., J.E. Mayer, B.D. Morrical, T. Dienes, D.P. Fergenson, and K.A. Prather, Real-time analysis of individual atmospheric aerosol particles: Design and performance of a portable ATOFMS, *Analytical Chemistry*, 69 (20), 4083-4091, 1997.
- Gautam, M., K. Chitoor, M. Durbha, and J.C. Summers, Effect of diesel soot contaminated oil on engine wear - investigation of novel oil formulations, *Tribology International*, 32 (12), 687-699, 1999.
- Heywood, J.B., *Internal combustion engine fundamentals*, xxix, 930 p., McGraw-Hill, New York, 1988.
- Hopke, P.K., and X.H. Song, Classification of single particles by neural networks based on the computer-controlled scanning electron microscopy data, *Analytica Chimica Acta*, 348 (1-3), 375-388, 1997.
- Isotalo, S., T. Kuljukka-Rabb, L. Rantanen, S. Mikkonen, and K. Savela, The effect of diesel fuel reformulation on the exhaust measured by Ames mutagenicity and DNA adducts, *International Journal of Environmental Analytical Chemistry*, 82 (2), 87-95, 2002.
- Kittelson, D.B., Engines and nanoparticles: A review, *Journal of Aerosol Science*, 29 (5-6), 575-588, 1998.
- Kleeman, M.J., J.J. Schauer, and G.R. Cass, Size and composition distribution of fine particulate matter emitted from motor vehicles, *Environmental Science & Technology*, 34 (7), 1132-1142, 2000.
- Lyyranen, J., J. Jokiniemi, E.I. Kauppinen, and J. Joutsensaari, Aerosol characterisation in medium-speed diesel engines operating with heavy fuel oils, *Journal of Aerosol Science*, 30 (6), 771-784, 1999.

- Marr, L.C., T.W. Kirchstetter, R.A. Harley, A.H. Miguel, S.V. Hering, and S.K. Hammond, Characterization of polycyclic aromatic hydrocarbons in motor vehicle fuels and exhaust emissions, *Environmental Science & Technology*, 33 (18), 3091-3099, 1999.
- May, K.R., Collision nebulizer. Description, performance, and application, *Journal of Aerosol Science*, 4 (3), 235-43, 1973.
- McLafferty, F.W., *Interpretation of Mass Spectra. 3rd Ed*, 303 pp. pp., 1980.
- Rhead, M.M., and S.A. Hardy, The sources of polycyclic aromatic compounds in diesel engine emissions, *Fuel*, 82 (4), 385-393, 2003.
- Rudnick, L.R., *Lubricant additives : chemistry and applications*, xiii, 735 p. pp., M. Dekker, New York, 2003.
- Sakurai, H., H.J. Tobias, K. Park, D. Zarling, S. Docherty, D.B. Kittelson, P.H. McMurry, and P.J. Ziemann, On-line measurements of diesel nanoparticle composition and volatility, *Atmospheric Environment*, 37 (9-10), 1199-1210, 2003.
- Schauer, J.J., M.J. Kleeman, G.R. Cass, and B.R.T. Simoneit, Measurement of emissions from air pollution sources. 5. C-1-C-32 organic compounds from gasoline-powered motor vehicles, *Environmental Science & Technology*, 36 (6), 1169-1180, 2002.
- Shields, L.G., D.T. Suess, S.A. Guazzotti, and K.A. Prather, Determination of single particle mass spectral signatures from heavy duty vehicle emissions in the 0.1 to 3 micrometer size range, *Environmental Science & Technology, manuscript in preparation*, 2005.
- Silva, P.J., and K.A. Prather, On-line characterization of individual particles from automobile emissions, *Environmental Science & Technology*, 31 (11), 3074-3080, 1997.
- Silva, P.J., and K.A. Prather, Interpretation of mass spectra from organic compounds in aerosol time-of-flight mass spectrometry, *Analytical Chemistry*, 72 (15), 3553-3562, 2000.
- Sodeman, D.A., S.M. Toner, and K.A. Prather, Determination of single particle mass spectral signatures from light duty vehicle emissions, *Environmental Science & Technology, accepted for publication*, 2005.
- Song, X.H., N.M. Faber, P.K. Hopke, D.T. Suess, K.A. Prather, J.J. Schauer, and G.R. Cass, Source apportionment of gasoline and diesel by multivariate calibration based on single particle mass spectral data, *Analytica Chimica Acta*, 446 (1-2), 329-343, 2001.
- Song, X.H., P.K. Hopke, D.P. Fergenson, and K.A. Prather, Classification of single particles analyzed by ATOFMS using an artificial neural network, ART-2A, *Analytical Chemistry*, 71 (4), 860-865, 1999.

- Suess, D.T., and K.A. Prather, Reproducibility of single particle chemical composition during a heavy duty diesel truck dynamometer study, *Aerosol Science and Technology*, 36 (12), 1139-1141, 2002.
- Toner, S.M., D.A. Sodeman, and K.A. Prather, Single particle characterization of ultrafine- and fine-mode particles from heavy duty diesel vehicles using aerosol time-of-flight mass spectrometry, *in preparation*, 2005.
- Wang, W.G., D.W. Lyons, N.N. Clark, M. Gautam, and P.M. Norton, Emissions from nine heavy trucks fueled by diesel and biodiesel blend without engine modification, *Environmental Science & Technology*, 34 (6), 933-939, 2000.
- Wang, Y.F., K.L. Huang, C.T. Li, H.H. Mi, J.H. Luo, and P.J. Tsai, Emissions of fuel metals content from a diesel vehicle engine, *Atmospheric Environment*, 37 (33), 4637-4643, 2003.
- Willermet, P.A., R.O. Carter, and E.N. Boulous, Lubricant-derived tribochemical films - an infrared spectroscopic study, *Tribology International*, 25 (6), 371-380, 1992.
- Zielinska, B., J. Sagebiel, J.D. McDonald, K. Whitney, and D.R. Lawson, Emission rates and comparative chemical composition from selected in-use diesel and gasoline-fueled vehicles, *Journal of the Air & Waste Management Association*, 54 (9), 1138-1150, 2004.

Analysis of Petroleum Based Lubricants with Different Detergent Additives and Used Engine Oils with Varying Soot Levels

6.1 Introduction

High concentrations of particulate matter associated with pollution episodes have been shown to cause deleterious health effects, leading to an increase in the morbidity rates of humans. Also, combustion emissions have been shown to affect climate through changes in cloud lifetime, and radiative forcing. Out of all the different particulate sources, fuel combustion has been shown to be a major contributor to PM in many urban areas in California. There is currently a large amount of research aimed at trying to evaluate the contributions of different sources to the overall aerosol burden in both urban and rural settings. As stated throughout this report, the major goal of the research conducted as part of this project is to develop ATOFMS so it can be used as a method for unraveling the relative impact of gasoline versus diesel engines on the environment. One step in doing this involves studying the components that make up the emissions in diesel and gasoline exhaust. As shown in this report, oil is a major component of diesel exhaust. Our goal is to determine where many of the markers we detect in engine exhaust originate, such as phosphate, calcium, and sulfur species, as well as determine whether there are any unique markers in the additive packages that can be used for source apportionment.

The goal of this study involved using aerosol time-of-flight mass spectrometry (ATOFMS) to evaluate several forms of oils and oil additive packages used in both gasoline and diesel engines: three fully formulated petroleum lubricates differing in their detergent content, three detergent additive packages, one base mineral oil, and six used oil samples which differ in their elemental carbon (EC) and polycyclic aromatic hydrocarbon (PAH) contents. Specifically, the goal was to look for unique chemical markers and chemical differences between the oil samples to aid in the apportionment of particulates detected in ambient studies in California.

6.2 Experimental

6.2.1 Oil Aerosol Generation

Oil and oil additive package samples were received from a major lubricant additive company that supplies such packages to over 50% of the world. Five different samples are distinguished as: 1) fully formulated oil with sulfonate detergent, 2) fully formulated oil with phenate detergent, 3) sulfonate additive package, 4) phenate additive package, and 5) mineral base oil with no additives. Six used oil samples that varied in the percent of soot by weight were also analyzed using an ATOFMS.

Aerosols of the oils and oil additive packages were generated using a Collison nebulizer, followed by two dilution chambers. Laboratory generated, charcoal filtered, dry, particle free air was used for aerosol production and subsequent dilution. A 2 L dilution chamber was utilized first, followed by a 1 L chamber. Each dilution chamber was made of Pyrex glass. The dilution chambers each gave about a 10-fold dilution for an overall dilution of the initial particle stream of approximately 100-fold.

6.2.2 Data Analysis

Data were imported into Matlab Version 6.1.0.450 release 12.1 (The Math Works, Inc.) containing YAADA version 1.2 [<http://www.yaada.org/>]. After importing the data into Matlab, a digital color stack mass spectrum was made for all particles with both a positive and negative mass spectrum for each individual sample. A digital color stack mass spectrum provides information on a collection of single particles, showing the fraction (y-axis) of particles that contain a certain m/z and the relative intensity (colored bars) of each peak area at different m/z values for all the particles within a sample. The range of peak areas at a particular m/z can be plotted as absolute areas which give one an idea of the amount of a given species in a particle or normalized to the total area for each individual mass spectrum (i.e. relative area). Relative area provides information on the contribution of an individual m/z to the total area for each mass spectrum. Relative areas are used in the digital color stacks presented in this chapter.

6.3 Results and Discussion

Figure 6.1 shows the digital color stacks for the a) sulfonate formulated oil, and b) sulfonate additive package. The sulfonate detergent additive is used in the formulation of gasoline engine oil lubricants. Particles from the formulated oil and the additive package shown in Figure 6.1 produce similar digital color stacks. Both have positive ion peaks attributed to organic carbon at m/z 27^+ , 29^+ and very intense peaks at m/z 40^+ and 57^+ attributed to Ca^+ and CaOH^+ . Other peaks in the positive ion spectra include m/z 65^+ , 96^+ (Ca_2O), 113^+ ($\text{Ca}_2\text{O}_2\text{H}$). The negative ion color stacks in Figures 6.1a and 6.1b both contain signals for phosphate $^{79}(\text{PO}_3)^-$, $^{95}(\text{PO}_4)^-$, and sulfite $^{80}(\text{SO}_3)^-$, and bisulfite $^{81}(\text{HSO}_3)^-$. Also intense peaks at m/z 26^- and 42^- are observed, and attributed to CN^- and CNO^- , and indicate the presence of N-containing organics in the samples. The sulfonate additive package has ions at m/z $^{16}\text{O}^-$, $^{17}\text{OH}^-$, 111^- , 183^- , and 213^- whereas the sulfonate oil formulation does not, possibly indicating the sulfonate species were “tied up” in complexes in the oil samples.

Figure 6.2 shows the digital color stacks for the a) phenate formulated oil, and b) phenate additive package. The phenate detergent additives are used in diesel engine oil lubricants. Similar to the sulfonate samples described above, both the formulated oil and additive package have positive ion peaks at m/z 27^+ , 29^+ , 40^+ , 57^+ , 65^+ , 96^+ , and 113^+ . The negative ion color stack also contains signals for phosphate $^{79}(\text{PO}_3)^-$, $^{95}(\text{PO}_4)^-$. The phenate additive package has ions at m/z $^{23}\text{Na}^+$, $^{16}\text{O}^-$, $^{17}\text{OH}^-$, whereas the phenate oil formulation does not. As expected, the

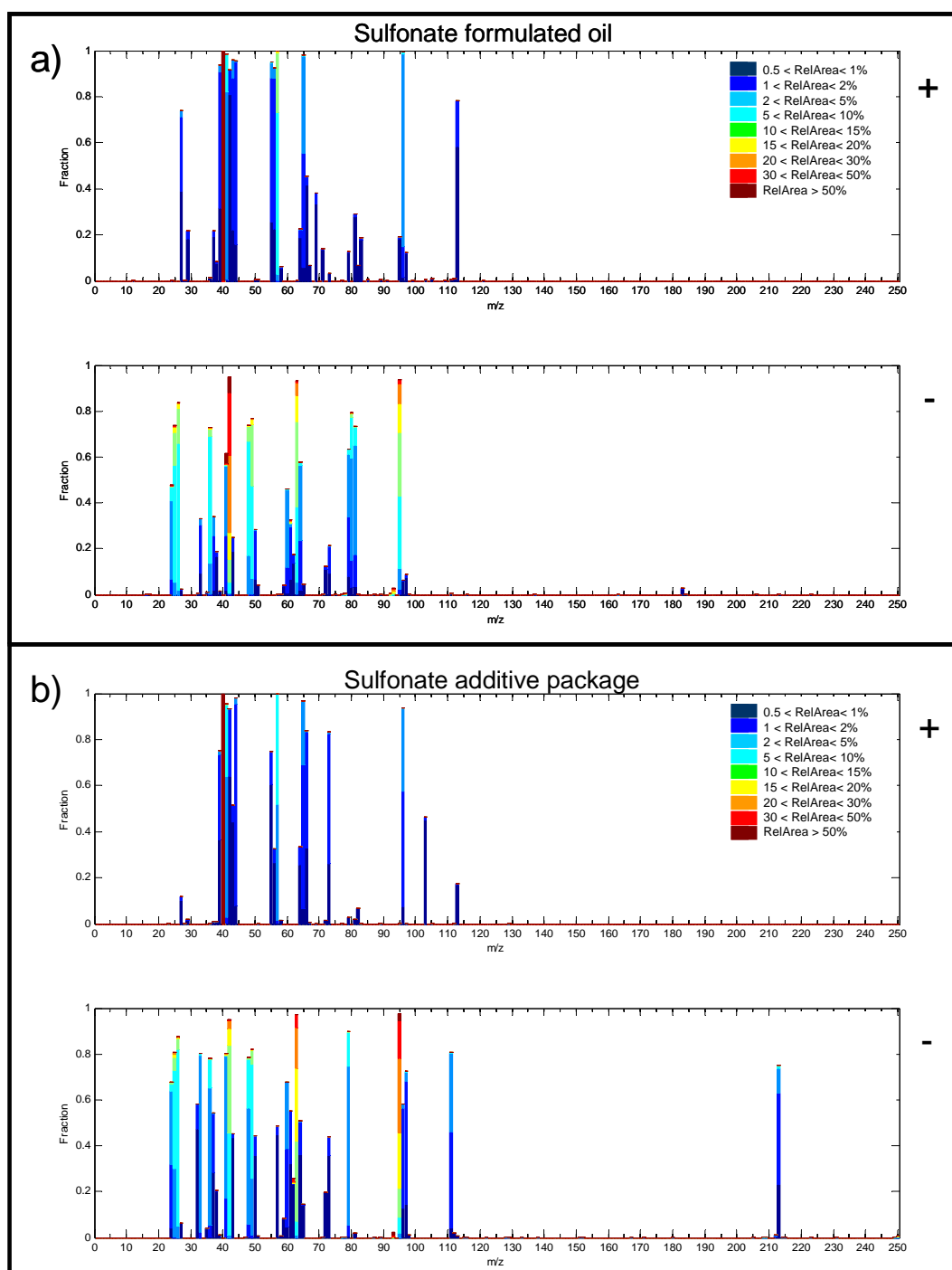


Figure 5.1 Digital mass spectrum color stack for both positive and negative ions of a) fully formulated oil with a sulfonate detergent additive and b) sulfonate detergent additive package

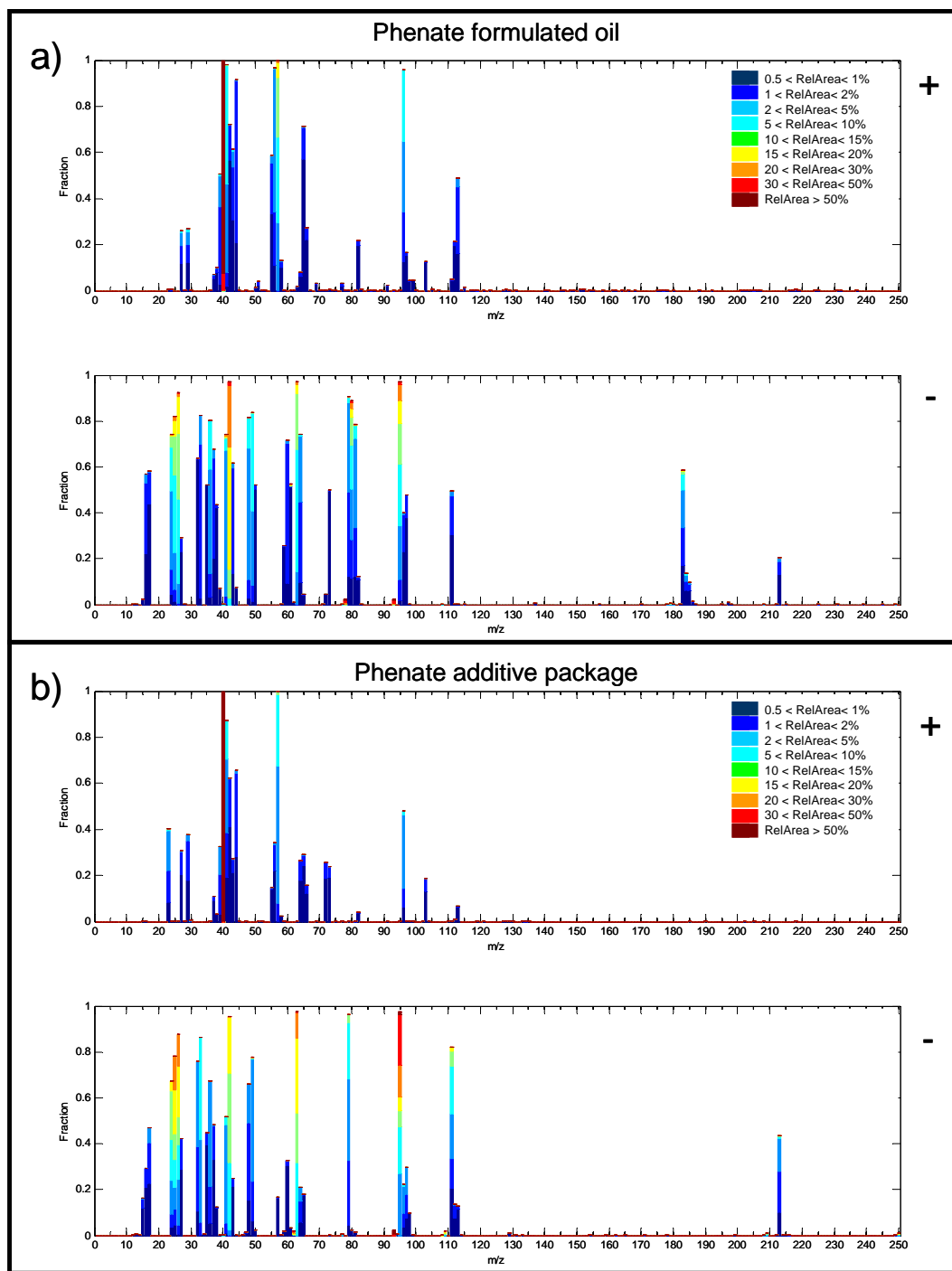


Figure 6.2 Digital mass spectrum color stack for both positive and negative ions of a) fully formulated oil with a phenate detergent additive and b) phenate detergent additive package

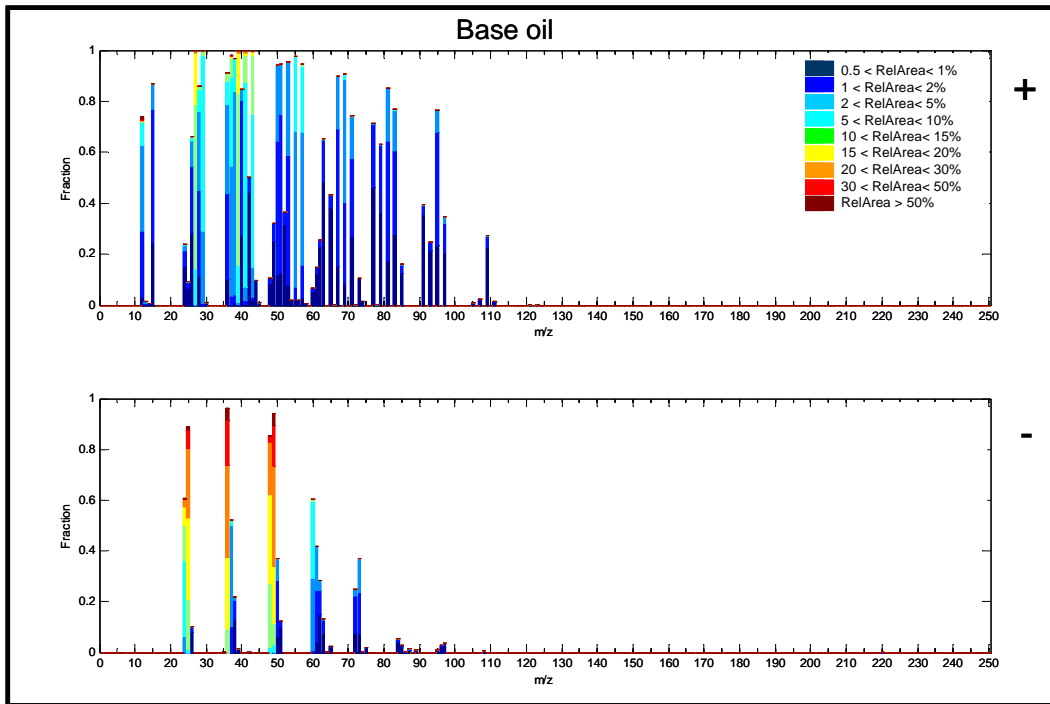


Figure 6.3 Digital mass spectrum color stack for both positive and negative ions of a mineral base oil with no additives

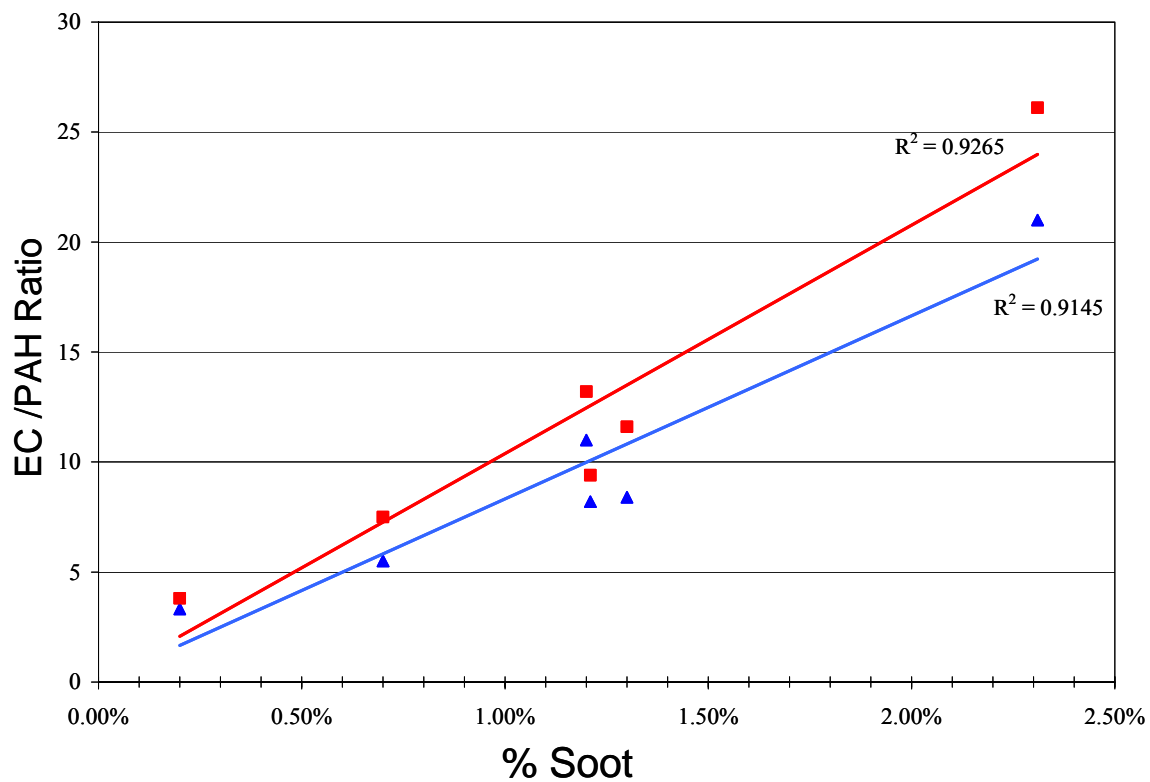


Figure 6.4 EC/PAH ratio for m/z $^{48}C_4^-$, and m/z 205^- (triangles) and the ratio of the sum of EC peaks $^{24}C_2^-$, $^{36}C_3^-$, $^{48}C_4^-$ to the sum of PAH peaks 205^- and 219^- (squares) versus the percent of soot for each sample

sulfite and bisulfite peaks at m/z $^{80}(\text{SO}_3)^-$, and $^{81}(\text{HSO}_3)^-$ are not observed in this sample, which differentiates these particles from the sulfonate oil samples shown in Figure 6.1. Such differences could potentially be used to distinguish between gas and oil samples in ambient air. Another distinguishing feature is that m/z 42^- is also much less intense in the phenate samples versus the sulfonate samples.

For comparison purposes, Figure 6.3 shows the digital color stack for the base oil, which contains no additives. This digital color stack contains positive ion peaks attributed to organic carbon at m/z $^{15}\text{CH}_3^+$, 27^+ , 29^+ , 43^+ , and 57^+ . Also observed is a pattern of odd-mass, positive ion peaks indicative of nitrogen-containing organic species. The negative ion spectrum contains carbon cluster peaks at $^{12}\text{C}^-$, $^{24}\text{C}_2^-$, $^{36}\text{C}_3^-$, $^{48}\text{C}_4^-$, $^{60}\text{C}_5^-$ as well as intense peaks at 25^- , 49^- . The base oil is easily distinguished from the fully formulated oils and the oil additive packages by the lack of inorganic ions such as $^{40}\text{Ca}^+$, $^{79}\text{PO}_3^-$, $^{80}\text{SO}_3^-$, $^{81}\text{HSO}_3^-$, and $^{95}\text{PO}_4^-$, supporting their assignments. The base oil also lacks a peak at m/z 213^- which was prevalent in all but one of the formulated oil and additive packages.

Six used oil samples that varied in the percent of soot by weight were aerosolized using a Collision atomizer and analyzed using an ATOFMS. The soot values were determined using an off-line method to be: 0.2%, 0.7%, 1.2%, 1.2%, 1.3%, and 2.3%. Each of the oil samples mass spectral fingerprint contained peaks attributed to EC at m/z $^{12}\text{C}^+$, $^{24}\text{C}_2^+$, $^{36}\text{C}_3^+$, $^{48}\text{C}_4^+$, $^{60}\text{C}_5^+$ and $^{24}\text{C}_2^-$, $^{36}\text{C}_3^-$, $^{48}\text{C}_4^-$, $^{60}\text{C}_5^-$. Also prevalent in the used oil samples were ions attributed to polycyclic aromatic hydrocarbons (PAH). There is an anti-correlation between the intensity of the PAH peaks and the carbon cluster ion peaks. In general, we were able to show using ATOFMS measurements the EC peaks correlate with the amount of soot in the sample. Thus, using ATOFMS we were able to show an anti-correlation between the relative amount of soot and PAH in the samples. The researchers at the additive company assumed the samples with less soot would have higher PAH and visa versa but had no way to measure the PAH in this complex of a sample. PAH represent the building blocks of soot, so chemically it is not surprising their presence is anti-correlated. Figure 6.4 shows a plot of the EC/PAH ratio for m/z $^{48}\text{C}_4^-$ and m/z 205^- (blue line), as well as the ratio of the sum of EC peaks $^{24}\text{C}_2^-$, $^{36}\text{C}_3^-$, $^{48}\text{C}_4^-$ to the sum of PAH peaks 205^- , and 219^- (red line) versus the percent of soot for each sample. There is a strong correlation between the measured percent of soot by weight and the ratio of EC to PAH. R^2 values using different peaks for the calculation were obtained of 0.9145 and 0.9265. This finding shows the ATOFMS can be used for the quantitative analysis of soot and PAH in complex used oil samples.

6.4 Conclusion

The analysis of different oil formulations and their additive packages using an ATOFMS has shown to be useful in identifying some key chemical species that are attributed to the oil additives versus the base oil. Inorganic compounds such as phosphate, sulfate, Ca, Na has been shown to be present in the oil additive packages and the formulated oils themselves, while the base oil seems to contain mostly organic and nitrogen containing organic species. An ion at m/z 213^- appears to be a unique ion to the oil formulations, and might prove useful as a marker for oil based aerosols in ambient ATOFMS measurements.

Analysis using an ATOFMS of used oils with varying soot concentrations showed a good correlation for the ratio of EC/PAH ion intensity. This could prove to be useful in quantifying the amount of soot or PAH in a used oils using an ATOFMS. Analysis of the formulated oils, oil additive packages and used oil samples is very preliminary and a more detailed analysis of these samples will be forthcoming.

Section IV

Evaluation of Source Signatures & Application to Apportionment Studies

Comparison of Light Duty and Heavy Duty Vehicle Emissions from Dynamometer and Tunnel Studies Using ART-2a

7.1 Introduction

Research has shown that vehicle emissions are a major source of pollution in urban areas [Fruin *et al.*, 2001; Marshall *et al.*, 2003; Mysliwiec and Kleeman, 2002; Rogge *et al.*, 1993; Vanvorst and George, 1997]. A goal of major federal and state agencies is to set regulations which lead to a reduction in these pollutants given growing concerns over their induced health effects [Pope, 2000; Riediker *et al.*, 2004; Seagrave *et al.*, 2002]. The ability to apportion light duty vehicle (LDV), heavy duty vehicle (HDV), and other combustion emissions in ambient aerosols will allow city and state agencies to channel their efforts and resources into targeting the major polluters (LDV, HDV, and other combustion sources) in their area. Out of all combustion sources, distinguishing between LDV and HDV represents the greatest challenge due to the similar chemical characteristics of the PM in their emissions, which result from their similar fuel and oil composition [Allen *et al.*, 2001; Fraser *et al.*, 2003; Kleeman *et al.*, 2000; Miguel *et al.*, 1998; Rogge *et al.*, 1993; Watson *et al.*, 1994]. In contrast, biomass combustion particle emissions with distinct potassium and levoglucosan signatures are readily distinguished from other ambient particles [Guazzotti *et al.*, 2003], and pulverized coal has distinct mass spectral signatures of metals (lithium, sodium, aluminum, potassium, calcium, and iron) in the positive ion and silicates, phosphates, and sulfates in the negative ion mass spectra [Suess, 2002].

Vehicle studies have been conducted on dynamometers [Bishop and Stedman, 1996; Cadle *et al.*, 2001; Kleeman *et al.*, 2000; Sagebiel *et al.*, 1997; Schauer *et al.*, 2002; Watson *et al.*, 1994], in tunnels [Dimashki *et al.*, 2000; Miguel *et al.*, 1998; Venkataraman *et al.*, 1994; Wingfors *et al.*, 2001], and alongside roadways [Gramotnev *et al.*, 2003; Harrison *et al.*, 2003; Ketzel *et al.*, 2003; Singh *et al.*, 2002; Vogt *et al.*, 2003]. Each of these studies has their own set of advantages and disadvantages. The dynamometer studies allow complete control over the vehicles tested and the driving conditions. However, only a small number of vehicles can be tested and particles emitted from brake pads and resuspended road dust are not characterized. There is also some question as to whether the dilution chambers used to mimic atmospheric dilution conditions produce particles that are representative of particles produced under true atmospheric conditions [Grashow *et al.*, 2000; Kawai *et al.*, 2004]. Tunnel studies can be conducted in locations where heavy duty and light duty vehicles are segregated into different bores within the tunnel. Tunnel studies also allow the sampling of emissions from a much larger vehicle fleet than dynamometer studies. However, tunnel studies offer little or no control over the driving conditions. Roadside studies offer the least amount of control over the vehicles and the cycles tested. However, roadside studies allow for sampling vehicular emissions that are atmospherically more dilute and can undergo photochemical aging on short timescales.

This chapter describes research conducted as part of a series of field campaigns focusing on the characterization of vehicle emissions using a single particle mass spectrometer, aerosol

time-of-flight mass spectrometry (ATOFMS). The studies carried out include an LDV dynamometer study [Sodeman *et al.*, 2005], two HDV dynamometer studies [Shields *et al.*, 2005; Toner *et al.*, 2005], a tunnel study (included herein), and a freeway study conducted in Summer of 2004. The goal of these studies is to utilize the signatures obtained from the dynamometer and tunnel studies to differentiate between LDV and HDV emissions in ambient aerosols. The ultimate goal is to use these signatures along with signatures from other combustion sources (e.g. biomass burning, coal combustion, and meat cooking) for ambient source apportionment. This paper addresses a number of issues, including determination of whether: 1) the chemical signatures obtained from dynamometer studies are representative of those observed in an ambient tunnel study, 2) there are any new particle types observed in the tunnel study, and 3) there are unique light duty versus heavy duty single particle signatures, and if so, detailing the different chemical types. Future work will address the relationship between the particle types observed in the dynamometer and tunnel studies and those found in the roadside study.

7.2 Experimental

Twenty-eight LDVs and thirteen HDVs were tested on a chassis dynamometer under various driving conditions. There were three dynamometer studies (one LDV and two HDV). The driving cycles for the LDV dynamometer study was predominately the Federal Test Protocol (FTP), a transient cycle. The other cycles consisted of a higher speed transient cycle, with faster accelerations and decelerations than the FTP cycle and a high speed (~60 mph) cruise cycle. For the HDV dynamometer studies, the driving cycle was the California Air Resources Board driving cycle for HDVs. This cycle consisted of idling, creeping (top speed of ~8 mph), transient, and cruising speeds. These driving conditions were representative of typical urban and freeway driving conditions. For each of the dynamometer studies, the emissions were sampled from a dilution and residence chamber [Hildemann *et al.*, 1989]. A more complete description of the sampling procedures and driving cycles has been provided previously [Shields *et al.*, 2005; Sodeman *et al.*, 2005; Toner *et al.*, 2005]. At all three of the dynamometer studies, an aerosol time-of-flight mass spectrometer (ATOFMS), and an aerodynamic particle sizer (APS TSI model 3020 for the Caldecott Tunnel study and one of the HDV dynamometer studies and a TSI Model 3021 for the LDV and the second dynamometer studies) were operated. An ATOFMS equipped with an aerodynamic lens (UF-ATOFMS) was also operated for the LDV and one of the HDV dynamometer studies (see Table 3.1). The mass spectrometers measure the aerodynamic diameter and chemical composition of single particles in real-time. The ATOFMS has a size range of 0.1 – 3.0 μm , while the UF-ATOFMS has a size range of 0.05 – 0.3 μm [Gard *et al.*, 1997; Su *et al.*, 2004]. The UF-ATOFMS has a detection efficiency for 0.2 μm particles that is at least three orders of magnitude higher than the standard ATOFMS [Su *et al.*, 2004].

The tunnel study was conducted at the Caldecott Tunnel, near Berkeley, CA from July 23rd through August 2nd, 2000. This tunnel is configured such that sampling of LDV only or mixed HDV-LDV is possible. See Table 7.1 for a list of the sampling times of the LDV only bore and the mixed HDV-LDV bore. Also included are the times in which videotaped data are available to determine the number of LDV and HDV traveling through the tunnels. Particles were drawn from the bores through 1/2 inch sampling lines with a flow rate of 67 liters per

Table 7.1 HDV-LDV and LDV only bores sampling times, along with available videotape of the traffic.

Day & Date	HDV-LDV Bore	LDV only Bore	Videotape
Sun 7/23	09:25 – 00:00		09:30 – 12:00
Mon 7/24	00:00 – 12:20 20:30 – 00:00	12:25 – 20:30	13:30 – 20:00
Tue 7/25	00:00 – 05:00 09:40 – 00:00	05:00 – 09:25	09:00 – 11:30 12:30 – 17:00 18:00 – 23:30
Wed 7/26	00:00 – 12:05 20:30 – 00:00	12:10 – 20:30	12:30 – 17:30
Thu 7/27	00:00 – 05:00 20:30 – 00:00	05:00 – 20:30	12:30 – 22:00
Fri 7/28	00:00 – 05:00 10:05 – 00:00	05:00 – 09:55	10:00 – 21:30
Sat 7/29	00:00 – 05:00 10:05 – 00:00	05:00 – 09:50	11:00 – 19:00
Sun 7/30	00:00 – 04:55 20:30 – 00:00	05:00 – 20:30	09:30 – 00:00
Mon 7/31	00:00 – 05:00 10:00 – 15:15 20:20 – 00:00	05:00 – 09:50 15:15 – 20:00	00:00 – 01:30 10:00 – 19:00
Tue 8/1	00:00 – 05:00	05:00 – 09:50	

minute into a $\sim 0.1 \text{ m}^3$ cylinder chamber. An ATOFMS and an APS each sampled from the chamber through a 3/8 in line. For all studies, the laser desorption/ionization was operated at the same nominal laser fluence, $\sim 2 \times 10^8 \text{ W/cm}^2$ ($\sim 1.5 \text{ mJ}$ per pulse (7 ns), focused to a 0.4 mm diameter spot size).

7.3 Results and Discussion

7.3.1 Dynamometer Studies

Detailed analysis on the vehicle variability and the influence the driving cycles have on the size and chemical composition during the three dynamometer studies have been described elsewhere [Shields *et al.*, 2005; Sodeman *et al.*, 2005; Toner *et al.*, 2005]. For each dynamometer study, a subset of the particles were analyzed with a neural network, ART-2a, at a vigilance factor of 0.85, a learning rate of 0.05, and 20 iterations to generate representative weight vectors or clusters of particles with similar compositions [Phares *et al.*, 2001; Song *et al.*, 1999; Wienke *et al.*, 1994; Xie *et al.*, 1994]. This analysis for this paper was conducted on all particles that contained both a positive and a negative ion mass spectrum in three different size ranges (0.05 – 0.1, 0.1 – 1.0, and 1.0 – 3.0 μm). All ART-2a clusters containing only one particle were discarded.

For a given size range, all HDV dynamometer particles in that particular size range were exclusively (i.e. each particle was allowed to match only the one cluster with which it had the highest dot product) matched to the combined set of HDV and LDV weight vectors using a vigilance factor of 0.85. After matching, the number of HDV dynamometer particles that matched the HDV weight vectors, the LDV weight vectors, or neither weight vectors was determined. The same was done for the LDV dynamometer particles. Figure 7.1 summarizes these results. These results indicate that greater than 85% of the HDV dynamometer particles are correctly matched to the HDV weight vectors and greater than 90% of the LDV dynamometer particles were correctly matched to the LDV weight vectors. Similar matching results were seen in all three size ranges (0.05 – 0.1, 0.1 – 1.0, and 1.0 – 3.0 μm). This analysis was done as a function of size since there are distinct size-chemical composition relationships as discussed in more detail in Sodeman *et al.*, Shields *et al.*, and Toner *et al.* [Shields *et al.*, 2005; Sodeman *et al.*, 2005; Toner *et al.*, 2005]. These results indicate that there are a relatively small fraction of similar particle types that look very similar. This is to be expected for particles generated by similar combustion processes.

Once the particles are emitted, aging processes (e.g. oxidation, condensation, and/or heterogeneous chemistry) will change the overall mass spectral fingerprint and make it challenging to distinguish some of the particle signatures in HDV and LDV emissions. These changes would decrease the similarity (dot product) between the aged particles and the dynamometer (non-aged) particles. This lowered similarity would decrease the number of particles matching the dynamometer weight vectors. To compensate for the lowered similarities, a lower vigilance factor could be used. However, this would increase the likelihood that LDV particles would match to the HDV weight vectors, and vice versa. Fortunately, most of these changes are not random and can be predicted based on known chemical processes. For instance, condensation and/or heterogeneous chemistry involving ammonium nitrate and/or sulfate will

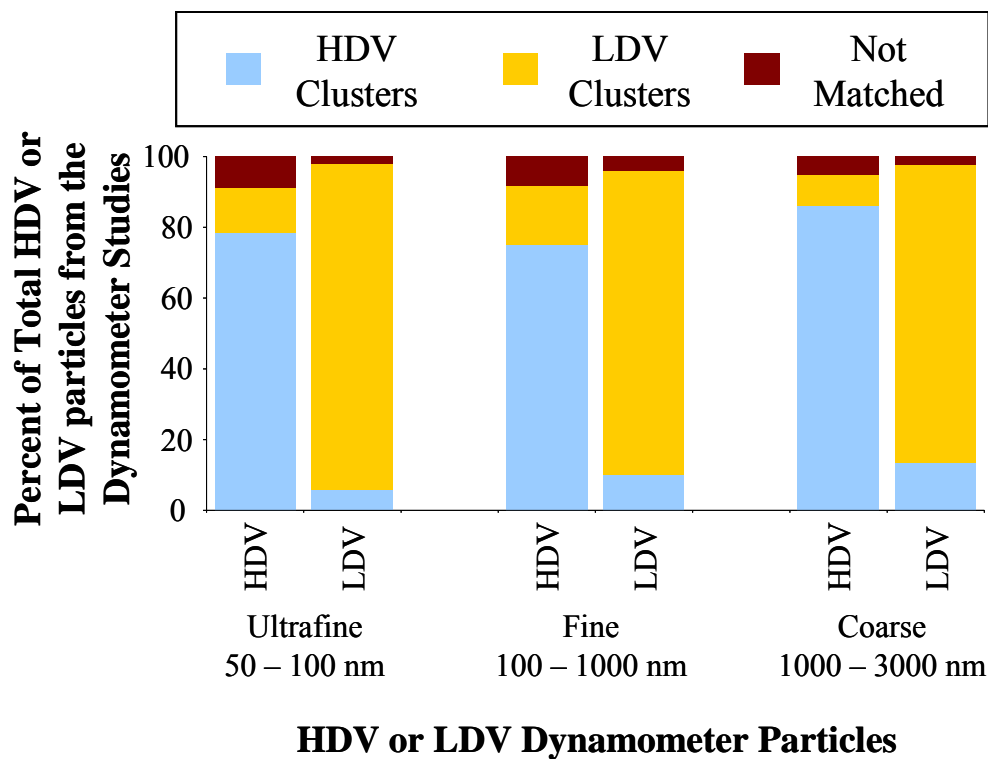


Figure 7.1 Exclusive matching of HDV and LDV dynamometer particles. Fraction of HDV and LDV particles that matched to the HDV, LDV, or neither HDV nor LDV weight vectors for three size ranges; 50 – 100 nm, 100 – 1000 nm, and 1000 – 3000 nm.

occur at specific m/z values ($^{18}\text{NH}_4$, $^{-46}\text{NO}_2$, $^{-62}\text{NO}_3$, and $^{-97}\text{HSO}_4$). One of the strengths and at the same time limitations of ART-2a is that it is a relatively simplistic data analysis tool package. Use of a different data analysis tool package that can be trained to take into account aging process may be necessary to accurately differentiate aged HDV from LDV emissions in ambient studies. This work is currently being investigated. However, ART-2a will be used to investigate the HDV and LDV particles types in the Caldecott Tunnel, where minimal aging of the aerosols is expected.

7.3.2 Caldecott Tunnel Study

Using the unique single particle signatures determined in the dynamometer studies, differences in the particle types detected in the two bores became apparent. It is important to note that an improvement was made in the data acquisition system between the two studies. For the Caldecott dataset, the dynamic range of the data acquisition system was lower resulting in every peak in the mass spectrum whose peak height intensity was above a certain threshold (256 arbitrary units) being truncated. In all of the dynamometer datasets, a wider dynamic range was used where the peak height truncation threshold was raised to 7520 arbitrary units (WDR) [Dienes, 2003]. This value was sufficiently high so that no peaks were truncated in the dynamometer studies. Since ART-2a analysis normalizes the cluster weight vectors, it is still possible to do comparisons of the particle types between the studies. One needs to be aware, however, that in the non-WDR Caldecott dataset, peaks whose heights are below the truncating value (256 arbitrary units) are relatively enhanced compared to the peaks with heights less than 256 arbitrary units in the WDR dynamometer datasets. Due to the high degree of similarity between the HDV and LDV weight vectors; this difference prevents accurate matching results of all particle types using high vigilance factors. However, even with this limitation, certain unique particle types are still quite comparable between the two studies as presented below.

Figure 7.2 shows the average area mass spectra of the top three clusters for three chemical classes detected in the Caldecott Tunnel (thick grey bars) that match three classes from the dynamometer studies (thin black bars), with similarity factors of 0.88, 0.81, and 0.91, respectively. Other particle types from the dynamometer study were also detected in the tunnel study, but only these three classes are shown since they are the dominant particle types detected in the dynamometer studies in the size range of 0.1 – 3.0 μm . The first class (Ca-EC-PO₃) is characterized by peaks from calcium (^{40}Ca , ^{56}CaO , $^{57}\text{CaOH}$, and $^{96}\text{Ca}_2\text{O}$), elemental carbon (^{12}C , $^{36}\text{C}_2$, $^{-36}\text{C}_3$, $^{-48}\text{C}_4$, $^{-60}\text{C}_5$, $^{-72}\text{C}_6$), phosphate ($^{-63}\text{PO}_2$, $^{-79}\text{PO}_3$, and $^{-95}\text{PO}_4$), and organic carbon (m/z 27 and 29). It is important to note that ATOFMS is much more sensitive to metals than carbonaceous compounds [Gross *et al.*, 2000a]. Thus, large ion signals from metals in the mass spectrum do not necessarily correlate with significant quantities of metals in the particles. The second class (EC-Ca-PO₃) is characterized by peaks from elemental carbon (^{12}C , $^{24}\text{C}_2$, $^{36}\text{C}_3$, $^{48}\text{C}_4$, $^{60}\text{C}_5$, $^{72}\text{C}_6$, and $^{84}\text{C}_7$), calcium (^{40}Ca), phosphate ($^{-79}\text{PO}_3$ and $^{-97}\text{H}_2\text{OPO}_3$), and organic carbon (m/z 27 and 29). The difference of this class from the previous one is the relative peak intensities between calcium and elemental carbon. In the positive ion mass spectrum of the first class, the majority of the ion intensity occurs at peaks corresponding to calcium and calcium oxides. In the second class, the majority of the ion intensity in the positive ion mass spectrum occurs at peaks that correspond to elemental carbon. These two classes have different size profiles (discussed below), and are believed to be derived from diesel lubricating oil

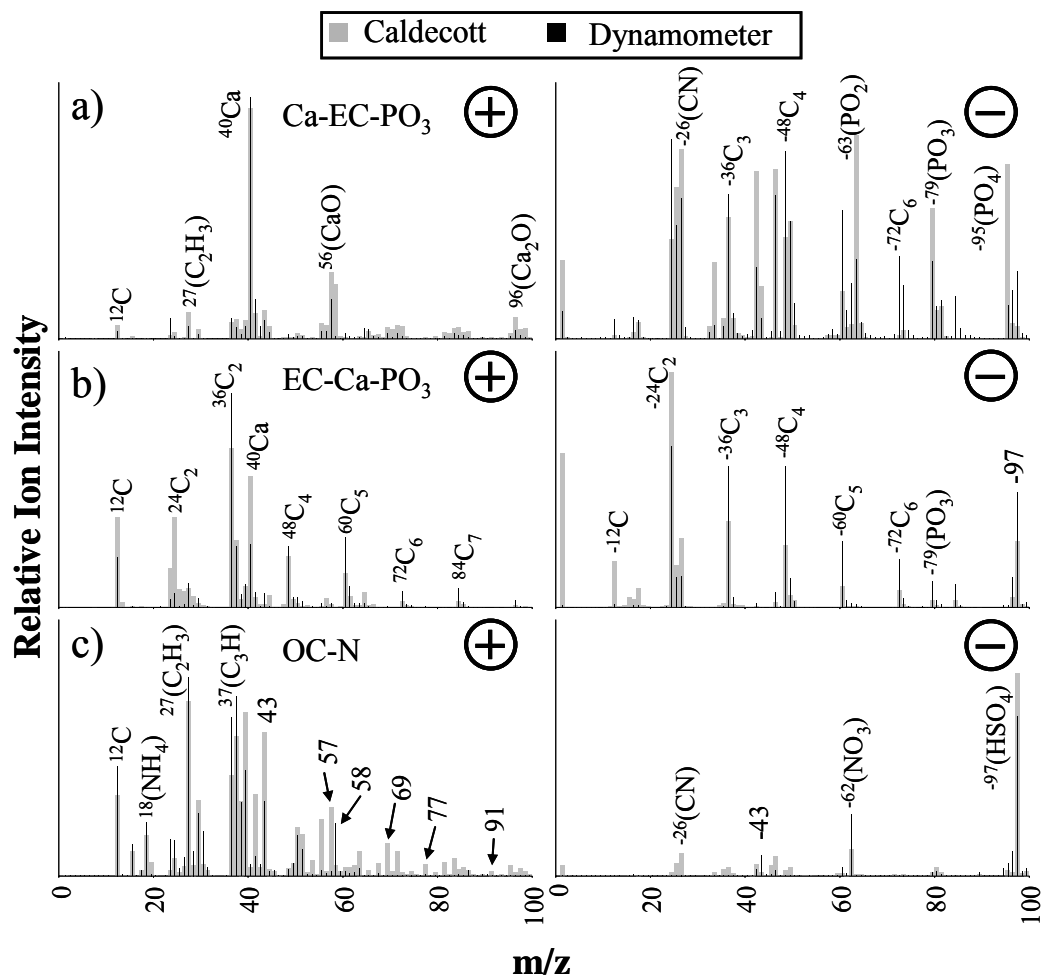


Figure 7.2 Comparison of three Caldecott Tunnel and dynamometer classes. a) Ca-EC-PO₃, b) EC-Ca-PO₃, and c) OC-N. Dot product (similarity) values are a) 0.88, b) 0.81, and c) 0.91. The thin black bars are the dynamometer classes, while the broad grey bars are the Caldecott Tunnel classes.

[Spencer and Prather, 2005]. Calcium is added to oil in the form of calcium sulfonate, phenate, salicylate, and/or carbonate as a detergent additive [Rizvi, 2003; Willermet, 1998; Yamaguchi et al., 2002]. Detergent additives function to neutralize acids (e.g. H₂SO₄ and hydroperoxides) and to keep insoluble contaminants (e.g. soot) from agglomerating. Phosphate is added to the oil as zinc dialkyldithiophosphate as an antioxidant and antiwear additive [McDonal, 2003 ; Willermet, 1998; Yamaguchi et al., 2002].

The third class (OC-N) is an organic carbon class with ammonium (¹⁸NH₄), nitrate (⁻⁴⁶NO₂ and ⁻⁶²NO₃), and sulfate (⁻⁹⁷H₂SO₄). This class is believed to derive from the incomplete or partial combustion of gasoline fuel. The ammonium probably is formed from ammonia reacting with sulfuric acid or nitric acid to produce ammonium sulfate and/or nitrate. Ammonia has been detected from LDV emissions, and it is formed in three way catalytic converters running under rich fuel – air mixtures [Fraser and Cass, 1998; Kean et al., 2000].

7.3.3 New Tunnel Classes

On average, the organic carbon particle classes in the tunnel have higher *m/z* peaks than the LDV dynamometer studies. The length of time the particles took to pass through the residence chamber during the dynamometer studies and time the particles spent in the sampling lines of the Caldecott were comparable (~2 minutes) and thus this cannot explain the observed differences. Insight into the extent of oxidation and/or condensation in the Caldecott dataset as compared to the dynamometer studies can be gained by examining the average area mass spectra and the digital mass spectra for all of the organic carbon particle types (identified from the ART-2a weight vectors) from each study. The organic carbon particle types were visually identified using the ART-2a weight vectors. The average area mass spectra and the digital mass spectra give complementary information. The average area mass spectra provide an indication of the relative ion intensity of each peak, whereas the digital mass spectra display the fraction of particles that contain a peak above a threshold value (area greater than 50 arbitrary units) within a chemical class [Liu et al., 2003]. This analysis is not affected by the non-WDR Caldecott Tunnel dataset, as the organic carbon particle types do not have peaks with heights above 256 arbitrary units.

Table 7.2 displays the ratio of the Caldecott value to the LDV dynamometer value for selected *m/z* for the digital mass spectra, as well as the average area matrix ratio for all of the organic carbon particle types. The ratio of ¹²C, ²⁴C₂, ³⁶C₃, and ⁴⁸C₄ in the digital mass spectra are all close to one, with the exception of ²⁴C₂. However, all of the average area matrix ratios are less than one. This indicates that even though the same fractions of the organic carbon particle types contain the above peaks, the average areas of these peaks are higher in the LDV dynamometer study than in the Caldecott Tunnel study. A characterization study of laser desorption/ionization on carbon black found that the majority of the ion intensity resides in C_n⁺ peaks, where n = 1 – 5 [Suess, 2002]. Organic carbon, on the other hand, has the majority of the ion intensity in C_nH_m⁺ peaks, where n = 2 – 4 and m = 1 – 5. [Silva and Prather, 2000]. Thus, even though organic carbon does yield C_n⁺ peaks, they are not the dominant peaks. With the organic carbon particles from the LDV dynamometer study having more intense peaks at C_n⁺ than the Caldecott Tunnel organic carbon particles, this indicates that the LDV dynamometer organic carbon particle types have more elemental carbon associated with them. One possible explanation is that the Caldecott Tunnel organic carbon particles have a thicker organic carbon coating on the elemental carbon

Table 7.2 Ratio of Caldecott values to the LDV Dynamometer values for individual m/z for average area mass spectrum and digital mass spectra for the organic carbon.

m/z	Digital Mass Spectra Ratio	Area Matrix Ratio	Type of Peak
12	1.02	0.56	EC
24	0.76	0.44	EC
36	1.03	0.60	EC
43	1.09	2.11	OC
48	1.02	0.82	EC
55	2.66	1.25	OC
57	2.78	6.84	OC
69	4.97	15.18	OC
77	2.80	3.22	OC
91	2.57	4.70	OC

core than the LDV dynamometer organic carbon particles. The laser utilized in these studies, a Nd:YAG operated at 266 nm, has an inhomogeneous laser beam profile. Analyzing particles in a “cold” spot of the laser (lower laser power than the average laser power of the entire spot) allows surface species to be preferentially detected [Wenzel and Prather, 2004]. Thus, if the entire particle is not analyzed, the chemical species at the core are underrepresented in the mass spectrum.

A larger fraction of particles contain organic carbon fragment ions above m/z 50 in the Caldecott Tunnel compared to the LDV dynamometer organic carbon particles. The average area mass spectra also show more intense peaks higher than m/z 50 in the Caldecott Tunnel organic carbon particles, indicating the presence of higher m/z fragments in the Caldecott Tunnel organic carbon particles. This could be the result of the beginning of the formation of organic carbon polymers as the organic species are oxidized [Tolocka *et al.*, 2004]. This would result in higher molecular weight organic carbon compounds, which would lead to higher m/z fragments in the ATOFMS mass spectrum.

An indication that oxidation is occurring for particles in the tunnel dataset compared to the dynamometer dataset is the presence and intensity of m/z 43 on the organic carbon particles. The peak at m/z 43 can be attributed to $C_2H_5N^+$, CH_3CO^+ and/or $C_3H_7^+$. Unfortunately, the mass resolution is not sufficient to be able to distinguish between the same nominal mass compounds for m/z 43. The digital mass spectra ratio is close to one (1.09), but the ratio in the average area mass spectra is 2.1, indicating that in the Caldecott Tunnel there is an additional source of m/z 43 relative to the LDV dynamometer study. Oxidation of organic carbon increases the oxygen content of the organic compounds as well as decreasing the vapor pressure of the organic carbon species, leading to a higher fraction of the oxidized species partitioning onto preexisting particle surfaces [Odum *et al.*, 1997; Seinfeld and Pandis, 1998; Yu *et al.*, 1999]. Oxygen-containing organics yield strong ion signals at m/z 43 in ATOFMS, which is most likely CH_3CO^+ based on the known stability of this cation due to resonance structures [Silva and Prather, 2000]. Thus, it is likely that the increase in intensity of m/z 43 can be at least partially attributed to CH_3CO^+ , which is a product of the oxidation of organic carbon, and thus contributes to secondary organic aerosol (SOA) [Grosjean, 1992; Grosjean and Seinfeld, 1989]. This indicates that a detectable amount of SOA exists within minutes after emission of its precursor. The peaks at m/z 77 and 91 (see Figure 7.2c and Gross *et al.*) are indications of substituted monoaromatic compounds [Gross *et al.*, 2004; McLafferty and Tureček, 1993]. Their presence is consistent with Odum *et al.* findings that the aromatic compounds in gasoline are precursors to SOA [Odum *et al.*, 1997].

One distinct particle type (Fe-Ba) observed in the tunnel that was not detected in the ATOFMS dynamometer studies is shown in Figure 7.3. This particle type average area mass spectrum contains sodium (^{23}Na), aluminum (^{27}Al), potassium (^{39}K), iron (^{56}Fe , ^{57}Fe , ^{58}Fe , ^{59}Fe , ^{60}Fe , ^{61}Fe , ^{62}Fe , ^{63}Fe , ^{64}Fe , ^{66}Fe , ^{67}Fe , ^{68}Fe , ^{69}Fe , ^{70}Fe , ^{72}Fe , ^{74}Fe , ^{76}Fe , ^{78}Fe , ^{80}Fe , ^{81}Fe , ^{82}Fe , ^{84}Fe , ^{86}Fe , ^{88}Fe , ^{90}Fe , ^{92}Fe , ^{94}Fe , ^{96}Fe , ^{98}Fe , ^{100}Fe), barium (^{138}Ba , ^{154}Ba), chloride (^{35}Cl), nitrate ($^{46}NO_2$ and $^{62}NO_3$), and phosphate ($^{63}PO_2$ and $^{79}PO_3$). Previous research found that iron and barium are common components of brake dust [Bush *et al.*, 1972; Hildemann *et al.*, 1991]. An ATOFMS analysis on new brake pads and brake dust from wheel drums of two vehicles show mass spectra similar to Figure 7.3 [Silva, 2000]. Thus, this class is generated from the wear of brake pads. The nitrate ($^{46}NO_2$ and $^{62}NO_3$) was also seen in the ATOFMS analysis of brake pads and so it can not be exclusively attributed to aging. Since the ATOFMS dynamometer studies focused on the emission of particles from the exhaust

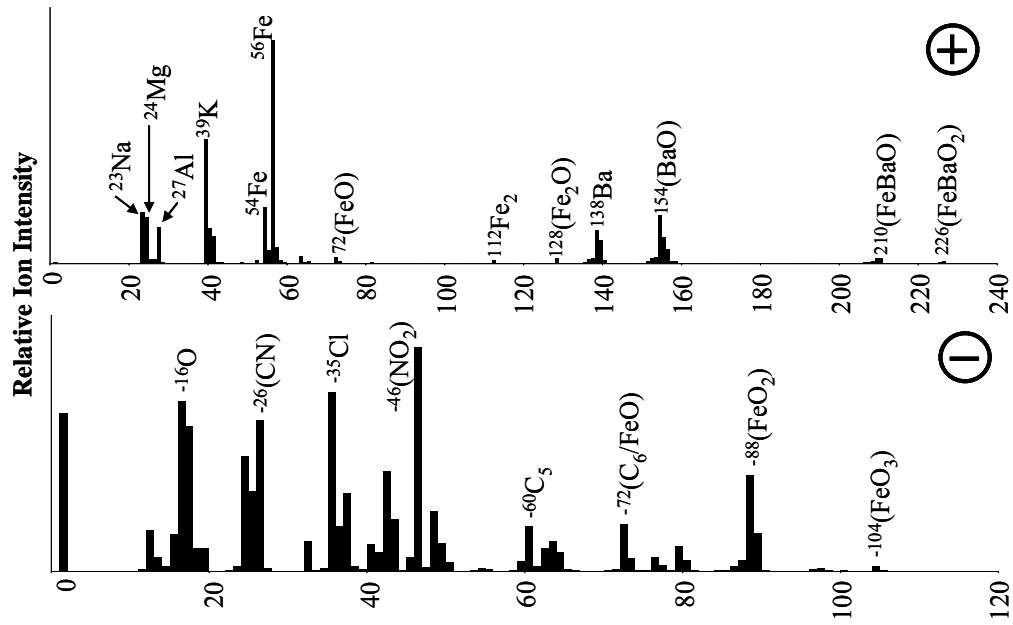


Figure 7.3 Average area mass spectrum of Fe-Ba class.

system, it is not surprising that this class was not detected in those studies [Shields *et al.*, 2005; Sodeman *et al.*, 2005; Toner *et al.*, 2005].

7.3.4 Size profiles

The relative size profiles (determined from the raw ATOFMS counts) of the four classes are shown in Figure 7.4. These size distributions display the relative fraction of each class per size bin and thus show information on size dependent chemical classes. Since the ATOFMS scaling procedures scale the chemical classes in each size bin by the same amount, scaling would not change the relative trends shown in Figure 7.4. One should note that since these size profiles are on a relative basis per size bin, they are not directly comparable to size profiles based on mass or number concentration. However, they are shown in this format to view any size dependences more easily. The brake dust class (Fe-Ba class) is strongly associated with the coarse mode ($> 1.0 \mu\text{m}$), which is expected given the mechanical (abrasive) formation process producing particles in this class. This is consistent with previous research conducted on brake dynamometers [Garg *et al.*, 2000; Sanders *et al.*, 2003]. The EC-Ca-PO₃ class is predominately in the smallest size bin ($< 0.4 \mu\text{m}$), which is consistent with past HDV dynamometer studies, where the mass concentration of EC peaks below $0.2 \mu\text{m}$ [Kleeman *et al.*, 2000]. The total of all of the OC classes (OC-Total) is predominately in the fine mode ($< 1.0 \mu\text{m}$), which is consistent with previous LDV dynamometer studies, where the mass concentration of OC peaks below $0.3 \mu\text{m}$ [Kleeman *et al.*, 2000]. The Ca-EC-PO₃ class was detected in both the fine and coarse modes, but with a larger relative contribution in the coarse mode. These three classes (EC-Ca-PO₃, Ca-EC-PO₃, and OC-Total) have the same general size profile as those observed in the ATOFMS dynamometer studies [Shields *et al.*, 2005; Sodeman *et al.*, 2005; Toner *et al.*, 2005].

7.3.5 Temporal Trends

The EC-Ca-PO₃ and the Ca-EC-PO₃ classes have been detected from LDVs in a dynamometer study; however, the EC-Ca-PO₃ class was predominately detected in the ultrafine sizes ($< 0.1 \mu\text{m}$) with minimal contribution in the fine mode. The Ca-EC-PO₃ class contributed less than 20% of the particle number concentration in the $0.1 - 2.5 \mu\text{m}$ size range for each of the LDVs vehicles tested in the dynamometer study [Sodeman *et al.*, 2005]. However, in the HDV dynamometer studies, this particle type accounted for 30 – 60% of the total particle concentration in the $0.1 - 2.5 \mu\text{m}$ size range [Shields *et al.*, 2005; Toner *et al.*, 2005]. More information regarding the dominant source of these two classes can be inferred from their temporal trends in the Caldecott Tunnel.

Figure 7.5 displays the hourly temporal distribution of the raw ATOFMS counts for the EC-Ca-PO₃, Ca-EC-PO₃, and OC-Total classes. These classes were scaled utilizing number concentration data from an APS as described by Allen *et al.* and Wenzel *et al.* and the results are shown in Figure 7.6 [Allen *et al.*, 2000; Wenzel *et al.*, 2003]. Both temporal profiles are shown so that high concentrations of the scaled classes can be explained by either high ATOFMS counts or by the scaling procedure (i.e. the APS measuring a high number concentration). Briefly, the ratio of the raw ATOFMS number concentration to the APS number concentration of the same size range gives the particle detection efficiency for that size range. The inverse of this ratio is the scaling factor needed to convert the raw ATOFMS number concentration to ambient number

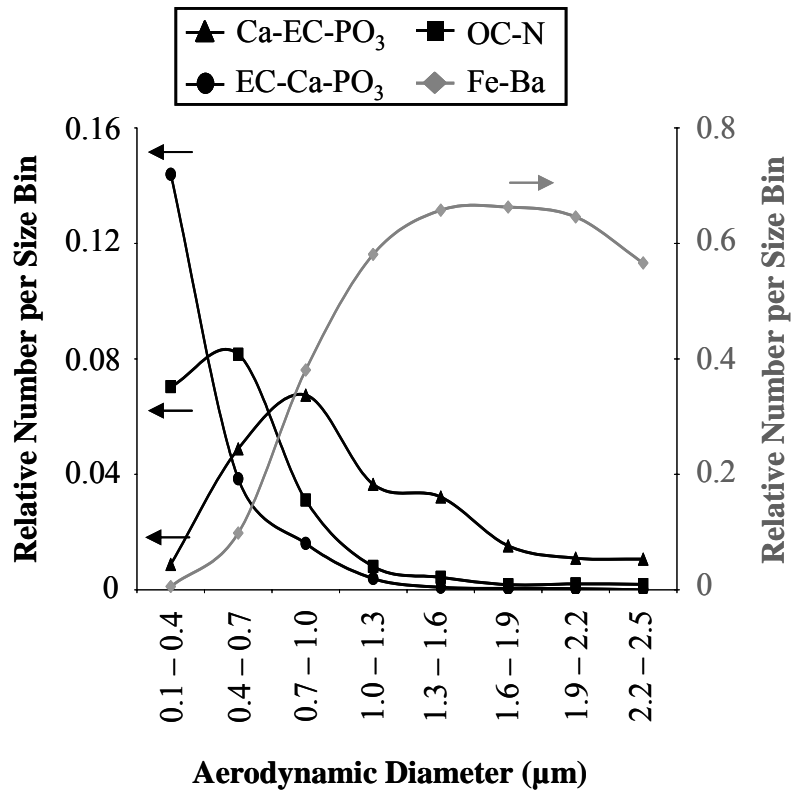


Figure 7.4 Relative size distributions of four chemical classes per size bin based on the ATOFMS raw counts. Each size bin displays the relative contribution of each chemical class for that size bin.

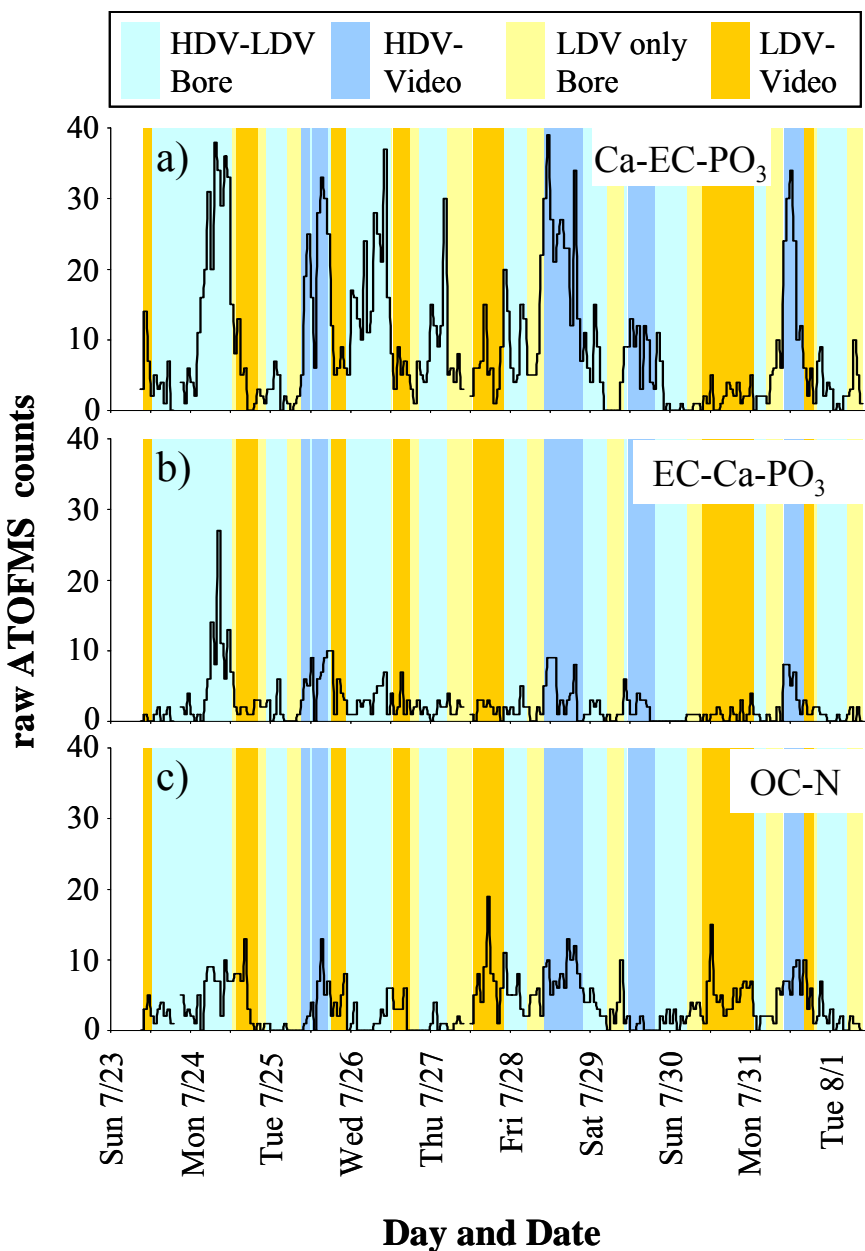


Figure 7.5 Hourly unscaled ATOFMS counts of the three major chemical classes. a) Ca-EC-PO₃, b) EC-Ca-PO₃, and c) OC-N. HDV-LDV Bore indicates when sampling was conducted from the mixed bore. HDV-LDV Video indicates when sampling was under the influence of HDVs (i.e. at least 1.5% of the vehicles were HDVs) based on video counts. LDV only Bore indicates when sampling was conducted from the LDV only bore. LDV Video indicates when sampling was under a relatively low influence of HDVs based on video counts (i.e. HDV were less than 0.8% of the total vehicles).

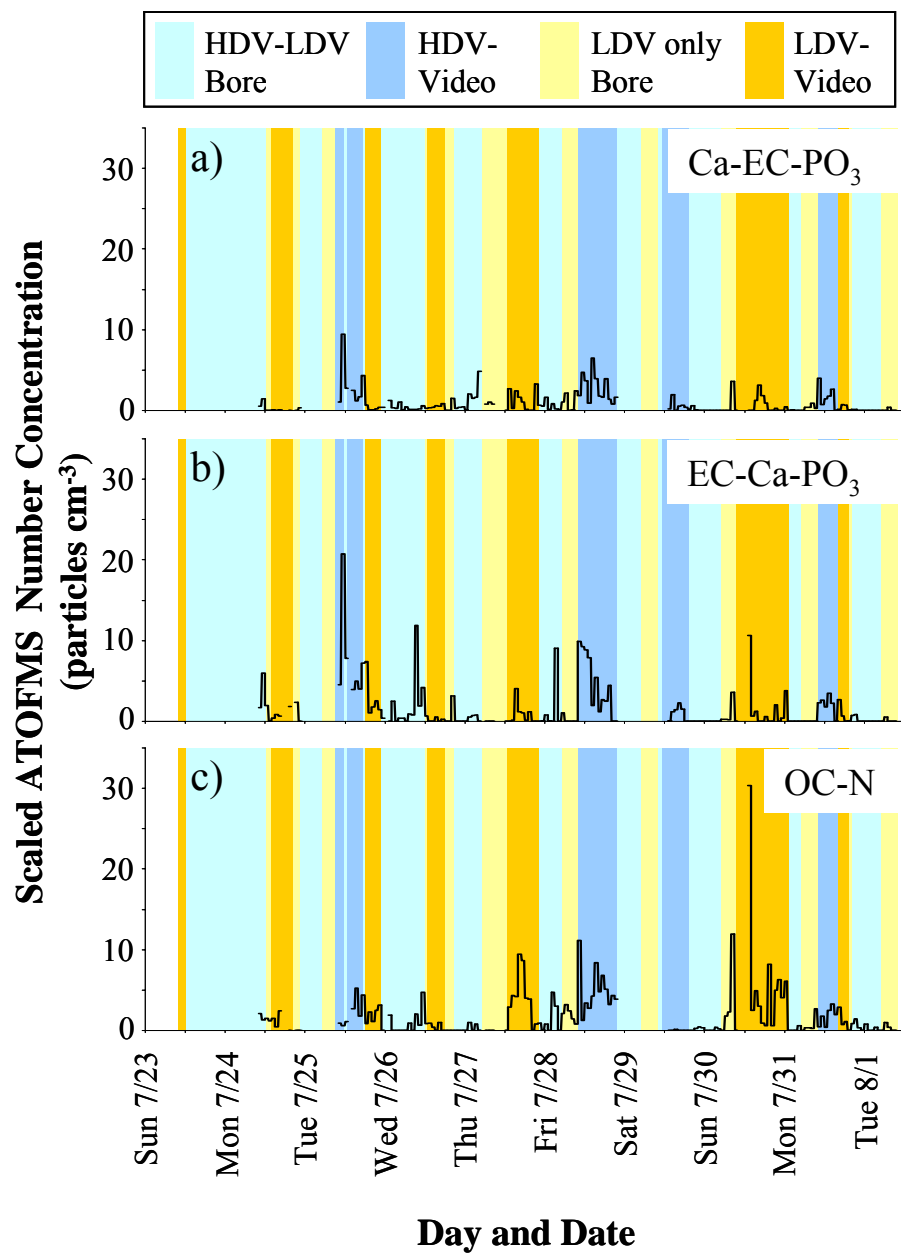


Figure 7.6 Hourly APS scaled ATOFMS number concentration of three chemical classes. a) Ca-EC-PO₃, b) EC-Ca-PO₃, and c) OC-N. HDV-LDV Bore indicates when sampling was conducted from the mixed bore. HDV-LDV Video indicates when sampling was under the influence of HDVs (i.e. at least 1.5% of the vehicles were HDVs). LDV only Bore indicates when sampling was conducted from the LDV only bore. LDV Video indicates when sampling was not under the influence of HDVs (i.e. HDV were less than 0.8% of the total vehicles).

concentration. The scaling factors were calculated hourly for five size bins in the range of 0.1 – 2.5 μm . To calculate the APS scaled ATOFMS number concentration for a particle type, the ratio of the number of particles of that particle type to the total number of particles for each size bin is multiplied by the scaling factor for that size bin. The coarse size resolution was necessary to obtain enough ATOFMS counts in each size bin to accurately scale the data. Low particle counts were mostly due to particle losses in the long sampling lines, which could not be avoided due to the location of the bores relative to the instruments. Since there were particle losses in the sampling lines, the measured APS number concentration is lower than the actual number concentration within the tunnel. Also shown in Figures 7.6 and 7.7 are the time periods when each bore (HDV-LDV or LDV only) was being sampled, as well as when the videotape counts acquired during selective time intervals indicate an influence of HDV or LDV only traffic. Table 7.3 shows the counts per hour of HDV and LDV for each videotaped time period. For the HDV influenced time periods, 1.5% to 4.5% of the vehicles were HDV, with a range of 20 – 40 HDVs per hour. During the LDV only influenced time periods, less than 0.1% to 0.8% of the vehicles were HDVs, with a range of less than one HDV to eight HDVs per hour.

In general, from Figures 7.5 and 7.6, the EC-Ca-PO₃ and the Ca-EC-PO₃ classes are primarily detected when the sampling was conducted in the HDV-LDV bore. This is especially evident in Figure 7.6 (the raw ATOFMS counts). Time periods of high contributions of the EC-Ca-PO₃ and the Ca-EC-PO₃ classes in the LDV only bore result from the APS scaling procedure, as those same time periods have low ATOFMS counts for those two classes. The OC-Total class was detected in similar concentrations from both bores, which is to be expected for particle types emitted from LDVs, as LDVs typically represented greater than 95% of the vehicles that traveled in the HDV-LDV bore.

These temporal profiles support the dynamometer studies that show the EC-Ca-PO₃ and the Ca-EC-PO₃ classes are primarily emitted from HDV, while the OC-Total class is emitted primarily from LDV [Shields *et al.*, 2005; Sodeman *et al.*, 2005; Toner *et al.*, 2005]. If the OC-Total class was being emitted from the HDV, it is expected that there would be an increase in the number of particle counts detected when ATOFMS was sampling from the HDV-LDV bore. However, this is not seen in Figure 7.5. The contribution of the Ca-EC-PO₃ and the EC-Ca-PO₃ classes in the LDV only bore can be attributed to the small number of HDVs, in addition to diesel passenger cars and diesel light and medium duty trucks. Diesel passenger cars and diesel light and medium duty trucks have not been characterized by ATOFMS, but since they have the same engine combustion technology (compression ignition) as HDVs, they are expected to emit particles with similar compositions. Allen *et al.* showed that the EC mass concentration in the Caldecott HDV-LDV bore was much higher than the EC in the LDV only bore (~60 versus ~15 $\mu\text{g m}^{-3}$) [Allen *et al.*, 2001]. With the EC-Ca-PO₃ and the Ca-EC-PO₃ classes being the dominant classes that contain EC and are primarily detected from the HDV-LDV bore, this is consistent with the findings by Allen *et al.* Thus, good markers for HDV emissions are the EC-Ca-PO₃ and the Ca-EC-PO₃ classes.

Investigators have found EC in both the HDV-LDV bore and the LDV only bore in the tunnel studies [Allen *et al.*, 2001; Gross *et al.*, 2000b; Laschober *et al.*, 2004; Miguel *et al.*, 1998]. However, the question remains: are there any mass spectral differences between the EC particle types in the Caldecott Tunnel? All of the elemental carbon particle types (identified from the ART-2a weight vectors) from the Caldecott Tunnel were combined into two sets; one for the HDV-LDV bore and the other for the LDV only bore. The time periods when the videotape data

Table 7.3 List of the number of LDV per hour, HDV per hour, and percent of HDV for each videotape period.

Videotape	LDV	HDV	% HDV
7/23 09:30 – 7/23 12:00	952	4	0.5
7/24 13:30 – 7/24 20:00	1190	2	0.2
7/25 09:00 – 7/25 11:30	1032	42	3.9
7/25 12:30 – 7/25 17:00	571	22	3.6
7/25 18:00 – 7/25 23:30	1017	8	0.8
7/26 12:30 – 7/26 17:30	1080	3	0.3
7/27 12:30 – 7/27 22:00	1110	3	0.2
7/28 10:00 – 7/28 21:30	820	26	2.9
7/29 11:00 – 7/29 19:00	828	13	1.5
7/30 09:30 – 7/31 01:00	709	<1	<0.1
7/31 10:00 – 7/31 16:00	883	40	4.4
7/31 16:00 – 7/31 19:00	1363	1	<0.1

indicates an influence of HDVs were used for the HDV-LDV bore analysis. These time periods are listed in Table 7.3 where the HDV counts were at least 1.5% of the vehicles. The time periods when the videotape data only indicates a low influence of HDVs (<0.8%) were used for the LDV only bore analysis. The digital mass spectra and the average area mass spectra were calculated for each bore, and the ratio of the HDV-LDV bore to the LDV only bore was calculated for a series of peaks that correspond to EC (C_n , where $n = 1 - 12$ and $-1 - -7$), as shown in Figure 7.7. The digital mass spectra and the average area mass spectra ratio are nearly one for all of the negative ion EC markers and the positive EC markers from $^{12}C_1 - ^{48}C_4$. After $^{48}C_4$, both ratios become greater than one, which indicates that there are more particles and greater mass spectral ion intensity at the EC marker peaks in the HDV-LDV bore than the LDV only bore. This signifies that the EC particle types from HDVs have higher m/z EC markers ions than LDVs. In the ATOFMS dynamometer studies, there was a higher fraction of the EC particles that had higher m/z EC marker ions in the HDV emissions than the LDV emissions particularly in the larger sizes [Shields *et al.*, 2005; Sodeman *et al.*, 2005; Toner *et al.*, 2005]. Watson *et al.* found in the thermal/optical reflectance method that EC1 (carbon that evolved at 550 °C in 98% He and 2% O₂) was twice as abundant in LDVs as HDVs, whereas EC2 (carbon that evolved at 700 °C in 98% He and 2% O₂) was ten times more abundant in HDVs than LDVs [Watson *et al.*, 1994]. Thus, it is a possibility that the EC2 from the thermal/optical reflectance method is the longer chain EC particle type (EC with $C_1 - C_{\geq 6}$) detected in the ATOFMS tunnel and dynamometer studies, whereas the EC1 from the thermal/optical reflectance method is the shorter chain EC particle type (EC with $C_1 - C_4$) detected in the ATOFMS tunnel and dynamometer studies. However, more work is needed to test this hypothesis.

7.4 Implications

The particle types measured during the dynamometer studies were detected in the Caldecott Tunnel, which validates that the chemical composition of particles produced in dynamometer studies using simulated dilution conditions are indeed representative of particle types emitted in real-world conditions. This indicates that the driving cycles tested on the dynamometer are representative of real-world driving conditions and that the dilution and residence chamber adequately simulate ambient dilution conditions, which is an important finding since dynamometers offer the highest degree of control over the vehicles and cycles tested.

Finally, these results show there are clear distinctions between light and heavy duty vehicle emissions at the single particle level. However, as shown, there is also quite a bit of overlap for some of the types and very subtle differences in composition for others. ART-2a is a straightforward analysis approach so this study represents a first step in source apportionment. It allows us to quickly assess the similarities and differences between HDV and LDV and dynamometer and tunnel conditions. It is clear that a multivariate approach such as positive matrix factorization (PMF) will be necessary for accurate source apportionment and the use of such approaches is currently underway.

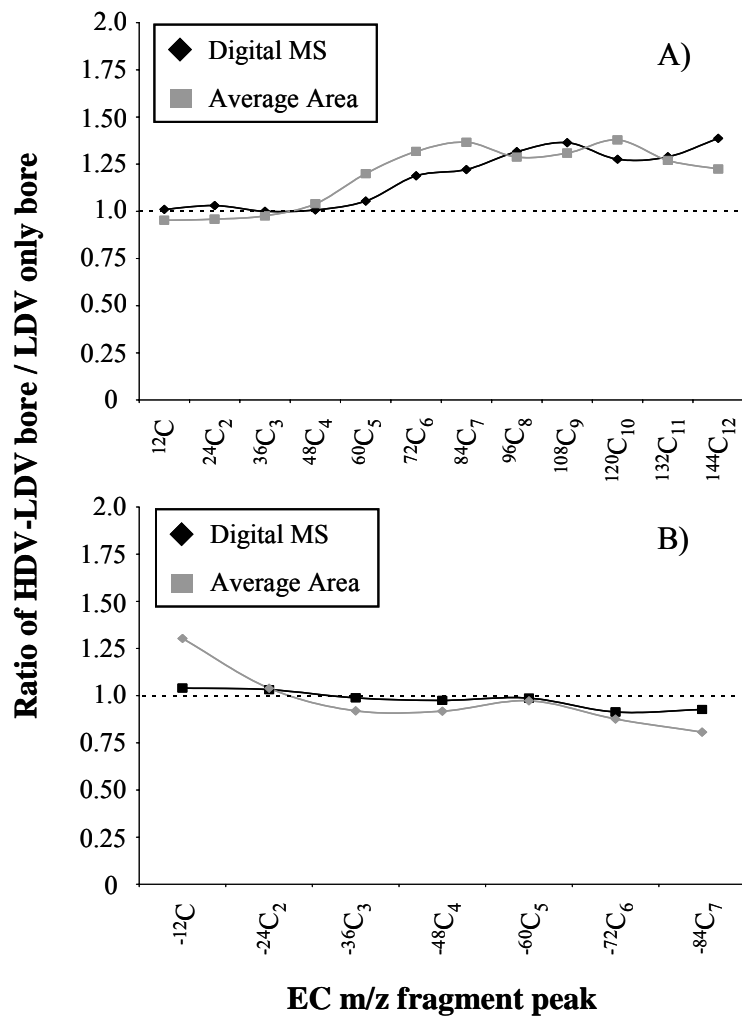


Figure 7.7 Ratios of HDV-LDV bore values divided by LDV only bore values for all EC particle types in the Caldecott Tunnel as a function of EC m/z fragments. Ratios greater than one indicate a higher detection of that m/z in the Caldecott Tunnel, whereas ratios less than one indicate lower detection of that m/z in the LDV dynamometer study.

7.5 Acknowledgements

The authors would like to thank Ellen M. Sukovich and Julia C. Jarvis for their help in the collection of the data from the Caldecott Tunnel, the Caltrans staff the Caldecott Tunnel, Mike Kleeman and Mike Robert for running the dilution and residence chamber utilized for two of the dynamometer studies, Barbara Zielinska for running the dilution and residence chamber utilized in one of the HDV dynamometer studies, and Shane Michael and the crew at California Air Resources Board (CARB) Haagan-Smit dynamometer facility in El Monte, CA for operating the LDV dynamometer. The authors express their gratitude to the Coordinating Research Council for their help and support in testing during CRC Project E55/E59, and the staff of the West Virginia University Transportable Heavy-Duty Emissions Testing Laboratory for their assistance with sample collection. Funding for this research was provided by CARB.

7.6 References

- Allen, J.O., D.P. Fergenson, E.E. Gard, L.S. Hughes, B.D. Morrical, M.J. Kleeman, D.S. Gross, M.E. Galli, K.A. Prather, and G.R. Cass, Particle detection efficiencies of aerosol time of flight mass spectrometers under ambient sampling conditions, *Environmental Science & Technology*, 34 (1), 211-217, 2000.
- Allen, J.O., P.R. Mayo, L.S. Hughes, L.G. Salmon, and G.R. Cass, Emissions of size-segregated aerosols from on-road vehicles in the Caldecott Tunnel, *Environmental Science & Technology*, 35 (21), 4189-4197, 2001.
- Bishop, G.A., and D.H. Stedman, Measuring the emissions of passing cars, *Accounts of Chemical Research*, 29 (10), 489-495, 1996.
- Bush, H.D., D.M. Rowson, and S.E. Warren, The application of neutron activation analysis to the measurement of the wear of a friction material, *Wear*, 20 (2), 211-225, 1972.
- Cadle, S.H., P. Mulawa, P. Groblicki, C. Laroo, R.A. Ragazzi, K. Nelson, G. Gallagher, and B. Zielinska, In-use light-duty gasoline vehicle particulate matter emissions on three driving cycles, *Environmental Science & Technology*, 35 (1), 26-32, 2001.
- Dienes, T., Development, characterization, and refinement of a transportable aerosol time-of-flight mass spectrometer, Ph.D. Thesis, University of California, Riverside, Riverside, 2003.
- Dimashki, M., S. Harrad, and R.M. Harrison, Measurements of nitro-PAH in the atmospheres of two cities, *Atmospheric Environment*, 34 (15), 2459-2469, 2000.
- Fraser, M.P., B. Buzcu, Z.W. Yue, G.R. McGaughey, N.R. Desai, D.T. Allen, R.L. Seila, W.A. Lonneman, and R.A. Harley, Separation of fine particulate matter emitted from gasoline

- and diesel vehicles using chemical mass balancing techniques, *Environmental Science & Technology*, 37 (17), 3904-3909, 2003.
- Fraser, M.P., and G.R. Cass, Detection of excess ammonia emissions from in-use vehicles and the implications for fine particle control, *Environmental Science & Technology*, 32 (8), 1053-1057, 1998.
- Fruin, S.A., M.J. St Denis, A.M. Winer, S.D. Colome, and F.W. Lurmann, Reductions in human benzene exposure in the California South Coast Air Basin, *Atmospheric Environment*, 35 (6), 1069-1077, 2001.
- Gard, E., J.E. Mayer, B.D. Morrical, T. Dienes, D.P. Fergenson, and K.A. Prather, Real-time analysis of individual atmospheric aerosol particles: Design and performance of a portable ATOFMS, *Analytical Chemistry*, 69 (20), 4083-4091, 1997.
- Garg, B.D., S.H. Cadle, P.A. Mulawa, P.J. Groblicki, C. Laroo, and G.A. Parr, Brake wear particulate matter emissions, *Environmental Science & Technology*, 34 (21), 4463-4469, 2000.
- Gramotnev, G., R. Brown, Z. Ristovski, J. Hitchins, and L. Morawska, Determination of average emission factors for vehicles on a busy road, *Atmospheric Environment*, 37 (4), 465-474, 2003.
- Graskow, B.R., M.R. Ahmadi, J.E. Moris, and D.B. Kittelson, Influence of fuel additives and dilution conditions on the formation and emission of exhaust particulate matter from a direct injection spark ignition engine, *Society of Automotive Engineers, SP-1551*, 261 - 271, 2000.
- Grosjean, D., In situ organic aerosol formation during a smog episode: Estimated production and chemical functionality, *Atmospheric Environment Part a-General Topics*, 26 (6), 953-963, 1992.
- Grosjean, D., and J.H. Seinfeld, Parameterization of the formation potential of secondary organic aerosols, *Atmospheric Environment*, 23 (8), 1733-1747, 1989.
- Gross, D.S., A.R. Barron, E.M. Sukovich, B.E. Warren, J.C. Jarvis, D.T. Suess, and K.A. Prather, Differentiation of heavy and light-duty emissions on the single particle level, *submitted to Atmos. Environ.*, 2004.
- Gross, D.S., M.E. Galli, P.J. Silva, and K.A. Prather, Relative sensitivity factors for alkali metal and ammonium cations in single particle aerosol time-of-flight mass spectra, *Analytical Chemistry*, 72 (2), 416-422, 2000a.

- Gross, D.S., M.E. Galli, P.J. Silva, S.H. Wood, D.Y. Liu, and K.A. Prather, Single particle characterization of automobile and diesel truck emissions in the Caldecott Tunnel, *Aerosol Science and Technology*, 32 (2), 152-163, 2000b.
- Guazzotti, S.A., D.T. Suess, K.R. Coffee, P.K. Quinn, T.S. Bates, A. Wisthaler, A. Hansel, W.P. Ball, R.R. Dickerson, C. Neususs, P.J. Crutzen, and K.A. Prather, Characterization of carbonaceous aerosols outflow from India and Arabia: Biomass/biofuel burning and fossil fuel combustion, *Journal of Geophysical Research-Atmospheres*, 108 (D15), 2003.
- Harrison, R.M., R. Tilling, M.S.C. Romero, S. Harrad, and K. Jarvis, A study of trace metals and polycyclic aromatic hydrocarbons in the roadside environment, *Atmospheric Environment*, 37 (17), 2391-2402, 2003.
- Heywood, J.B., *Internal combustion engine fundamentals*, 930 pp., McGraw-Hill, New York, 1988.
- Hildemann, L.M., G.R. Cass, and G.R. Markowski, A dilution stack sampler for collection of organic aerosol emissions: Design, characterization and field-tests, *Aerosol Science and Technology*, 10 (1), 193-204, 1989.
- Hildemann, L.M., G.R. Markowski, and G.R. Cass, Chemical composition of emissions from urban sources of fine organic aerosol, *Environmental Science & Technology*, 25 (4), 744-759, 1991.
- Kawai, T., Y. Goto, and M. Odaka, Influence of dilution process on engine exhaust nanoparticles, *Society of Automotive Engineers, SP-1862*, 113 - 119, 2004.
- Kean, A.J., R.A. Harley, D. Littlejohn, and G.R. Kendall, On-road measurement of ammonia and other motor vehicle exhaust emissions, *Environmental Science & Technology*, 34 (17), 3535-3539, 2000.
- Ketzel, M., P. Wahlin, R. Berkowicz, and F. Palmgren, Particle and trace gas emission factors under urban driving conditions in Copenhagen based on street and roof-level observations, *Atmospheric Environment*, 37 (20), 2735-2749, 2003.
- Kleeman, M.J., J.J. Schauer, and G.R. Cass, Size and composition distribution of fine particulate matter emitted from motor vehicles, *Environmental Science & Technology*, 34 (7), 1132-1142, 2000.
- Laschober, C., A. Limbeck, J. Rendl, and H. Puxbaum, Particulate emissions from on-road vehicles in the Kaisermuhlen-tunnel (Vienna, Austria), *Atmospheric Environment*, 38 (14), 2187-2195, 2004.

- Liu, D.Y., R.J. Wenzel, and K.A. Prather, Aerosol time-of-flight mass spectrometry during the Atlanta Supersite experiment: 1. Measurements, *Journal of Geophysical Research-Atmospheres*, 108 (D7), 8426, 2003.
- Marshall, J.D., W.J. Riley, T.E. McKone, and W.W. Nazaroff, Intake fraction of primary pollutants: Motor vehicle emissions in the South Coast Air Basin, *Atmospheric Environment*, 37 (24), 3455-3468, 2003.
- McDonal, R.A., Zinc dithiophosphates, in *Lubricant additives: Chemistry and applications*, edited by L.R. Rudnick, pp. 29 - 44, Marcel Dekker, New York, 2003.
- McLafferty, F.W., and F. Tureček, *Interpretation of mass spectra*, 371 pp., University Science Books, Mill Valley, Calif., 1993.
- Miguel, A.H., T.W. Kirchstetter, R.A. Harley, and S.V. Hering, On-road emissions of particulate polycyclic aromatic hydrocarbons and black carbon from gasoline and diesel vehicles, *Environmental Science & Technology*, 32 (4), 450-455, 1998.
- Mysliwiec, M.J., and M.J. Kleeman, Source apportionment of secondary airborne particulate matter in a polluted atmosphere, *Environmental Science & Technology*, 36 (24), 5376-5384, 2002.
- Odum, J.R., T.P.W. Jungkamp, R.J. Griffin, R.C. Flagan, and J.H. Seinfeld, The atmospheric aerosol-forming potential of whole gasoline vapor, *Science*, 276 (5309), 96-99, 1997.
- Phares, D.J., K.P. Rhoads, A.S. Wexler, D.B. Kane, and M.V. Johnston, Application of the ART-2a algorithm to laser ablation aerosol mass spectrometry of particle standards, *Analytical Chemistry*, 73 (10), 2338-2344, 2001.
- Pope, C.A., Review: Epidemiological basis for particulate air pollution health standards, *Aerosol Science & Technology*, 32 (1), 4-14, 2000.
- Riediker, M., W.E. Cascio, T.R. Griggs, M.C. Herbst, P.A. Bromberg, L. Neas, R.W. Williams, and R.B. Devlin, Particulate matter exposure in cars is associated with cardiovascular effects in healthy young men, *American Journal of Respiratory & Critical Care Medicine*, 169 (8), 934-940, 2004.
- Rizvi, S.Q., Detergents, in *Lubricant additives: Chemistry and applications*, edited by L.R. Rudnick, pp. 113 - 136, Marcel Dekker, New York, 2003.
- Rogge, W.F., L.M. Hildemann, M.A. Mazurek, G.R. Cass, and B.R.T. Simoneit, Sources of fine organic aerosol 2: Noncatalyst and catalyst-equipped automobiles and heavy-duty diesel trucks, *Environmental Science & Technology*, 27 (4), 636-651, 1993.

- Sagebiel, J.C., B. Zielinska, P.A. Walsh, J.C. Chow, S.H. Cadle, P.A. Mulawa, K.T. Knapp, and R.B. Zweidinger, PM₁₀ exhaust samples collected during IM-240 dynamometer tests of in-service vehicles in Nevada, *Environmental Science & Technology*, 31 (1), 75-83, 1997.
- Sanders, P.G., N. Xu, T.M. Dalka, and M.M. Maricq, Airborne brake wear debris: Size distributions, composition, and a comparison of dynamometer and vehicle tests, *Environmental Science & Technology*, 37 (18), 4060-4069, 2003.
- Schauer, J.J., M.J. Kleeman, G.R. Cass, and B.R.T. Simoneit, Measurement of emissions from air pollution sources 5: C-1-C-32 organic compounds from gasoline-powered motor vehicles, *Environmental Science & Technology*, 36 (6), 1169-1180, 2002.
- Seagrave, J., J.D. McDonald, A.P. Gigliotti, K.J. Nikula, S.K. Seilkop, M. Gurevich, and J.L. Mauderly, Mutagenicity and in vivo toxicity of combined particulate and semivolatile organic fractions of gasoline and diesel engine emissions, *Toxicological Sciences*, 70 (2), 212-226, 2002.
- Seinfeld, J.H., and S.N. Pandis, *Atmospheric chemistry and physics: from air pollution to climate change*, 1326 pp., Wiley, New York, 1998.
- Shields, L.G., D.T. Suess, S.A. Guazzotti, and K.A. Prather, Determination of single particle mass spectral signatures from heavy duty vehicle emissions, *in preparation*, 2005.
- Silva, P.J., Source profiling and apportionment of airborne particles: A new approach using aerosol time-of-flight mass spectrometry, Ph.D. Thesis, University of California, Riverside, Riverside, 2000.
- Silva, P.J., and K.A. Prather, Interpretation of mass spectra from organic compounds in aerosol time-of-flight mass spectrometry, *Analytical Chemistry*, 72 (15), 3553-3562, 2000.
- Singh, M., P.A. Jaques, and C. Sioutas, Size distribution and diurnal characteristics of particle-bound metals in source and receptor sites of the Los Angeles Basin, *Atmospheric Environment*, 36 (10), 1675-1689, 2002.
- Sodeman, D.A., S.M. Toner, and K.A. Prather, Determination of single particle mass spectral signatures from light duty vehicle emissions, *accepted for publication, Environment Science & Technology*, 2005.
- Song, X.H., P.K. Hopke, D.P. Fergenson, and K.A. Prather, Classification of single particles analyzed by ATOFMS using an artificial neural network, ART-2A, *Analytical Chemistry*, 71 (4), 860-865, 1999.
- Spencer, M.T., and K.A. Prather, Atomization of gasoline and diesel fuel and oil, *in preparation*, 2005.

- Stamatelos, A.M., A review of the effect of particulate traps on the efficiency of vehicle diesel engines, *Energy Conversion & Management*, 38 (1), 83-99, 1997.
- Su, Y.X., M.F. Sipin, H. Furutani, and K.A. Prather, Development and characterization of an aerosol time-of-flight mass spectrometer with increased detection efficiency, *Analytical Chemistry*, 76 (3), 712-719, 2004.
- Suess, D.T., Single particle mass spectrometry combustion source characterization and atmospheric apportionment of vehicular, coal, and biofuel exhaust emission, Ph.D. Thesis, University of California, Riverside, Riverside, 2002.
- Tolocka, M.P., M. Jang, J.M. Ginter, F.J. Cox, R.M. Kamens, and M.V. Johnston, Formation of oligomers in secondary organic aerosol, *Environmental Science & Technology*, 38 (5), 1428-1434, 2004.
- Toner, S.M., D.A. Sodeman, and K.A. Prather, Determination of single particle mass spectral signatures from heavy duty vehicle emissions for ultrafine and fine particles, *in preparation*, 2005.
- Vanvorst, W.D., and S. George, Impact of the California Clean Air Act, *International Journal of Hydrogen Energy*, 22 (1), 31-38, 1997.
- Venkataraman, C., J.M. Lyons, and S.K. Friedlander, Size distributions of polycyclic aromatic hydrocarbons and elemental carbon 1: Sampling, measurement methods, and source characterization, *Environmental Science & Technology*, 28 (4), 555-562, 1994.
- Vogt, R., U. Kirchner, V. Scheer, K.P. Hinz, A. Trimborn, and B. Spengler, Identification of diesel exhaust particles at an Autobahn, urban and rural location using single-particle mass spectrometry, *Journal of Aerosol Science*, 34 (3), 319-337, 2003.
- Watson, J.G., J.C. Chow, D.H. Lowenthal, L.C. Pritchett, C.A. Frazier, G.R. Neuroth, and R. Robbins, Differences in the carbon composition of source profiles for diesel-powered and gasoline-powered vehicles, *Atmospheric Environment*, 28 (15), 2493-2505, 1994.
- Wenzel, R.J., D.Y. Liu, E. Edgerton, and K.A. Prather, Aerosol time-of-flight mass spectrometry during the Atlanta Supersite Experiment: 2. Scaling procedures, *Journal of Geophysical Research-Atmospheres*, 108 (D7), 8427, 2003.
- Wenzel, R.J., and K.A. Prather, Improvements in ion signal reproducibility obtained using a homogeneous laser beam for on-line laser desorption/ionization of single particles, *Rapid Communications in Mass Spectrometry*, 18, 1525-1533, 2004.
- Wienke, D., Y. Xie, and P.K. Hopke, An adaptive resonance theory based artificial neural network (ART-2a) for rapid identification of airborne particle shapes from their scanning

- electron microscopy images, *Chemometrics & Intelligent Laboratory Systems*, 25 (2), 367-387, 1994.
- Willermet, P.A., Some engine oil additives and their effects on antiwear film formation, *Tribology Letters*, 5 (1), 41-47, 1998.
- Wingfors, H., A. Sjodin, P. Haglund, and E. Brorstrom-Lunden, Characterization and determination of profiles of polycyclic aromatic hydrocarbons in a traffic tunnel in Gothenburg, Sweden, *Atmospheric Environment*, 35 (36), 6361-6369, 2001.
- Xie, Y., P.K. Hopke, and D. Wienke, Airborne particle classification with a combination of chemical composition and shape index utilizing an adaptive resonance artificial neural network, *Environmental Science & Technology*, 28 (11), 1921-1928, 1994.
- Yamaguchi, E.S., S.H. Roby, M.M. Francisco, S.G. Ruelas, and D. Godfrey, Antiwear film formation by ZnDTP, detergent, and dispersant components of passenger car motor oils, *Tribology Transactions*, 45 (3), 425-429, 2002.
- Yu, J.Z., D.R. Cocker, R.J. Griffin, R.C. Flagan, and J.H. Seinfeld, Gas-phase ozone oxidation of monoterpenes: Gaseous and particulate products, *Journal of Atmospheric Chemistry*, 34 (2), 207-258, 1999.

Using Mass Spectral Source Signatures to Apportion Exhaust Particles From Gasoline and Diesel Powered Vehicles in a Freeway Study

8.1 Overview of Freeway Study

As described in this final report, mass spectral signatures have been obtained directly by sampling exhaust emissions from heavy duty diesel vehicles (HDDV) and gasoline powered light duty vehicles (LDV) in dynamometer studies using ATOFMS. In order to test the feasibility of using the dynamometer signatures for ambient source apportionment, a study using three ATOFMS instruments was performed near a major San Diego freeway (Interstate-5) from July 21-Aug. 25, 2004. There were several major goals for this study:

Major goals

- 1) Measure the size-resolved composition of ambient particles using three ATOFMS instruments.
- 2) Determine whether the single particle mass spectral signatures acquired with ATOFMS during the dynamometer studies are representative of those detected near a roadway.
- 3) If the ambient particles resemble the dynamometer particles, determine the percentage of ambient particles near a major roadway which match the dynamometer source seeds.
- 4) Compare single particle signatures and relative number concentrations between the roadside site and the background locations.
- 5) Use a combination of gas and particle phase instrumentation to determine whether particles from light duty vehicles can be distinguished from diesel vehicles.
- 6) Examine the temporal evolution of the particles over time and determine the relative contributions from particle sources other than vehicles.

Further studies

- 7) Compare the evolution of gas phase, particle phase, and meteorological data to use information from a combination of instruments as an approach for source apportionment.
- 8) Apportion particles based on single particle signatures to HDDV or LDV, and determine the fractions of particles from each source. We will examine how source contributions of particles from different sources vary as a function of size by apportioning particles in separate size bins (i.e. 50-100 nm, 100-500 nm, and 500-1000 nm).
- 9) Compare single particle apportionment results from different data analysis tools that are being applied to single particle data in the Prather group.
- 10) Compare ATOFMS source apportionment results with those from conventional filter based sampling by Prof. Mike Kleeman's group at UC Davis.

This chapter provides an overview of our progress to date in analyzing the freeway dataset.

8.2 Experimental Approach and Study Location

Two sites were chosen for this study. First, a “clean” upwind site (Figure 8.1 – yellow circle) was stationed at the Prather Laboratory in Urey Hall at the University of California, San Diego (UCSD) with the goal of determining the signature of the background ambient aerosols (GPS position N32°52.520’ W117°14.482’). This site is close to the ocean so the prevailing winds (from the west) should introduce no new sources other than sea spray (in theory). This site housed an ATOFMS instrument which use standard particle inlet (200-2500 nm) along with an aerodynamic particle sizer (APS) (TSI Model 3321 – Minnesota) and a scanning mobility particle sizer (SMPS) (TSI Model 3936L10 – Minnesota). The second site (Figure 8.1 – green circle) was stationed in a low-use parking lot (particularly during the summer) on the UCSD campus directly adjacent to the I-5 freeway (GPS position N32°52.831’ W117°13.680’) with the sampling line within 10 meters of the freeway. The trailer housed a suite of instruments including an ATOFMS and an UF-ATOFMS. A detailed summary of the instrumentation operated at both sites is provided in Table 8.1. Dr. Michael Kleeman (UC Davis) also sampled at both sites with micro orifice uniform deposit impactors (MOUDI’s), Anderson Impactors, an APS, and an SMPS. His group sampled from July 21-Aug. 1. Their measurements focused on obtaining size-resolved concentrations of organic and metal tracers that can be used for conventional source apportionment. Ultimately, when their results are available, a comparison will be made between the ATOFMS apportionment results and the filter-based predictions. Meteorological stations were operated on each side of the freeway for complete wind trajectory information.

A digital Webcam was used for freeway traffic monitoring and recorded digital video continuously throughout the study. Some preliminary analysis shows that the measurements track trends in traffic quite well, especially during heavy traffic events in the morning and evening hours. Further trends will ultimately be explored in greater detail, such as establishing correlations between elemental carbon (EC) classes and CO concentrations (both indicators of fresh emissions), PAH-containing particles with trends in the photoelectric aerosol sensor (PAS), as well as many other potential trends between the peripheral instruments and the ATOFMS size-resolved chemistry PM measurements.

8.3 Results and Discussion

8.3.1 Quality assurance of ATOFMS data

Data from the three ATOFMS instruments as well as all peripheral instruments have been loaded into a database that allows for direct comparison of the temporal trends of gas phase, particle phase, and meteorological data. Before beginning data analysis of the ATOFMS chemical types, quality assurance (QA) graphs were prepared for all three instruments over the relevant size ranges for the course of the study.



Figure 8.1 Aerial view of the UCSD campus showing the upwind (yellow circle) and downwind (green circle) sampling sites of the freeway.
(Picture from <http://maps.ucsd.edu/Viewer.htm?Map=Aerial2002>)

Table 8.1 List of instruments used for the upwind/downwind freeway study in 2004.

Instrument	Make & Model	Measurement	Units	Sample Interval	Site	Sampling Period
Ultrafine Aerosol Time-of-Flight Mass Spectrometer (UF-ATOFMS)		size range: 50-400 nm		real-time	trailer	Jul 21 to Aug 25, 2004
Standard Aerosol Time-of-Flight Mass Spectrometer (ATOFMS) 1		size range: 200-3000 nm		real-time	trailer	Jul 21 to Aug 25, 2004
Standard Aerosol Time-of-Flight Mass Spectrometer (ATOFMS) 2		size range: 200-3000 nm		real-time	laboratory	Jul 21 to Aug 2, 2004
					trailer	Aug 10 to Aug 25, 2004
					parking lot	Aug 25, 2004
Aerodynamic Particle Sizer (APS) 1	TSI Model 3321	particle number conc. (0.5-20 μm)	$\#/ \text{cm}^3$	5 min	trailer	Jul 21 to Aug 25, 2004
Aerodynamic Particle Sizer (APS) 2	TSI Model 3321	particle number conc. (0.5-20 μm)	$\#/ \text{cm}^3$	5 min	laboratory parking lot	Jul 21 to Aug 2, 2004 Aug 25, 2004
Scanning Mobility Particle Sizer (SMPS) 1	TSI Model 3936L10	particle number conc. (10-500 nm)	$\#/ \text{cm}^3$	5 min	trailer	Jul 21 to Aug 25, 2004
Scanning Mobility Particle Sizer (SMPS) 2	TSI Model 3936L10	particle number conc. (10-500 nm)	$\#/ \text{cm}^3$	5 min	laboratory parking lot	Jul 21 to Aug 2, 2004 Aug 25, 2004
Aethalometer	Magee Scientific 'Spectrum' AE-3 Series	optical absorption cross-section per unit mass	$\mu\text{m}/\text{m}^3$	5 min	trailer	Jul 21 to Aug 25, 2004
Nephelometer	Radiance Model M903	light scattering coefficient (bscat)	km^{-1}	5 min	trailer	Jul 21 to Jul 22 & Jul 25 to Aug 25, 2004
Photoelectric Aerosol Sensor (PAS)	EcoChem Model 2000	concentration of total particle-bound PAH	ng/m^3	5 min	trailer	Jul 30 to Aug 25, 2004
Tapered Element Oscillating Microbalance (TEOM)	Rupprecht & Patashnick (R & P) Series 1400a	mass concentration (PM _{2.5})	$\mu\text{m}/\text{m}^3$	30 min	trailer	Jul 21 to Aug 25, 2004
Chemiluminescence NO-NO ₂ -NO _x Analyzer	Thermo Environmental Instruments (TEI) Model 42C	NO & NO _x concentration levels	ppb	1 min	trailer	Aug 5 to Aug 25, 2004
CO Analyzer	Advanced Pollution Instrumentation (API) Model M300	CO concentration levels	ppm	5 min	trailer	Jul 30 to Aug 10 & Aug 13 to Aug 25, 2004
Webcam	Creative Model PD1001	traffic video surveillance		real-time	trailer	Jul 21 to Aug 25, 2004

A question that often arises is: how can one be sure any non-absorbing particle classes are not being “missed” in the LDI analysis step. In order to check for the presence of chemical biases, temporal plots are compared of the number of particles which scatter light to the number of particles which scatter light and produce a mass spectrum. If there is a chemical bias, where a particular type is being “missed”, it will show up in this type of plot as a period when there were lots of “scatters” with very few “scatters + mass spectra”. These plots were made for all three ATOFMS instruments over multiple size ranges for the full duration of the study. An example of this type of plot is shown in Figure 8.2. It should be noted that all temporal plots for ATOFMS data shown in this chapter show unscaled ATOFMS number concentrations, in contrast to previous chapters which report scaled ATOFMS data. As will be shown, the unscaled temporal trends of the ATOFMS track the peripheral instruments without scaling; the main reason for scaling is to obtain atmospherically representative concentrations that can be directly compared to other studies.

It is important to note that the smallest sized particles have the highest probability of showing a chemical bias since smaller particles are more “pure” (i.e. less chemically complex). In the freeway study, there was no major evidence of any particle types being missed by the ATOFMS in any of the size ranges examined (50-1000 nm). This is not surprising since combustion emissions from vehicles strongly absorb the ultraviolet light used for laser desorption/ionization process.

As part of the QA, it is also important to compare the two ATOFMS instruments temporal trends when they were sampling side-by-side for the last part of the study near the freeway. Figure 8.3 shows a comparison, demonstrating how when the instruments were located at the same site almost identical trends in particle counts are obtained, demonstrating the reproducibility of the two ATOFMS systems.

8.3.2 Comparison with standard particle counts

Another way to determine whether the trends observed with the ATOFMS reflect ambient particle concentrations involves comparing the ATOFMS size distribution measurements with those from other particle instruments located at the same site. Figure 8.4 shows a comparison of the SMPS (5 minute temporal resolution) against the UF-ATOFMS (30 minute temporal resolution) for sub-100 nm particle counts. Since the SMPS data are plotted with short 5 minute resolution, the data appear noisy; however, it is still evident that the basic trends measured by these two instruments track one another quite well, providing additional validation of the ATOFMS temporal trends. In general, the ultrafine counts were found to correspond to periods when the winds were blowing from the west directly to the sampling site. At night the wind speeds typically became quite small, the traffic was reduced, and the ultrafine particle counts were reduced. This pattern was repeated over the entire study.

The two standard inlet ATOFMS systems measured particles in the larger size modes. Figure 8.5 shows a comparison over the entire study of one of the ATOFMS instruments sampling 100-1000 nm by the freeway with the Aerodynamic Particle Sizer (APS) counts. The APS only samples particles down to 500 nm so a slightly different size range is covered, and the standard ATOFMS detected very few particles below 300 nm due to limitations in the transmission efficiency of the inlet. The important thing to note about this comparison is how strongly correlated the trends are, offering further credence to the temporal variations observed

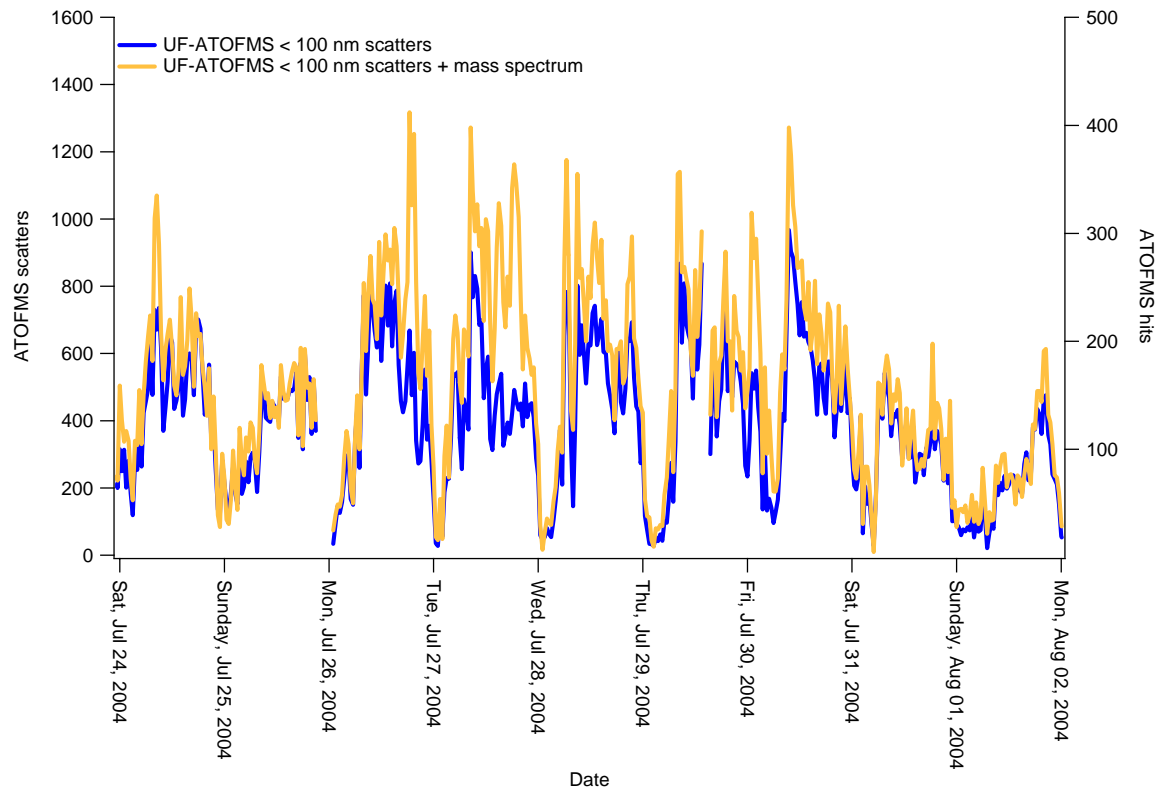


Figure 8.2 Temporal trends (30 minute resolution) showing those particles which scatter light versus those that scatter light and also produce a mass spectrum.

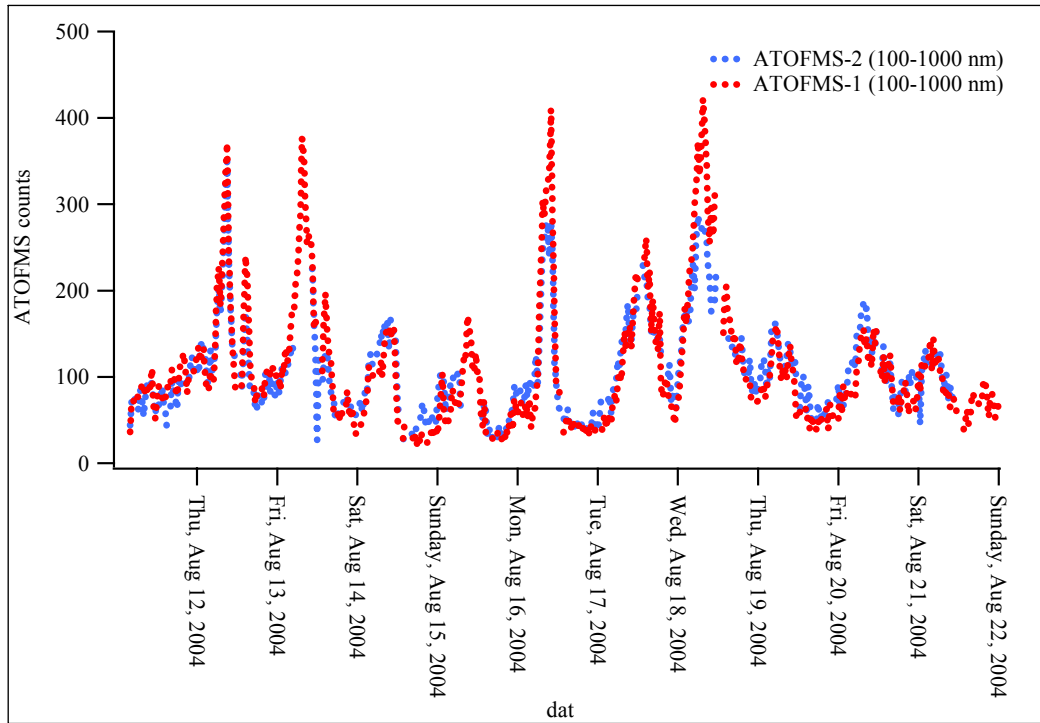


Figure 8.3 Comparison of temporal trends for two ATOFMS instruments in the 100-1000 nm size range.

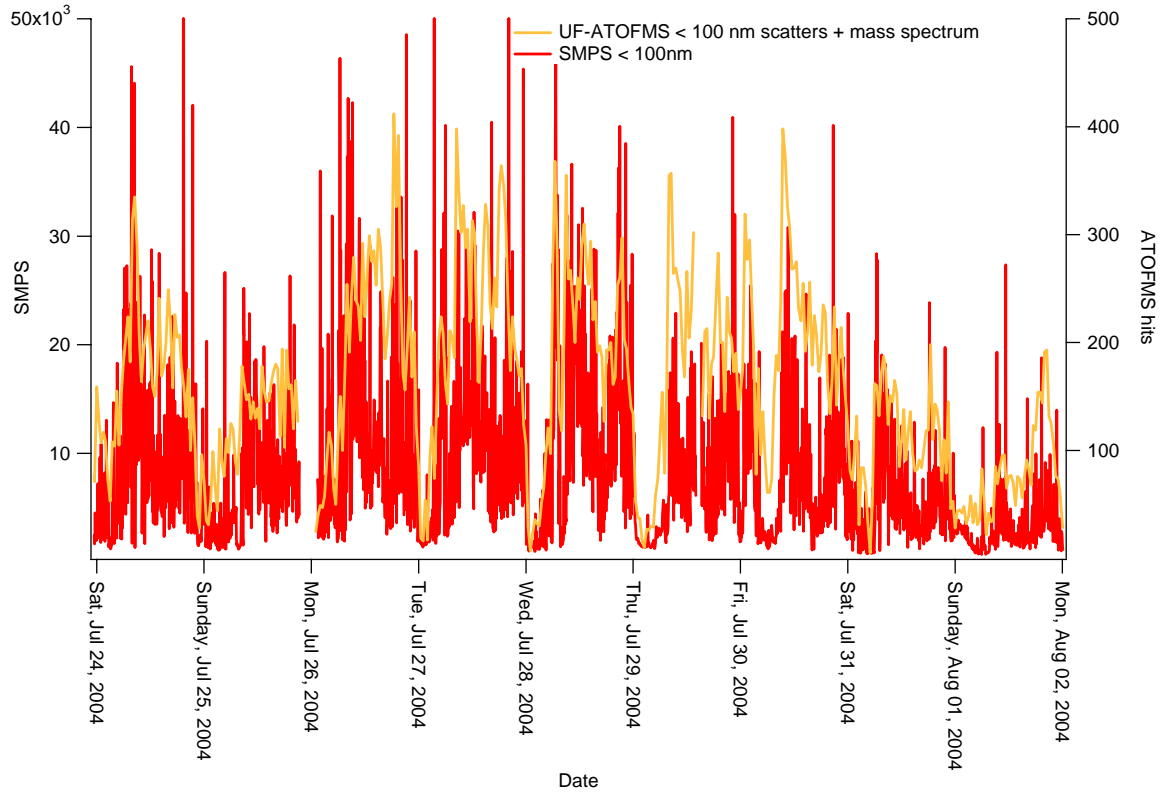


Figure 8.4 Comparison of ATOFMS counts for sub-100 nm particles versus those measured by the scanning mobility particle sizing system.

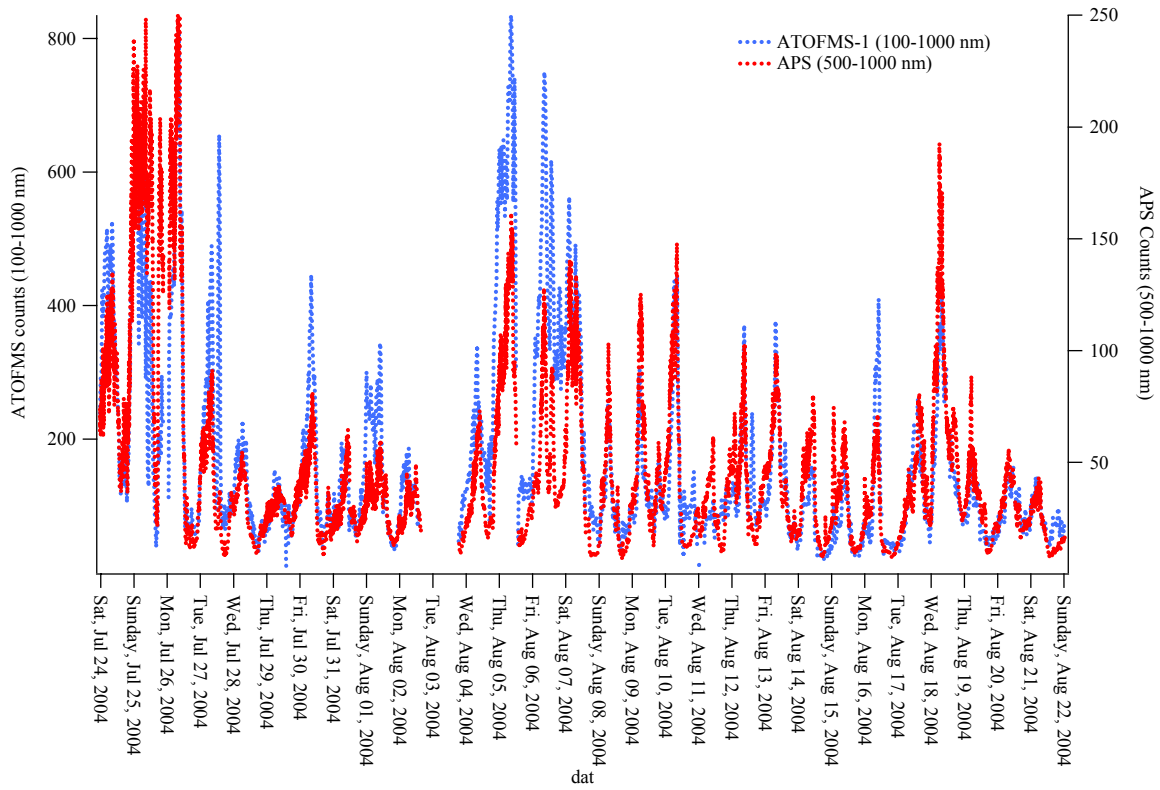


Figure 8.5 Comparison of temporal trends of aerodynamic particle sizer (APS) counts to the ATOFMS counts with 1 hour temporal resolution for the duration of the study.

with the ATOFMS. Both Figures 8.4 and 8.5 both show the ATOFMS instruments correlate well with particle number concentrations measured using traditional particle sizing instruments over a broad range of sizes. This validation step is extremely important to future studies probing the temporal variability of different source contributions to the various ambient particles sampled by ATOFMS.

8.3.3 Comparison of temporal trends from peripheral instruments

Analysis of gas phase species such as NO_x and CO coupled with aethalometer data can provide insight into the time periods when freeway plumes were impacting the sampling site. There is some speculation that this combination of instruments coupled with ultrafine size distribution measurements made with an SMPS may be used to identify HDDV impacted events. Figure 8.6 shows a comparison of the aethalometer and NO_x measurements made over a time period when all instruments were operational. In general, strong trends were observed between the ultrafine particle concentrations (<100 nm), CO, aethalometer, and NO_x measurements when the wind was blowing towards the sampling site, which occurred mostly during daytime hours.

By comparing the aethalometer and NO_x concentrations, one can see the trends track very well. In addition, one can see there are increases during weekdays as has been reported in previous studies. This has been attributed to a relative increase in truck traffic during the week. We plan to explore composition differences for weekday/weekends to see if the truck/car split is evident in the single particle data. One thing to note, based on an initial viewing of traffic count data, in addition to fewer trucks being on the road on weekends, there are also fewer cars overall. The traffic flow in general is much lower on this freeway on weekends.

Figure 8.7 shows the correlations observed between ultrafine particle concentrations measured with an SMPS, aethalometer, and gas phase NO_x concentration. A correlation of high values between these 3 instruments will help isolate time periods where fresh particles emissions from HDDV may dominate such as August 9-13 and 16-20 shown above.

8.3.4 Comparison of particle phase and gas phase data

It is interesting to compare the UF-ATOFS measurements with gas phase measurements. Figures 8.8 and 8.9 show a comparison of gas phase CO and NO_x concentration measurements versus UF-ATOFS counts, indicating time periods where fresh emissions were impacting the sampling site. Figure 8.8 shows an expanded view of each gas phase species plotted along with the ATOFS data. Figure 8.9 shows a comparison of the UF-ATOFS against NO_x and CO over the full time period when all gas phase instruments were operational during the study. These plots are important because it is expected that time periods where UF particles and CO peak may be indicative of car exhaust periods, whereas increases in NO_x concentrations could be more indicative of HDDV emissions.

8.3.5 Upwind/Downwind Sampling

A major goal of the freeway study involved determining the contributions of vehicle emissions to ambient air near a major freeway. As described in the introduction, an upwind sampling site was established so a comparison could be made between source contributions at a

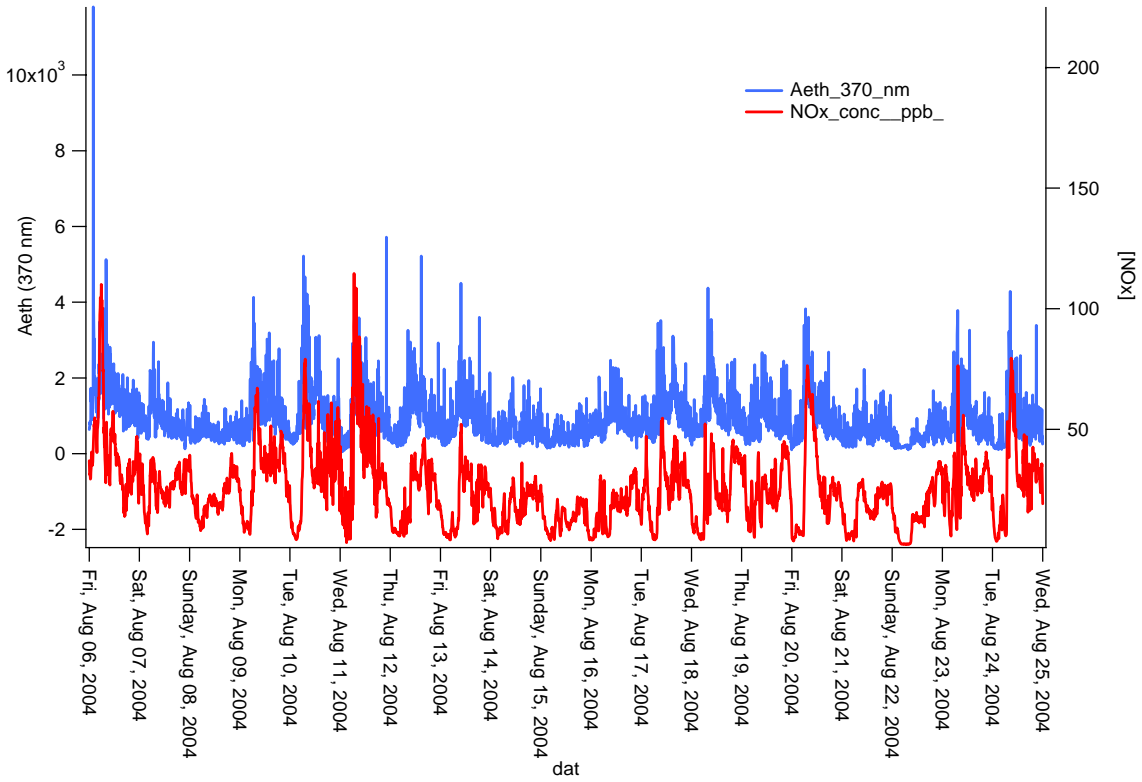


Figure 8.6 Temporal trends for the aethalometer (370 nm) versus gas phase NOx concentrations.

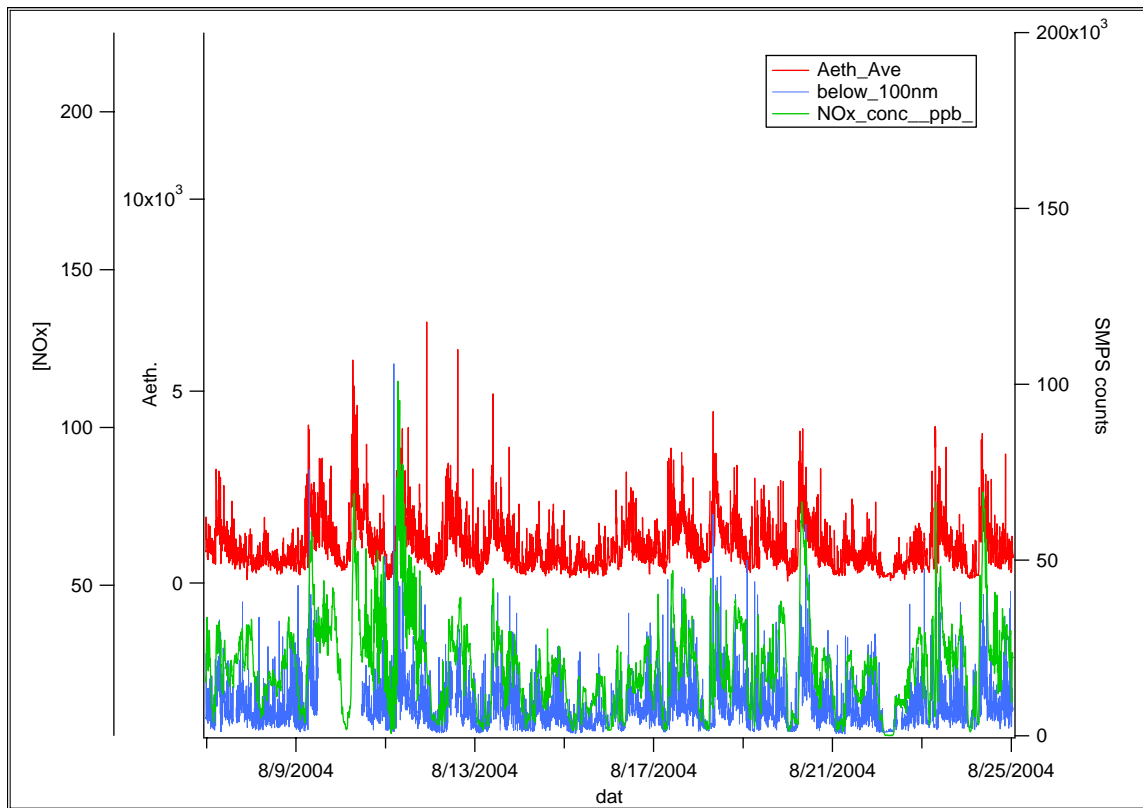


Figure 8.7 Temporal trends of NOX, aethalometer, and particle number concentrations for sizes below 100 nm measured with the SMPS.

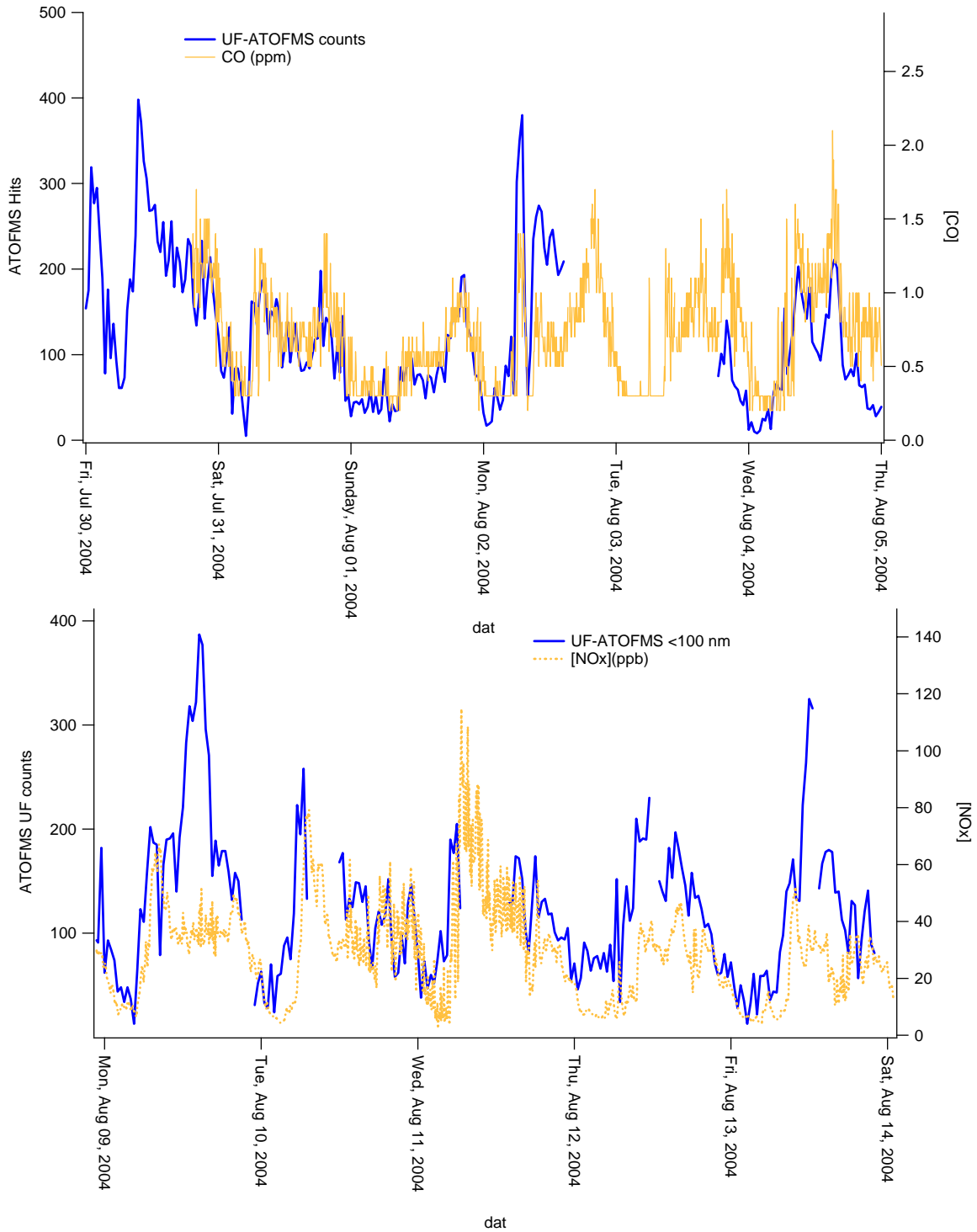


Figure 8.8 Comparison of ATOFMS ultrafine particle counts with gas phase measurements of CO (top) and NOx (bottom).

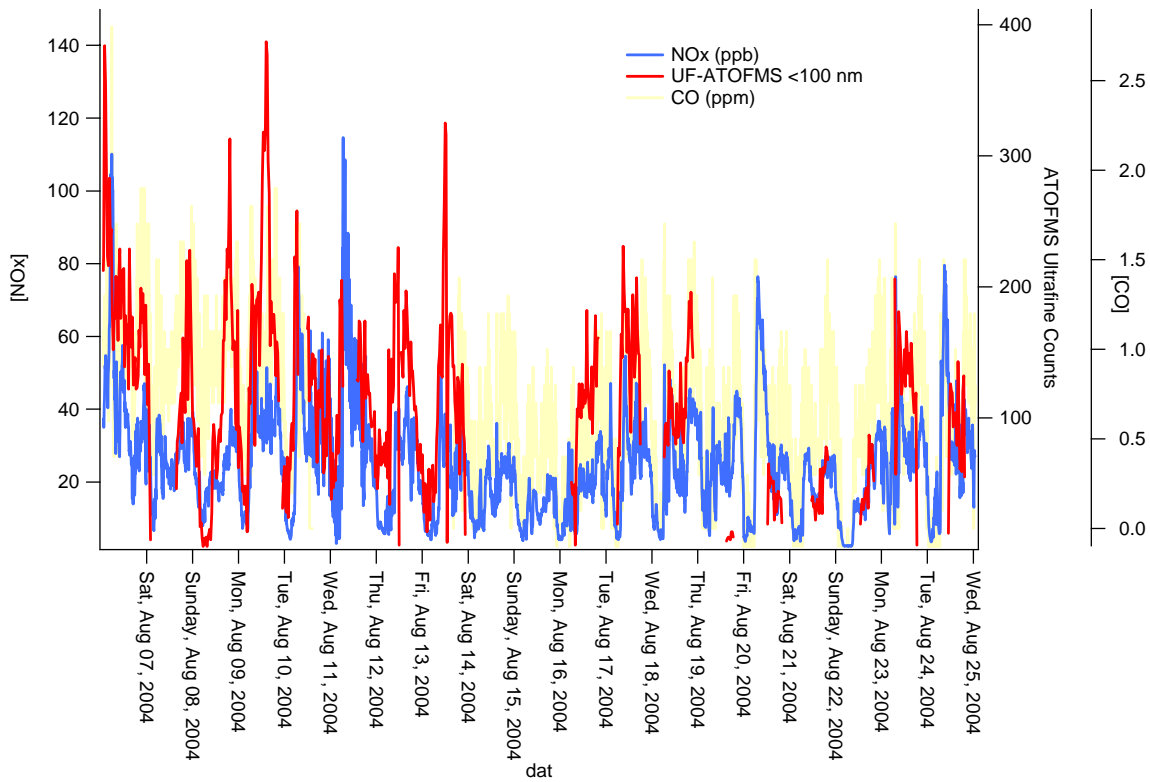


Figure 8.9 Comparison of temporal trends of CO, NO_x, and UF-ATOFMS (50-100 nm) particle counts.

freeway-impacted site and a background (upwind) site. In addition to composition measurements being made with the ATOFMS and filters (by the Kleeman group), size distribution measurements were made using an APS and SMPS combination at both locations.

Figure 8.10 shows the APS and SMPS concentrations for the period between July 24 and August 2, 2004. The temporal trends of the particle concentrations in all size ranges are very similar at the two locations, suggesting a strong regional contribution to the ambient PM levels at both sites. It is important to note that the wind was blowing from the upwind site (onshore) towards the freeway site during daytime hours when the concentrations show maxima in the ultrafine particle number concentrations at both locations. This figure shows that the concentrations of accumulation mode particles at the upwind/background site were not lower than those at the freeway site, and at times they were actually higher. As shown in Figure 8.10, the accumulation mode concentrations peaked between midnight and noon, much of the time when the wind speed was almost non-existent. This indicates the freeway was not substantially impacting the overall ambient accumulation mode particle concentrations during this period of the study. Figure 8.11 shows the concentrations of particles in the larger sizes (1000-2500 nm) were actually higher at the upwind site than the freeway site. ATOFMS measurements show the majority of particles in this size range are sea salt, and thus it is not surprising these concentrations were higher closer to the ocean.

The ultrafine mode and lower end of the accumulation mode size range (50-500 nm) show higher concentrations at the freeway location (Figure 8.11), suggesting the freeway is making detectable contributions to particles in the 50-500 nm size range. However, it is interesting to note that on July 27 and 28, at around noon, significantly higher ultrafine and accumulation mode concentrations are observed at the upwind site indicating contributions from a local source near the laboratory site. The standard instrument (ATOFMS-2) was sampling at the upwind location during this period. An examination of the single particle composition reveals a unique single particle signature, shown in Figures 8.10 and 8.12. The spectra shown in Figure 8.12 are the particle types identified by ART-2a as the major types at both sites by the two ATOFMS instruments when the concentrations peaked on July 27. This signature has been detected as a major particle type in meat cooking emissions in previous meat cooking studies conducted in our laboratory. The fingerprint for this particle type shows indicators of long chain (fatty) acids (odd/alternative hydrogen m/z envelopes), sulfur species (-97), and well as polycyclic aromatic hydrocarbon (PAH) species at m/z 178. A large potential source of PM on the UCSD campus near the sampling site is a cafeteria that charbroils hamburgers. The peak in emissions corresponds to lunch time preparation hours and this is the period of the day when the most people eat at this establishment. Of note, in our lab we often smell the emissions at around noon on many days. On July 27, this particle type was detected by both the UF and standard ATOFMS at the freeway site. The APS shows an increase (Figure 8.10) and also, the standard ATOFMS shows an increase at almost the same time. Meteorological data show the wind was blowing directly from the upwind site to the freeway with an average wind speed of 4 m/s. A common marker used for meat cooking emissions is oleic acid which shows a specific peak in the negative ion spectra of the ATOFMS. A search on this peak for all 3 instruments provides an indication of the relative impact of meat cooking emissions on PM concentrations at both sites. The temporal trends of particles containing oleic acid are shown in Figure 8.13 along with the meteorological data which show the link between the transport and temporal trends of the meat cooking emissions. This figure shows the upwind site has higher concentrations due to this

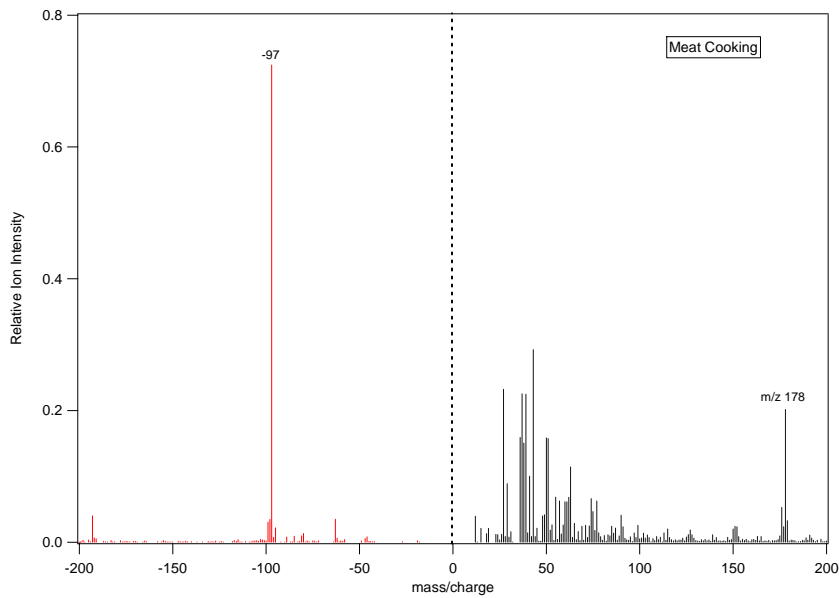
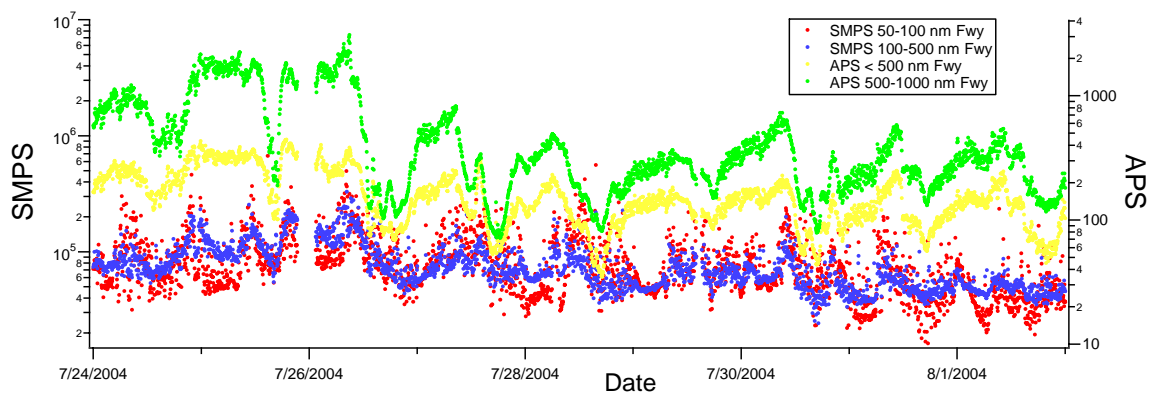
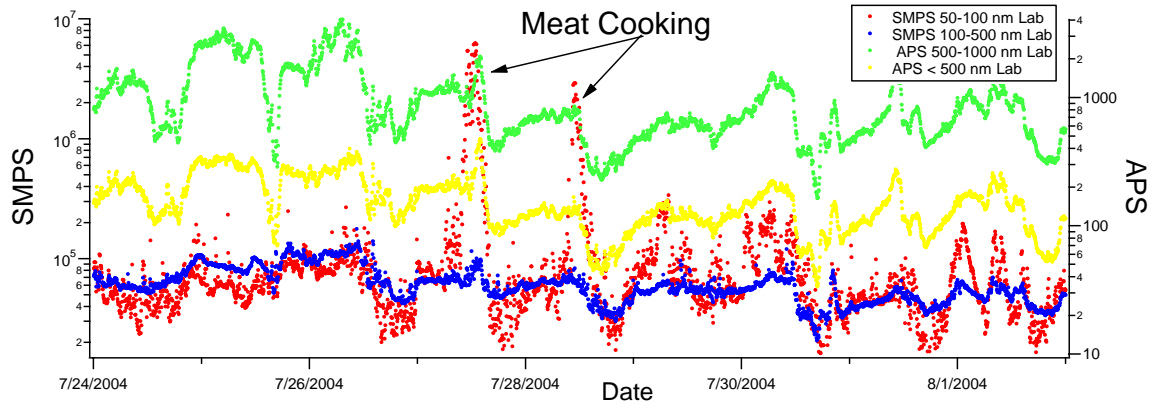


Figure 8.10 Comparison of SMPS and APS concentrations at freeway and upwind sites.

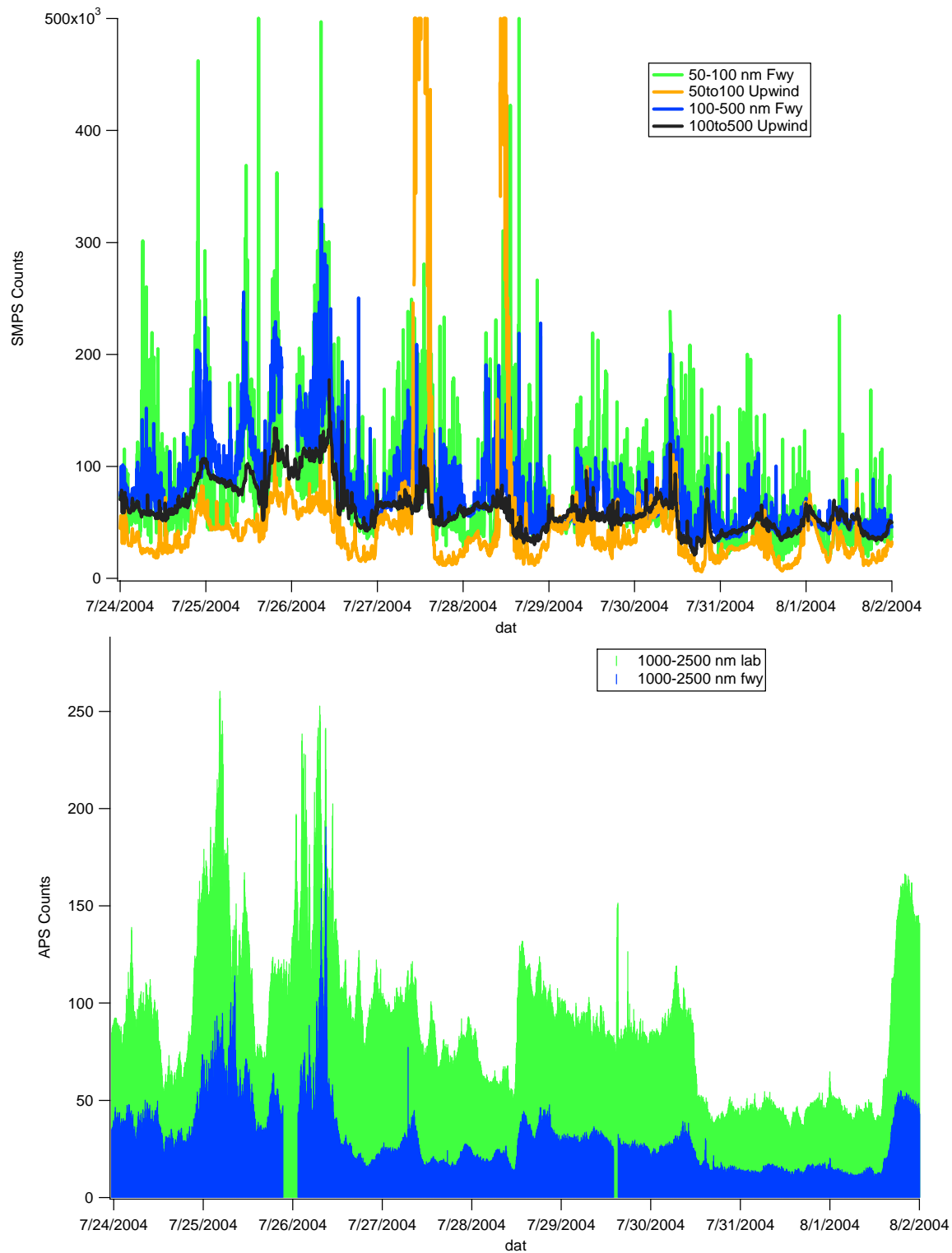


Figure 8.11 Comparison of ultrafine particle concentrations (upper) and 1000-2500 nm size ranges made using an SMPS and APS, respectively.

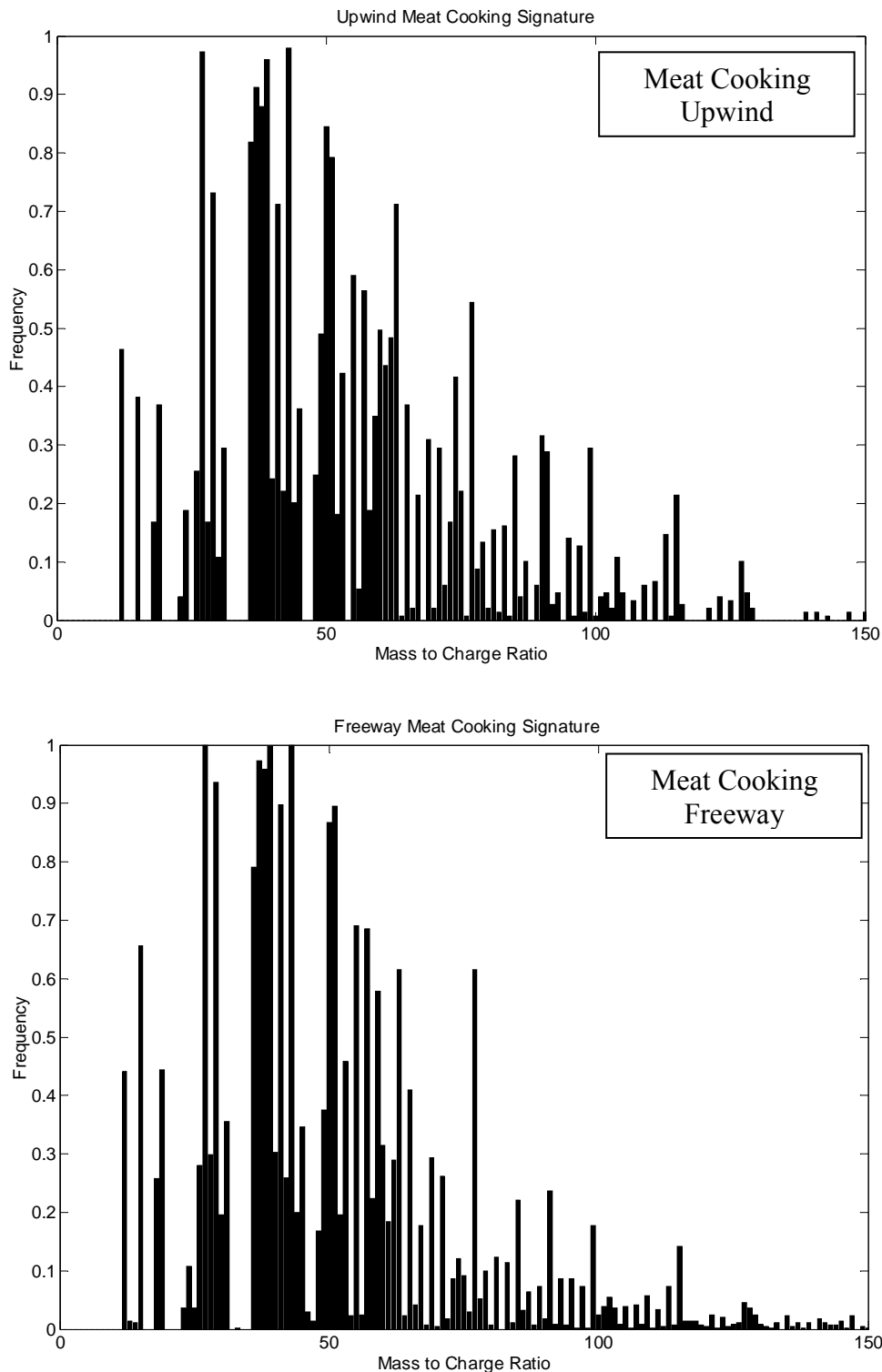


Figure 8.12 Single particle spectra of meat cooking particles detected in ultrafine mode at upwind site and accumulation mode (100-1000 nm) at freeway site. Note unique signature of odd spaced peaks at higher m/z ratios. These are indicative of fatty acids. See Figure 8.13 for temporal trends.

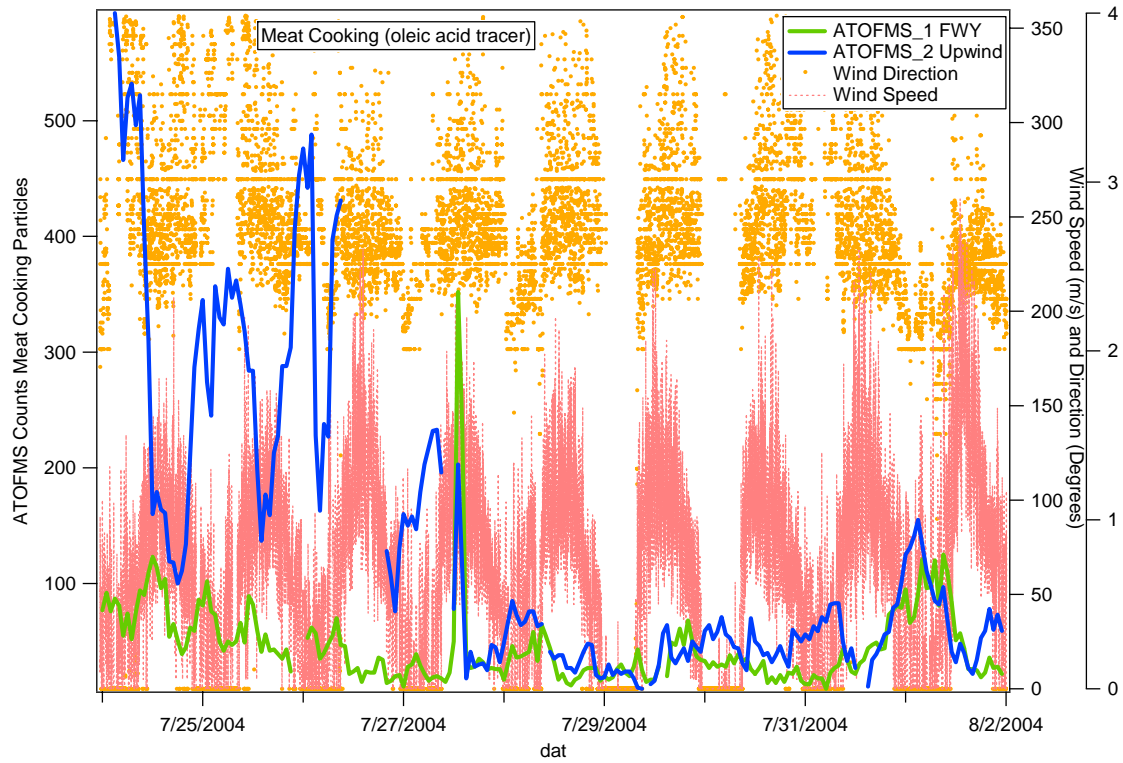


Figure 8.13 Temporal trends for meat cooking particles (oleic acid marker) for upwind (lab) and freeway locations.

source overall. The concentrations peak in the accumulation mode peak at the beginning of this period (July 24-26); one should note that this could be due to regional contributions as opposed to fresh emissions as the UF mode does not show the same corresponding increase on July 27.

As shown in Figure 8.14, regional background PM concentrations appear to be making significant contributions to the accumulation mode. By comparing the size distributions of the two ATOFMS instruments (lab and freeway), one can see that the size distributions are almost identical in the accumulation mode size range. Evident in this figure is a relatively high PM concentration in this mode from July 24-26. In contrast, the ultrafine mode shows higher concentrations during the week, suggesting it will most likely be more reflective of vehicle influences. This will make unraveling the source signatures near the freeway more challenging than anticipated. The SMPS and APS data confirm these same trends and indicate the ultrafine mode had higher concentration differences between the upwind and downwind sites. One of the ultimate goals of this study is to compare single particle source apportionment with the filter-based samples acquired during this study. Single particle measurements will hopefully be able to distinguish unique source signatures superimposed on a high ambient background concentrations that may not be apparent in filter-based mass concentrations where only slight changes are due to vehicle emissions (at least for the accumulation mode).

Due to these background contributions, other particle types including biomass and metal-containing particles were detected during this study that did not match the dynamometer clusters. The mass spectrum and temporal trends measured for a vanadium-type particle are shown in Figure 8.15. Again, this particle type peaked during the first few days of the study in the accumulation mode at both sites mostly at night when the winds were low, possibly indicating a regional contribution. There are a number of possible sources for such particles including ships. It is interesting to compare the temporal trend for these V-particles in the accumulation mode versus the ultrafine mode. On August 1, the number concentration of these particles shows a sharp increase that is not apparent in the accumulation mode, mostly likely indicating a local source.

On July 29 and 30, ultrafine concentrations at the upwind site peaked at approximately 6 am (see “SMPS 50 to 100 Lab” in Figure 8.10) and most likely came from traffic on a local road that circles the campus located close to the upwind site which is highly traveled at this hour of the day. In general, ultrafine particle concentrations show the highest spatial variability and represent ideal markers for local source inputs, as they spike only near the emission source. The ultrafine particles are also the most straightforward to identify and apportion since they have undergone very little aging and thus their signatures closely resemble the source (in this case dynamometer) testing signatures.

In general, all major particle types observed at the freeway site were also detected at the laboratory site. The similarities between the major particle types sampled by the standard ATOFMS instrument that was initially located at the upwind site (ATOFMS-2) and then moved to the freeway site were compared by taking the dot product of the top clusters detected at each site (see Section 1.3 for a further description). In general, all particle types detected at both sites had matching clusters with vigilance (similarity) factors of 0.85 and greater, meaning their mass spectral signatures were very similar to one another (a dot product of 1 indicates they are identical to one another). It is important to keep in mind that slight modifications due to uptake of organic carbon, ammonium, nitrate, and other secondary species will not have much of an

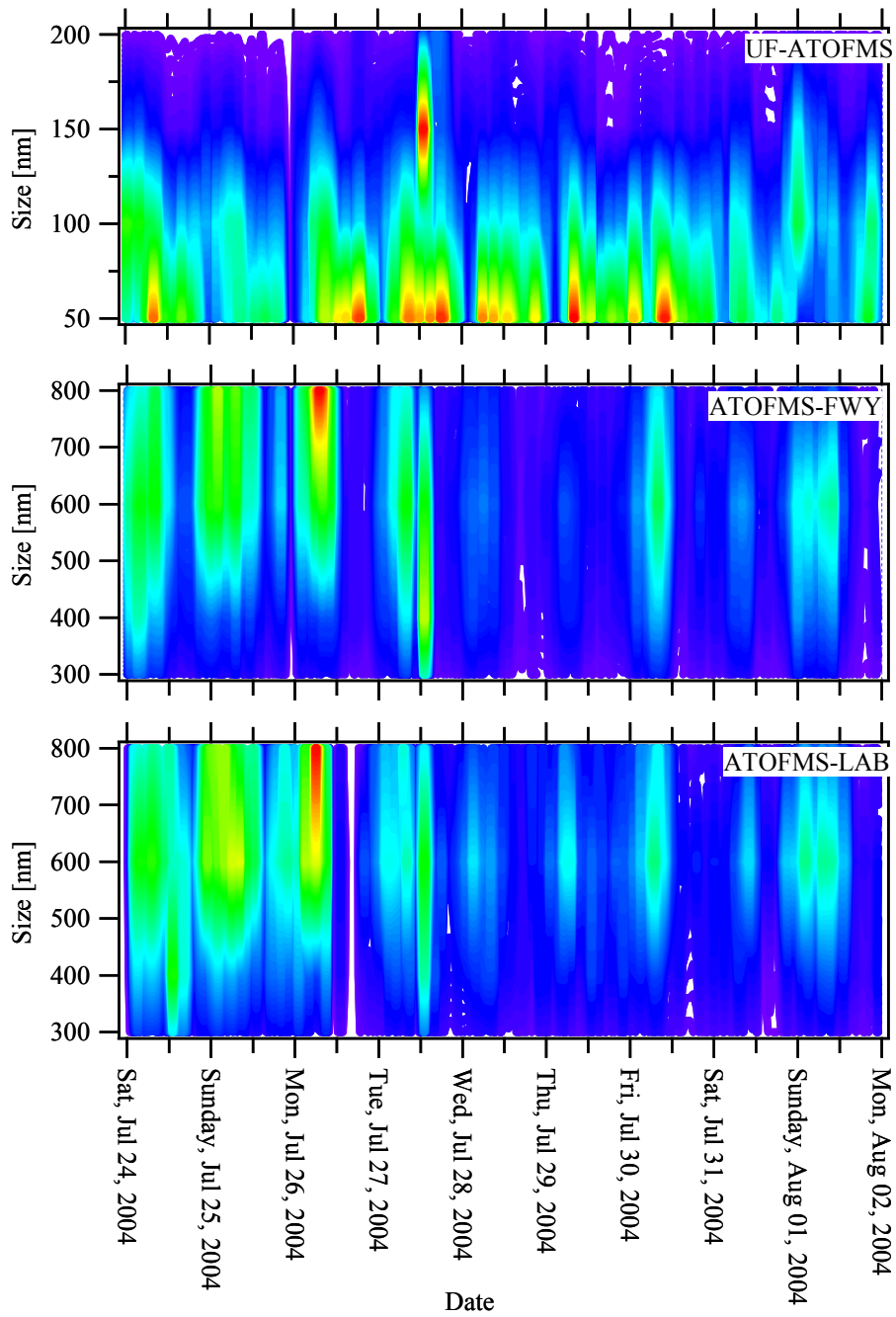


Figure 8.14 Size distributions for total hit particles as measured for the 3 ATOFMS instruments between July 24-31, 2004.

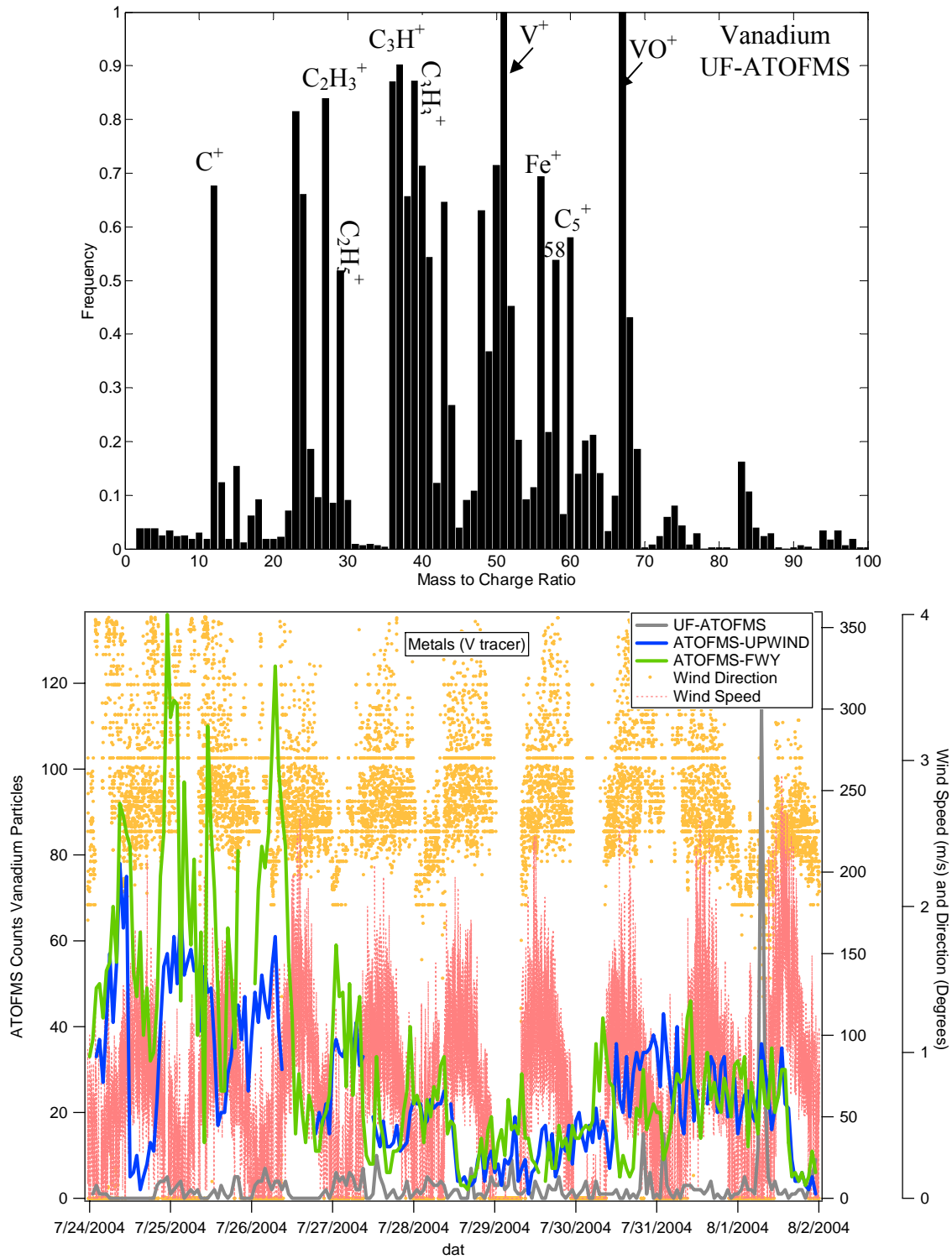


Figure 8.15 Common V-containing particle type detected at both locations and temporal trends for 3 instruments.

effect on the comparison as the ART-2a weight vectors are sensitive to the most intense peaks in the spectra. The particle types deemed as “unique” at both sites were mainly sea salt particles. This is because they had undergone less processing in general at the upwind site than the freeway site since it is closer to the ocean. The spectral modifications due to heterogeneous processing involve the loss of one peak from a relatively complex particle spectrum and the addition of another. Reducing the vigilance factor to 0.7 instead of 0.85 resulted in all particle types at the freeway site, including sea salt, matching the clusters at the upwind site. As would be expected, the rank order (based on the number of particles in each cluster) of the various types and their relative contributions to ambient PM was different at the two sites.

8.4 Data Analysis Approaches Used for Apportionment

8.4.1 ART-2a Analysis

Over the past several months, data analysis efforts aimed at exploring the potential for using source signatures obtained from the dynamometer studies performed as part of this project to distinguish gasoline LDV from diesel HDDV particulate emissions has begun on several fronts. Currently, a number of data analysis techniques beyond ART-2a are being explored in an effort to find the most appropriate ones that will provide accurate source apportionment of ambient particles using the particle class signatures from the dynamometer studies. To date, the ART-2a neural network analysis method has already provided some initial promising results showing that a significant fraction of the HDDV and LDV particle types acquired during dynamometer sampling are indeed representative of those produced near a roadway. The initial results focus on particles sampled with the two ATOFMS instruments sampling near the freeway for the entire experiment (UF-ATOFMS and ATOFMS-1; see Table 8.1), in the 100-1000 nm size range since particles in this size regime denote freshly emitted particles that would have a greater probability of originating from vehicular traffic on the freeway. As a first step, ART-2a clusters were made of all ambient particle types sampled near the freeway. These were then compared to the clusters created from the HDDV and LDV dynamometer particle types. The top 100 clusters from the HDV 2001 and HDV 2003 were combined with 200 clusters from the LDV 2002 study and used for this analysis. More clusters were used from the LDV studies due to the fact particles were sampled from a much higher number of vehicles (covering a wide range of ages and catalyst technologies) and cycles during the LDV studies. In general, the complexity of particles in the LDV exhaust is higher than those particles emitted from HDDV vehicles. The “matching” procedure involves taking the dot product of the ART-2a weight vectors (matrices) of the major particle types. The dot product values range (denoted as a Vigilance Factor or VF) from 0 to 1 with a value of 1 indicating the particle types are identical. For this analysis, a relatively high VF of 0.85 was used. If the ambient particle has a VF of 0.85 or higher, it will be “matched” to that particle source cluster. Each ambient particle is compared one-by-one to the source “seeds”.

Table 8.2 shows that on average, 65-73% of the ambient particles in the 100-1000 nm size range match the most common source seeds created from the dynamometer study particles. As stated, 300 clusters from all vehicles (100 HDV and 200 LDV) were created so only the top particle types were used for this analysis. It should be noted that approximately 15-20 of the

Table 8.2 Percentage of particles matched to dynamometer source seeds using a vigilance factor of 0.85 for all particles in the 100-300 nm (UF-ATOFMS) and 100-1000 nm (ATOFMS-1) size ranges.

Instrument/ Time Period	Matched	Remaining	% Matched VF = 0.85
UF-ATOFMS I	34,604	15,517	69%
ATOFMS-1 I	55,960	20,519	73%
UF-ATOFMS II	38,367	18,531	67%
ATOFMS-1 II	60,319	31,929	65%
UF-ATOFMS III	32,588	15,833	67%
ATOFMS-1 III	42,497	18,472	70%

major types explained 80% of the particles or more during the source tests. However, when grouping tens of thousands of particles from multiple cycles, sizes, and vehicles of many vintages, one can obtain 100-200 particle types for each source. In other words, it takes many clusters (containing relatively few particles) to explain the variability of the remaining 20% of the more unique particle types. Upon examination of the non-matched particle types, it was noted that there is still a significant fraction (~5-10%) of the particles that were not matched because ion peak assignments in their mass spectra were improperly calibrated. This occurs mainly for smaller particles because as the particles become smaller, the complexity of the resulting mass spectra is greatly reduced. This often results in the negative ion spectra only containing a single ion peak (i.e. sulfate). When this occurs, the automated calibration procedure often shifts the position of this peak and assigns it to an incorrect m/z value. We are currently re-calibrating these spectra and re-importing the data and will redo this same analysis. The question is: which particle types make up the remaining ~20% of the unmatched particles? Basically, there is a range of other types including metal dominated particles (not apportioned at this time), highly aged organic carbon, meat cooking, biomass burning particles (which peaked at midnight on weekends and most likely came from local campfires), and a few percent as yet unidentified particle types. It is important to note that these results were obtained from the very first attempt to use dynamometer source clusters and “match” them to ambient data. Before this study was performed, there were questions as to whether any of the ambient particles would match the dynamometer particle types. With this in mind, the numbers are quite encouraging and will most likely improve as we work through the dataset. We will also apply other data analysis algorithms besides ART-2a. Ultimately, we will need to decide whether the apportionment numbers are reasonable. This will be accomplished through a combination of comparing our apportioned results to gas phase, meteorological, and the Kleeman apportionment predictions.

ART-2a “matching” was also performed on the ultrafine size range (50-100 nm) of the UF-ATOFMS. Approx. 90% of the ambient particles matched the source seed particle types. This higher percentage is not surprising since one would expect most of the ultrafine particles to be freshly emitted vehicle exhaust right next to a major freeway. Interestingly, upon examining which particles types are the most populated (i.e. best matched) for the ultrafine mode and comparing them with those source seed clusters matching the accumulation (100-1000 nm) mode, there are obvious differences, suggesting the source apportionment results could be quite different for ultrafine versus fine ambient particles. The distribution of the number of ambient particles in each of the matched clusters for the 300 source seeds can be plotted to examine the differences between ultrafine and fine matching. This is shown in Figure 8.16. Comparing the distribution of the number of particles falling in clusters for the ultrafine mode (upper) with those in the accumulation mode (lower), it is apparent the complexity of types increases (more seed particle types are “matched”) as particle size gets larger and different cluster distributions occur for these two different particle size ranges. This finding suggests it is extremely important to perform source apportionment using source seeds created for the same size range as the ambient data being apportioned. For this reason, the final source apportionment results will be obtained in 3 size modes which will most likely be: 1) 50-100 nm, 2) 100-1000 nm, and 3) 1000-2500 nm. It is reassuring to note that even though some overlap occurs in the particle types produced by HDDV and LDV, it appears one can use size as an extra dimension of information to help separate their relative contributions.

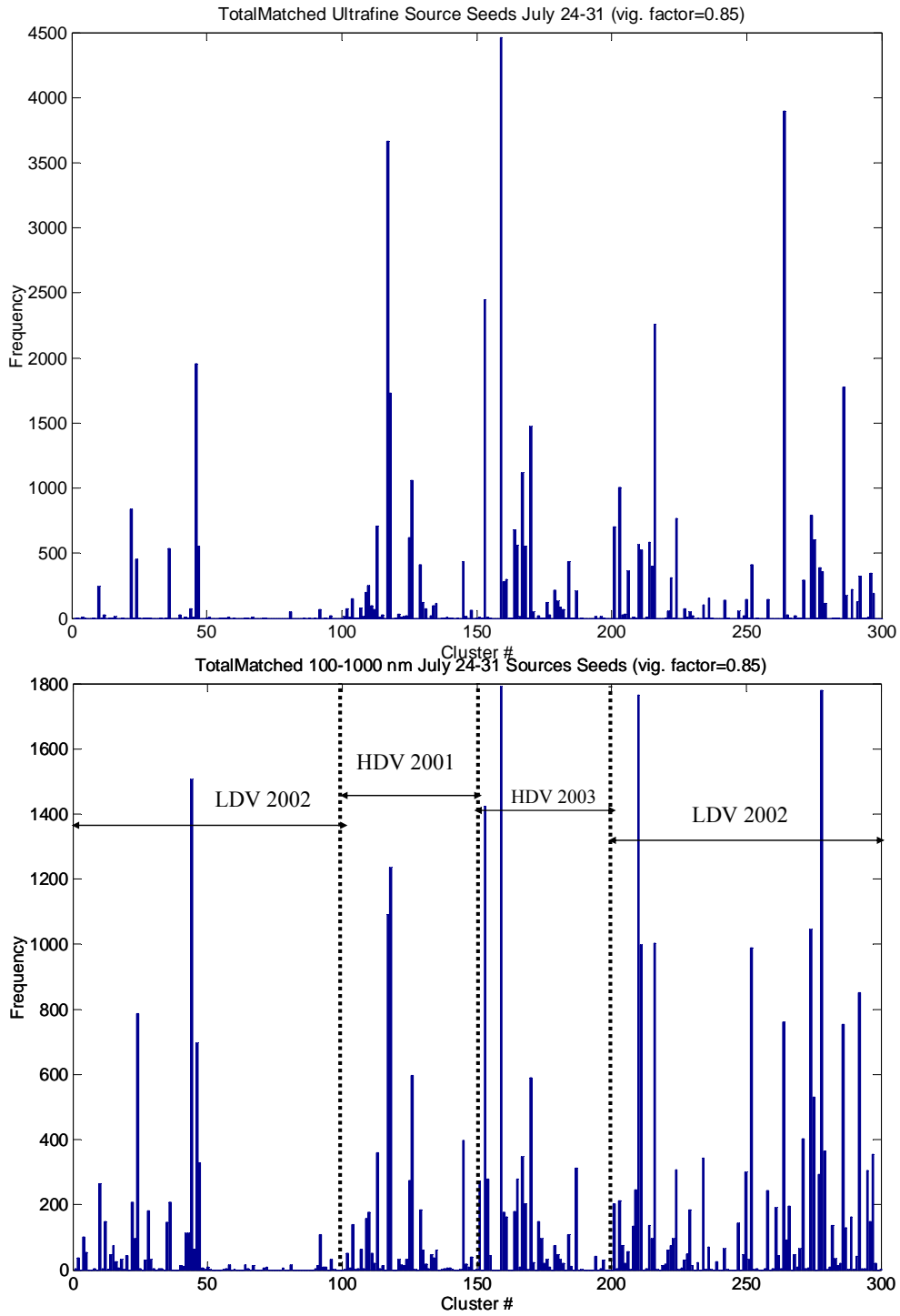


Figure 8.16 Particle population distributions in each of the 300 source clusters used for ambient matching.

8.4.2 Major particle types near roadway

In general, the particle types sampled by the UF and standard inlet (ATOFMS-1) instrument near the freeway were very similar. The ordering of the clusters based on particle populations varied between the two instruments. To further examine the similarities, particles in the 100-1000 nm size range (only up to 300 nm for the UF-ATOFMS) from each instrument were analyzed using ART-2a analysis separately for the last portion of the study. The dot products of the similar particle types in the top 30 clusters from each instrument were compared and were 0.85 and higher. The different numbers of particles in the various classes support the fact that there are strong size-composition relationships. We have briefly examined the sub-100 nm sizes and super-micrometer sizes and are finding there are a significant number of particle types that are distinct from those in the accumulation mode (100-1000 nm) particles. This is further discussed in the HDDV analysis section of the report. These differences are expected since different formations mechanisms produce particles in each of these 3 distinct size modes. The weight matrices for two of the more common particle types detected during the freeway study are shown in Figure 8.17. Using ART-2a, these particle types match (with a vigilance factor of 0.85 or greater) those discussed in the LDV and HDDV sections of this final report. In general, the highest ranked particle types (based on particle populations in each cluster) produced during dynamometer testing matched the top types detected in ambient data. This further indicates the dynamometer produced chemically representative particles during vehicle testing.

We have determined that the ATOFMS measurements (both size and composition) were consistent between instruments, size ranges, as well as with other gas phase (CO and NO_x) and particle phase (aethalometer, SMPS, APS) instruments. The goal of ATOFMS studies is to go beyond number concentration of basic compounds and obtain size resolved composition changes of source specific particle types over time to develop a better understanding of the variability of source contributions on shorter timescales. As discussed earlier in this report, the ATOFMS commonly detects elemental carbon (EC), organic carbon (OC), and mixed elemental carbon/organic carbon (EC/OC) particle types from vehicle emissions. Figure 8.18 shows a plot of the temporal evolution of ultrafine EC particles sampled near the freeway versus the aethalometer (absorption) data. One would expect the aethalometer data to track the EC data given the strongly absorbing nature of soot particles, and such a correlation is in fact observed. The same temporal correlations are not observed when plotting the OC dominated particle types versus the aethalometer data. We are now working to relate the different EC and OC signatures observed during the freeway study to specific vehicular sources. As mentioned previously, both LDV and HDDV emit EC; however, they are emitted in different size fractions, show different fragmentation patterns, and contain different relative amounts of other species such as additives (calcium, phosphate) that should allow for their differentiation.

8.5 Source apportionment progress

As described, ART-2a analysis was used to “match” source seeds to ambient data for the duration of the study. Figure 8.19 shows the apportionment for the first part of the study averaged over several days. Using a time resolution 30-60 minutes, the percentage of the number of ambient particles matched to HDDV varied from 2% to 28%, with those matching

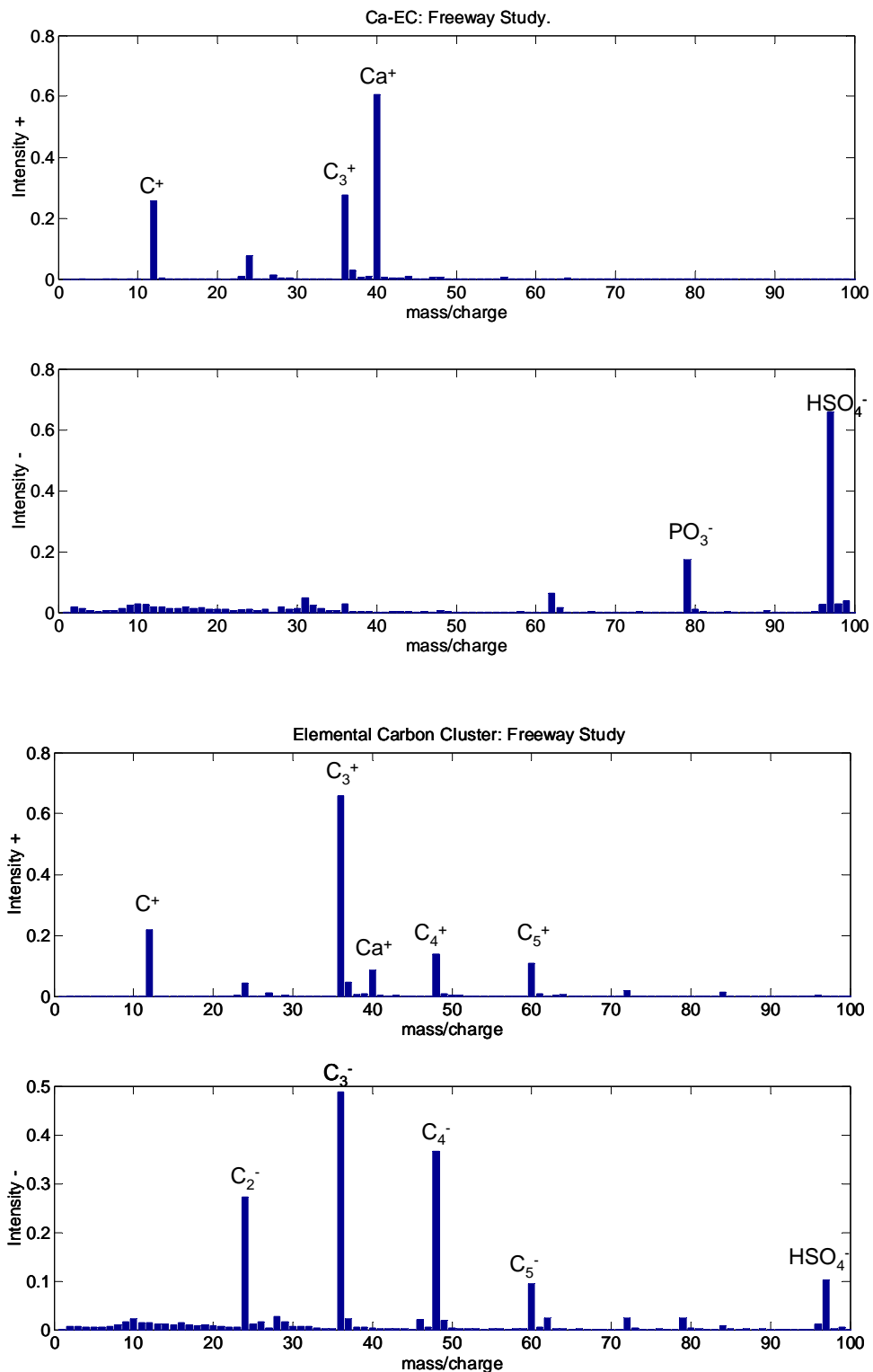


Figure 8.17 Weight matrices of two most common types of particles observed in the 50-300 nm size range during the freeway study. These types are very similar to the major types sampled from vehicles during previous HDDV and LDV dynamometer studies.

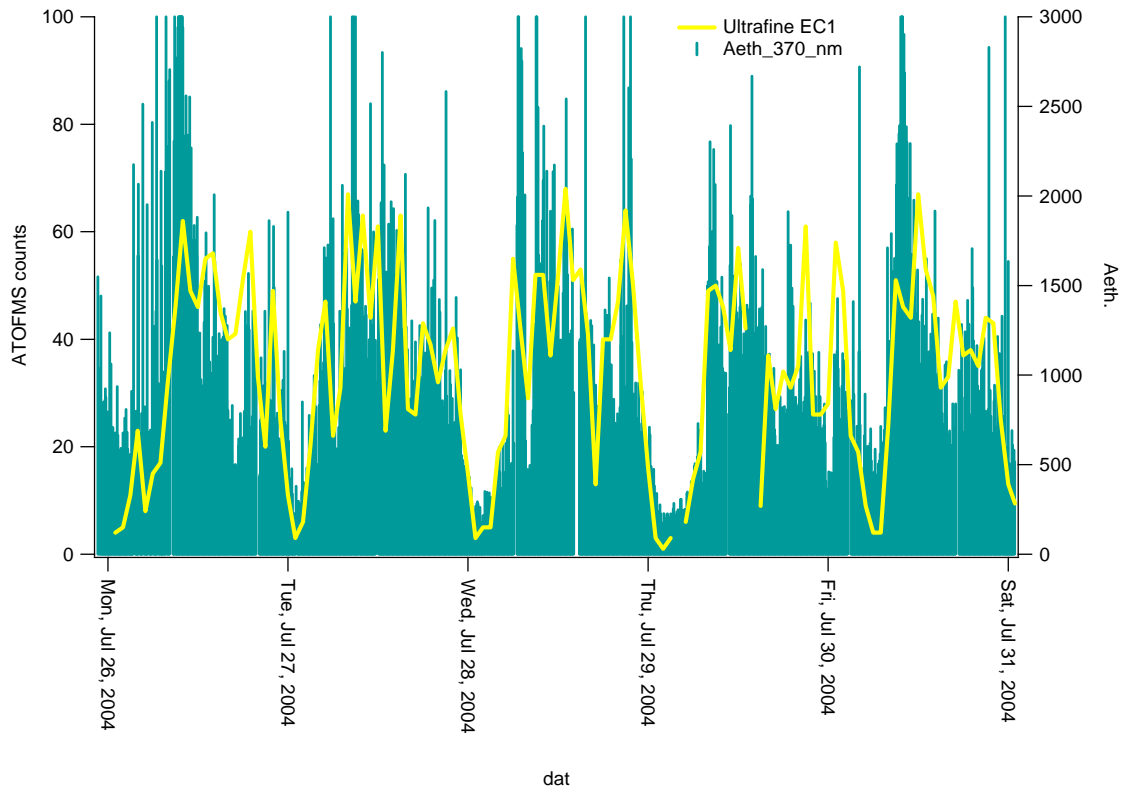


Figure 8.18 Ultrafine EC particle counts detected by ATOFMS compared to aethalometer data.

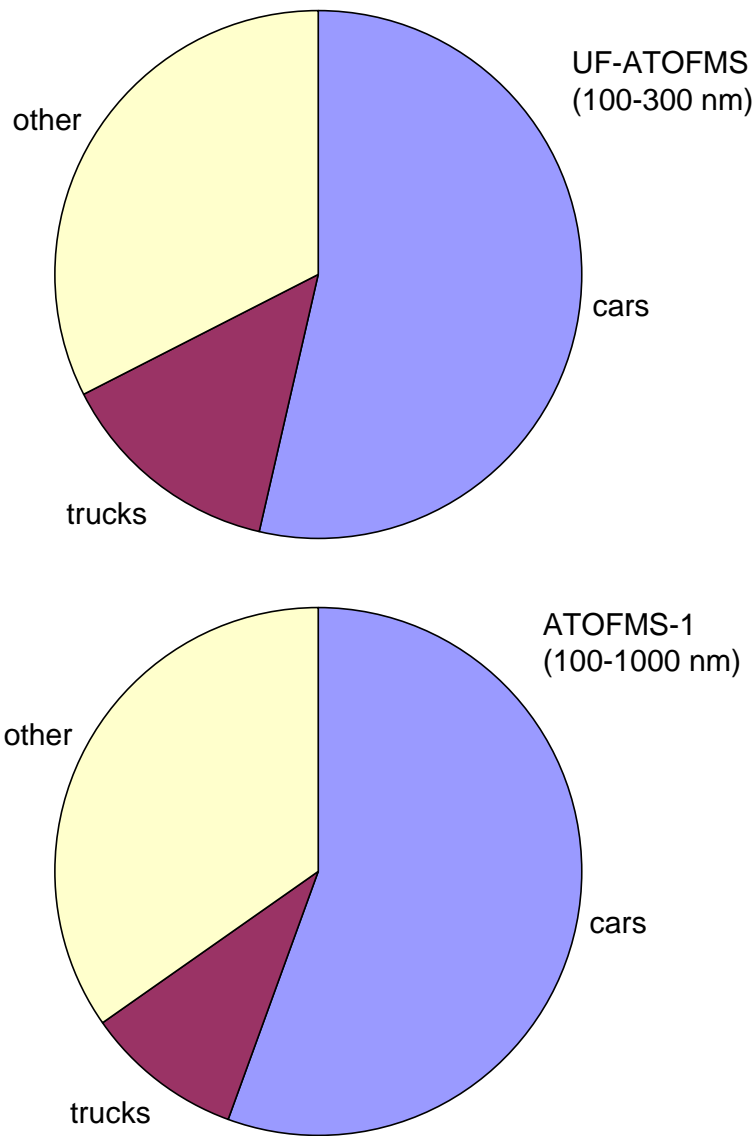


Figure 8.19 Source apportionment of LDV (cars) vs. HDDV (trucks) for one time period during the study for particles in the 100-1000 nm size range.

LDV varying between 42% and 68% in the accumulation mode. In the ultrafine (50-100 nm) size range, particles attributed to HDDV emissions range from 4% to 48%. The percentage changes depending on the time of day, traffic conditions, meteorological conditions, and a number of other factors. It is expected that LDV will make up the majority of particles in this particular freeway environment since LDV represent on average approximately 99% of the fleet on the Interstate 5 freeway. However, by reviewing video footage taken, we plan to focus on periods with greater HDDV influence to see if the matching percentages show corresponding shifts towards HDDV emissions. Another option is to use known shifts in traffic patterns where for example, one expects the amount of HDDV traffic to be reduced on weekends. Figure 8.20 shows the difference in apportionment results for ultrafine particles sampled during weekend versus weekday time periods. It shows hourly temporal bins of unscaled ATOFMS data. It is important to recognize there were still medium duty trucks and other trucks traveling on weekends. In addition, PM emissions from LDVs go down on weekends. The time periods where HDDV represent the smallest fraction of the emissions are the early morning hours on weekends, as indicated by the arrows in the above graphs. Figure 8.20a shows 2 days on the weekend where the HDDV contributions in the early morning hours are low, but pick up around noon on both days. These patterns are significantly different on the weekdays where trucks make substantial contributions during these late night-early morning periods as well.

One should note that all results presented here are based on one relatively simplistic univariate data analysis approach using ART-2a. However, even with this simplistic approach, the results are quite promising and it is obvious how single particle data can be used to measure source contributions to ambient data. Ultimately, correlations will be established between multiple particle types, gas phase data (when available), aethalometer data, and meteorological data. In addition, other data analysis techniques, including tree-regression, hierarchical and nearest-neighbor approaches are also being implemented to evaluate the variations in source apportionment depending on the analysis method chosen. Some preliminary results with test data (from the dynamometer experiments) have resulted in signature matching with 99.7% accuracy using a nearest neighbor data analysis technique. Since these data were matched to a prepared unknown set consisting of fresh LDV and HDDV dynamometer emissions, they are only partly representative of the freeway-side sampled particles. Particle aging, coating, agglomeration, and water uptake will play important roles in affecting changes in the particle composition from the freeway experiment. These changes will, undoubtedly, make matching to source signatures more challenging in particular at locations further from the source. However, there are unique features to the sources that should make matching consistent, whether the particles have aged or not. One of the most important factors is that HDDV particles tend to have calcium and phosphate associated with them in an elemental carbon/calcium type particle (EC-Ca). LDV particle have much less calcium and/or phosphate associated with them, but do produce elemental carbon particles in the UF size mode. These kinds of distinctions can be used to “pre-filter” data prior to matching to better improve the accuracy of identifying LDV vs. HDDV. These issues are addressed in the chapter comparing HDDV and LDV signatures to the Caldecott tunnel 2000 field campaign. Also, Figure 3.7 in the ultrafine/fine HDDV study displays the top three HDDV classes compared to three classes observed with the UF-ATOFMS sampling alongside the freeway. This figure further confirms that the dynamometer classes are indeed detected in ambient air, and can be readily distinguished using the current ART-2a technique.

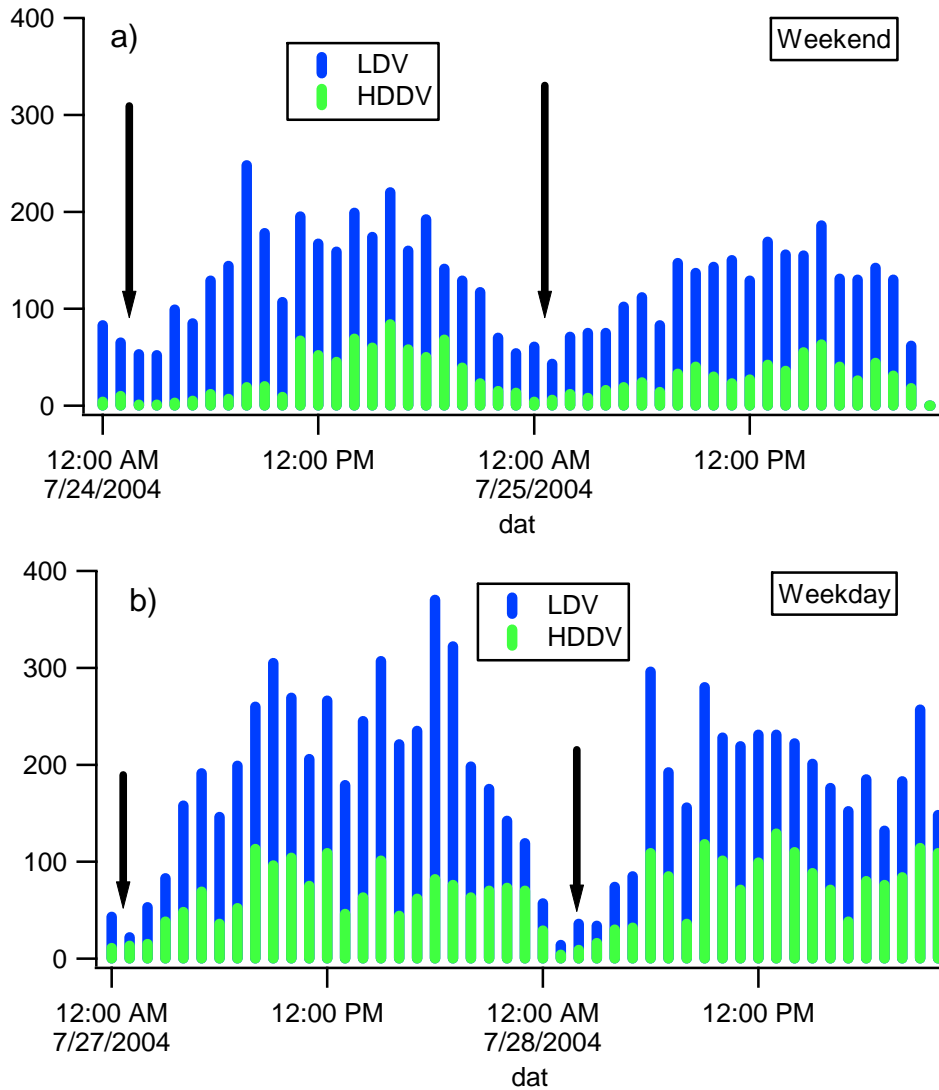


Figure 8.20 Apportionment of ultrafine particles during 2 days on the weekend (top) and weekday (bottom). The arrows indicate time periods when the proportion of LDV to HDDV show the greatest differences (i.e. late night-early morning hours).

8.6 Conclusions and future work

A tremendous amount has already been learned from the analysis of this dataset. Specifically, we have been able to identify the largest fraction of particles in the ambient air during the freeway study are indeed representative of those sampled from HDDV and LDV vehicles on a dynamometer. To date, we have shown there are strong correlations between the ATOFMS instruments with one another as well as with peripheral gas and particle phase instruments. We are now in position to go into more detailed analysis on certain time periods and use new algorithms that may ultimately replace or at the very least supplement ART-2a. ART-2a has limitations but it has been able to show us for this study the signatures for HDDV and LDV do show distinctions, especially when taking into account size, which should allow for their differentiation in ambient data. The next steps in this project include:

- Use traffic count data coupled with meteorology to understand variations in trends of different particle types and sources.
- Study the correlations between all instruments and apply a multivariate approach to further separate contributions from particle types with chemically similar signatures.
- Establish size-resolved percentages of HDDV and LDV as well as other ambient particles with one-hour temporal resolution.
- Establish single particle source libraries for various sources (i.e. dust, sea salt, meat cooking, LDV, HDDV, biomass) that can be apportioned in real-time as particles are acquired in field.
- Compare the ATOFMS source percentage predictions with those of Prof. Mike Kleeman's group based on organic tracer filter based methods.
- Compare size-resolved amounts of ammonium, nitrate, sulfate upwind and downwind of the freeway (M. Jacobson, Stanford and J. Seinfeld, Caltech) with model predictions to develop a better understanding of particle evolution processes in the atmosphere.

8.7 Acknowledgements

The authors would like to thank Dan Cayan and Alex Revchuk of the Scripps Institution of Oceanography (SIO) at UCSD for setting up the micro-meteorological stations and providing the data for this study.

Section V

Future Data Analysis

Techniques

Identifying Particle Source in Ambient Air Using New Data Analysis Techniques

9.1 Introduction

This chapter describes our current methods for extracting information from single particle spectra and future directions for data analysis that will allow source apportionment of ambient particles. As shown in Chapters 2-4, a combustion source of particulate matter (PM) can produce many different particle types; moreover, aerosol time-of-flight mass spectrometry (ATOFMS) can map several observed spectra [Wenzel and Prather, 2004]—this is called a “one-to-many” mapping. Due to shot-to-shot variability of the laser used to desorb/ionize species from each particles, two particles that are almost identical in size and composition can yield different ion intensities. The laser can desorb a particle differently depending on the particle chemical composition but mostly due to the particle location within the inhomogeneities the laser beam energy profile. In addition, compounds have different levels of stability, so that some ions will be produced more easily than others; moreover, ATOFMS has high and low sensitivities to particular species [Gross *et al.*, 2000], so that the observed intensity of one species in the ATOFMS spectrum must be calibrated to the concentration of that species in the particle using lab standards. Despite these variations, the trained human eye can readily identify and estimate the sources of most ambient particle spectra acquired by ATOFMS. Thereby, the one-to-many mapping can be converted back from the different types of resulting spectra to the original single type of particle. The long term goal of the proposed machine learning methods is to create tools that catch up with, and eventually improve over, the human recognition rates.

Underlying the automatic identification approach, there is the assumption is that the one-to-many mapping, from particle source to true particle type to particle spectrum, creates for each source a limited variety of distributions in the spectral space. This assumption is supported empirically [Steele *et al.*, 2003]. Each source gives off several types of particle, and each type creates distributions in the spectral space that can be distinguished. Particle distributions do not have to be condensed on a single spectrum, but we expect that given the high dimensionality of the spectral space they will overlap little with distributions issued from another type of particle. Any overlap in the distributions of two sources will result from the existence of similar particle types in these sources. For example, the particles emitted from light duty vehicles (LDV) and heavy duty vehicles (HDV) undergo similar formation mechanisms and produce some overlap [Sodeman *et al.*, 2005]. Figure 9.1 is a ternary plot that illustrates the variety that can be obtained from particles of the same source. Ternary plots represent the relative composition of three specified peaks of the spectrum (see Appendix A2 for a full explanation of how ternary plots are made and read). In Figure 9.1, 17,000 fine particles ($100 \text{ nm} < D_a < 1000 \text{ nm}$) measured as LDV exhaust have been projected in the plane ($[12^+] + [24^+] + [36^+] = 1$). The figure is bimodal, with some particles exhibiting a strong m/z 24 peak and others a mix of m/z 36 and 12. From the spectral information alone, it is difficult to determine whether similar particles have been split by the ATOFMS measurement into two populations, or whether the exhaust may contains two

different types, but in either case, because the clusters only occupy a small portion of the space, they should be identified as LDV clusters. In summary, Figure 9.1 illustrates the existence of sub-distributions for the same source of particle.

Given the variety of spectral distributions issued from each single source, recognition algorithms will run faster if they can use a catalogue of particle clusters or clustering rules.

The research program that is being used in the Prather group consists of three steps:

1. identify and catalog, offline, all possible microclusters of particle spectra;
2. regroup and label, offline, these microclusters under source labels; and
3. create a fast recognizer that matches in real-time an incoming particle with one of the catalogued fine clusters, and links it with the corresponding source label.

Currently, there is no real-time apportionment technique. Source identification is done off-line and separately for each study. Using the ART-2a algorithm [*Carpenter et al.*, 1991], [*Song et al.*, 1999], particles are classified into several clusters, and the clusters of substantial size are then labeled by hand. When the study is large, only a fraction of the particles (about 20,000) is used by ART-2a to determine the initial “seed” clusters, and the remainder of the particles are compared to these. There are several drawbacks to this approach. ART-2a attaches each particle to the closest already defined cluster, unless their distance is too large, in which case the particle is used as a seed for a new cluster. The original center of the clusters is therefore arbitrary, depending on the order in which particles are classified. The particle list is reviewed several times, and with each iteration, cluster centers slowly move towards the recently attached particles, but by the same token clusters move slowly towards regions of high density. ART-2a therefore does not necessarily converge in reasonable time scales, or if it does, does not always converge to the same classification [*Murphy et al.*, 2003].

Besides the problems inherent to ART-2a per se, the approach of generating ad hoc clusters and labeling them by hand for each new study means that nothing is currently retained for automatic classification from one study to the next. Several other algorithms have also been used to determine clusters in single studies: Hierarchical Clustering and Principal Component Analysis [*Xhoffer et al.*, 1992], Fuzzy Clustering [*Hinz et al.*, 1999]. The strength of these approaches lies in their robustness against changes in the measuring process and settings. But such single-study classification leaves many of the infrequently detected particles without a label, because these particles do not occur frequently enough to generate a level of density in the spectral space that will create a cluster. In contrast, the proposed method rests on the assumption that spectra obtained from different instruments or from the same instrument under different conditions are comparable (yet this assumption is mitigated because the proposed method handles well the one-to-many splitting of true particle types to observed spectra). By pooling studies, the proposed method aggregates massive numbers of particle spectra, allowing both very narrow clustering criteria and low rates of unclustered and hence unclassified particles.

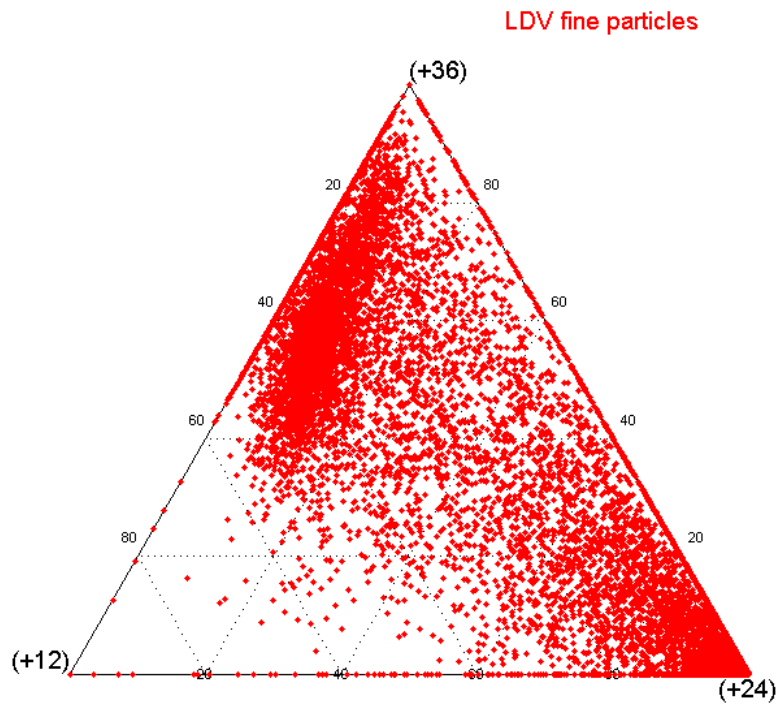


Figure 9.1 LDV particles projected in the plane of their spectral peak areas on peaks 12, 24 and 36. (See appendix B about ternary plots). The distribution is bimodal.

9.2 Details of Future Data Analysis Methods Beyond ART-2a

9.2.1 Clustering as Narrowly as Possible

The first step of the future classification method is to identify all the narrow clusters, or “microclusters” of particles in a large corpus of data (ideally, all the group studies). There are two main reasons why we want the first step of classification to define very narrow clusters. First, clusters from different sources can coincide. For example, we expect some particular clusters to derive indiscriminately from LDVs and HDVs. By separating different clusters belonging to the same source, we retain the ability to track the unambiguous clusters separately from their ambiguous siblings. Secondly, most clustering processes produce convex clusters (“blocks”, in which all spectra interpolated between two points of the cluster also belong to that cluster), or at least produce better results when forced to produce convex, rather than arbitrarily shaped clusters. The narrow clustering approach can make use of these algorithms and still capture bean-shaped distributions by dividing them into adjacent convex clusters.

Preliminary studies concur with the current literature to use pre-processing steps for the spectra. First, we considered the square root of peak areas rather than the peak area itself or the peak height. Murphy & al. (2003) prefer to use a combination of peak area and its logarithm to balance the influence of larger and smaller peaks. Taking the square root has the same effect. In fact, if peaks were of similar shape (taller peaks get proportionally wider), the square root of the area would be homogeneous to the peak height; but it is a more robust measure. This method of preprocessing has been tested by comparing the efficiency of several powers of pre-processing scaling (from 0.3 to 1.0) on classification of known source particles. Afterwards, the square roots of the spectra are normalized by their Euclidian norm (“ L_2 ”), to obtain relative values rather than absolute values.

Clustering can be done by several algorithms including ART-2a [Carpenter *et al.*, 1991], which we use currently, neural network methods such as Kohonen Maps [Kohonen, 1995], or other unsupervised learning techniques like K-Means or hierarchical clustering (for a review of many unsupervised clustering algorithms, see [Duda *et al.*, 1997]). Narrow clustering comes from specifying stringent requirements, and as a result, when the clustering is very fine, different algorithms tend to deliver the same results. A side effect of very narrow clustering is that fewer particles are clustered (i.e. many end up alone in a cluster), but this effect is compensated by operating the algorithm on large numbers of particles, because in the sparse regions of the spectrum the limiting factor to clustering is particle distance and therefore cluster size increases proportionally to the total number of particles (In the denser regions of the spectrum clustering is limited by competition with other clusters). The trade-off between total particle number and clustering narrowness has to be explored empirically, and depends on the distribution of distances between particles and on the particular clustering algorithm used.

Because of computational complexity, the clustering of existing data must be done off-line. Clustering N particles generally takes a multiple of N^3 operations, so clustering directly millions of particles is computationally intractable; however, it is possible to break down the corpus by size, and into overlapping spectral “sectors”. Even though the primary input for clustering is the spectrum, it makes sense to separate particles into broad categories of size and make separate analyses for each size, because particles above one micron size are more likely to be agglomerates as well as produced by different sources. After separating by size, for example,

one can consider dividing the spectral space; for example three intervals for the ratio of elemental carbon peak 12 to peak 36: less than one, more than one, and between 0.5 and 2; these sectors overlap to avoid artificially dividing legitimate clusters that would ride astride a boundary. Each sector will have about half the particles in the corpus (allowing for a 1/8 runtime), and every microcluster will be well within one of these sectors. By multiplying such partitions, the computational difficulty can be overcome offline. It is all the more important to ensure a fast runtime as the optimal solution will depend on parameters such that have to be optimized by multiplying runs.

9.2.2 Regrouping and Labeling Microclusters

The second step will involve labeling the identified microclusters. The three sources of labels are: human pattern recognition, automatic labeling by similarity with controlled, one-source studies, and analysis of correlations between cluster occurrences in ambient studies.

Human pattern recognition relies on good visual representations. Figure 9.2 shows three slightly different representations of a cluster: the mean spectrum, augmented with standard deviation, the median spectrum, augmented with 1st and 3rd quartiles, and the digital color stack. All three give an idea not only of the average particle in the cluster (the centroid) but also of the dispersion around it. Ternary plots such as the one in Figure 9.1 can also be of some use to zoom in on particular peak area ratios.

Humans can focus on less intense but informative markers, to which automatic techniques may give less weight. For example, particles with high sodium are much more likely to be sea salt if they also have peaks at m/z 81 and m/z 83 (Na₂Cl peaks). Figure 9.2 shows a sea salt cluster, the 81 and 83 peaks are much lower in intensity than many other peaks. Humans are also good at adapting their judgment according to context; so for example if the negative spectrum of a particle shows a lot of nitrates (peaks m/z -46 and m/z -62), then it is possible for sea salt not to have the Na₂Cl markers, because nitrate will have displaced the chloride (Gard, 1998). In short, the human mind is much more apt to use reasoning and nonlinear criteria. However, the downside of human classification is speed. Therefore, human classification is acceptable for small numbers of spectra, up to a very few hundred, for example by looking at all the centroids of clusters found automatically, but difficult for a whole study with thousands to millions of particles.

Automatic labeling compares the fine clusters to particles from a known source, obtained from controlled studies (e.g. dynamometer studies for vehicles). By assuming that all the microclusters observed belong to one or another of the sampled sources, we can say that these clusters implement a Bayesian classifier and, therefore, assign them to the maximum likelihood type (the most frequent single source of the known particles). A Bayesian classifier partitions the space in which new exemplars may fall according to exemplars already known, in such a way that the observed classification pattern (the type of the known exemplars) is the most likely one. This type of labeling depends strongly on the variety and the quality of the sources obtained, because clusters without a close match will nonetheless be attributed a label. For example, a cluster made of five sources in almost equal shares will be assigned to the most frequent source even though this source represents a 20% minority. One way to soften this weakness is not to label clusters which attract particles of various sources, or to allow a “fuzzy classification”, in which some microclusters (and consequently, the particles that produce them) belong jointly to

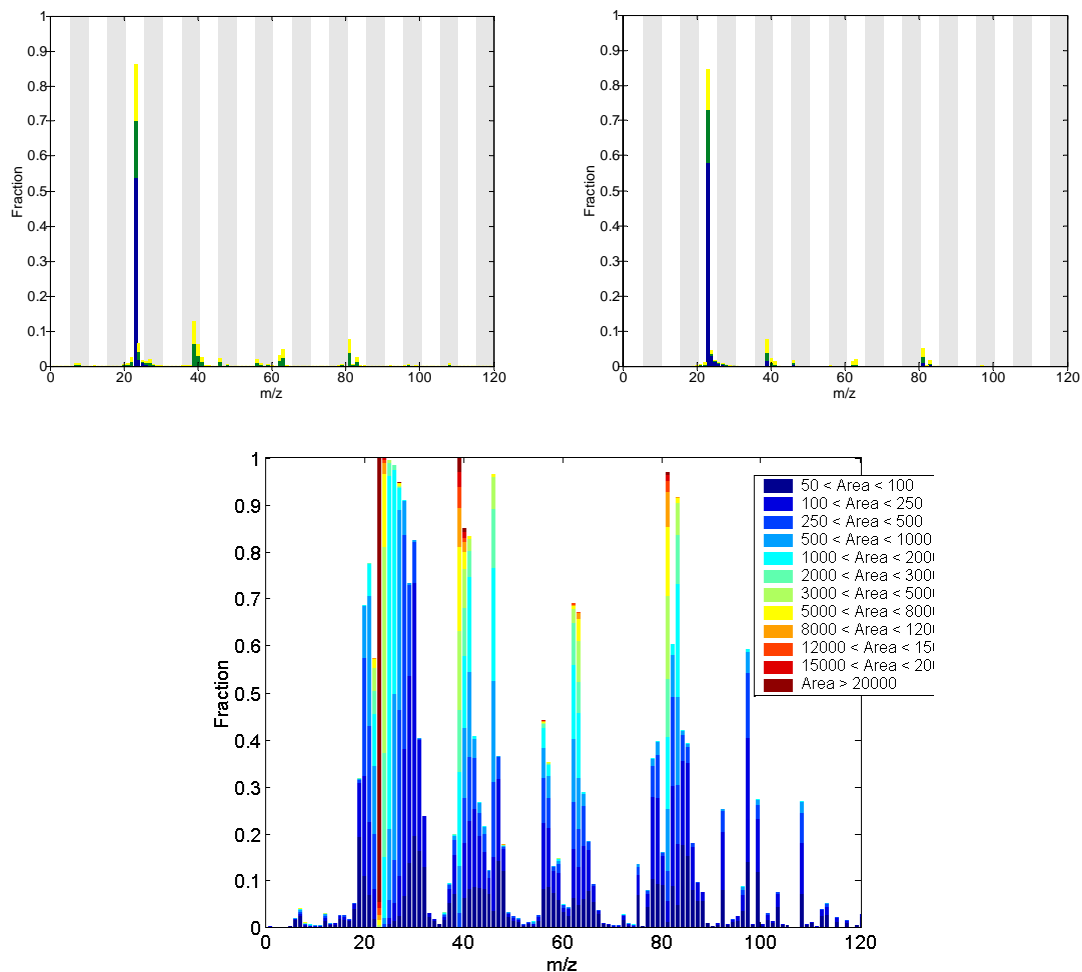


Figure 9.2 Three representations of the same cluster. Fig. 9.2.a. (top left) shows the mean of the relative areas of peaks. Each peak is shown as a dark bar. Standard deviation is shown by a yellow bar extending the peak, and by a color change (blue to green) for the part of the bar stretching one standard deviation downwards of the mean. Fig 9.2.b (top right) shows the median of relative peak areas, indicating first quartile, median and third quartile with the blue/green/yellow color scheme. Fig. 9.2.c (bottom) shows for each peak the proportion of particles in the cluster that have areas larger than a given color-coded threshold. Large peak areas are in warm colors, so that a high reddish bar indicates that most particles in the cluster have a large area for this particular peak.

several sources. This may be the case for some of the combustion particle clusters, in order to keep the closely related LDV and HDV sources separate. Another case in which a cluster source assignment is dubious is when the cluster attracts only far particles (with a distance greater than twice the median distance between particles of this cluster) that have nowhere else to fall. In this case, it may be better to refuse labeling the cluster at all, since it likely does not belong to any of the sources used in the automatic identification.

Analysis of correlations between cluster occurrences in ambient studies is based on the assumption that particles produced together from a particular source tend to remain near each other in the same air mass. When one type from a particular source is sampled, other types of the same source are likely to be sampled as well. Therefore, the temporal distribution of one cluster may be useful in the classification of other clusters with similar temporal profile. The time course of a cluster is obtained by computing its proportion in rolling window of fixed width (number of particles) or fixed time interval. The correlation between their time courses can be used to associate different but co-occurring clusters.

9.2.3 Using the Catalogue for Fast Recognition

The microcluster list can be used for fast recognition by a nearest neighbor match. The principle of the match is that an unknown particle is compared to all clusters by computing its distance to the cluster center, and the closest cluster indicates the category to which the particle belongs. In practice, the cluster list can be structured to reduce the comparison to a series of three-choice decisions, so that the computing time increases only logarithmically with the number of clusters. An incoming particle is compared to the most distant types of clusters, and depending on the result it belongs to one or two of three overlapping sub-lists of clusters, and the process can be repeated within each sub-list, until there is only one possible cluster. With this method, at most a few tens of between-spectral distances have to be computed, and the particle can be classified as fast as they are currently acquired (up to 20 particles per second).

9.3 Two Examples of Automatic Labeling Using Source Studies Method

9.3.1 Direct Apportionment by Nearest Neighbor

In preliminary studies, we have looked at direct automatic apportionment by the K-nearest neighbor method. So, without taking the microclustering step, we used source study examples to directly label particles obtained during an ambient study at the Fresno Supersite during CRPAQS between Jan 19, 2001 and Feb 3, 2001. Source particles and ambient particles to be labeled from a given source were limited to the 0.1 micron – 1 micron aerodynamic diameter size range. The distance between spectra was obtained by Euclidian distance in the space of normalized vectors of the square roots of peak areas. Using this distance, each Fresno particle was connected to known neighbors— particles from the source studies which had the most similar spectra—and if the closest ten neighbors belonged to the same source, the Fresno particle was assumed to be from that source too. The possible sources were HDV, LDV, biomass, coal, sea salt and dust. HDV and LDV sources were obtained by dynamometer studies. Biomass, coal, sea salt and dust sources were obtained by careful selection from ambient studies

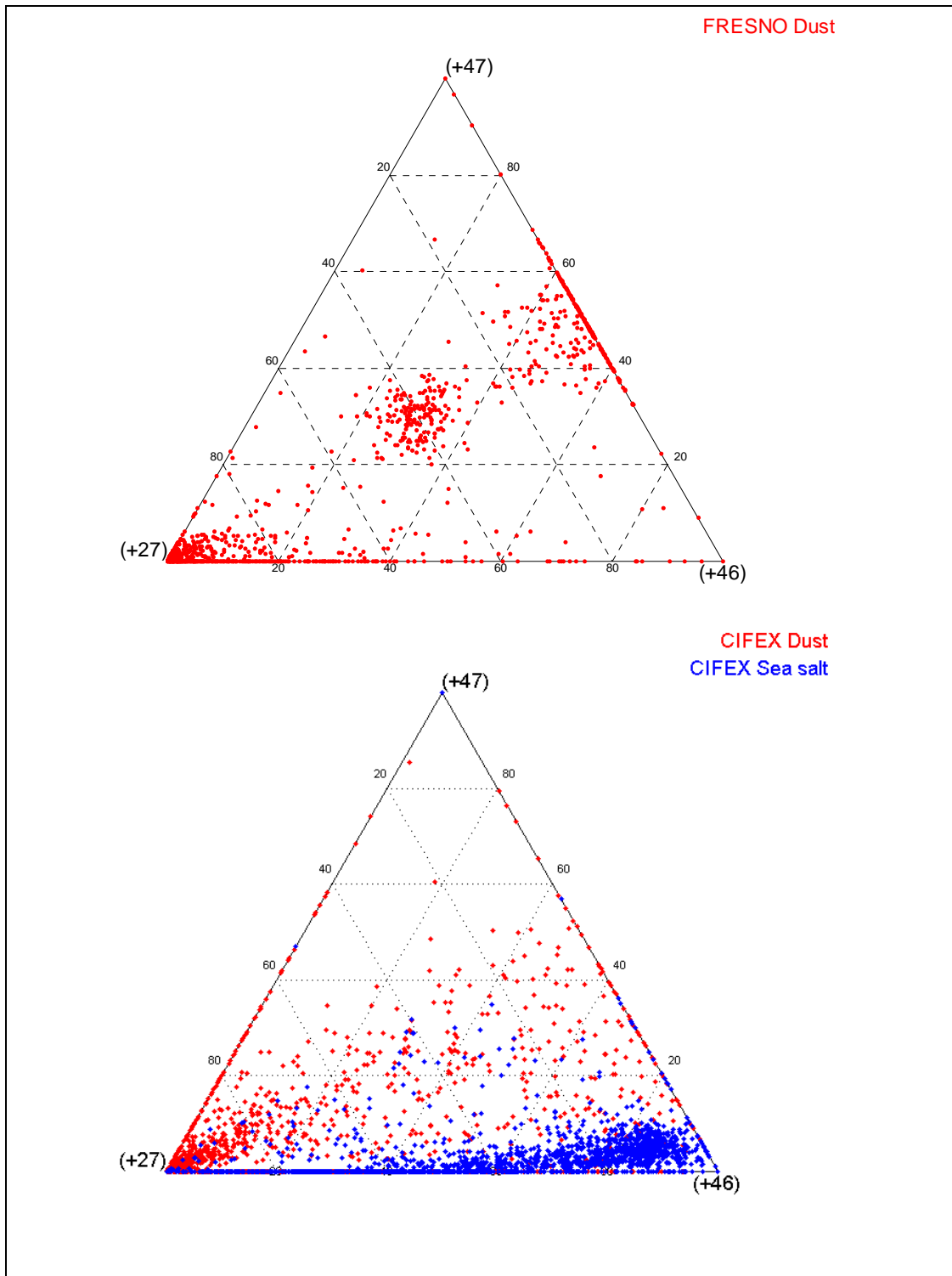


Figure 9.3 (Top) Fresno particles labeled “Dust” by a nearest neighbor method. Below, sea salt and dust particles from CIFEX, selected by human criteria. A peak at 27 in dust is due to aluminum.

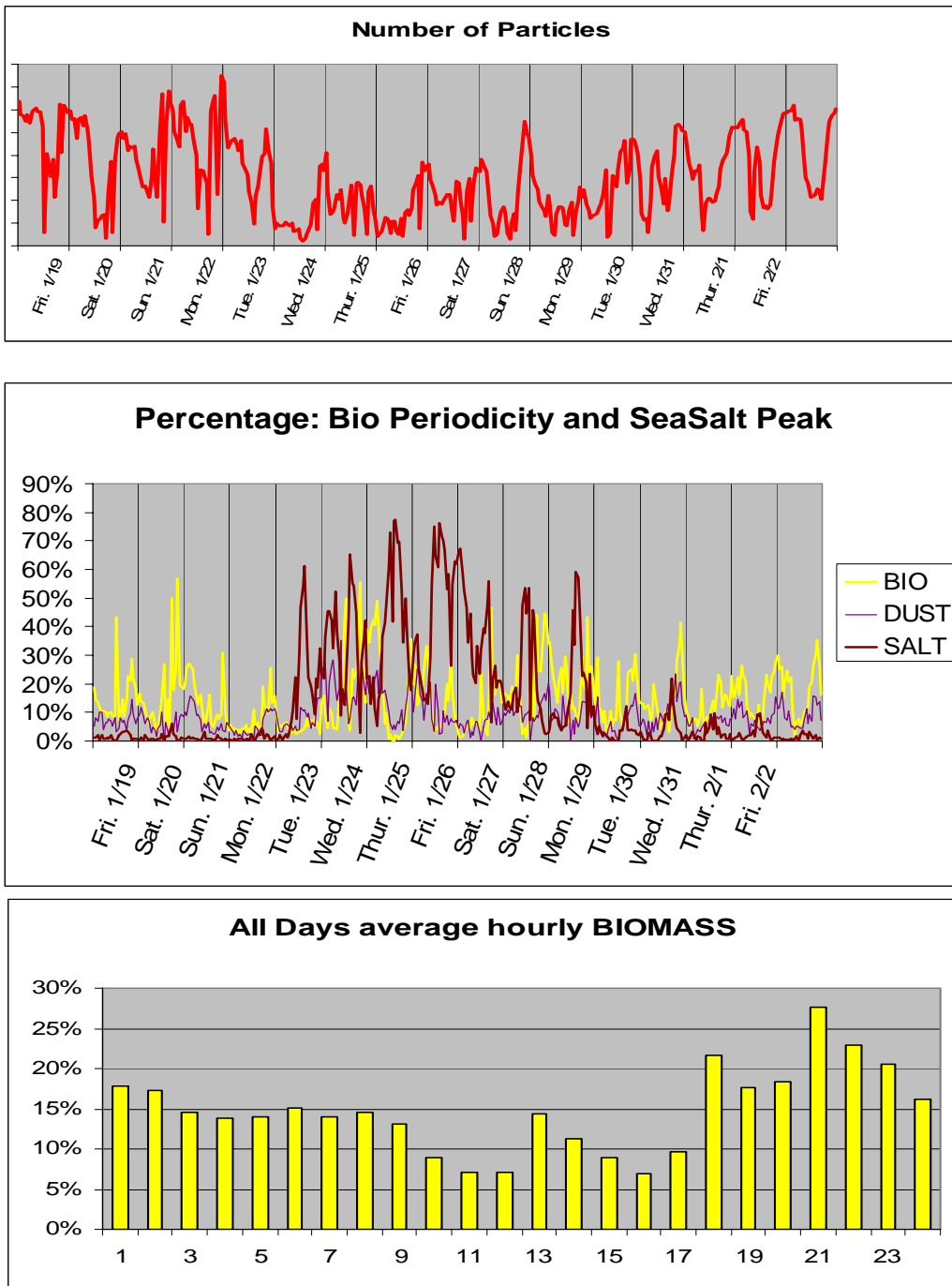


Figure 9.4 Timeline for Fresno Nearest-Neighbor Apportionment: 9.4A shows decrease in particle counts from Wed 1/24 to Mon 1/29. This coincides with crustal element frequently present in dust particles. Peak 46 can be either Na_2 or an isotope of Ti. In salt, 46 tends to be Na_2 , but in dust it is 6% of the Ti content with a peak 47 7% of the Ti content. Fresno particles labeled “dust” follow the same 46/47 ratio as CIFEX dust does.

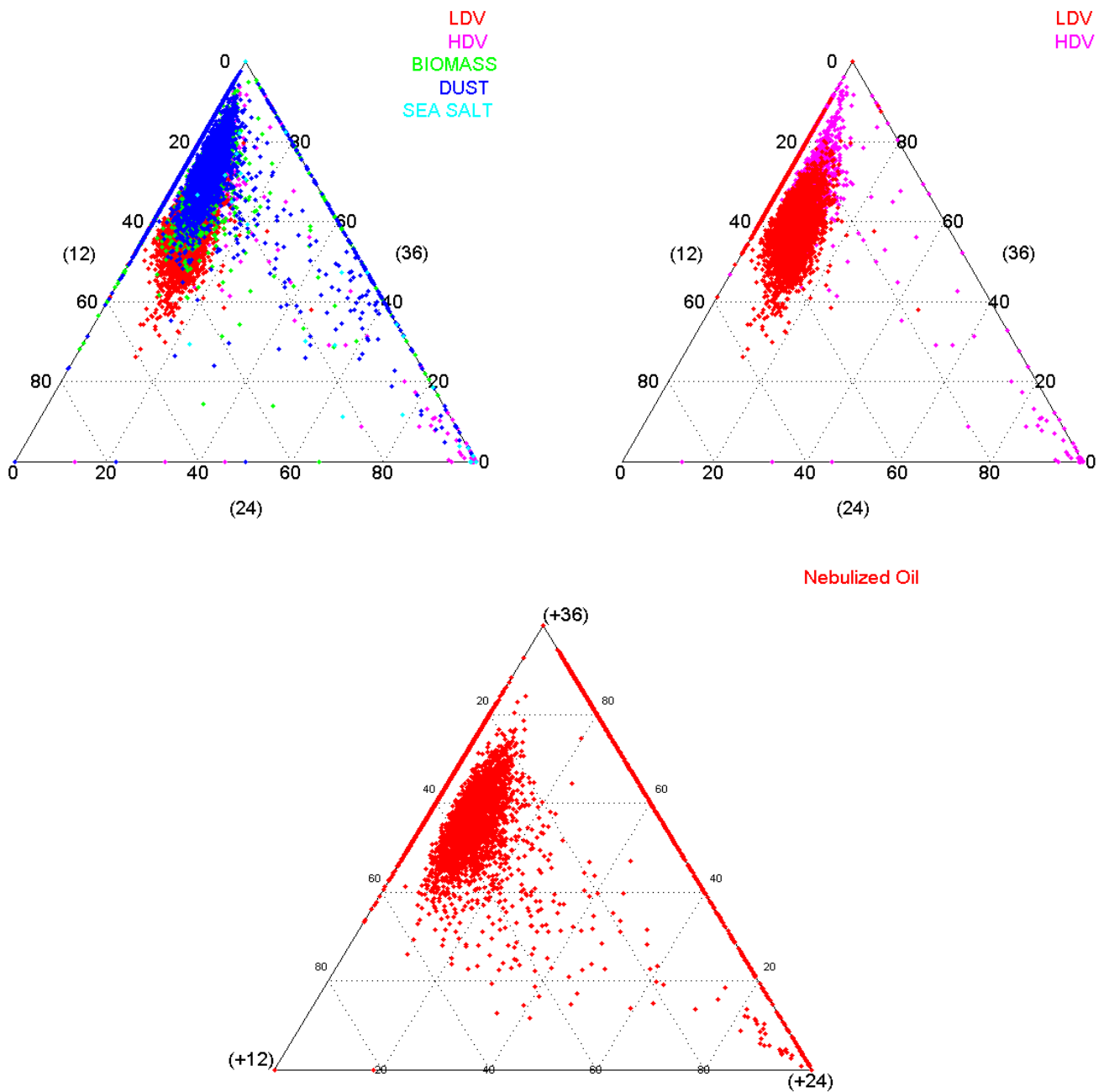


Figure 9.5 Fresno Particle Apportionment, comparing the HDV, LDV and other particles at m/z 12, 24, and 36. Only LDV differs, but it still overlaps with HDV. The third plot is obtained from nebulized oil particles measured in the laboratory. Even this pure source in very controlled conditions presents the same variations as LDV do in ambient studies, which is further evidence the desorption process generates at least a substantial part of the spectral variation observed in ambient particles.

than those observed in the Fresno study. The distribution of Fresno “labeled-dust” particles coincides with the distribution of CIFEX dust, but not with the distribution of CIFEX sea salt. Figure 9.4 shows temporal distributions. In 9.4A and 9.4B the apportionment indicates the arrival of westerly winds: in 9.4A the particle count drops strongly from using ART-2a clusters that have been manually labeled, in conjunction with a selection on particular peak areas and ratios. Figures 9.3, 9.4 and 9.5 illustrate the results from this method. Figure 9.3 shows type recognition by comparing the Fresno dust particles to the dust/sea salt apportionment in the Wednesday 1/24 until Tuesday 1/30. Simultaneously, the sea salt and dust proportions increase heavily, as shown in Figure 9.4B, presumably because westerly wind carried oceanic air masses and had been strong enough to pick up dust along the way. Figure 9.4C shows the daily cycle of biomass particles, which increase in the early night hours. Figure 9.5 is a ternary plot analyzing the proportions of different carbon peaks (12, 24 and 36) and shows that the populations labeled as HDV and LDV are different; the apportioned fractions overlap in the spectrum space, but only the LDV differs substantially from the average particle in terms of the m/z 12 to m/z 36 ratio. This plot also shows that it is impossible to differentiate HDV, coal, biomass, dust and sea salt using only the ratios of m/z 12 to m/z 36 or of m/z 24 to m/z 36. Overall, when using controlled study sources for automatic labeling, the labeling correlates well with identifiable source (as in Figure 9.3) and with external events (Figure 9.4), but it has to be curtailed to avoid forced classification of particles for whose source no samples are available at the time of analysis, such as different types of dust, or particles with a much higher or lower degree of aging than the source particles.

9.3.2 Regrouping Clusters by Analysis of Correlations

A preliminary study of the time correlation method was made on 20,000 Fresno particles, sampled on Jan 19, 2001 between 00:00 and 11:26AM. For the narrow clustering step, we used a SAHN (Sequential, Agglomerative, Hierarchical, Non-overlapping, see [Day and Edelsbrunner, 1984] algorithm, identical to that used by Murphy et al. (2003). Using the root-normalized spectra, this algorithm starts with one cluster per particle, and gradually merges clusters (finding the closest two, and replacing them by their centroid—with a correction for sphericity because the spectra had been normalized. This algorithm builds a tree that eventually has only one root cluster, but it can be interrupted at any time; in this case we put a limitation on the distance between merged points, by requesting that the distance between normalized spectra be smaller than 0.06 (this corresponds to a dot product of 0.998, or, in planar geometry, to an angle of $3^\circ 26'$). At the end of the narrow clustering step, 10,005 particles were associated in 487 clusters of various sizes from 4,698 to 2 particles (the remaining 9,995 particles were still alone in their individual “clusters”). The time course of clusters was then computed by averaging the dominance of that cluster over a rolling window of 100 particles (about 3 minutes of sampling). Thus, a pair of particles A in cluster 1 and B in cluster 2 would start contributing to a good correlation if they were sampled within 6 minutes of each other. The correlation matrix was then converted into a distance matrix and the same SAHN clustering algorithm, (weighted by cluster size) was used to collect the microclusters (based on spectra) into megaclusters (based on time course). The stopping point was for a distance corresponding to a +0.3 correlation.

To estimate the quality of the results, the graduate student in charge of the study labeled the microclusters according to her own categories (based on ART-2a data). We labeled each megacluster according to the category of its lead microcluster (the largest). We then computed the percent of the other particles in the mega-cluster that had that same label. Thus, in a megacluster with one large dominant microcluster (the usual case), the percent correct indicates how well the other microclusters match the lead cluster type. The overall percent correct is 81%. This means that, of the particles not in the lead clusters, 19% were incorrectly labeled; since the lead cluster itself is tautologically correct (it is the cluster used to determine the label of the mega-cluster), the absolute error rate is only 5.3% of the particles. Interestingly, the larger the lead cluster, the more reliable the apportionment is, as shown in Figure 9.6. For lead cluster size over 500 members, the method is very reliable, with less than 10% of misclassified particles. This was to be expected because large microclusters have a smoother time course and are not as likely to be accidentally correlated to other microclusters as are small microclusters.

Appendix C shows the median microcluster spectra and the type identified by the graduate student, for some of the microclusters of more than 12 particles. In these graphs, each bar shows relative peak areas at the corresponding m/z ; the blue part of the bar indicates the third quartile (75% of the particles in the cluster have a relative area larger than the blue/green transition), the blue+green bars indicate the median (half the particles have a relative area larger than the green/yellow transition) and the yellow indicates the first quartile (less than 25% of the particles in this cluster have a peak larger than the yellow bar). White and grey background stripes are there to facilitate localizing the peaks.

Appendix C illustrates several properties of the future method of data analysis. Microclustering creates many more clusters than ART-2a would determine with the standard vigilance setting of 0.8, and for this reason only the largest clusters are shown. This is because the goal of the first step was to define really narrow clusters, with the confidence that the second step would bring back together pieces that would be artificially separated.

Another observation is that the more numerous types are over-represented. The aged organic carbon (OC) and biomass types are dominant, and only 4 microclusters out of 41 are not biomass or aged OC. The bias in favor of the most numerous types of particles comes from the microclustering stage; this bias diminishes when more particles are considered in the clustering process. This reflects the importance of doing such studies over large numbers to empower both the microclustering and the temporal correlation stages. The proposed approach is to pool as much data as possible, computing the microclusters from several studies pooled together, and also regrouping them by combining the temporal correlation in all of these studies. Microclustering can only collect particles that are close to each other and benefits from higher densities in the spectral space; for Fresno particles, with the same stopping parameters, only 8% of the particles are clustered if the study covers 4,000 particles, versus 50% for a study of 20,000 particles. Temporal correlation works better when the study covers a longer time with more natural variations, such as day versus night, and various wind regimes. Moreover, time courses are smoother with a wider rolling window. Ideally, the rolling window must stay relatively short compared to the expected variation in source composition, but still encompass as many particles as possible. So, in high winds, a wide temporal window will smear the effect of varying volumes of air. Since the Fresno study, a bottleneck in the acquisition software has been removed, and the maximum sampling rate has been increased by a factor of 4, which should allow for a finer

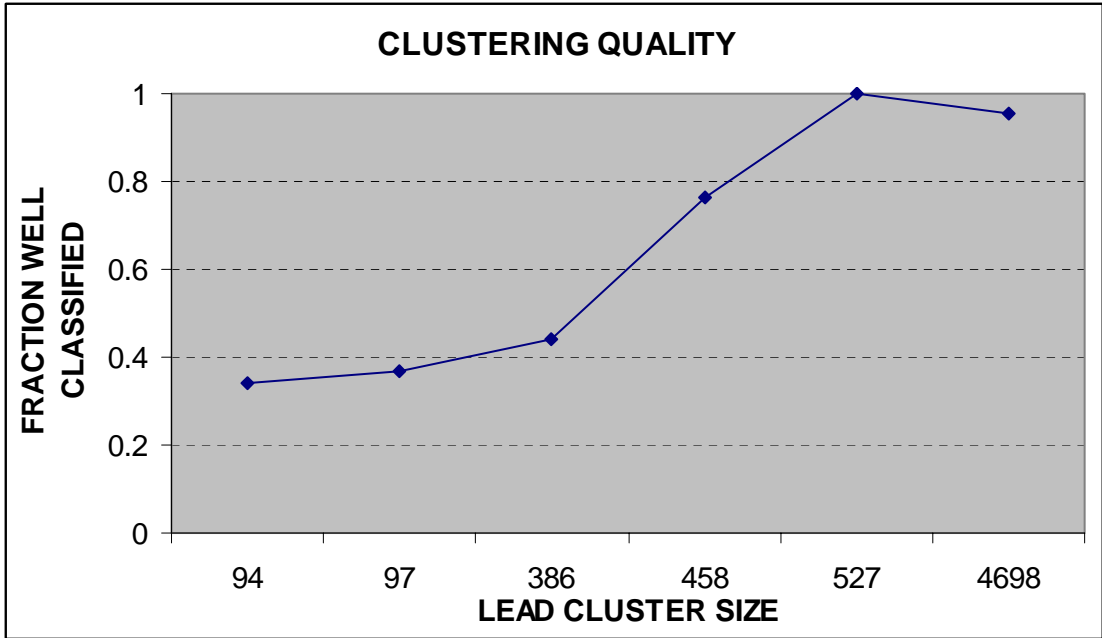


Figure 9.6 The percent of particles, not from the lead microcluster, that match the type of this microcluster as a function of lead cluster size.

correlation analysis. This increase in particle counts, coupled with using the whole duration of a study rather than just a few hours, will make time correlation analysis a very accurate method.

9.4 Other Modeling Approaches and Open Questions

Human based recognition is based on rules more than on quantitative analysis. For example, as explained earlier in this chapter, the presence of sea salt is strongly indicated by markers at peaks 81 or 83 (Na_2Cl) even though these peaks have smaller intensities than others in the spectrum. Alternative approaches to clustering methods for the fine clustering step would be to use discriminant analysis [Tan *et al.*, 2002], or decision trees mimicking the human decision making. Both of these methods allow apportionment into pre-defined classes only. Discriminant analysis (DA) uses for each class one template called a “discriminant”, which is a particular linear combination of spectral peak areas; to classify a particle, all its discriminants are computed, and the particle is labeled with the class of the highest discriminant. The templates are chosen by algorithms that work from pre-labeled training sets. Decision trees use a series of binary choices, for example the test “if the relative area of peak 23 (Na) is greater than 0.2 then the particle is either sea salt, burned biomass, or dust” will be followed by the test “if there is a peak 81 and there is a peak 83 and there is either a peak -35 with a smaller peak -37 (Chloride) or a peak 46 or a peak 62 (Nitrate), then this particle is a sea salt”, etc. In decision trees the tests can be more flexible than those of discriminant analysis, but the formulas are pre-determined by human knowledge without the automatic detection of the best discriminants that DA does. The strength of these methods is to handle well smaller markers, but their weakness is to be unable to identify new classes by themselves.

Another open avenue is the study of peak attribution. Some peaks are unambiguous, but many can represent different compounds. Humans are usually able to disambiguate peaks based on the presence of other peaks. For example, peak 27 likely can be attributed to aluminum in a particle whose spectrum also is indicative of aluminum oxide and other crustal metals but can be labeled as C_2H_3 in a particle that has mostly organics elsewhere. Some peaks can also be disambiguated by isotopic considerations. Bayesian analysis and Independent Component Analysis could both help disambiguating peaks, and would be a good preliminary step to quantitative fine clustering. Bayesian analysis can exploit human labeled examples, for example, using a set of particles in which peak at $m/z+39$ is labeled as either K^+ or C_3H_3 to determine what patterns in the rest of the spectrum are most likely to be associated with the [K] or the [C_3H_3] labels. This information is then used in reverse, to predict the probability that observed +39 peaks are [K] or [C_3H_3] peaks. Independent Component Analysis (ICA) [Bell and Sejnowski, 1995] looks at the components that have the best statistical independence. It differs from the better known Principal Component Analysis (PCA): PCA finds the most important orthogonal sources of variance whereas ICA finds non-orthogonal but statistically independent components. If a time-varying signal is made by adding two sources A and B that are somewhat but not entirely correlated, PCA will recover linear combinations of A and B, but ICA will isolate A from B. Applied to spectra, ICA can identify independent components that both show the +39 peak, but in some components this peak will be entirely [K] and in some others entirely [C_3H_3].

The existence of reaction lines in the spectra is also a point of interest that will eventually find its way into the models. For example, aging creates a continuum in the chloride/nitrate

balance in sea salt and dust particles, and other markers based on chloride (e.g., 81 and 83 for sea salt) will disappear along with the m/z 35 and 37 peaks. Therefore, it is possible to preprocess the spectra and combine the replaced peaks with those replacing them, for example by replacing the chlorine fraction (m/z at peaks -35 -37) by a linear combination of themselves and the nitrate fraction (m/z at peaks -46 or -62). This will substitute the line in the original spectral space by a point in the new one, thereby facilitating clustering and apportionment.

Finally, two questions related to the best use of the instrumental data deserve empirical study: the dependence of the measured spectra to the instrument design, and the vulnerability of various clustering methods to miscalibration (shifting the entire spectrum by 1 m/z) or to filtering and preprocessing immediately after data acquisition. Most analysis methods used currently work after a preprocessing step of peak detection and peak area computation. In the Prather group, this step is accomplished by the TasWare software. TasWare receives a series of 15,000 points per spectrum (ion current as a function of time) and converts it to a peak list for m/z varying from 1 to 350. To do so, it makes use of calibration points defined by the experimenter; the same calibration is used automatically for many spectra (usually for a day or at least several hours of measurement). Occasionally (for less than 2% percent of the particles), the acquisition board shifts the starting point in time by up to 1 m/z : this is a mis-calibration. Peak detection depends on threshold parameters that are set by experimenter, and also on filtering that can affect differently peaks of different area and aspect ratio. For example, it might be beneficial to use low-pass filtering at the 1 m/z bandwidth to remove noise before computing the peaks. Even then, signal noise is occasionally large enough to be above threshold, so that the spectra may be noised a by a few spurious small peaks. The same data pre-processing steps that reduce the influence of large peaks tend to increase the influence of these smaller noise-generated peaks. It is therefore necessary to optimize the parameters of preprocessing and of clustering on a several data sets that represent well the variation in signal noise across the studies that the optimized algorithm has to be used on.

9.5 Current Status and Next Steps

At of the writing of this report, we have a first operational version of the programs that use the SAHN Hierarchical Clustering Analysis for the microclustering and time correlation mega-clustering steps. The next two steps in this line of research will be first to implement a sectoring algorithm, to allow these programs to work fast on large numbers of particles (the current limit is 40,000 particles—which take 3 days to run), and second to explore the parameter space (distance for which the microclustering stops, width of the temporal rolling window, correlation for which the mega-clustering stops) and the conditions of use of this model, especially whether we can pool data from different instruments. The third step will be validation, on well known studies such as the Caldecott data set by comparing the apportionment with external variables like the observed numbers of LDVs and HDVs. Afterwards we plan to process all our available studies, constitute the catalog, and design of the fast recognizer program itself.

9.6 Conclusion

In conclusion, the method that we will use for future source studies will involve creating a catalogue of existing particle types for different sources, perhaps dependant on some particular conditions such as humidity, or the instrument used. Unlike the current ART-2a method, this one will accumulate knowledge from several studies. Work is currently underway to optimize these parameters. Using this catalogue will require matching the particle to one of a few hundred or thousand basic clusters—a task that computationally can be done at the same speed as particle sampling. This catalogue approach should enable real-time apportionment in the future.

9.7 References

- Bell, A.J., and T.J. Sejnowski, An information-maximization approach to blind separation and blind deconvolution, *Neural Computation*, 7, 1129-1159, 1995.
- Carpenter, G.A., S. Grossberg, and D.B. Rosen, ART 2-A: An adaptive resonance algorithm for rapid category learning and recognition, *Neural Networks*, 4, 493-504, 1991.
- Day, W.H.E., and H. Edelsbrunner, Efficient algorithms for agglomerative hierarchical clustering methods, *Journal of Classification*, 1, 7-24, 1984.
- Duda, R.O., P.E. Hart, and D.G. Stork, *Pattern Classification, second edition*, Wiley Interscience, 1997.
- Gross, D.S., M.E. Gälli, P.J. Silva, and K.A. Prather, Relative sensitivity factors for alkali metal and ammonium cations in single-particle aerosol time-of-flight mass spectra, *Anal. Chem.*, 72 (2), 416-422, 2000.
- Hinz, K.-P., M. Greweling, F. Drews, and B. Spengler, Data processing in on-line laser mass spectrometry of inorganic, organic, or biological airborne particles, *Journal of the American Society for Mass Spectrometry*, 10 (7), 648-660, 1999.
- Kohonen, T., *Self-Organizing Maps*, Springer, Berlin, Heidelberg, New York, 1995.
- Murphy, D.M., A.M. Middlebrook, and M. Warshawsky, Cluster analysis of data from the particle analysis by laser mass spectrometry (PALMS) instrument, *Aerosol Science and Technology*, 37, 382-391, 2003.
- Sodeman, D.A., S.M. Toner, L.G. Shields, D.T. Suess, D.S. Gross, and K.A. Prather, Comparison of light duty and heavy duty vehicle emissions from dynamometer and tunnel studies using ART-2a, *accepted for publication, Environmental Science & Technology*, 2005.

- Song, X.-H., D.P. Fergenson, P.K. Hopke, and K.A. Prather, Classification of single particles analyzed by ATOFMS using an artificial neural network, ART-2A, *Anal. Chem*, 71 (4), 860-865, 1999.
- Steele, P.T., H.J. Tobias, D.P. Fergenson, M.E. Pitesky, J.M. Horn, G.A. Czerwieniec, R.S. C., L.C. B., E.E. Gard, and M. Frank, Laser power dependence of mass spectral signatures from individual bacterial spores in bioaerosol mass spectrometry, *Anal. Chem*, 75 (20), 5480-5487, 2003.
- Tan, P.V., O. Malpica, G.J. Evans, S. Owega, and M.S. Fila, Chemically-assigned classification of aerosol mass spectra, *Journal of the American Society for Mass Spectrometry*, 13 (7), 826-838, 2002.
- Wenzel, R.J., and K.A. Prather, Improvements in ion signal reproducibility obtained using a homogeneous laser beam for on-line laser desorption/ionization of single particles, *Rapid communications in mass spectrometry*, 18, 1525-1533, 2004.
- Xhoffer, C., L. Wouters, and R. Van Grieken, Characterization of individual particles in the north sea surface microlayer and underlying seawater: Comparison with atmospheric particles, *Environmental Science and Technology*, 26 (11), 2151-2162, 1992.

Section VI

Conclusion

Concluding Remarks

The combination of a chassis dynamometer and a dilution system for studying complex combustion aerosol sources yielded highly reproducible chemical compositions at the single particle level. Therefore, ATOFMS source profiles and chemical obtained for different vehicles and driving cycles can be attributed to actual chemical differences and not to innate variations from instrumental variability or lack of a statistically relevant sample. Several distinct chemical classes were observed in the vehicular exhaust emissions during the dynamometer studies. The dominant particle types emitted by HDDV were determined to originate from lubricant oil. This observation was supported by the direct analysis of the vehicular fluids, oil and fuel. The high temporal resolution of ATOFMS provided insight to the chemical composition of single exhaust particles as the driving conditions changed; it revealed the preferential production of an elemental carbon particle types during the beginning of the cold start of LDV and of an organic carbon chemical class during the idling and low speed operation of HDDV. The particle types observed in the dynamometer studies created source profiles for LDV and HDDV, which were applied and evaluated in an apportionment study. The source signatures were detected in the tunnel study, and a new vehicle-related particle type (brake dust) was revealed. The observation of the dynamometer source signatures in this study shows great promise for ambient apportionment studies.

A significant fraction (close to 70% of accumulation mode and 85% of ultrafine mode) of ambient particles during the freeway study was matched to the dynamometer signatures. It was also demonstrated how the ATOFMS can identify particle types from other major combustion sources in ambient air including biomass and meat cooking. This finding is significant because these particle types represent a significant fraction of anthropogenic particles in the accumulation mode, particularly in other regions of California such as central California. The freeway study demonstrated the strength of using a combination of gas and particle phase instruments coupled with meteorological data for source apportionment. High correlations between the temporal variations of particle types measured with ATOFMS instruments were shown with peripheral gas and particle phase instruments. A tremendous amount has already been learned from the analysis of this dataset. Ultimately, the freeway study apportionment results will be compared with filter-based results from the Kleeman group once the off-line results become available. We are now in position to go into more detailed analysis on certain time periods and use new algorithms that may ultimately replace or at the very least supplement ART-2a. ART-2a has certain limitations as described in this report, however in spite of this it has been shown to be capable of distinguishing between the signatures for HDDV and LDV in ambient air. The next steps will include:

- Use traffic count data coupled with meteorology to develop an understanding of the variations in trends of different particle types and sources.
- Study the correlations between all instruments and apply a multivariate approach to further separate contributions from particle types with chemically similar signatures.

- Establish size-resolved percentages of HDDV and LDV as well as other ambient particles with one-hour temporal resolution.
- Compare the ATOFMS source percentage predictions with those of Prof. Mike Kleeman's group based on organic tracer filter based methods.
- Establish single particle source libraries for various sources (i.e. dust, sea salt, meat cooking, LDV, HDDV, biomass) that can be apportioned in real-time as particles are acquired in field.
- Compare the ATOFMS size resolved composition data with models (i.e. M.Z. Jacobson, J. Seinfeld) which predict roadside particle evolution to derive a better understanding of particle evolution in the atmosphere.

Section VII

Appendices

Publications and Presentations

A.1 List of Publications

Gross, D. S., M.E. Galli, P.J. Silva, S.H. Wood, Liu Don-Yuan, and K.A. Prather, Single particle characterization of automobile and diesel truck emissions in the Caldecott Tunnel, *Aerosol Science and Technology*, 32 (2), 2000, 152-163.

Gross, D. S., Barron, A. R., Sukovic, E. M., Warren B.S., Jarvis, J. C., Suess, D. T., and K. A. Prather, Differentiation of heavy and light-duty vehicle emissions on the single particle level, *Atmospheric Environment*, in press, 2005.

Suess, D.T., and K.A. Prather, Reproducibility of single particle chemical composition during a heavy duty diesel truck dynamometer study, *Aerosol Science and Technology*, 36 (12), 1139-1141, 2002.

Sodeman, D.A., S.M. Toner, and K.A. Prather, Determination of single particle mass spectral signatures from light duty vehicle emissions, *Environmental Science & Technology*, 2005, *accepted for publication*.

Shields, L.G., D.T. Suess, S.A. Guazzotti, and K.A. Prather, Determination of single particle mass spectral signatures from heavy duty diesel vehicle emissions in the 0.1 to 3 micrometer size range, *in preparation*.

Sodeman, D.A., S.M. Toner, L.G. Shields, D.T. Suess, D.S. Gross, and K.A. Prather, Comparison of light duty and heavy duty vehicle emissions from dynamometer and tunnel studies using ART-2a, *in preparation*.

Toner, S.M., D.A. Sodeman, and K.A. Prather, Single particle characterization of ultrafine- and fine-mode particles from heavy duty diesel vehicles using aerosol time-of-flight mass spectrometry, *in preparation*.

Spencer, M.T., and K.A. Prather, Comparison of oil and fuel signatures with gasoline and diesel emissions, *in preparation*.

A.2 List of Presentations

Jarvis, J.C., E.M. Sukovich, D.T. Suess, K.A. Prather, and D.S. Gross. Relationship between size distribution and individual particle composition from individual particles sampled in a road

tunnel, 49th Annual ASMS Conference on Mass Spectrometry and Allied Topics, Chicago, May 2001. (Poster presentation)

Sukovich, E.M., J.C. Jarvis, D.T. Suess, D.T. K.A. Prather, and D.S. Gross. Identification of marker ions from emissions of gasoline and diesel fueled vehicles by single particle aerosol time-of-flight mass spectrometry, 49th Annual ASMS Conference on Mass Spectrometry and Allied Topics, Chicago, May 2001. (Poster presentation)

Gross, D.S., J.C. Jarvis, E.M. Sukovich, W.J. Galush, A.M. Silverberg, D.T. Suess, and K. A. Prather. Aerosol time-of-flight mass spectrometry in a road tunnel: Correlations between single-particle and traditional measurements, American Society for Mass Spectrometry Asilomar Conference, Asilomar, CA, October 2001. (Poster presentation)

Guazzotti, S.A. and K.A. Prather. Using individual particle signatures to discriminate between HDV and LDV emissions, HEI Workshop: Improving Estimates of Diesel and Other Emissions for Epidemiologic Studies, Baltimore, MD, December 2002. (Invited oral presentation)

Guazzotti, S.A., M. Sipin, D.A. Sodeman, Y. Su, D.T. Suess, S. Toner, and K.A. Prather. Single particle characteristics of gasoline and diesel powered vehicular emissions: Classification, differentiation and source apportionment, Am Assn for Aerosol Research Particulate Matter: Atmospheric Sciences, Exposure and the Fourth Colloquium on PM and Human Health (AAAR PM) Meeting, Pittsburgh, PA, April 2003. (Oral presentation)

Spencer, M.T. and K.A. Prather. PM analysis of PALAS generated elemental carbon particles coated with fuels using ATOFMS, 22nd Annual AAAR Conference, Anaheim, CA, October 2003. (Poster presentation)

Spencer, M.T. and K.A. Prather. Detection of the mixing state of individual organic carbon and elemental carbon particles, 2003 AGU Fall Meeting, San Francisco, CA, December 2003. (Poster presentation)

Prather, K.A., D.A. Sodeman, L.G. Shields, S.M. Toner, D.T. Suess, and S.A. Guazzotti. Single particle mass spectral signatures from diesel- and gasoline-powered vehicles on a dynamometer system: Can these signatures be used for source apportionment, 14th CRC On-Road Vehicle Emissions Workshop, San Diego, CA, March 2004. (Oral presentation)

Shields, L.G., D.T. Suess, and K.A. Prather. Determination of single particle mass spectral signatures from heavy duty diesel vehicle emissions in the 0.1 to 3 micrometer size range, 229th ACS National Meeting, San Diego, CA, March 2005.

Spencer, M.T., L.G. Shields, and K.A. Prather. Chemical analysis of used and new petroleum based lubricants using ATOFMS, 229th ACS National Meeting, San Diego, CA, March 2005.

Toner, S.M., L.G. Shields, D.A. Sodeman, and K.A. Prather. Using mass spectral source signatures to apportion exhaust particles from gasoline and diesel powered vehicles in a freeway study, 229th ACS National Meeting, San Diego, CA, March 2005.

Reading Spectral Ternary Plots

B.1 Ternary Plots

Ternary plots are a way to represent a narrow slice of spectral data for a large set of particle. Only three spectral components (the values for three chosen peaks) are used, which allows to plot each particle as a point on a plane. The plot represents only the relative composition of each particle in those peaks regardless of all other peaks. For example if we chose peaks 12, 24, and 36 (which frequently correspond to elemental carbon ions (organic carbon also show these peaks)), the plot is going to summarize the ratios $[12]/([12]+[24]+[36])$, $[24]/([12]+[24]+[36])$ and $[36]/([12]+[24]+[36])$. Mathematically this is done simply by creating a point-based planar coordinate system. (Note that using 3-D plots we could likewise represent 4 peaks at a time). Geometrically, as shown in Figure B.1, the particles are projected from their original $([12], [24], [36])$ coordinates onto the plane of equation $(x+y+z = 1)$.

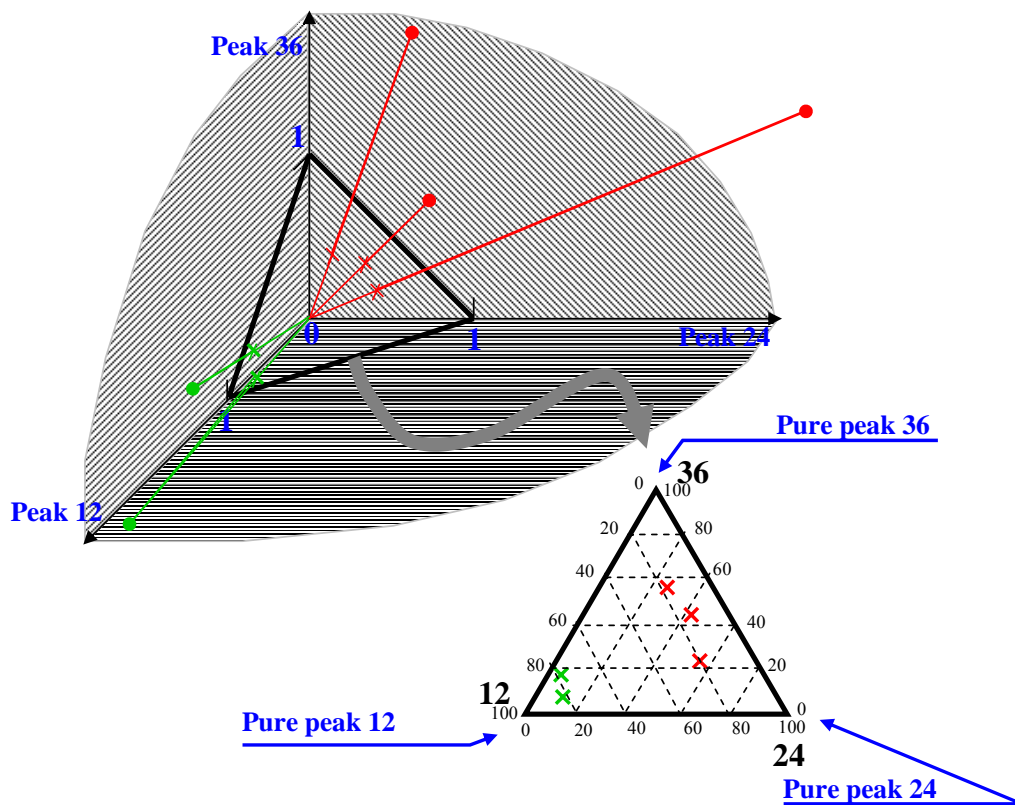


Figure B.1 Creating a ternary plot. From their 3-D coordinates (concentrations in [12], [24] and [36]), individual particles are projected into the triangle defined by $(x+y+z = 1)$. Here for example the green particles have strong peaks at m/z 12 whereas the red ones have only about 20% of [12]. The sides are labeled with a 0-100% scale and the peak that this scale applies to. Reference lines (dotted lines) allow a better reading of the particle composition.

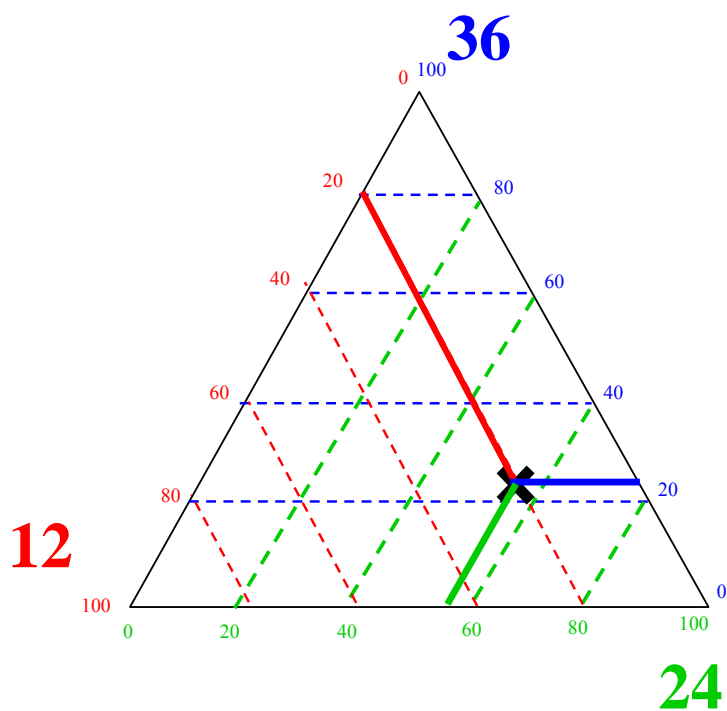
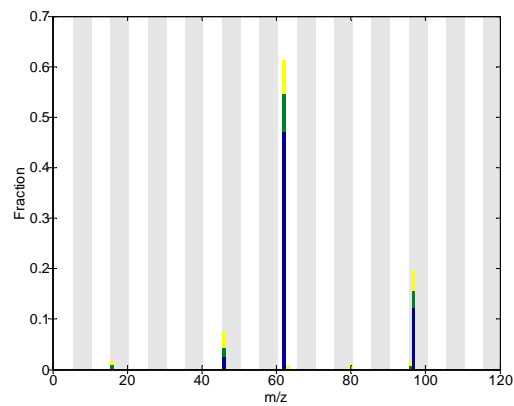
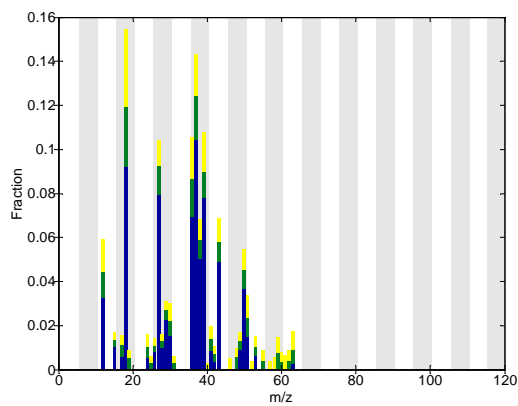


Figure B.2 Reading relative composition from the ternary plot: the main component is the triangle corner that the point is closest to. In this case, peak 24. The composition is in proportion of the proximity to the pure peak corners. The exact composition can be read by projecting the point onto the axes by following lines opposite to the corner of which we are reading the percentage. In this case, the particle has [24] ~ 55% found by following the green line down to the green scale; [12] ~ 20% by following the red line, and [36] ~ 25% read by following the blue line.

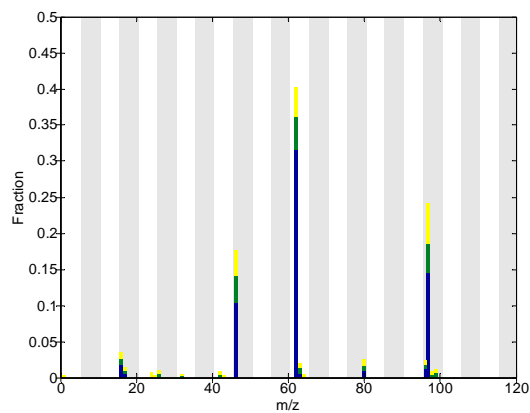
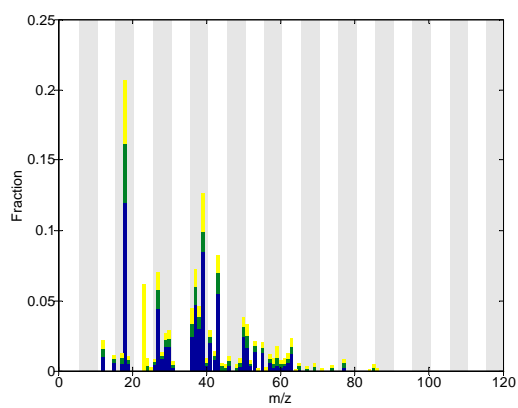
Megaclusters for Fresno 20,000 Particles

C.1 Example 1: MEGA 1: Aged Organic Carbon

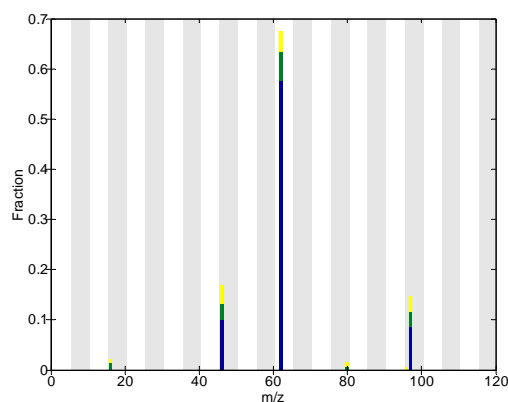
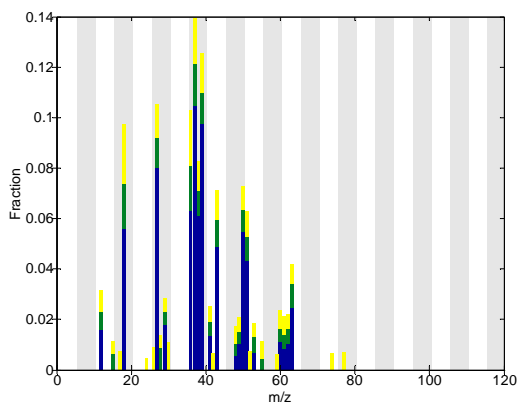
Cluster 1: 4,698 particles : Aged OC



Cluster 4: 525 particles : Aged OC



Cluster 20: 397 particles : Aged OC



Cluster 11: 203 particles : less aged OC (not shown): well-classified

Cluster 13: 152 particles : Aged OC (not shown): well-classified

Cluster 73: 46 particles : Aged OC (not shown): well-classified

Cluster 53: 45 particles : Biomass (not shown): mis-classified

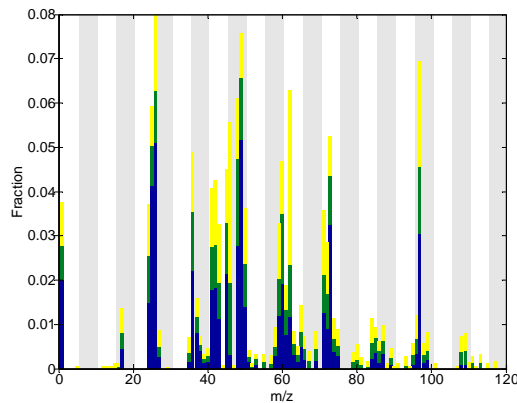
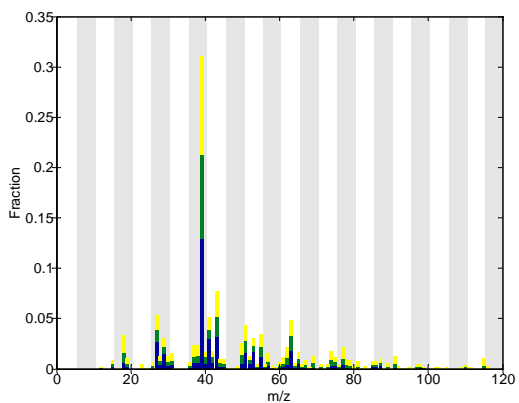
Cluster 24: 18 particles : Biomass (not shown) : mis-classified

Cluster 48: 12 particles : Aged OC (not shown): well-classified

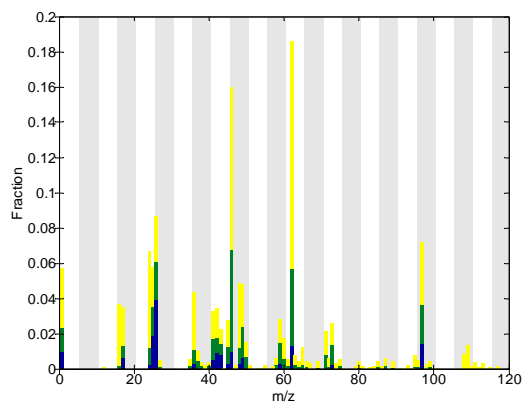
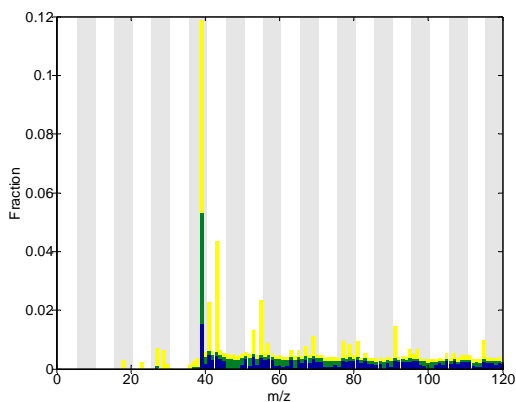
Total Particles NOT in the lead cluster: 1398, well classified: 1335, misclassified: 63, % correct: 95.5%

C.2 Example 2: MEGA 3: Biomass

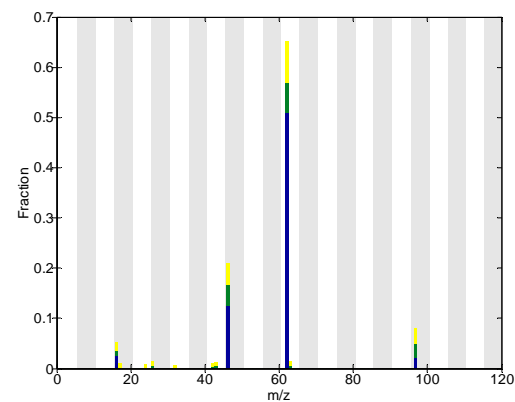
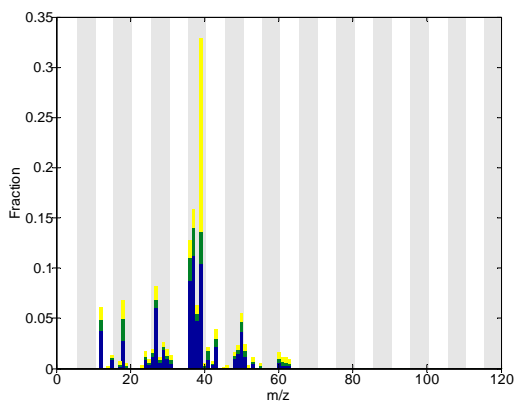
Cluster 8: 459 particles : Biomass



Cluster 6: 337 particles : Biomass



Cluster 27: 77 particles : Aged OC : misclassified

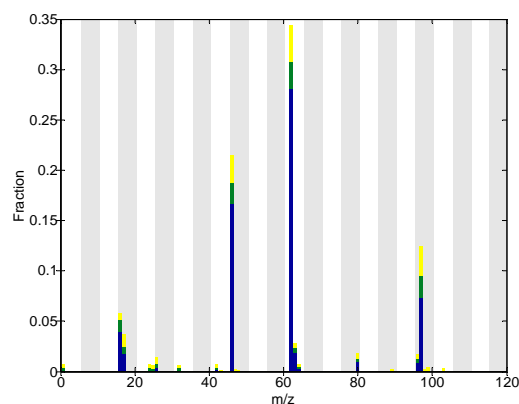
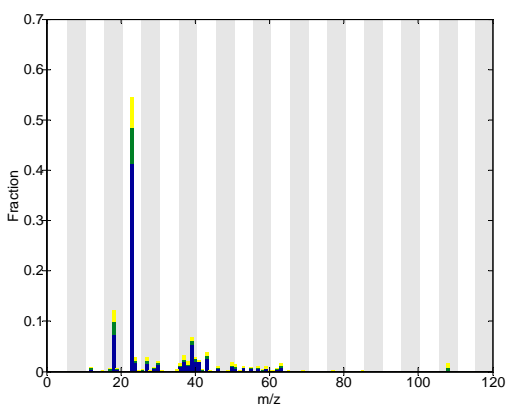
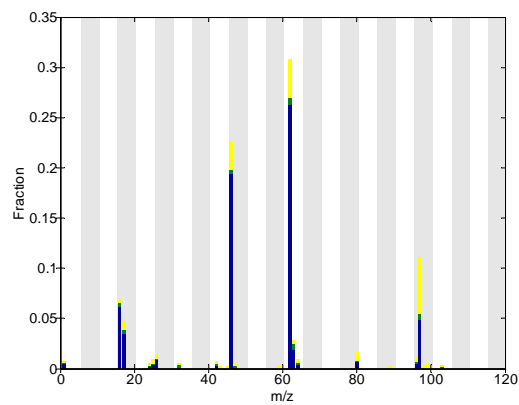
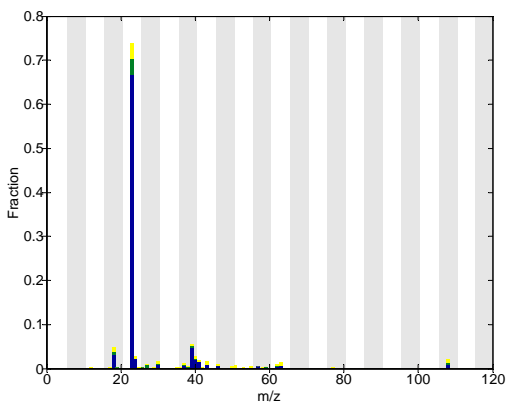


- Cluster 14: 58 particles : Biomass
- Cluster 15: 46 particles : Biomass
- Cluster 3: 45 particles : Aged OC
- Cluster 16: 35 particles : Biomass
- Cluster 32: 15 particles : Aged OC
- Cluster 259: 14 particles : Biomass
- Cluster 101: 14 particles : Sea Salt

Total Particles NOT in the lead cluster: 641, well classified: 490, misclassified: 151, % correct: 76.4%

C.3 Example 3: Clusters of “minor types” (not biomass or aged organic carbon)

Clusters 57 (58 particles), and 101 (14 particles) : Sea Salt



Clusters 102 (36 particles) and 180 (18 particles): Calcium Dust

